

Multiscale Analysis of High Resolution Digital Elevation Models using the Wavelet Transform

THÈSE N° 4610 (2010)

PRÉSENTÉE LE 5 MARS 2010

À LA FACULTÉ ENVIRONNEMENT NATUREL, ARCHITECTURAL ET CONSTRUIT
LABORATOIRE DE SYSTÈMES D'INFORMATION GÉOGRAPHIQUE
PROGRAMME DOCTORAL EN ENVIRONNEMENT

ÉCOLE POLYTECHNIQUE FÉDÉRALE DE LAUSANNE

POUR L'OBTENTION DU GRADE DE DOCTEUR ÈS SCIENCES

PAR

Michaël KALBERMATTEN

acceptée sur proposition du jury:

Prof. I. Smith, président du jury
Prof. F. Golay, directeur de thèse
Dr D. Van De Ville, rapporteur
Prof. R. Weibel, rapporteur
Prof. J. Wood, rapporteur



ÉCOLE POLYTECHNIQUE
FÉDÉRALE DE LAUSANNE

Suisse
2010

An idea is always a generalisation, and generalisation is a property of thinking. To generalise means to think.

Georg Hegel

Abstract

At the end of the nineties the emergence of high resolution (1 *m*) digital elevation models (DEMs) settled the context of high precision geomorphological analysis. These new elevation models permitted to reveal structures that remained heretofore undetectable. Earth scientists henceforth benefit from a field of analysis with a textural richness that was never attained before.

However, the complexity and the volume of the data reveal a series of questions and problems. The storage size has increased, the computational processes have become heavier, and the visual or digital interpretation has become more complex. Moreover, these new models make it possible to characterize and analyse much smaller phenomena than previously. "Traditional" DEMs with resolutions ranging from 10 *m* to 90 *m* can be used to analyse a valley or a hillside. Transposed to a cartographic scale, this corresponds at best to a 1 : 25 000 ratio. As for high resolution DEMs, they show much more detailed structural levels and can be used to analyse geomorphological features of 2 – 3 meters, this corresponding to scales ranging from 1 : 10 000 to 1 : 1 000.

Yet, in the abundance offered by this growing resolution, large geomorphological structures are still present, including the finer structures. They are even the actuators of processes relevant to larger cartographic scales. Consequently, high resolution DEMs contain a multitude of structures, which exist throughout their interactions with other structures at other scales. This is the context of the present study.

Geomorphometry - the quantitative counterpart of exploratory geomorphology - permits to explore and quantify a wide range of shapes and terrain indicators. At higher resolution however, the methods of this discipline can hardly be used. Geomorphometrical methods are based on a geometric model (a quadratic surface) and few of these methods can be applied it in a multiscale context. Furthermore inappropriate techniques are frequently used, hence the idea to move to a multiscale approach called the wavelet transform. The latter had previously been explored by few researchers within the geomorphometry community, but never thoroughly to micro- and to meso-scales.

Due to the non-stationarity of DEMs, the wavelet transform was preferred to the Fourier transform in order to decompose DEMs into multiscale spaces. This facilitates a coherent navigation from scale to scale, but also makes new scale specific phenomena emerge for different frequencies. The wavelet transform is a technique widely used in image analysis. It allows decomposing a signal according to its frequency components, but also according to the position of the frequencies in the signal. Its multi-scale capacity is an effective analytical tool in multiple domains. More particularly in geomorphology, structural components - specific to a specific phenomenon - are well

determined in these sub-spaces specific to the scale continuum. Finally an in-depth analysis of the phenomena enabled us to understand processes and their and their phenomenological inter-dependencies.

In order to understand the effects and outcomes of the approach we developed an artificial landslide. We then computed some profiles and analysed the autocorrelation, slope attenuation and local fractal indicator. The resulting high-pass information of the wavelet transform has also been analysed and filtered using several types of filters. In a case study we used a real-world landslide to validate the transform and to understand its impact on geological structures.

Within this case-study we conducted a web-based survey that allowed the participants to analyse the landslide using wavelet results and to make comments on the potential of the wavelet transform in the field of geomorphometry. Moreover, important contributions of this thesis are new algorithms that allow the illustration of the structural coherence in relation to each subspace. These are based on the theory of vision of Marr and on structure tensors.

The results of our studies show a high consistency. The wavelet transform thereby extends the range of tools in geomorphometry. The different structural scale levels show that such these methods are needed to better understand the phenomenology of geomorphological processes.

Keywords:

DEM, high resolution, multiscale, wavelets, Marr wavelets, geomorphology

Résumé

Depuis la fin des années 90, les modèles numériques de terrain (MNT) à haute résolution (1 *m*) ont fourni un contexte d'analyse géomorphologique d'une précision inégalée. Le terrain modélisé laisse apparaître des structures qui restaient invisibles auparavant. Les géologues, géomorphologues et ingénieurs de l'environnement ont désormais accès à un champ d'analyse d'une grande finesse.

Ces données ont cependant fait émerger toute une série de questionnements et de problèmes. La taille des fichiers à traiter a explosé, les processus de calcul se sont alourdis, et l'interprétation, visuelle ou numérique, est devenue plus complexe. De plus, la taille des phénomènes que ces modèles permettent d'analyser s'est aussi considérablement réduite. Les MNT "traditionnels" (de 10 à 90 *m* de résolution) permettent de traiter des vallées ou des versants entiers, ce qui correspond à une échelle cartographique de 1 : 25 000 environ. Les MNT à haute résolution permettent d'aborder des niveaux beaucoup plus fins, et correspondent à des échelles cartographiques du 1 : 10 000 au 1 : 1 000 environ. Structurellement, cela signifie que des éléments géomorphologiques de tailles avoisinant 2 à 3 *m* deviennent visibles et peuvent être analysés. Toutefois, les énormes possibilités offertes par le grand niveau de détail de la haute résolution ne doivent pas faire oublier le fait que les grandes structures géomorphologiques sont toujours présentes et qu'elles se superposent aux plus petites structures. Celles-ci peuvent même constituer les moteurs de processus qui se déroulent à des échelles plus grossières. Par conséquent, les MNT à haute résolution contiennent une multitude de structures qui coexistent en interaction avec d'autres structures détectables à d'autres échelles. C'est dans cette perspective multi-échelle que s'inscrit la présente étude.

Les indicateurs géomorphométriques, instruments quantitatifs de la géomorphologie exploratoire, permettent d'explorer et de quantifier toute une série d'indicateurs de forme et de caractéristiques du terrain. Leur utilisation est cependant limitée dans le contexte de la haute résolution: ils sont basés sur une modélisation géométrique - une surface quadratique - et rares sont les techniques qui permettent de les appliquer dans le cadre d'une approche multi-échelle. Comme leur implémentation est souvent effectuée au moyen de techniques d'analyse inappropriées, il a semblé pertinent de changer de méthode et d'explorer l'approche par transformée par ondelette. Cette dernière n'avait jamais été utilisée et validée d'une manière aussi approfondie dans le cadre de phénomènes à micro- ou méso-échelle jusqu'ici.

Les MNT sont non-stationnaires. La transformée par ondelette a donc été préférée à la transformée de Fourier pour décomposer les MNT en une succession d'échelles. Les ondelettes, et la transformée qui leur est associée, constituent une technique largement utilisée en analyse d'image. Elles permettent non seulement de décomposer un signal suivant les fréquences qui le compose,

mais aussi suivant la position de ces fréquences dans le signal. Leur capacité à dissocier les échelles en fait un outil d'analyse efficace dans une multitude de domaines. Plus particulièrement en géomorphologie, les composantes structurales - spécifiques à des phénomènes particuliers - apparaissent ainsi dans ces sous-espaces spécifiques du continuum de l'échelle. Enfin, leur analyse fine a permis de mieux comprendre les processus et leurs inter-dépendances phénoménologiques.

Pour comprendre les tenants et les aboutissants de l'approche, un glissement de terrain artificiel a été produit et soumis à plusieurs analyses entreprises sur les résultats de la transformation: calcul de profils, indice d'autocorrélation, analyse de l'atténuation des pentes et coefficient local de fractale. L'information passe-haut résultante de la transformée par ondelette a aussi été analysée et filtrée suivant plusieurs typologies de filtres. Un glissement de terrain réel a aussi été utilisé pour valider la transformée et comprendre son impact sur les structures géologiques. La validation a été poursuivie par la mise en place d'une enquête sur Internet qui a permis à des utilisateurs de faire une analyse utilisant les ondelettes et de commenter la valeur ajoutée de la transformée par ondelettes.

Pour clore l'étude, de nouveaux développements algorithmiques ont permis d'illustrer de la cohérence structurale par rapport à chaque sous-espace. Ceux-ci se basent sur la théorie de la vision de Marr et sur les tenseurs structurels.

Les différents résultats démontrent que le traitement et le rehaussement de MNT est possible en utilisant la transformée par ondelettes. De plus, ils montrent la haute cohérence de la méthodologie et permettent d'élargir le panel d'outils géomorphométriques. L'imbrication structurale dans les niveaux d'échelle montre aussi que de telles méthodes sont nécessaires afin de mieux comprendre la phénoménologie des processus géomorphologiques.

Mots-clés:

MNT, haute-résolution, multi-échelle, analyse et filtrage fréquentiels, ondelette, ondelette de Marr, géomorphologie

Acknowledgements

This research started as a reflection at the GIS laboratory (LaSIG) at EPFL regarding high resolution digital elevation models (DEMs). Moreover the Swiss authorities had acquired these models and we were asked to develop methods for specific analysis purposes.

Through discussion with Régis Caloz, former scientific adjunct of the LaSIG, we wanted to explore the wavelets analytical capabilities applied on DEMs. These turned out to become my PhD research field. Therefore I first would like to thank Régis Caloz without whom I would never have had such a research thought. I would also like to thank Abram Pointet, another former member of the LaSIG, for his unconditional support and for his “unconditional” criticism. His ideas, suggestions and challenges pushed me forward to accomplish this work. I have really enjoyed (and still enjoy) exchanging ideas with him. My thanks also go to Stéphane Joost. His friendly scientific support during the last two years of this PhD work have been valuable.

Prof. François Golay gave me the opportunity to work in an academic environment and accepted to be my thesis director. I would especially like to thank him! Even if my research field was a bit obscure for him, I hope that he had some pleasure to follow my work! I would like also to thank him for all the invaluable help and feedback.

Wavelets would still equal to a day of disappointment for surfers of the lake Léman to me without the encounter of Prof. Dimitri Van de Ville. I was lucky to meet somebody who has so much patience! I will keep his mathematical papers and explanations to remind me that everything is possible. A great thank also to the members of his former laboratory - The Biomedical Imaging Group of the EPFL, directed by Prof. Michael Unser -, even if they had the habit to call me “le géographe”, I felt that all my questions were always answered!

Another person who followed and helped me during my whole journey through my PhD is Pascal Turberg - my geological adviser. His optimism regarding my research was always a wonder for me compared to some other feedbacks that the geological community gave me. I would like to thank him a lot for all his reading and advise!

A great thank to Marc Riedo from the Système d’Information du Territoire Neuchâtelois without whom I would not have had my nice landslide case study. Within a week after the landslide, Marc decided to fly over the landslide, which was a great opportunity for me!

I thank the president and board members of my committee who have accepted to evaluate my research: Prof. Ian Smith (EPFL), Prof. Jo Wood (City University, London), Prof. Robert Weibel (University of Zurich) and Prof. Dimitri Van De Ville (EPFL).

A huge thank you to all LaSIG members of these past seven years for the atmosphere, which is unforgettable. Of course, François Golay has a lot to do with that. He always manages to make people feel comfortable inside of his team. A great thank to Véronique, which has always been able to get me out of the mess of the school administration. Thanks also to all former members: Joël (long live musical experiments!), Karine (supporting all those men), Gilles (do not be shy), Eduardo (I still do not understand everything you say), Mathieu (the African way of life), Elena (again supporting all those men, do you not agree “Loulette”?), Thierry (how is junior today?), Nicolas (admit it “tabernacle”, you love to play the drums!), Claudio (do not hesitate to offer me some Portuguese wine) and Sylvie (physics and straight humor).

I am very grateful to my main LaSIG mate Roger - Doctor Jens Ingensand - who had to bear my moods for almost seven years! I think that without him (and his German sense of humour) I would not have achieved anything. The scientific and human exchanges we had were really important to end the worst days and to start the best days! I am almost jealous of his next office colleague - parting is going to be hard! Thanks also for all the things he helped me with and for all his advice.

I am infinitely grateful to my family and to my friends for their support. They surely felt a bit abandoned, which is sometimes hard to understand and to accept. I will try to catch up! I promise!

And last but not at least, I would like to thank Marie-Claude: for her unconditional support over the last few months, even if I have not always been really present, and for the great correction work of my English writing, even if she did not really understand what I was trying to prove. Her help, encouragement and support are indefinable.

Table of Contents

Abstract	I
Résumé	III
Acknowledgements	V
1. Introduction	1
1.1 Research goals	2
1.2 Outline	4
2. Digital elevation model and geographical information systems	7
2.1 Airborne laser scanning - Basic principles	8
2.1.1 Acquisition of ALS data	8
2.2 DEM - Digital Elevation Model	11
2.3 Visualisation	14
2.3.1 Shading	14
2.3.2 Contour lines	17
2.3.3 3D	18
2.4 Geomorphometric indicators	19
2.4.1 Quadratic surface and derivatives	19
2.4.2 Hydrological indicators	21
2.4.3 Other geomorphometric indicators	22
2.4.4 Geomorphometric patterns	23
3. Scale and scaling process	25
3.1 Scale	25
3.1.1 Scale specifications in geography	26
3.1.2 Geographical information processes and scale	28
3.2 Spatial resolution	31
3.3 Scaling	33
3.3.1 Scaling process in raster data	34
3.4 Geomorphology and scale	39
3.5 Multiscale analysis in geomorphometry	40
3.6 New multiscale framework in geomorphometry	41
4. Multiscale DEM using wavelets	45
4.1 Wavelet for generalisation	45
4.1.1 Fourier transform	45
4.1.2 Wavelet transform	47
4.1.3 Inverse wavelet discrete transform	52
4.2 Generalisation of high resolution DEMs	52

4.2.1	DEMs and wavelet	52
4.2.2	Validating the wavelet approach	53
4.2.3	Wavelet function choice	54
4.2.4	Wavelet transform effect - A simple model	56
4.2.5	Global surface statistics	60
4.2.6	Profiles on generalisations	61
4.2.7	Slope to elevation distribution	62
4.2.8	Local fractal validation	69
4.2.9	Global spatial autocorrelation	71
4.3	Wavelet coefficients	72
4.3.1	Coefficient filtering	72
5.	Case study	79
5.1	Introduction to the case study	79
5.2	Global statistical indicators	79
5.3	Profiles on generalisation	80
5.4	Slope to elevation distribution	86
5.5	Local fractal indicator	89
5.6	Global spatial autocorrelation	91
5.7	Wavelet coefficient analysis and filtering	92
5.7.1	Global landslide context analysis	92
5.7.2	Profile on the accumulation zone	99
5.7.3	Geomorphological visual analysis	104
5.8	Conclusion on the case study	115
6.	Methodological validation	117
6.1	Introduction	117
6.2	GAS - Geomorphometric Analysis System	117
6.2.1	Purpose and objectives	117
6.2.2	The survey	118
6.2.3	Results	122
6.2.4	Conclusions	123
6.3	Multiscale pattern analysis	127
6.3.1	Unsupervised classification of geomorphometric indicators	127
6.3.2	Fuzzy k-means	128
6.3.3	Application to DEM pixel classification	128
7.	A vision for multiscale DEM analysis	139
7.1	From wavelets to Marr's vision theory	139
7.2	Marr's theory of vision	139
7.3	Marr's decomposition	140
7.3.1	Magnitude and phase of the complex wavelet subbands	141
7.3.2	Subband-selective reconstruction	145
7.4	Structure tensors	150
7.5	Exploratory geomorphological mapping	153
8.	Discussion	157
8.1	Wavelets and DEMs	157
8.2	Wavelet transform applied to geomorphological characterization	159
8.2.1	Geomorphological scale and the wavelet transform	159
8.2.2	Patterns & multiscale DEMs	160

8.3	Marr's vision and DEMs	161
8.4	Framework benchmark	163
9.	Conclusion	165
9.1	Review of the goals	165
9.2	Final outcome	167
9.3	Perspectives	167
9.3.1	Energy of wavelet coefficients	167
9.3.2	Vision for geomorphometry	168
9.3.3	Linking geological space and decomposition levels	168
9.3.4	Dissemination of the wavelet transform applied to DEM analysis.....	168
	Bibliography	171
	Glossary	181
	Mathematical notations	183
A.	Fractional B-splines and Wavelets	185
A.1	B-spline Interpolation	185
A.1.1	B-spline basis function	185
A.1.2	B-spline coefficients	186
A.1.3	Filter autocorrelation	187
A.2	Wavelets	188
A.2.1	Mirror filters.....	188
A.3	Computing the wavelet transform	189
B.	Fractional spline wavelet and scaling functions	191
B.1	Fractional spline wavelets.....	191
B.2	Choice of B-spline degrees	191
B.2.1	Frequency composition of low-pass reconstructions....	191
B.3	Profiles on generalised DEMs	196
B.4	2D shape of fractional B-spline scaling and wavelet functions.	197
C.	Profiles on generalised surface	201
D.	Hurst coefficient	209
D.1	Hurst coefficient	209
D.1.1	Example of Hurst coefficient computation	209
D.2	Hurst coefficient on virtual landslide	211
E.	Detail coefficient of the virtual landslide	213
F.	The Travers landslide description	221
F.1	Data.....	221
F.1.1	DEM	221
F.1.2	Geological Map	226
F.2	Description of the Travers landslide	228
G.	Profiles on generalised DEM of Travers	231
H.	Detail coefficients on the Travers DEM	239

I. Fold profiles	249
J. Linear structural elements on the Travers DEM	253
K. GAS - Geomorphometric Analysis System	255
K.1 Result analysis	256
K.1.1 First questionnaire results	256
K.1.2 Second questionnaire results	257
K.1.3 Third questionnaire results	258
K.1.4 General comments	258
K.2 Acknowledgement	259
K.3 Questionnaires	261
L. Multiscale pattern analysis results	263
L.1 Generalised Least-Square Errors - fuzzy k-means	263
L.1.1 Confusion Index	263
L.1.2 F, partition coefficient	264
L.1.3 H, classification entropy	264
L.2 Results for the Travers DEM	265
L.2.1 Correlation of geomorphometric information	265
L.2.2 Confusion index	265
L.2.3 Result of the fuzzy k-means classification	267
M. Laplace-gradient wavelet pyramid and structure tensor ...	285
M.1 Laplace-gradient wavelet pyramid	285
M.2 Structure Tensor	287

1. Introduction

In the early 2000s, the emergence of high resolution ($\sim 1\text{ m}$) elevation data allowed exploration of our environment and its morphology under new aspects, like analysing micro-faults on a cliff. The enthusiasm of researchers, but also authorities, engineers and geologists, has been enormous since then. Nevertheless, new techniques have to be developed in order to process all this new information. The content of these digital elevation models (DEMs), with reference to their high resolution, has caused multiple problems to emerge, such as storage, computation and interpretation. Moreover, the visual perception, i.e. the visible phenomena or relevant structures, has evolved considerably due to the finer description the model permits. Indeed, it is now possible for instance to analyse visually a hillside and its details. By details, we refer to elements of only a few meters. Multiscale analysis of such models has therefore appeared like a new way of analysis and perception of geomorphology and its underlying phenomenology.

Over the same period, research on developing form indicators, called geomorphometry indicators, has also progressed significantly; note the important contribution of Wood (1996) in the development of these indicators. However, these are geometric indicators, because they are computed using the adjustment of a mathematical surface on elevation models.

The motivation for the present research emerged through internal discussions at the GIS laboratory of the École Polytechnique Fédérale de Lausanne. Indeed, the frequency approach issue arose following a study on these geomorphological indicators and their evolution through scale. In fact, there have been only few attempts to analyse elevation models using frequency domain approaches. Yet, our environment is composed of frequency information, as well as some phenomena that are inherent in its evolution (e.g. earthquakes or mass movements). The limitation, which made most studies fail, is that almost no natural phenomenon related to Earth science is stationary and homogeneous. It consists of a nesting of processes and structural elements, which are interdependent, have various scales, and interact in the natural system. This means that the size and shape of every structure depends on the phenomenon it belongs to, but also on the functional scale of the system.

That is the reason why we chose to use a frequency analysis tool, the wavelet transform, for the multiscale analysis of elevation models. Unlike the Fourier transform which is the best known frequency analysis tool, the wavelet transform is spatially well-defined and results in a multiscale view of the analysed data.

1.1 Research goals

As we are dealing with natural phenomena and their representation in elevation models, our hypotheses are strongly linked to the description of landscape in a geomorphological perspective. As thread, we use assumptions inspired by the work of Meentemeyer and Box (1987) on “Principles of scale”. They will help us define the aim and goals of the study. The following assumptions are used:

- Fewer variables may be needed for modelling larger study areas; conversely, smaller study areas may have more external effects, thus requiring more variables.
- Dynamics observed at finer scales cause the equilibrium observed at broader scales.
- Distance decay: everything is related to everything else, but near things are more related than distant things (Tobler, 1970).
- Apparent detail is lost using areas at broad scale; at fine scale, apparent new detail may appear in the area.
- Broad scale system size involves emergent properties; fine scale systems lose some interactions and thus some functional properties.
- A quantitative description of a system cannot be made using only one scale.
- Rough areas must be analysed at relatively finer scales than the rest of the study landscape.
- Roughness and structural density can be described using a frequency space.

Wavelet theory, and its underlying analysis, is related to these assumptions. The wavelet analysis is applied to the frequency space representing the entire spectrum of a 1D or 2D signal. It is a dyadic discretization of this space at each successive analysis. Moreover, the energy of the spectrum is reduced. As for spatiality, it is respected by the fact that the transformation is localized. We know exactly where and how it is applied throughout its results. These are multiscale views of coefficients, which reflect a successive reduction of details and roughness. Therefore, there is a strong relation between the assumptions adapted from Meentemeyer and Box (1987) and the methodology developed in this study.

These assumptions involve scale, modelling, spatial distances, geomorphological structures and quantitative systems. Thus, the general aim of the study is:

The multiscale analysis of geomorphological structures and manifestations of processes using the wavelet transform

Using the previous general aim, we will now define the specific research goals to this study. Regarding this aim, the following goals are defined:

To define a good scaling method for elevation models and, if possible, to implement multiscale analysis approaches.

In order to analyse multiscale processes and structures in geomorphology, the scaling method has to respect the structural elements of the elevation model. Scaling through interpolation may be implemented using several methods and techniques, but not all are appropriate in all circumstances. They must not inject noise and artefacts into the scaled model. We want to implement a scaling process which does not generate new structures. Therefore, it will be necessary to define what a multiscale elevation model is.

To transfer information from fine scale to broad scale and keep the best structural geometry

As our main data will be of high resolution¹, the scaling process will be defined as going from fine scale to broad scale. The problem is to conserve structural elements through the process until their specific scale level is reached. The methodology is not appropriate if it injects distortions to broad scaled elements as it goes through the different levels. For example, if we take a large-scaled hill, it has to remain structurally preserved until the process reaches its scale level.

Using scale analysis to generalise and simplify information by retaining only the essential data for multiscale geomorphological analysis

The central interest of this study is to find out how frequency like analysis may be applied to geomorphological analysis using elevation models. Thus, combining scale, frequency analysis and geomorphology, we want to retrieve only the data of interest related to our system or phenomenon.

To interface scales of interest by combining data at different scales

If we create discrete scale intervals, the representation of the model that we will have at a specific scale level does not allow us to link the various scale levels, besides spatial overlay. We must indeed find a way to combine these different discrete spaces in order to analyse and study the different interactions. However, multiscale analysis does not make sense if it is limited to separate structural elements simply into discrete intervals of scale. Thus, it is still necessary to find a way to recombine these different intervals as required by a structural analysis which is specific to a phenomenon. Only then can its nested structures be represented and analysed.

To produce and recognise geomorphological structures through these scale levels

Geomorphological structures are like fingerprints on a glass, they have a spatial coverage and a certain shape in elevation models. Thus, we may be wondering whether the imprint may be recognised or not, consequently if it can be extracted and isolated in the model. We might here see a link with geometric pattern recognition. However, it should be specified that our analysis domain is topography in the form of an elevation model and its underlying geomorphology. The latter, given its nature, is extremely complex and heterogeneous. And this already greatly limits the application of pattern recognition techniques.

¹ By “high resolution”, we mean what is usually called “very high resolution”, thus resolutions from 0.5 to 2 m. But for clarity purposes, we will use the term “high resolution” instead of “very high resolution” in this study.

To identify scale domains and scale thresholds regarding geomorphological phenomenology

The purpose of any discretization analysis is to simplify and threshold an information. In a structural perspective, the question is here to understand the efficiency of the thresholds in the creation process of new scale intervals. It will then give a geomorphological sense to these new created intervals. Due to the very definition of “interval”, and whatever its nature is, it has limits. These may of course be strict (or compact) or fuzzy. However, the scale discretization results in mathematically well-defined intervals. It will therefore be necessary to verify in which type of extent they are defined: compact or fuzzy.

1.2 Outline

Following this introduction, which focuses on the motivations and goals of the present thesis, the next chapters and sections are structured as follows:

Chapter 2

In this chapter, we introduce the main kind of data and its properties that we are going to use throughout the study: from the acquisition of elevation data to the establishment of a regular gridded model. Besides, existing methods and their underlying indicators, as quantitative methods for geomorphological analysis, will be shortly presented.

Chapter 3

This chapter is an introduction to scale concepts. It is not supposed to express new theories or concepts of scale. There are already plenty of studies and theoretical background in the current literature. We make a review of scale concepts related to geographical information science (GISc) and moreover to raster data. Although geomorphology is not directly related to GISc and its underlying data, we will make a short review of scale issues as it is our main analytical framework.

Chapter 4

This chapter is the core of the study. It introduces multiscale elevation models produced using the wavelet transform. The transform is applied to a virtual model in order to assess the methodology and to understand better the issues and effects of the transform. This is done by visual analysis, but also using some statistical and textural indicators.

Chapter 5

A real elevation model is used to assess the methodology developed in chapter 4. Thus, the same indicators as for the virtual model are computed and analysed. A qualitative study, based on geological information and terrain observation completes the case study. Some conclusions are given regarding all the elements analysed in this chapter.

Chapter 6

This chapter is a validation of the wavelet transform applied in chapters 4 and 5. Two distinct analysis are undertaken: a web-survey called Geomorphometric Analysis System (GAS) and an attempt to classify geomorphometric indicators computed using the low-pass wavelet transform results. GAS shows how the wavelet transform results might be used for the interpretation of geomorphological structures by an expert audience. The classification shows the relation of features through scale and their potential interactions.

Chapter 7

As seen through the web-based survey (GAS, chapter 6) experts (geomorphologists, geologists, environmental engineer and so on) encounter many problems analysing multiscale information, which is often also multivariate information, in multiple layers. Using the elevation model of the case study of chapter 4 and the results of the web-based survey, this chapter states that we have to go one step further in the multiscale analysis and introduce also visualisation of multiscale data. The innovative methodology developed by Van De Ville and Unser (2008) enables to reduce the number of representative dimensions. A short case study is thus undertaken in this chapter and some new approaches for the geomorphological characterization are introduced.

Chapter 8

This chapter consists of a discussion of the proposed methodology. We discuss the solutions and exploratory analysis of the study regarding the response of geomorphological structures using frequency analysis. As an introduction to the study's perspectives, it is a summary and the conceptual explanation of the undertaken analysis. The web-survey (see chapter 6) assesses the methodology and the impact of the developed approach on quantitative terrain analysis and interpretation.

Chapter 9

Finally, this chapter concludes the study by taking into review all the goals we expressed above. Perspectives, regarding the wavelet methodology, the representation of filtering processes and further work on the vision concept of chapter 5 are given. A final conclusion completes these perspectives.

2. Digital elevation model and geographical information systems

In the Swiss federal mapping history, one of the first representation of relief appeared on the Dufour maps (1842-1864) as lines representing more or less the slope directions in order to simply represent the presence of slopes. However, this way of representing the topography makes the map difficult to read because these lines or stripes take a lot of space on the map (Imhof, 2007). In the second generation of the Swiss national maps (Siegfried, 1870-1892), the stripes slope gradients were abandoned and replaced by contour lines and manual relief shading. In the current national maps, the topography is still represented that way (note that the shading azimuth is 315°).

With the emergence of digital methods and geographical information system (GIS) tools, the contour lines were digitized. But this kind of vector data is not easy to use numerically for relief analysis. It is indeed difficult to calculate a slope gradient using contour lines. They were then interpolated into regular grids, hence the appearance of raster elevation models. These terrain models are called digital elevation models (DEMs) and, since, they are used for a better understanding and modelling of our environment. For instance, in GISc, DEMs are used for terrain analysis in a defined spatial process. A lot of functions enable DEM calculus, contouring, derivation, hydrological process modelling, feature network extraction and solar irradiation. Research in 3D DEM representation and computation has grown rapidly over the past ten years by the emergence of public 3D viewers. Currently 3D remains a representation mode of DEMs, and data is mostly computed in 2D before being represented in 2.5D¹.

The first DEMs used in GIS were interpolated using cartographic contours or computed through parallax measures in aerial photography interpretation (Moore *et al.*, 1991). Synthetic aperture radars (SAR) interferometry and radargrammetry appeared through the evolution of space technology, e.g. the shuttle radar topography mission (SRTM) of the National Aeronautics and Space Administration (NASA). Although these new technologies enabled the acquisition of global terrestrial coverage, the DEM resolutions remained in ranges of 15–90 meters. Only terrestrial methods, like levelling, GPS measures and, in some cases, aerial photography and interferometry can result in high resolution DEMs (1–5 m). Airborne laser scanning (ALS) appeared about 15 years ago for DEM acquisition purposes (Baltasvias, 1999b). This active system enables the acquisition of high resolution DEMs over a wide spatial coverage and even over dense vegetation through its canopy penetration properties. We will focus this study on ALS data, but as a remainder

¹ 2.5D refers to the fact that a DEMs is a 2D representation (regular matrix) of 3D data (elevation) (Monnier, 1997). It should give a 3D cognitive approach to 2D data.

the following techniques are or were used for DEM data acquisition (Li *et al.*, 2005):

- Aerial photography: through two stereo photographs an image matching is fulfilled; coordinates (x, y and z) can then be measured.
- Radargrammetry and SAR interferometry: space techniques in which the interferometry of phase is measured. This is an active system using microwaves. Like carrier phase tracking with a GPS, coordinates can then be derived from the phase differences.
- Cartographic interpolation: the swiss national DEM (25 meter resolution) was created using a cubic interpolation from cartographic contour data (swisstopo, 2004).
- Manual terrestrial acquisition: using GPS or levelling techniques, on site coordinates are measured and interpolated.
- Light detection and ranging (LIDAR): for more details, see next sections.

The data used in this study are issued from ALS (or LIDAR). From now on, we will only consider and describe ALS data.

2.1 Airborne laser scanning - Basic principles

ALS for DEM acquisition purposes was first described in the late 90's (Baltasvias, 1999a,b; Wehr and Lohr, 1999). At this time only few companies had such a system, but since, ALS has become a common and rapid system for data acquisition. Many national institutions acquired high resolution DEMs using ALS measured data. A lot of applications were developed in order to process this data in fields as different as forestry (Gachet, 2009), geomorphology (Theiler and Reynard, 2008; McKean and Roering, 2004), ecology (Lassueur *et al.*, 2006), urban planning, and architecture (Rottensteiner and Briese, 2002). This list is not exhaustive, several other fields use high resolution DEMs.

2.1.1 Acquisition of ALS data

ALS systems are a combination of two other systems: the LIDAR unit and the positioning unit (*POS* in figure 2.1). The first one is composed of the LASER unit and of the computational units which calculate the distance covered by the laser beam and the current position of the aircraft. The latter measures the absolute position using differential the global positioning system (GPS) and an inertial navigation system (INS).

Differential global positioning system.

The differential GPS (DGPS) system measures the differential positioning (X, Y and Z) of the aircraft in the WGS84 datum. For an accurate position, two receivers using two different frequencies (called L1 and L2) are used. The obtained precision is about 10 *cm*. "Differential" stands for the correction of the aircraft GPS measures with a ground GPS which measures its position on a point. The coordinate of this point are know in the projection system.

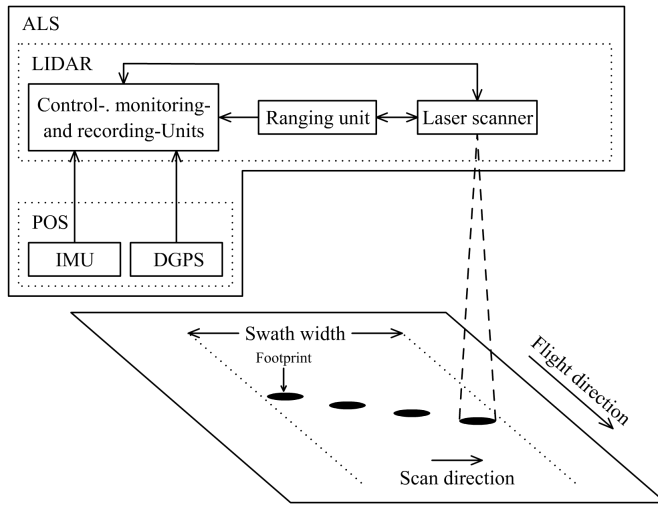


Fig. 2.1. ALS system, adapted from Wehr and Lohr (1999)

Inertial navigation system.

The inertial system measures the accelerations and the attitude (rolling, pitch and yaw) of the aircraft (figure 2.2). In opposition to the DPGS, this measure degrades itself with time.

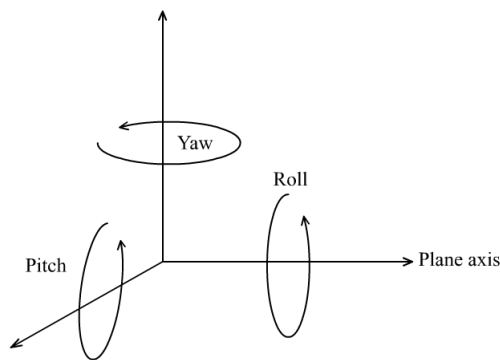


Fig. 2.2. Aircraft attitude

By integrating the measured data, an accurate navigation position can be obtained for the aircraft. Unfortunately, the INS drifts in time, reducing the accuracy of the attitude and consequently the position. The measure frequency is between 100 – 400 Hz.

Combining GPS and INS data enables to obtain enough accurate positions for laser elevation data. This combination makes it possible to compensate the errors of both systems. The INS drift is corrected by the GPS positioning and the lack of GPS measures is compensated by the INS measures.

Light detection and ranging.

The LIDAR telemeter is generally assembled on the INS platform, so that the aimed direction is generally known. Then the telemeter emits a high frequency laser beam ($\sim 80 \text{ kHz}$). The transceivers enable the measure of emittance - reflectance time. Exciting light at a specific frequency using mirrors produces a concentration of light. This one is released and forms a beam (or laser beam). The diameter of this beam on the ground, because of the propagation divergence, depends on the height above ground of the aircraft. Generally, this diameter is between $15 - 30 \text{ cm}$.

The LIDAR produces a laser pulse which propagates through the atmosphere and which is more or less reflected depending on the nature of the impact point. The propagation speed of this pulse is light speed. The echoes are consequently detected before the next pulse is emitted.

Principles of laser measures.

The LIDAR systems enable to measure more than only one echo. For ground and surface investigations, we will limit ourselves to the first and last echoes. These result from the penetration potential of the laser beam. The first echo gives the distance of the first reflecting encountered object. The first measured distance is the tree foliage and the last one is the ground (figure 2.3).

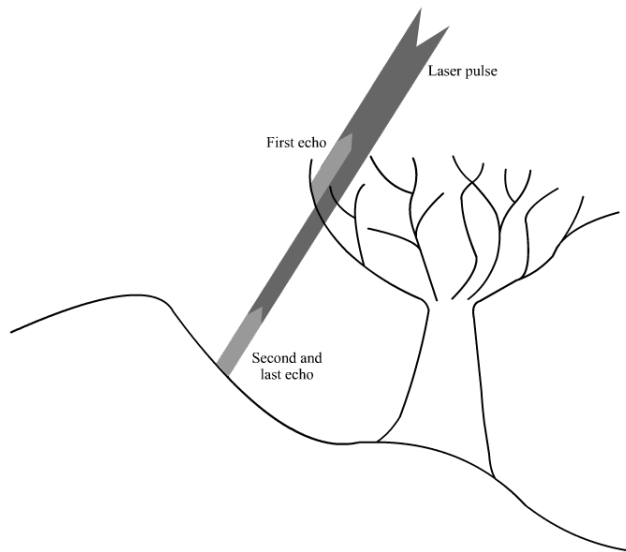


Fig. 2.3. Laser penetrating vegetation - echoes

The laser beam goes from the emitter to an object and back to a receiver. Knowing the speed (light speed, $c = 3 \cdot 10^8 \text{ m/s}$) of the beam, it is easy to calculate the distance:

$$distance = \frac{c \cdot t}{2} \quad (2.1)$$

with t the run time.

Current laser systems enable the measurement of terrain stripes. The following different systems are distinguished:

- Multiple telemeter systems: each telemeter is oriented in a different direction (regular angle increment).
- Mobile optic systems: the laser beam is deviated periodically by a rotating mirror.
- Augmented mobile optic systems: same principle than the previous one, but augmented by a glass fibre bundle which increases the mechanical stability of the system².

The scanner bands enable stripe from 250 *m* to 700 *m*, depending on the opening angle to be captured (up to 30°). For more details on ALS systems and specifications, see Baltsavias (1999a,b); Gachet (2009); Wehr and Lohr (1999).

Classification and interpolation.

Most terrain indicators are computed and modelled using matrices. This comes from the fact that, in computer science, it is much easier to set an indicator using regular computational steps, but also because regular data is easier to handle, store and compress. Thus a lot of developments concerning elevation were done on elevation data matrices, the so-called DEM.

To define a regular matrix using LIDAR data points, two operations have to be achieved: a point classification, followed by an interpolation. The classification is the separation of the echoes into ground or surface points:

- Ground points: raw terrain points (no vegetation, no human infrastructures), e.g. if the LIDAR survey is done over a forest, ground points will often be considered as the last echo returning from the ground to the aircraft.
- Surface points: first echoes and human infrastructures.

Part of this classification process is undertaken automatically by applying an elevation threshold to the point regarding the mean slope for example or by using object-oriented data classification (Brennan and Webster, 2006). Afterwards, a visual verification has to be done in order to assess the automatic classification. Expert software exist for this purpose, and we will not go further into the classification discussion here.

Following the classification, an interpolation needs to be performed between these points and a regular grid. Gachet (2005); Li *et al.* (2005); Monnier (1997) analysed the most common techniques for DEM interpolation. The DEMs used in this study were interpolated using triangular irregular network (TIN) interpolation proposed in the Terrasolid³ software.

2.2 DEM - Digital Elevation Model

The term "DEM" takes its origins from physical terrain model (Li *et al.*, 2005). Since the appearance of numerical technologies, DEM has widely been accepted as a term for the characterization of elevation matrices. Multiple terms are used. In order to avoid any confusion, a short definition of each term used in this study is given:

² see <http://www.toposys.com/> for details, accessed 25 May 2009

³ <http://www.terrasolid.fi>, accessed 29 January 2010

- DEM - Digital Elevation Model: DEM is the term that will be used as a generic for the description of general proprieties and process of matrix elevation data.
- DTM - Digital Terrain Model: DTM is the part of elevation data that represent the terrain, but only its natural structures and without vegetation. Sometimes, even large rocks are removed. DTM will be the main type of DEM used in this study (see chapters 4 and 7).
- DSM - Digital Surface Model: DSM is the model of surface, namely all elements independently of their kind (natural or human infrastructures), including vegetation, trees or buildings. If a model does not contain any of those objects, then the DSM is equivalent to the DTM.
- DHM - Digital Height Model: DHM is a derived model of the last two. However, it is not a representation of elevation, but a representation of height. By computing the difference between the DSM and DTM, a DHM containing differences of surface and terrain is generated. This kind of model is often used to determine tree heights (Gachet, 2009) and building heights.

The terrain is a continuous field (x, y) referring to a continuous measure z , the elevation (Cova and Goodchild, 2002). This field is a tensor field of multiple directions and amplitudes. As suggested by Cova and Goodchild (2002), terrain can be represented as a spatial tessellation, which may be regular, irregular or even hybrid. The basic function of such tessellation is:

$$z_i = f(x_i, y_i) \forall i \text{ location} \quad (2.2)$$

So at all spatial locations, the model is defined, thus continuous. It can be represented in many ways such as a triangular network (see next section) or a regular grid.

In this study, the terms DEM, DTM, DSM and DHM will always refer to the model in the form of a regular grid (even if a TIN is also a DEM).

So, for us, a DEM is a regular matrix containing interpolated elevation data, thus an aggregated continuous variable represented by a discrete spatial grid. This basis is used as a spatial model for indicator computation. In this study, we will distinguish three different matrix components (figure 2.4):

- Node: computational model (black crosses, figure 2.4)
- Mesh: connection network of nodes (dot lines, figure 2.4)
- Grid: visual representational model using cells (gray squares, figure 2.4)

Regarding the above definition, **a terrain model is spatially continuous in the space (x, y) , discrete in the grid, but thematically continuous in both (z) .**

We are going to compute new information using the nodes. The mesh is a purely conceptual framework of neighbouring and adjacency used for the definition of a convolution (or moving) window (figure 2.4, z_i). Regarding the chosen size of this computational window ($3 \times 3, 5 \times 5, \dots, n \times n$, n defines the size and is odd most times), mesh defines which nodes are needed for the convolution operation. Convolution will be defined more thoroughly in section 3.3.1. Finally, the grid is only a concept for visualisation purposes. In fact, it is the visual element which is displayed when a DEM is visualised in a GIS, the node value is then applied to its relative cell in the grid.

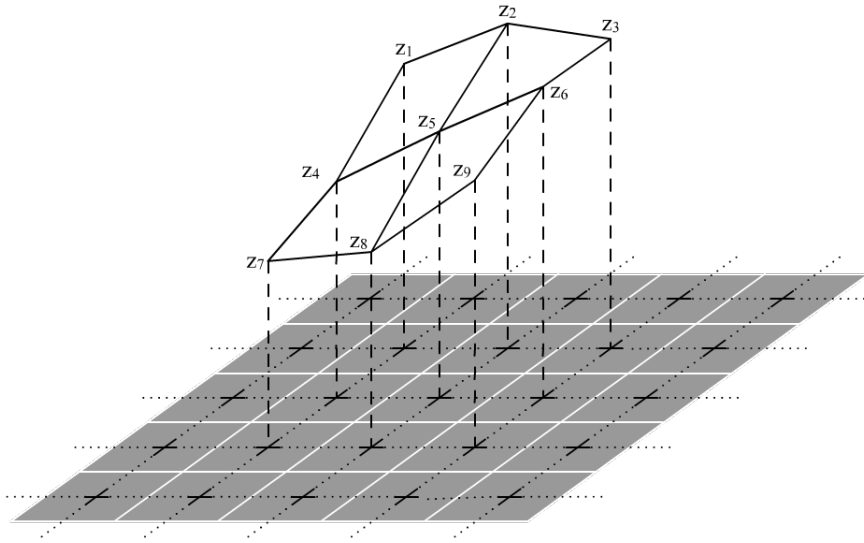


Fig. 2.4. Conceptual description of DEM elements

We will specify the following properties of DTMs:

- Resolution (r): size of a grid cell (or distance between two non-diagonal adjacent nodes).
- Width (m): number of columns of the matrix. $m \cdot r$ gives the east-west extend of the DTM.
- Height (n): number of lines of the matrix. $n \cdot r$ gives the north-south extend of the DTM.
- Minimum (min): the minimum pixel value, thus the minimum elevation over the DTM's spatial coverage.
- Maximum (max): the maximum pixel value, thus the maximum elevation over the DTM's spatial coverage.
- Range: $max - min$ gives the range of elevations. The range gives an indication of the type of terrain (abrupt or flat) covered by the DTM. It is also highly scale dependent.

The three last statistical indicators give a first overview of the type of DTM we are dealing with. The minimum and maximum indicate in which kind of environment the DTM is located. Range specifies the vertical spatial coverage, showing if there is a great elevation difference, thus if the landforms are steep and mountainous. But all these properties are completely dependent on the spatial extension of the DTM and, thus, are dependent on the width, height and resolution.

As we are mostly interested in landscape feature analysis and recognition, we shall focus on the definition of DTMs (see section 2.2 for the difference between DEM and DTM). *Terrain* is used as the term for specifying the scope on which the DEM matrix is centred:

Terrain:

*a stretch of land, especially with regard to its physical features.*⁴

However, this definition is not explicit enough and *terrain* remains an obscure term. As Li *et al.* (2005) suggested, a DTM contains topographical or non-topographical information. In this study, we will limit ourselves to topographical information, thus elevations above the sea level in a particular projection system, including landforms, rocks, rivers, seas and land infrastructures such as roads; but no elevated infrastructures (bridges or buildings).

DTM are used in landform analysis (Lane *et al.*, 1998), geomorphology (Bishop and Shroder Jr, 2004; Wilson and Gallant, 2000), terrain modelling and visualisation (Li *et al.*, 2005). Geomorphometric indicators (see section 2.4) were developed for DTM analysis. Even if they are used on DSM or DHM, their first scope was DTM.

2.3 Visualisation

Visualisation means only the visualisation of DEMs in GIS software, either in 2D matrix visualisation or in 2.5D modelling. The advantage is that rendering a matrix is easy, because of its image-like structure.

We will not further develop visualisation concepts, but briefly give an overview of DEM visualisation in GIS software. For more details, refer to Weibel (1989a); Wood (1999); Buckley *et al.* (2004) and Li *et al.* (2005).

2.3.1 Shading

Shaded relief is the common way of DEM visualisation in GIS. There are many different methods to compute a shading using a DEM (Batson *et al.*, 1975; Horn, 1981). Most of them use two parameters, the sun incidence angle and the sun azimuth, and two variables derived (or approximated) from the DEM, the slope and the aspect (see section 2.4 for more details). Often, relief shading (or hillshading) is applied with an azimuth of 315° degrees. As Burrough and McDonnell (1998) mentioned, this azimuth has “more to do with human faculties for perception than with astronomical reality”. Indeed, cognitive visual faculties are, for most people, better in feature recognition and analysis for this shading azimuth. Other azimuths enhance other aspects of terrain properties (e.g. figure 2.5).

Batson *et al.* (1975) gave a simple method for computing hillshading on a DEM (equation 2.3). Using trigonometric relation between slope and aspect of a pixel and the incidence angle and azimuth of the lightening source, the light intensity can be computed (figure 2.7).

$$I = \frac{1}{1 + \frac{\cos \epsilon}{\cos i}} \quad (2.3)$$

where (figure 2.6):

- I : intensity of the reflectance
- ϵ : angle between the observer and the slope normal
- i : angle between the direct sun beam and the slope normal

⁴ Compact Oxford English Dictionary: [http://www.askoxford.com/results/?view=dev_dict &field-12668446=terrain&branch=13842570&textsearchtype=exact&sortorder=score%2Cname](http://www.askoxford.com/results/?view=dev_dict&field-12668446=terrain&branch=13842570&textsearchtype=exact&sortorder=score%2Cname), accessed 18 May 2009

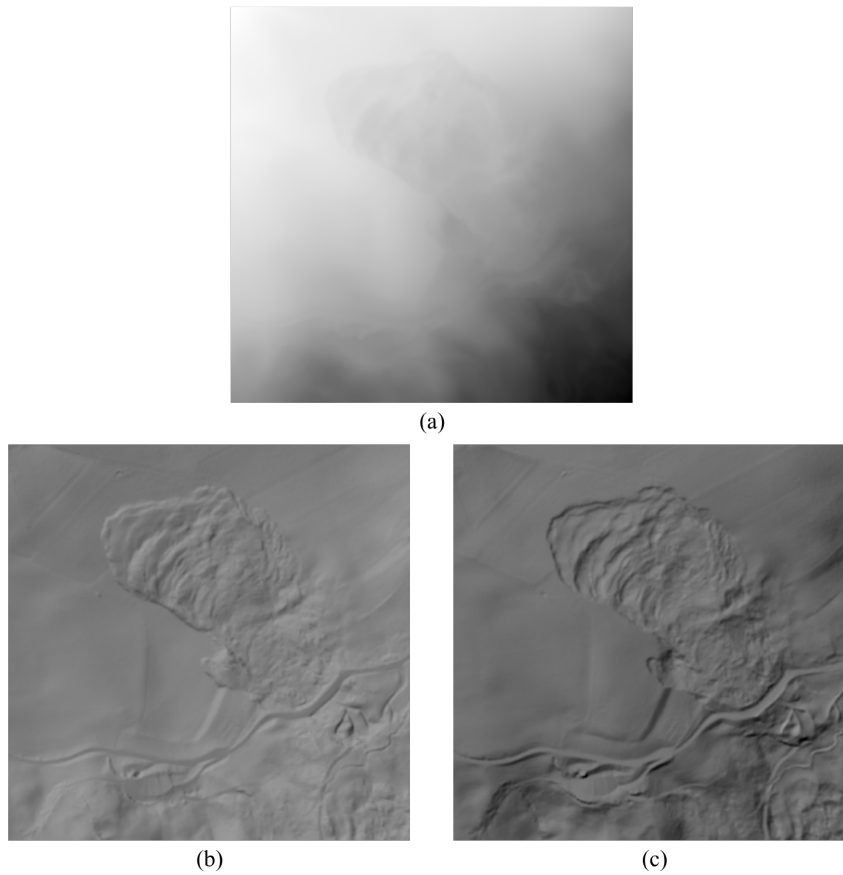


Fig. 2.5. 2D DEM representation (resolution 1 meter), a grayscale intensity of the elevation values representation does not reflect local structures of the DEM (a), hillshading (azimuth: 315°) enhances local structures and landforms (b). Using another azimuth (135°), as in subfigure (c), gives another description of the terrain shapes and structures, DEM©SITN

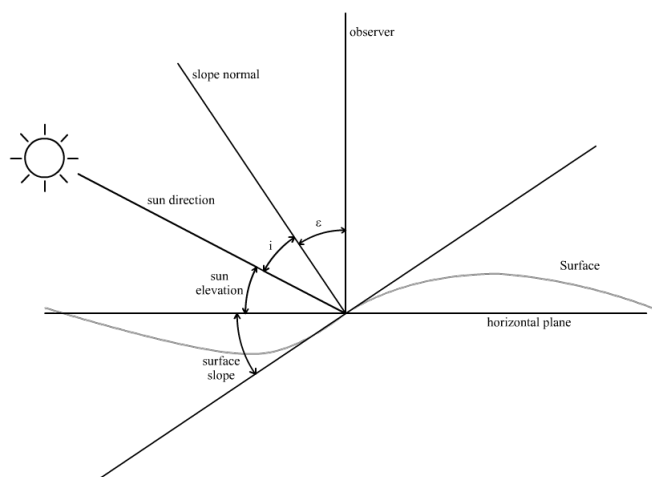


Fig. 2.6. Hillshading concept and angles (Batson *et al.*, 1975)

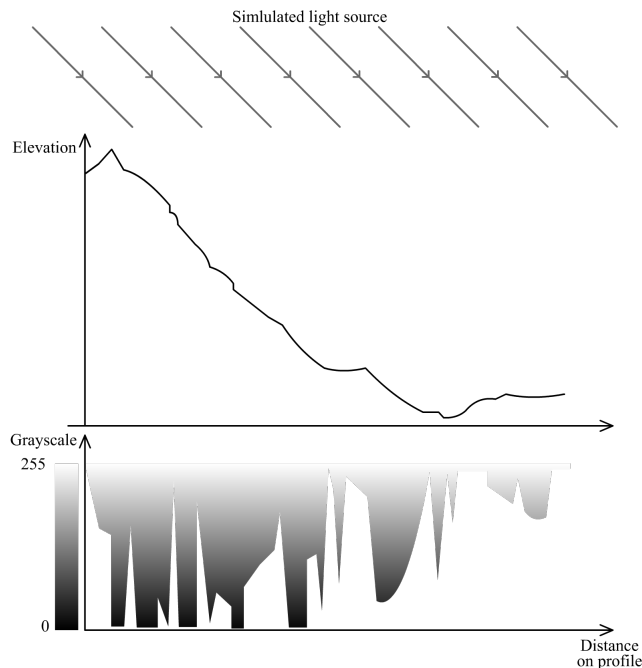


Fig. 2.7. Hillshading example on a DEM profile, the grayscale intensity is computed using the slope and aspect of each pixel and incidence angle and azimuth of the lightening source.

Remarks concerning relief shading

A lot of techniques and methods were developed for digital relief shading. For a review refer to the relief shading website⁵.

Regarding the above mentioned azimuth, we have to introduce “terrain inversion”. Shading is a so-called psychological cue in depth perception (Toutin, 1998), thus it is essentially a cue which is acquired with experience and learning. Consequently, we see a hill because we have learned that this kind of illumination shows a hill. As Imhof (2007) stated “*Many map users are so completely conditioned to a light source from above left that they subconsciously expect this direction of lighting ... The result is the inversion of the positive impression of shape to a negative one.*” In relief shading this issue has always been problematic (Rudnicki, 2000) and there is no proper solution at the present for the definition of an optimal azimuth angle. As most people expect an azimuth of 315° and this angle is mostly set to this value there is no major issue. Problems however appear if people are not aware of this angle or if the azimuth is set to another value. Then, terrain inversion might become a major concern when analysing the geomorphological features of a DEM. In this study, all the maps and images will always be oriented to the north and illuminated with a 315° azimuth.

⁵ <http://reliefshading.com>, accessed 13 October 2009

2.3.2 Contour lines

Contour lines interpolated from a DEM are often used to give elevation information for a visual analysis of the shaded DEM. The shaded relief gives a terrain overview. No information about elevation is given, nor contained in it, hence its combination with contour lines. They are iso-elevation lines, which are most of the time interpolated over the grid using linear or spline interpolation (De Smith *et al.*, 2008).

As we have seen at the beginning of this chapter, historically, geomorphologists and geographers often use contours for their analysis. It is their way to look at continuous value in a discrete way. As Lane *et al.* (1998) mentioned, they represent a discrete view of the continuous grid, thus an easier interpretation of terrain structures and forms. However, there is a loss of accuracy, and, subsequently to the chosen contour interval, features may not be illustrated by them (see figure 2.8 for an example). An analysis using only contour lines is almost impossible, because there is a complete lost of context. Therefore, often contour lines are overlaid to another media (cartographic map, aerial photography or DEM) in order to reveal the context.

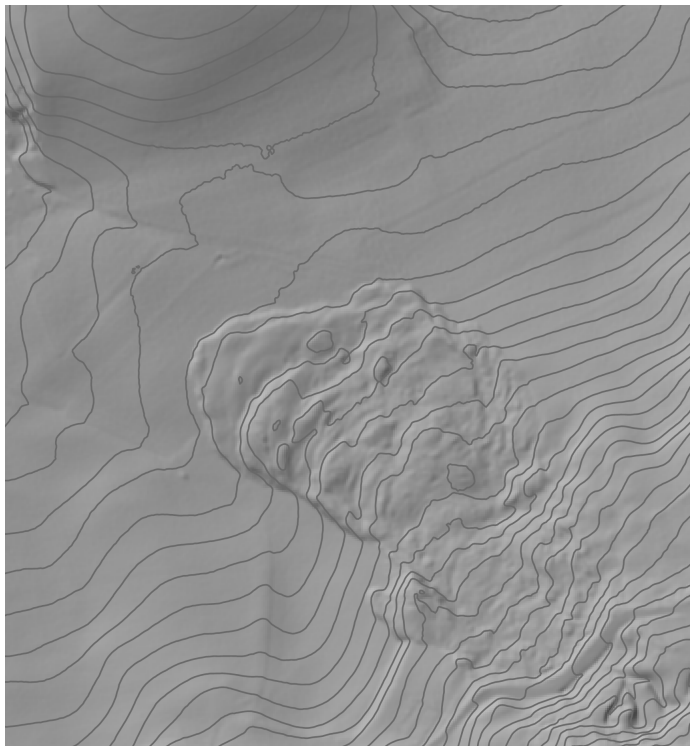


Fig. 2.8. Contours (elevation interval: 2m) overlaid to a 1 m resolution DEM, DEM©SITN

2.3.3 3D

Visualisation of elevation data became one of the main purpose of DEM acquisition due to the rise of free 3D viewers⁶. But for many years (Weibel, 1989a; Burrough and McDonnell, 1998), visualisation has been a tool for draping spatial analysis results on a 3D (or 2.5D) surface. Currently, most GIS software have a 3D module in order to make such representations. Thus computation of new data is made in 2D and its representation in 3D, but this kind of representation, as Buckley *et al.* (2004) pointed out, is mainly an “impressive analytical perspective view”. Analytical perspective enables to reconstruct the vision we have of topography when we look at our world. Thus through the 3D representation, the viewer has more cognitive faculties for the recognition of topographical elements than in 2D. This only because 3D representations tend to the natural representation human cognition is used to, when looking at natural (or landscape) phenomenon (e.g. see figure 2.9).

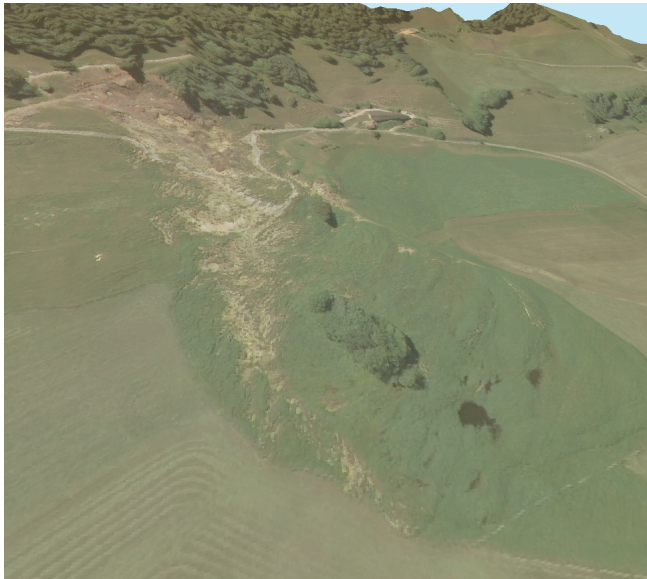


Fig. 2.9. 3D visualisation of a landslide, DEM and aerial photography©SITN

Ware (2004) suggested some remarks concerning 3D versus 2D (not exhaustive):

- 3D environments are more difficult to create than 2D environments with similar capabilities.
- 3D is (self-evidently) richer than 2D.
- 3D adds far less visual information than it might be supposed.
- 3D must only be used if there are sufficiently more subtasks which might be achieved regarding 2D.

⁶ e.g. Google Earth (<http://earth.google.com/>, accessed 18 May 2009) or Virtual Earth (<http://www.microsoft.com/virtualearth/>, accessed 18 May 2009)

Consequently the type of representation (2D or 3D) clearly depends on the needs and tasks (Ware, 2001). The 3D representation is not obvious to use and, in DEM analysis, 3D does not bring any benefit in quantitative computation. As Ware (2001) stated, it takes people a longer time to generate a mental map of such space than as for a 2D representation. Moreover, it is actually difficult to get a good overview of a type of topography. 3D rendering often reduces the level of detail of the model, thus a smoothing effect. In addition, the computation of indicators is still done on the matrix. The results can potentially be draped on the 3D model, but the overview will not be improved. It is currently easier to perform morphological analysis in 2D. Therefore we will not explore 3D representations any further.

2.4 Geomorphometric indicators

Geomorphometry, as used in almost all GIS software, was defined conceptually by Evans (1972). A few years later, Evans (1979) went from a conceptual definition to a mathematical description using quadratic surfaces (see section 2.4.1). He gave the next definition of general geomorphometry:

Definition 2.4.1 (Evans (1972)). *General geomorphometry as a whole provides a basis for the quantitative comparison even of qualitatively different landscapes, and it can adapt methods of surface analysis used outside geomorphology.*

Since Evans (1979) attempt to mathematically describe surface indicators, many authors have given their own equations, modifying the mathematical definition of the quadratic surface, for e.g. Zevenbergen and Thorne (1987); Shary (1995). Others (Skidmore, 1989; Burrough and McDonnell, 1998; Schmidt *et al.*, 2003) made a comparison between the different methods and techniques. The result showed that all methods give similar results and that the differences are not significant for visual interpretation.

Moore *et al.* (1991) and Pike (2002) made a review of the indicators which can be computed using DEM for quantitative geomorphological analysis, thus geomorphometry. Applications (Wilson and Gallant, 2000; Bishop and Shroder Jr, 2004) showed that geomorphometry is the geometrical indicator of geomorphological analysis. However this one depends on the DEM and its resolution. For example, slopes computed on a 90 m or a 1 m resolution DEM do not give the same geomorphological information. So far, few authors have given a solution for this complex problem.

2.4.1 Quadratic surface and derivatives

Only Evans (1979) solution is developed. Most other solutions are elaborated through modifications of the quadratic equation (Zevenbergen and Thorne, 1987; Schmidt *et al.*, 2003). A real surface can be approached by a quadratic surface.

$$f(x, y) = z = b_0 \cdot x^2 + b_1 \cdot y^2 + b_2 \cdot xy + b_3 \cdot x + b_4 \cdot y + b_5 \quad (2.4)$$

By convoluting each DEM pixel with a convolution window of size 3×3 , it is possible to adjust a local quadratic surface for each pixel of this DEM. The quadratic equation is composed of six unknowns, which are described as the equation parameters. Using a 3×3 window, we have nine observations, which is enough to solve the equation. Depending on the authors, the equation may slightly be modified, changing the type of equation or the number of observations taken into account to solve the equation using least squares. Some authors take only the four cardinal pixels (north, south, east and west) and the central pixel into account for computation. This can be seen as a solution without over-determination. Evans (1979) gave a solution computed by using Lagrange's polynomial solution to approach the parameters. These ones are a combination of the variables (the pixels in the convolution window).

Using the previous definition of a quadratic surface (equation 2.4), the partial derivatives can be defined. As the equation is of second degree, we can compute first and second derivatives.

First derivative.

The first partial derivative of the quadratic surface results in the magnitude (slope) and polar angle (aspect) of central pixel z :

$$slope = g \left(\frac{\partial f}{\partial x}; \frac{\partial f}{\partial y} \right) = \frac{\partial f}{\partial xy} = \sqrt{\left(\frac{\partial f}{\partial x} \right)^2 + \left(\frac{\partial f}{\partial y} \right)^2} \quad (2.5)$$

$$aspect = h \left(\frac{\partial f}{\partial x}; \frac{\partial f}{\partial y} \right) = \arctan \left(\frac{\partial f}{\partial y} / \frac{\partial f}{\partial x} \right) \quad (2.6)$$

Second derivative.

The second derivative of a quadratic surface gives the curvature of the surface. However, we have to evaluate curvature for given points and in the desired directions of interest. In fact, curvatures in directions x and y (north-south and east-west axis) are not relevant, but they should be oriented preferably in the direction of the maximum slope gradient (in *profile*) and in the orthogonal direction of this gradient (in *plan*).

Profile curvature (PRC) is the given curvature along the slope gradient where the gravitational effects are maximised (Wilson and Gallant, 2000). A vector \mathbf{s} has to be defined to represent the slope magnitude in the centre of the quadratic approximation (the pixel where we want to compute the curvature).

$$PRC = \frac{d^2 z}{ds^2} = g \left(\frac{\partial^2 f}{\partial x^2}; \frac{\partial^2 f}{\partial y^2} \right) \quad (2.7)$$

To define the plan curvature (PLC), we have first to define a vector \mathbf{s}_\perp orthogonal to \mathbf{s} and which has the same magnitude.

$$PLC = \frac{d^2 z}{ds_\perp^2} = h \left(\frac{\partial^2 f}{\partial x^2}; \frac{\partial^2 f}{\partial y^2} \right) \quad (2.8)$$

Curvatures have the following meaning:

- Profile curvature measures the rate of change of the slope gradient and is important for flow speed changes and sediment transport processes.
- Plan curvature measures topographic convergence and divergence. It shows the convergence probability of water flow on a surface.

Convention is defined as positive values (case *PLC I* and *PRC I* in figure 2.10) for convex values and negative for concave values (case *PLC II* and *PRC II* in figure 2.10).

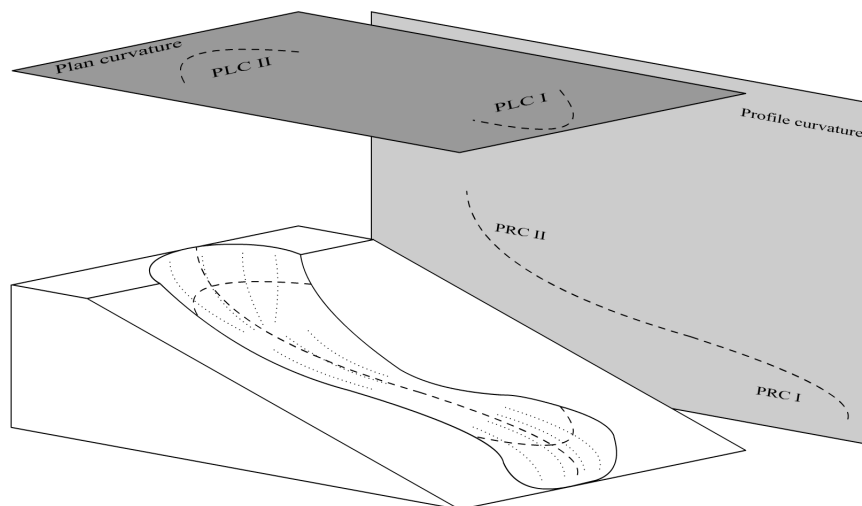


Fig. 2.10. Illustration of plan (PLC) and profile (PRC) curvatures on the horizontal and vertical planes

Using these two definitions of curvature, several other types of curvature evolve, such as tangential curvature (multiplication of PLC and the sine of slope) or total curvature (Wilson and Gallant, 2000). Each of these curvatures has specific issues and application domains. As example (Wilson and Gallant, 2000), tangential curvature was developed to study flow convergence and divergence. Refer to Schmidt *et al.* (2003) for a complete review of all curvature indicators and the explanation of their meaning.

Multiscale version of derivatives.

Wood (1996) proposed a multiscale version of the first and second derivatives of the quadratic surface. It consists to take into account a larger neighbourhood than the proposed 3×3 window. Thus, the redundancy of the equation system increases and the solution is given by normal equations. Wood (1996) used also weighted least squares to give more importance to pixels nearer to the central pixel by introducing a distance decay on the weights. Consequently, by increasing the size of the convolution window, the computation of the local indicators is extended to more general features of the DEM. Fisher *et al.* (2004) used these developments to define the spatial extend of mountains. They illustrated the concept of Wood (1996) by showing that the considered window size had a great impact on the values of the indicators.

2.4.2 Hydrological indicators

Hydrological indicators are indicators of water behaviour on a surface (or DEM). There is a multitude of them (flow direction, catchment area, flow width, wetness index, watershed, LS-factor and more). Some are strongly

correlated with others, others may bring new structural information to DEM quantitative analysis. In our case, interest is given to the wetness index (WI). Beven and Kirkby (1979) gave the first definition for this index in the development of their hydrological conceptual model *TOPMODEL*. Many authors improved this definition, which are compared by Sorensen *et al.* (2006). Inasmuch we are not interested in the absolute value of the wetness index (see section 6.3), but rather more in the relation between it and other morphometric indicators. Thus, we will use the basic wetness index of Beven and Kirkby (1979).

$$WI = \ln \left(\frac{A_s}{\tan \beta} \right) \quad (2.9)$$

where:

- A_s : specific catchment area, defines which quantity of upslope flow runs through each pixel of the DEM.
- β : slope (see section 2.4.1).

The WI is used to characterize the soil wetness potential (or soil moisture). In topography, thus by computing it using a DEM, it “quantifies the role of topography for redistributing water in the landscape” (Reuter and Nelson, 2009). Indeed, it shows which pixels will be subjected to what surface water pressure and flow.

2.4.3 Other geomorphometric indicators

There are many indicators which were developed in surface analysis. We chose to develop only those used in this study. Many recent techniques apply geomorphometric indicators for the computation of surface specific parameters. Wilson and Gallant (2000) developed and explained indicators, like sun lightening indicators, for Earth sciences. Li *et al.* (2005) developed some textural indicators (roughness). This one is part of textural image analysis (Parker, 1997). Thus, a lot of image analysis processes may be applied to surface analysis. Conceptually, a grid surface is an non-normalised image, the only difference is that the pixels values are not bounded by the usual interval $[0, 255]$.

Another surface tool is the analysis of networks. Rana (2004); Schneider (2003) and Wood (2000) developed a multiscale approach for the analysis of surface networks. The conceptual ideas are taken from purely geometric properties of a mathematical surface (Pfaltz, 1976). This latter gave a solution to determine specific surface points (pits, peaks and passes) and the connective network of those points.

Frequency analysis using Fourier transforms are another type of geomorphometric analysis. In DEM spectral analysis, Pike and Rozema (1975) were the first to give a hint about the frequency composition of surfaces, but natural features are non-stationary from a frequency point of view, thus a link to fractal theory may be more appropriate. The idea of fractal theory is that “*there exists a hierarchy of ever-finer detail in the real world*” (Russ, 1994). Looking to all the concepts and theories which were described in this chapter, there might be a link between the perception of DEMs structural information and fractals. Some of the fractal concepts developed by Russ (1994) will be applied further in this study in order to point out local self-similarity in

DEMs and to specify how neighbouring values evolve in our models through the scale intervals we will define. However, we will not explore the fractal dimensions of DEMs any further, but chapter 4 will explore more thoroughly the spectral properties of DEMs.

2.4.4 Geomorphometric patterns

As seen in the previous sections, geomorphometry can produce a lot of indicators and derived variables. Geomorphologists often want to reduce this multidimensional space into a single component and to characterize territorial zones defined by classes. This process is called classification of surface landforms using geomorphometric parameters. However, there are many possibilities for the classification of geomorphometric information. A non-exhaustive list is made hereunder. The first technique is specific to geomorphometry and the others were adapted from classification of multidimensional data:

- Subjective conceptual classification: As example, using Dikau’s curvature classification (using the profile and plan curvature), it is possible to define nine types of terrain which are combinations and thresholding of plan and profile curvatures (see figure 2.11) (Dikau, 1994, 1989). Some recent developments showed that using object-oriented classification, it was possible to obtain a good partition into patterns using this type of curvature discretization (Dragut and Blaschke, 2006). There are many other ways to classify geomorphometric information, for example by using the swiss soil classification scheme (BGS, 2002) or a specific partition of topographical properties like what Hammond (1964) did. But, one has to retain that these types of classifications impose to define multiple thresholds for each used information.
- Unsupervised multidimensional classification: the aim is to define the best hyperplanes in all the dimensions of the used data. Thus, there are many possibilities for the separation of hyperplanes in multi-dimensional spaces. The main problem is to build the multi-dimensional space using the appropriated variables, which is decisive in the classification quality.

These two schemes for the definition of geomorphometric patterns are different. In the first one, thresholds have to be applied, thus a partition of the data into intervals which results in a specific property of the terrain, like Dikau’s scheme (figure 2.11). The second techniques are less constrained by thresholds, but the results strongly differ from a region to another. It is not possible to normalise the approach, because of topographical variations, and thus variations on the values and intervals defined by the derived geomorphometric information. The hard clustered patterns are only dependent on the features that the DEM represents and on the convergence threshold as we will see hereunder.

MacMillan and Shary (2009) gave some remarks concerning pattern detection using DEMs. We retained the most interesting ones for our study, respectively remarks 3, 6, 7, 8 and 9:

- *Remark 3*: classification of landforms are commonly specific to a particular scale or narrow range of scales.
- *Remark 6*: landform elements can be extracted automatically by using land-surface parameters such as slope, curvatures, catchment area, distance to streams, peaks and depression depth.

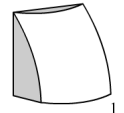
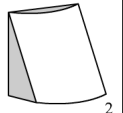
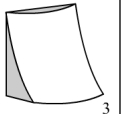
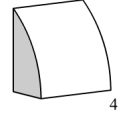
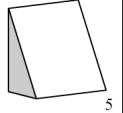
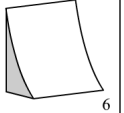
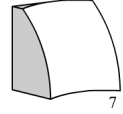
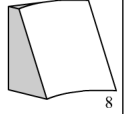
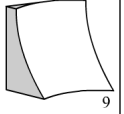
		Profile curvature		
		Convex	Flat in profile	Concave
Plan curvature	Convex	 1	 2	 3
	Flat in plan	 4	 5	 6
	Concave	 7	 8	 9

Fig. 2.11. Dikau's curvature classification scheme

- *Remark 7:* a geometric signature is a set of measures that describes topographic form well enough to distinguish among geomorphological disparate landscapes.
- *Remark 8:* it is not possible to select any single fixed dimension for a moving window that will perfectly capture the wavelength of all landform features of interest in any given area.
- *Remark 9:* extraction of landform types and elements from DEMs commonly consist of: (a) preparation of the legend, (b) preparation of the land surface parametrizations (LSPs) (inputs), (c) creation of the rules, (d) extraction of landforms and (e) assessment of accuracy.

These remarks show some important properties about multiscale DEMs and their underlying geomorphometric indicators. The first, phenomena inherent, is that a particular scale will only inform about forms related to it (remark 3). Thus its geomorphometric indicators will also be strongly scale-dependent and only frequency information described in the specific scale will be retrieved (remarks 6 to 8). This scale issue is developed in the next chapters, and a multiscale classification is performed in section 6.3.

3. Scale and scaling process

Since spatial data and spatial operations using numerical data appeared, researcher and engineers have been confronted to scale issues. Using raster data for example, Gallant and Hutchinson (1996) stated that topographical analysis results are sensitive to the resolution of the generalised source. Also, Quattrochi and Goodchild (1997) analysed how to manage scale issues in remote sensing. They tried to give solutions to relate remote sensing data and data obtained from geographical information science (GISc) methods using vector data. Besides, in order to analyse scale effects on vector data, Openshaw (1984) gave solutions to deal with aggregation problems on vector data.

Scale is a central concept not only in the geographical description of our world but also in modelling environmental patterns and processes. Indeed, every environmental phenomenon can be described partially at a specific scale. More precisely, a single feature¹ is scale specific, but the phenomena, to which the feature belongs, is a combination of different features that are described by different scales. Thus a natural (or environmental) phenomenon is always composed of multiscale processes. Even local phenomena are described by a multiscale combination of features. Multiple authors have treated territorial scale effects so far.

So, if any geographical information refers to a specific analysis scale, every environmental data acquisition is correlated to its environmental and territorial scale. Some space-scale effects are illustrated in figure 3.1, but none of them is scale specific. Scale is not a discrete variable, neither in GISc nor for environmental phenomena. However, there is no other way to characterize continuous scale than to interpret phenomena by data discretization.

3.1 Scale

Scale is not only a scientific generalisation or specialisation concept. Indeed, all phenomena, which have an impact on our environment, are scale dependent. If a lot of researches were carried out concerning scale, one of the most complete was written by Marceau (1999), in which she gave the following general definition for scale:

¹ In this study, the term “feature” is used as a specific topographical structure located at a particular place in the sense of the definition of the dictionary of the Oxford University Press: something important, interesting or typical of a place or thing. - http://www.oup.com/oald-bin/web_getald7index1a.pl, accessed 22 October 2009. Thus it represents a discrete piece of landform in this study.

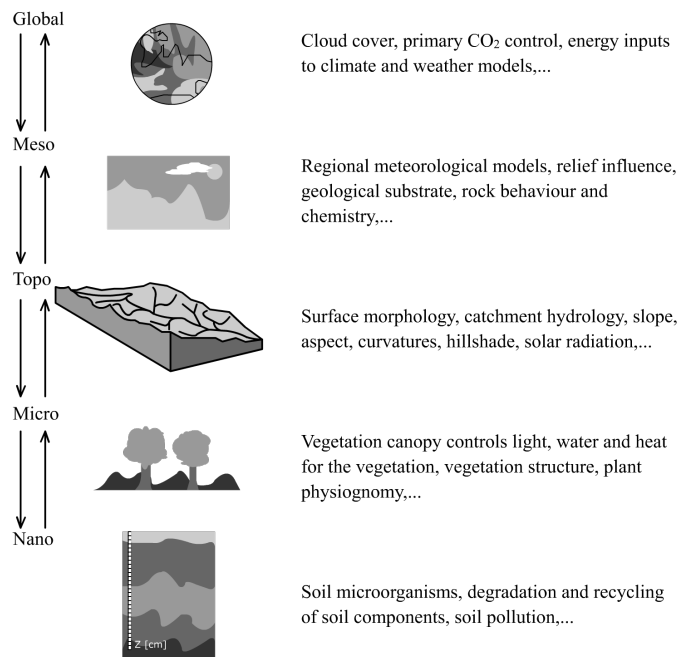


Fig. 3.1. Scale dependencies, multiresolution, adapted from Wilson and Gallant (2000), page 2.

Definition 3.1.1 (D. J. Marceau 1999). *Scale refers to the spatial dimensions at which entities, patterns, and processes can be observed and characterized. Scale is recognized as a central concept in the description of the hierarchical organisation of the world.*

So, scale is a continuum: entities, forms and even processes are continuous in scale; the interpretation we make using these different elements, however, is not.

If scale is described by discrete intervals defining scale of “interest”, then an underlying scale threshold is applied (figure 3.1). Between these intervals, a continuum of entities, features and processes can be observed and joined together (Marceau, 1999). These intervals are related to specific organisational levels in the scale hierarchy of natural features and processes. They are defined by the elements one wants to analyse or describe.

With our cognitive capabilities, we can only find interest in a limited number of phenomena on which we then apply methodologies in order to understand them. Moreover, computer analysis and processing needs discrete scale steps. Hence, there is a need to have discrete systems, which are consistent mathematically, but also which, through scientific methods, make sense. Creating scale levels (or intervals) is the most common action amongst the scientific community in order to reveal natural phenomena.

3.1.1 Scale specifications in geography

There are many references for scale definition in geography. Two major trends can be distinguished (Marceau and Hay, 1999): relative/absolute

scales, and what we will call functional scale definitions. The former, defined by Meentemeyer (1989), is clearly more conceptual than the functional one defined by Marceau. There is a clear difference between these trends. We will review them in the next two sections and from a mathematical perspective, as this is relevant to our study.

Absolute and relative scales.

Absolute scale is related to the Euclidean space. The localisation of elements is given in a regular coordinate system, which defines the scale of those elements. In conventional geography and cartography, this definition is often widely used, enabling the representation and localisation of spatial data. In this case, scale is only defined by the frame of the coordinate system. Therefore, the smallest element which can be taken into account cannot be smaller than the grid definition itself. Hence absolute scale is associated with representation and localisation of elements, but not with interaction or process between them. In spatial image analysis, this definition is slightly different, as shown in section 3.2.

Besides this absolute scale, Marceau and Hay (1999) stated that, in relative space, scale becomes an intrinsic variable related to spatial entities, forms, function and processes. From a geomorphological perspective, it is this scale which enables the characterization of processes and phenomena. The definition of relative scale is thus complementary to absolute scale. Space is defined by the spatial elements and processes taken into consideration, such as the relations inherent to their association. This space, defining relative scale, is not a Euclidean space, as even distances are relative. What's more, it is impossible to make a projected map out of the relative space. However this space characterizes the interactions of features at different scales. As for example, the interaction between local faults in a slope and stability of this same slope, i.e. a multiscale relation between features.

Functional scales.

The above definitions lead us to define functional scales in order to understand the interactions between absolute and relative scales, since it is impossible to conceptualize processes inherent to geomorphological phenomena by focusing only on the absolute or relative scale. Cao and Lam (1997) gave four types of scale definition: cartographic, geographical, operational and measure scales. Pointet (2007) preferred to group them in three distinct scales used in geographical sciences and spatial analysis. These three types of functional scales are relevant from a geographical and geomorphological point of view and they are:

- Cartographic scale: represents the ratio of a distance on a map to the corresponding distance in reality (Marceau (1999) and references therein). This scale is strongly related to absolute scale as it is a representation of territorial features in a certain coordinate system.
- Observation scale: represents the scale at which measures and data acquisition are undertaken (Pointet, 2007). It refers to the resolution of measures. In remote sensing, this would be the considered surface taken into account by the measure of reflection.
- Operating scale: refers to the scale at which processes occur. There is a strong relation to the phenomenon, according to Cao and Lam (1997): “*A phenomenon observed at one scale may not exist at another scale*”. This

links operating scale to the scale at which a phenomenon was observed and it is represented by figure 3.1.

The interpretation and analysis of geomorphological phenomena are strongly dependent on the observation scale (Pointet, 2007). The adequacy between observation scale and representation is carried out through data scaling, based on the hypothesis that the observation scale is not consistent with the chosen representation level(s). The interpretation and analysis of geomorphological phenomena is a confrontation between observation and operating scale. It is always a subtle interplay of functional scales, on the one hand for the interpretation and analysis of geomorphological phenomena and on the other hand for the representation of results.

3.1.2 Geographical information processes and scale

Any process or model of the territory needs geographical information (GI). It is made of many conceptual data models, depending on the user's needs and goals (Goodchild, 1992). For instance, a process in GI is a spatial problem solved using a spatial method applied to a dataset. If we look at the geometric definition of data or measure, each type (e.g aerial photography, terrain measures, land registry, geological surveys) has been acquired at a defined scale and in a certain manner. As seen in the previous section (3.1.1), scale has many definitions. From a GI point of view, it is strongly dependent on the nature of data and on its level of detail, thus GI processes are scale dependent.

In geographical information systems (GIS), two main types of data can be considered: vector and raster data. They are used to represent most GIS processes. Thus scale and processes issues on these data will have an effect in cartography too. In the next two sections, we will analyse scale effects on these two kinds of data from a geometrical and mathematical point of view.

Vector data.

Vector data is one of the main components in GIS methods, and can be made of points, polylines or polygons. A lot of spatial geometrical operation were developed using this kind of data. As far as space, scale and geometry are concerned, a compromise is made for the description of a geographical feature. It means that the resolution (or the scale definition) of vector objects² is always linked to what they describe. For instance, the length of a boundary is highly dependent on the resolution (thus the operating scale) of a vector object. A boundary (of a district or a country) will not have the same length regarding a vector object when representing it at two different scales (figure 3.2).

Couclelis (1992) stated that *“it is only at some phenomenon-specific but generally ill-defined scale that points, lines and polygons become reasonable approximations, if at all”*. This shows the difficulty to apprehend scale for vector data. Often GISc specialists prefer having too precise data in order to have smooth data on their screen. The problem is however not to have smooth data, the problem is computational, because visual noise and redundancy has to be avoided.

² The term “object” is used in this study as a representation on a map of a feature of interest.

A line object is always defined by nodes in GIS. Measuring a line is highly scale dependent (or dependent on the resolution, thus the distance, between nodes). If we take a detailed scale object (object (a) in figure 3.2), we will be able to measure a certain distance. If conceptually we take the same object at a coarser scale or resolution (object (b) in figure 3.2), we will get another distance, which will be lower than the first one only because of the resolution. The same could be shown measuring the area of a polygon.

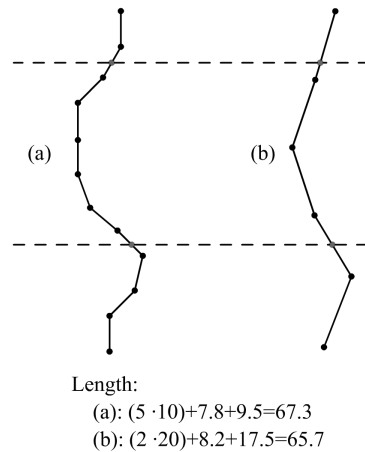


Fig. 3.2. Distance measured (between the dashed lines) using a detailed scale object (a) and a coarser scale object (b). Results show that the higher the resolution is, the more complex a path (a) will be. Its measure will be longer than for a less complex path (b).

To sum up, there is never an absolute measured distance. An object is always scale-dependent and so are GISc processes. The first reaction would be to increase the resolution. Conceptually this would increase the number of nodes toward the infinite and the measured distance too, which is impossible. This shows that there is always a choice of scale to make and how crucial this choice can be regarding GI processes. Sadly, most GIS users make this choice unconsciously, just using data at the scale they acquired it or received it.

Raster data.

Raster data scale is limited by the spatial resolution of the pixel matrix (see section 3.2 for the definition of spatial resolution). GIS use raster data for background purposes, sampling of land cover and land use, raster pattern classification, and representation of all variables which are spaced regularly, may they be continuous or not. As a matter of fact, pixel resolution has a great impact on what can be done with these products. As examples, figures 3.3 and 3.4 illustrate the Geneva lake region using two different products: satellite imagery (Landsat ETM+) and aerial imagery. GIS processes or territorial image processing, through this effective scale difference, will not be the same for these two pictures. Thus, resolution has a great impact on what can be done. But what follows will explore this more thoroughly.

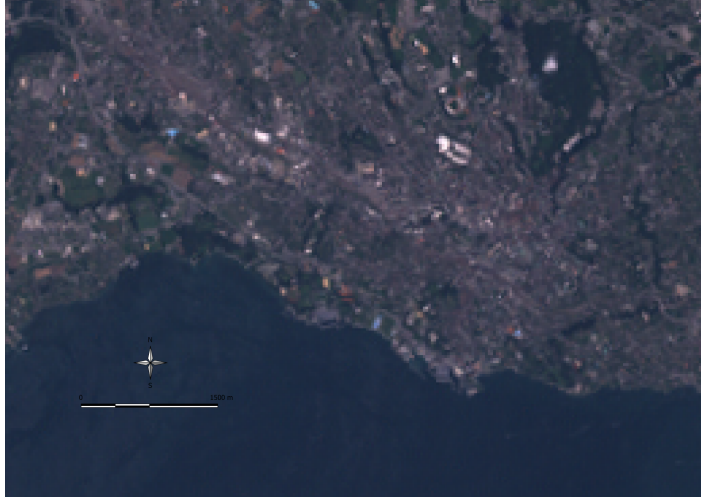


Fig. 3.3. True color Landsat ETM+ image of Lausanne, resolution 30 *m*

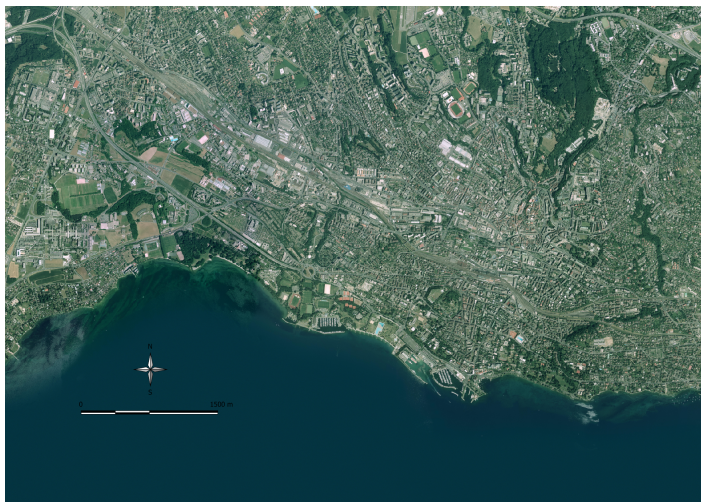


Fig. 3.4. True color aerial image of Lausanne, resolution 0.5 *m*, aerial photography ©swisstopo

3.2 Spatial resolution

Spatial resolution (see definition 3.2.1), similarly to scale, is defined in many ways. For image analysts, it may be the sampling rate of a numerical instrument. For ecologists, it is the grain of their patterns. Finally, for GISc specialists working on vector data, spatial resolution is linked to the geometry of an object, i.e. the shape size for a polygon, the line length or the distance between two adjacent points (Bian, 1997). For raster data (like gridded elevation models or spatial imagery), it is linked to observation scale (Woodcock and Strahler, 1987; Tobler, 1987). Resolution characterizes the separability of two features and is thereby the dimension at which features can be distinguished. Marceau (1999) showed that modifying spatial resolution affects the precision of classification, hence the strong relation between resolution and classification. Due to the analytical sensibility of the spatial unit's definition used to collect data, this case is linked to the modifiable areal unit problem³ (MAUP). Many others studies (Cao and Lam, 1997; Wong, 2009) showed that applying the same spatial analysis method to raster data set at different resolutions gives different results. Thus there is an actual relation between environment and spatial resolution, suggesting some spatial structure. Tobler (1987) has already suggested this in his definition of spatial resolution:

Definition 3.2.1 (Tobler, W. 1987). *Spatial resolution is defined as the content of the geometric domain of observation divided by the number of observations, all raised to the power one over the spatial dimension. The size of the smallest detectable feature is twice that of the resolution. The usefulness of a Geographic Information System is constrained by its spatial resolution. Systems with the same resolution can be compared.*

In remote sensing, spatial resolution defines the highest operational scale which can be reached, creating interdependence between scale and resolution. Grain is the smallest distinction that is made of ground elements. It often depends on the imagery optical system or on the density of the measured laser ground points (see section 2.1). Amongst the scientific imagery community, it is generally admitted that a point feature has to cover at least two pixels to have a chance to be detected by visual analysis or image processing. We prefer to raise this number of pixels to three. Tobler (1987) gave an interesting conversion table (table 3.1) of the relation between cartographic scale, resolution and feature detection. In addition, he defined the resolution in relation to the domain (or spatial extend) and the number of observations:

$$\text{Average Spatial Resolution} = \left(\frac{\text{Domain}}{\text{Number of observations}} \right)^{1/\text{Dimension}} \quad (3.1)$$

³ Openshaw and Abrahart (2000) defined the modifiable areal unit problem (MAUP) as the sensitivity of analytical results in relation to the definition of the spatial units. Spatial units can be seen as the smallest unity which can be identified in a dataset. Openshaw (1984) suggested that “*Spatial aggregation is necessary in order to create a relevant data set*”, thus to unveil areas relevant to some considered phenomenon. From a mathematical perspective and regarding Openshaw (1984), the MAUP is defined as a combination of two problems: the scale problem (scale of interest) and the aggregation problem (manner of aggregating data).

The *Domain* is the area covered by an interest zone whereas the *Dimension* is the spatial dimension (2D or 3D) in which the analysis is made.

Weibel (1989b) used this definition to explain the implication of resolution in DEM analysis. He expressed this in visualisation and computational issues, too. The latter illustrates that if products computed from different spatial resolution layers are overlaid in GIS, scaling problems will rapidly appear (e.g. overlaying 1 *m* resolution computed slopes to a 30 *m* resolution Landsat satellite image).

Cartographic scale	Resolution	Detection
1 : 2 000	1 <i>m</i>	2 <i>m</i>
1 : 10 000	5 <i>m</i>	10 <i>m</i>
1 : 50 000	25 <i>m</i>	50 <i>m</i>
1 : 100 000	50 <i>m</i>	100 <i>m</i>
1 : 1 000 000	500 <i>m</i>	1000 <i>m</i>

Table 3.1. Tobler’s relation table between cartographic scale, resolution and detection (Tobler, 1987)

Regarding raster data, a limitation to the above explanations appears by taking into account the context. The recognition and identification of a spatial feature which has an imprint on a media can be made even if it does not respect the given limitation. Indeed, regarding the geometric context, a feature can still be identified, and this, even if it is smaller than the resolution, but its localisation cannot be better than the resolution. As example, if we look at a highway - a linear feature - in a Landsat image (figure 3.5), the luminance of the pixel will vary compared to neighbouring pixels and the highway recognized, but its localisation cannot exceed the resolution.

Woodcock and Strahler (1987) put forward methodologies to avoid effects due to raster scale (or resolution), which we have slightly modified:

- If the resolution is a lot finer than the feature of interest, pixel value measures (of the feature) will be strongly correlated with their neighbouring pixels. The local variance will be small.
- If the resolution is equal to the feature of interest, neighbouring equivalence will diminish and local variance increase.

These two points illustrate how hard it is to evaluate which resolution should be used, regarding what has to be achieved with raster data. These assertions are deduced from Tobler’s first law of geography (Tobler, 1970): “*Everything is related to everything else, but near things are more related than distant things*”.

As seen, these principles are well defined in the binary case and classified data. However, the definitions become less obvious and much less stable when applied on continuous data which represents geomorphological features. Moreover, if we take the phenomenological perspective of nature, the imprint

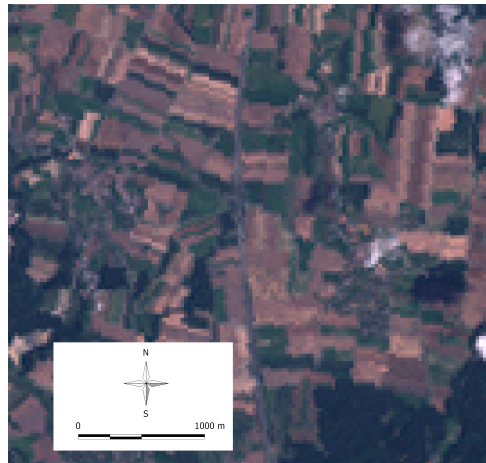


Fig. 3.5. Highway (width ~ 25 m) in a true colour Landsat ETM+ image ($r = 30$ m). The highway is located in the middle of the image and goes from the south to the north.

of related features will have a fuzzy definition. Indeed, it seems that the measure and representation are defined in terms of scale, but presently almost no evidence brings us back to the phenomenon.

3.3 Scaling

Jelinski and Wu (1996) showed that scale and aggregation affect the adjustment of a model and the estimation of its parameters. Generalisation of spatial data is therefore limited by the lack of rules and methods dealing with multiscale spatial phenomena (Ratcliffe and McCullagh, 1999). Therefore, scale continuum implies discretization in some units which are relevant of a process or phenomenon. We will now analyse more thoroughly scaling processes of spatial data and their impacts on multiscale geomorphological phenomena.

The number of variables needed for modelling and spatial analysis is changing through scale (Meentemeyer and Box, 1987). Scale modifies the structures of a model because the number of variables is generally reduced by decreasing scale. Thus, scaling is not a linear process and is defined as a data transfer from one scale to another. This can be done using several techniques and methods, but it always results in a modification of the structural geometry of the data. Scaling process involves taking information or data at one scale and using it to derive processes at other scales (Jarvis, 1995); it is a transition concept which links processes through the different scale intervals.

Spatial data is scale dependent and heterogeneous. It follows that spatial data is autocorrelated and non-stationary. In addition, it might be irregularly spaced and discontinuous. Meentemeyer and Box (1987) concluded that spatial data does not follow any rule for parametric statistical analysis. This affirmation contradicts most of the theoretical background used for spatial analysis. Jarvis (1995) stated that scaling was non-linear and heterogeneous. Regarding the properties of spatial data and scaling issues, it is difficult to

define or propose a single method or technique for scaling geographical data. There is a strong dependence to the thematic property of the data and its spatial context.

Besides, two types of scaling can be defined: downscaling and upscaling. Raffy (1992) showed that there is a clear difference between them. The potentials of methods and relations in scale discretization processes are not equal subsequently to the specialisation (upscaling) or generalisation (downscaling) of the data (Golay, 1992):

- Upscaling: taking information at broader scales to derive processes at finer scales; this can be seen as a specialisation or decomposition process. Using raster data, this means to “invent” or bring in some new data.
- Downscaling: decomposing information at one scale into its constituents at broader scale; this can be made explicit as a generalisation or aggregation process. When generalising, some details are lost. Meentemeyer and Box (1987) showed that some interactions were invisible at detailed scale. Therefore, new proprieties might appear because of a better synergy between phenomena at a broader scale.

In this study, we will only look at geometrical scaling processes and not at scaling processes using thematic properties or attributes. The following definitions will be used to specify scaling processes (figure 3.6):

- Scale: general description of scaling process
 - Generalisation: general term to describe the transition from fine scale to broad scale.
 - Specialisation: general term to describe the transition from broad scale to fine scale.
- Raster data:
 - Downscaling: downscaling data is done by spatial aggregation of pixel values using an appropriate method.
 - Upscaling: like downscaling, upscaling is done by interpolation or spatial aggregation of pixel values using an appropriate technique. But upscaling does not bring any supplementary information, it is only redundancy regarding the original data.
- Vector data:
 - Simplification: vector data generalisation, e.g. simplification by suppressing vector nodes defining this data. Several techniques exist (such as Douglas & Peucker’s line simplification algorithm) and applied in GIS software.
 - Segmentation: this operation only injects new nodes to an existing line or areal feature using some relevant method, no precision is therefore made or created.

As the present study is based on raster data generalisation, the next sections develop scale and scaling processes on this specific type of data.

3.3.1 Scaling process in raster data

Raster data is usually a regular matrix or a group of pixels defined by:

$$\{f(m, n)\}, m = 0, 1, \dots, M - 1, n = 0, 1, \dots, N - 1, (m, n) \in \mathbb{Z}^2 \quad (3.2)$$

where M is the number of columns of the data and N the number of lines.

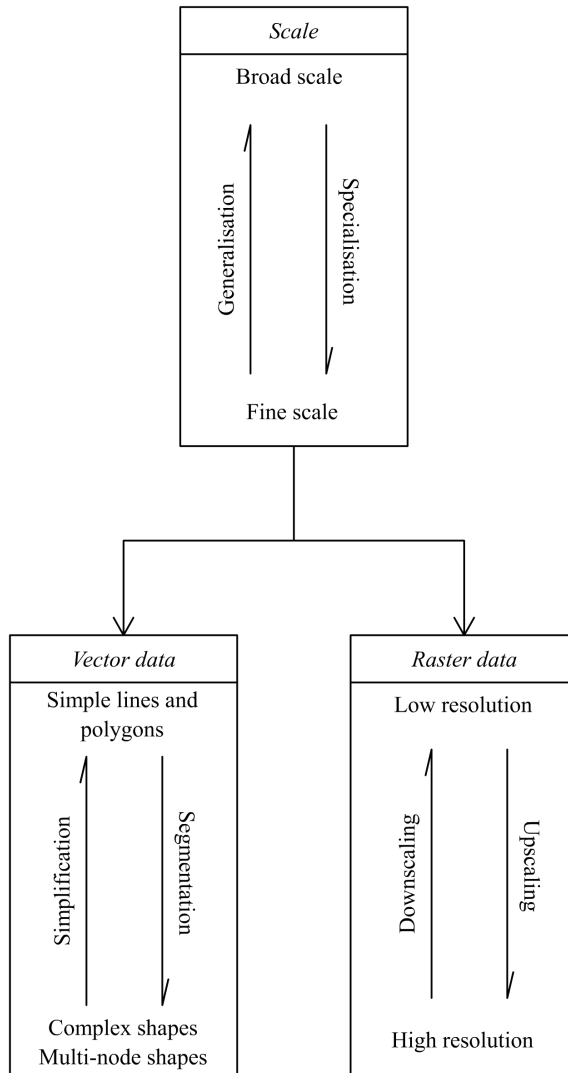


Fig. 3.6. Scaling - differences between vector and raster data (for vector data, we consider only the geometrical issues and not the thematic ones, which would bring us to the MAUP.)

This 2D sequence is called an image, a surface or a matrix, depending on the values of its pixels and on the field of application. It is a discretization of a continuous space into cells which does not affect the conceptual spatial and thematic dimensions (see section 2.2 for more details). $f(m, n)$ is a function which represents a measure of light intensity in photography or a measure of elevation in DEMs. There are multiple types of operations that can occur in this 2D sequence (non-exhaustive):

- Global transforms: e.g. contrast or brightness
- Spectral global transforms: e.g. Fourier transform and filtering
- Local transforms: e.g. spatial filters
- Geometric transforms: e.g. rotation and deformation

Local transforms include the convolution of a 2D mask or a filter (h) over a set of pixels. The latter is a “moving” window which is convoluted over dimensions M and N (figure 3.7). It is purely a mathematical operation over a set of pixels.

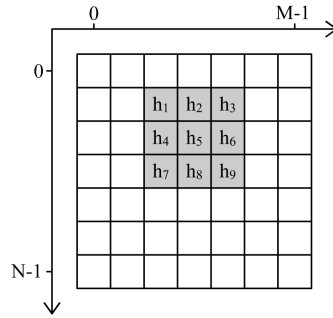


Fig. 3.7. 2D 3×3 Convolution mask h

Definition 3.3.1 (Convolution, adapted from Jähne (2005)). A function $h(\mathbf{x})$ is zero except for a small area and is denoted as the convolution mask. The convolution of a filter $h(\mathbf{x})$ with a signal $f(\mathbf{x})$ results in a new function $g(\mathbf{x})$ whose values are a kind of weighted average of $f(\mathbf{x})$ in a small neighbourhood around \mathbf{x} . It changes the signal in a defined way and is often called a filter.

Mathematically, a continuous convolution is defined by the integration of the filter over the signal (or image):

$$g(\mathbf{x}) = (h * f)(\mathbf{x}) = \int_{-\infty}^{+\infty} h(\mathbf{t})f(\mathbf{x} - \mathbf{t})d\mathbf{t} \quad (3.3)$$

The discrete form of this transform is defined by:

$$g_{m,n} = \sum_{m'=0}^{M-1} \sum_{n'=0}^{N-1} h_{m',n'} f_{m-m',n-n'} \quad (3.4)$$

Convolution is a local transformation of the central pixel value of a window through a filter function or an aggregation function. The size of the convolution mask (or window) is in most usual cases 3×3 . In data scaling process, if a mask has to be applied to an image, either the size of the mask has to be changed, or the image has to be downscaled (or generalised).

As seen in section 2.4 in quantitative geomorphology, this operation is typically used to compute the derivative of the quadratic surface (see equation 2.4, section 2.4.1). The filter function computes this derivative for each pixel. If we consider that we have a high resolution DEM, the computation of a derivative using a 3×3 window involves a small spatial coverage. If we are interested in computing a less local derivative, we have to extend the spatial coverage of the window. Currently, there are two concepts which allow this. Either the values of the DEM are aggregated to decrease the resolution by using an appropriate generalisation function, then the derivatives calculated, or the spatial coverage of the convolution window is extended and the computation of the filter function adapted. We will call these two operations respectively spatial aggregation and thematic filtering (figure 3.8).

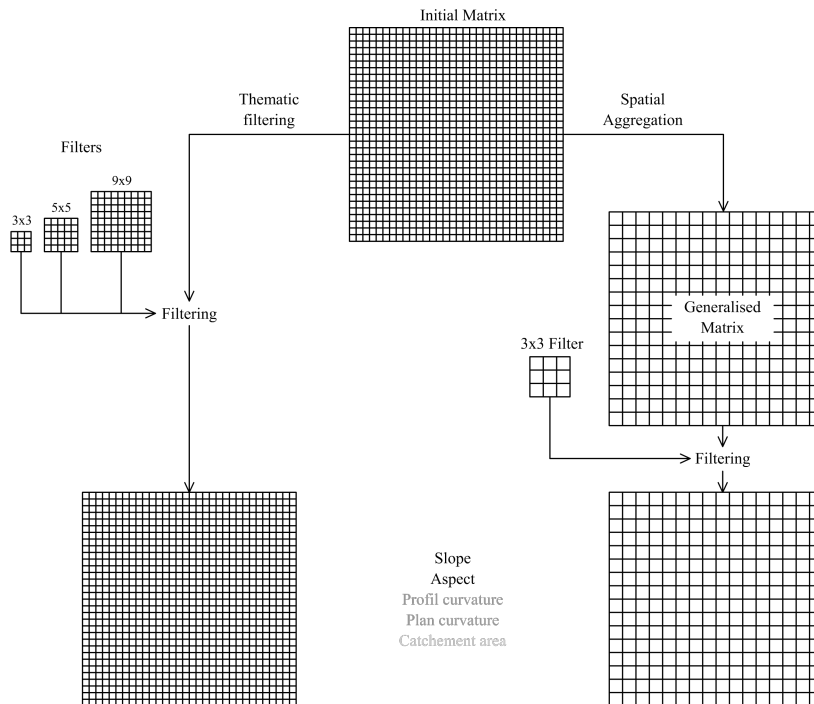


Fig. 3.8. Thematic filtering and spatial aggregation in raster data scaling processes

Spatial aggregation and thematic filtering are differentiated by:

- Spatial aggregation: first, the matrix information (or pixel values) is aggregated using an appropriated technique. The information has to be aggregated to the desired scale, in other words, the local neighbourhood of each pixel has to correspond to the scale of the desired analysis. By local neighbourhood it is meant the adjacent pixels, this in order for the matrix

to fit the 3×3 convolution mask, then the filter is convoluted with the image. Spatial aggregation results in a reduction of information throughout the resolution decrease. In our example (figure 3.9), the generalisation filter size is 8×8 and the operator it represents may be purely mathematical (a function like the average operator for example) or thematic (like focal functions). Thus, the choice of the function can be multiple, and it always depends on what needs to be preserved or illustrated through the generalisation process.

- Thematic filtering: the size of the filter is adapted to the size of the elements contained in the matrix. This one is not downsampled, but the local neighbourhood is enlarged in order to take into account non-adjacent neighbouring effects ($n \times n$) and, moreover, to include a mathematical function describing a multiscale operator. In quantitative geomorphology, this is illustrated by the work of Wood (1996).

The data generalisation using spatial aggregation results in an information loss and, visually, the surface is a less smooth. Spatial aggregation affects simultaneously the operating scale (change of resolution) and the representation scale. Thematic filtering is a more local analysis to the extent that local structures are taken into account during the convolution (figure 3.9).

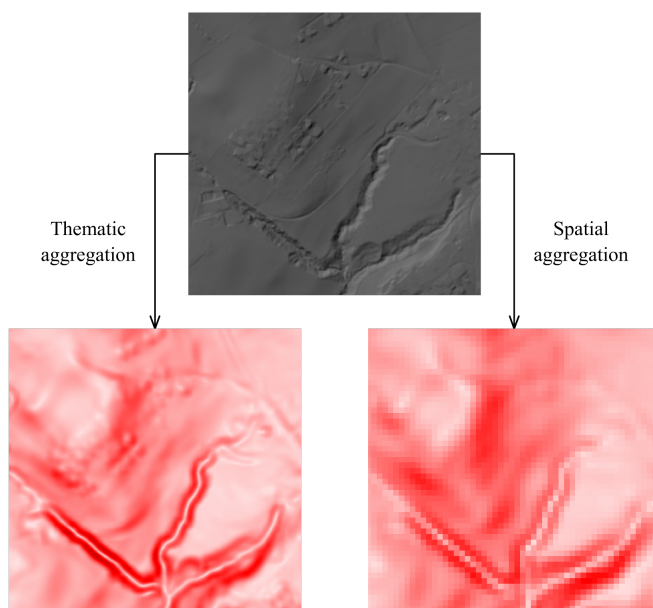


Fig. 3.9. Slopes computed using a $2\ m$ original DEM. Slopes using the thematic filtering were computed using a 9×9 convolution window. Spatial aggregation slopes were computed by first generalising the DEM (8×8 aggregation filter) in order to have a $16\ m$ resolution DEM and then slopes were computed using a 3×3 convolution window. DEM©swisstopo

3.4 Geomorphology and scale

In section 2.4, we have introduced geomorphometry and a series of terrain indicators. Geomorphometry is the quantitative counterpart of geomorphology. From the definition of geomorphometry (definition 2.4.1), we will now enlarge the scope of scale concepts applied to geomorphology; first by defining it, and second by investigating the impact of scale in geomorphological analysis and interpretation.

Geomorphology:

*the study of the physical features of the surface of the earth and their relation to its geological structures.*⁴

With this definition, geomorphology appears to be a branch of landscape analysis completely related to physical properties of a landscape. Landscape has multiple definitions in earth sciences, ecology, sociology and history. Here, we will only consider landscape from the earth science point of view, and specifically the physical impact and trace of landscape structures.

Scale in geomorphology remains a complex problem, because geomorphological processes may arise at various scales and depend on the interactions between hierarchical scale elements. Qi and Wu (1996) expressed this problem notably: “*Because of the spatial heterogeneity and hierarchical properties of landscape systems, understanding the effects of changing scale on the analysis of landscape patterns is critical to our ability to predict landscape dynamics across scale*”. Thus the appropriate observation scale is function of the environment and of the type of desired information (Woodcock and Strahler, 1987). Mark and Aronson (1984) stated that the separation between landscape scale (and the related geomorphological analysis) and geomorphological processes are strongly related to the scale of interest, but then, we might ask ourselves what are the scales of interest? Because a geomorphological shape and its size are strongly related to the scale of interest, it is undeniably necessary to define shapes in their scale context or at the scale of interest. And, actually, many geomorphological phenomena are defined by a combination of typical behaviours and structures at different scales. These hierarchical imbrications of shapes and processes brought several researchers to fractal⁵ landscape analysis (Mark and Aronson, 1984; Meentemeyer and Box, 1987; Klinkenberg, 1992; De Boer, 1992; Lloyd and Atkinson, 1998). Klinkenberg (1992) stated that for interpretation of geomorphological phenomena geomorphologists had to choose between the study of the associated scaling process and the nesting of scale-specific processes. Thus, either the analysis or interpretation of a phenomenon is the result of a scaling operation, or it is composed of multiple process which are nested in the scale continuum. There is still no absolute answer to the geomorphological scaling issues, but all these developments show that dealing with scale in earth science has a great impact on the vision we have of earth processes and interaction. Applying a scaling process to a geomorphological phenomenon already assumes that there is a scale nesting. As we expect this nesting, we will introduce a framework to explore it thoroughly.

⁴ Compact Oxford English Dictionary: http://www.askoxford.com/concise_oed/geomorphology?view=uk, accessed 25 March 2009

⁵ Fractals are a description of shapes where each part of which has the same statistical character as the whole, Compact Oxford English Dictionary: http://www.askoxford.com/concise_oed/fractal?view=uk, accessed 25 March 2009. See Goodchild and Mark (1987) for details

3.5 Multiscale analysis in geomorphometry

DEMs contain rich and diverse topographical information. The visual analysis of a shaded DEM efficiently supports the detection of a great amount of features at various scales. Earth science experts, such as geologists and geomorphologists, use high resolution DEMs to visually assess geomorphological features.

The detection of the same features using geomorphometric indicators (slope, aspect, curvature) and hydro-morphological indicators (wetness index, watersheds, streams) is complicated due to the fact that they are only dedicated to local scale analysis. Moreover, in high resolution DEMs, features are nested one into the other rendering the interpretation of indicators difficult. This is a computational scale problem (see Lassueur *et al.* (2006), and references therein).

Wilson and Gallant (2000) showed that the characterization of landscape processes and features based on one specific scale is far too simple to model our environment. In recent years, multiresolution analysis tools based on a generalisation of Evan's (1972) geomorphometric indicators have been developed (Wood, 1996). These tools provide multiple results for one indicator at multiple scales. There is no feature extraction, but rather a multi-scale/multiresolution topographical analysis and geometric network extraction.

Geological phenomena are composed of different topographical features. Klinkenberg (1992) suggested that a phenomenon fits over scale and its features are nested in discrete scale intervals, leading to a strong correlation between features and phenomena (Mark and Aronson, 1984). In human vision, the neural network is able to distinguish specific features in relation to a corresponding scale (Marr, 1982), as well as to carry out a multiresolution analysis. As suggested by Marr (1982), our visual system is probably linked to tuned cells or, in other words, it has specific frequency intervals which it is sensitive to. Therefore, computer systems and the visual representations we make of processed data should reflect this. Nevertheless, in most current systems, information is perceived like a static image, and whatever it represents, our visual system has to analyse the multiple scale levels that it contains. However, there are two ways to interpret information in an image: either we know what the image, or data, contains and we focus on retrieving this information using the most appropriated technique or method; or we do not know what the image contains. In this case, we use a more general method to identify and differentiate relevant content in the data. This latter applies for DEM analysis. Often a specific DEM contains specific information, like a geological phenomenon, but the identification of its component is not straight forward. Consequently, topographical features have to be classified according to their representative scale. In other words, it is necessary to find the best correlation between a certain level of generalisation (of the DEM) and the scale of a particular feature of the topography. This process is called a multiscale analysis of structural topographical features (Marceau and Hay, 1999).

As we have seen in chapter 2, elevation data gathering techniques such as ALS have been used for a few years. In most developed countries, high resolution DEMs have been made available by national mapping authorities.

These DEMs, through their high resolution, have fundamentally changed the way we perceive elevation information. High resolution describes very fine structural levels that stem from different processes. As example, a micro-fold may be resulting from a landslide or from usual erosion. Thus, the imprint of this feature will not be contained in the same spatial context regarding its relation to coarser features. Although high resolution allows us a much better visual rendering of the territory and of its structures, the relations between topographical structures and formations are more complicated, hence they represent a new challenge for quantitative geomorphologist and geomorphometry. How can we then identify phenomena which have a multiscale imprint? In fact, we can still apply the same algorithms and the same methods used before, but we can no longer confine ourselves to the unique result we obtain at one scale or using a 3×3 convolution window, such as defined by Evans (1979).

Multiscale DEMs are either produced using a top-down approach, or a bottom-up approach (De Floriani *et al.*, 1996; Schroeder *et al.*, 1992). The top-down approach involves refinement, going from a coarse resolution to the desired fine one, called upscaling (see section 3.3). Generalisation, the bottom-up approach, is a concept connecting phenomena through different scale levels, from fine to coarse. It is linked to downscaling, which is made possible by decomposing information in order to reach its constituents at coarser scales (Marceau, 1999; Jarvis, 1995). Using high resolution DEMs, we have now moved from a top-down approach (low resolution to high resolution) to a bottom-up approach, which will be developed in the next chapter. Within this scaling process, structures have to be transferred from one scale to another. In order to be able to detect a phenomenon (thus its underlying feature(s)) at a specific scale, it is necessary to have access to the specific scales at which significant features and their intrinsic relations emerge.

The comparison between generalised DEMs and a basic shape, representing an elementary landscape structure, could result in a correlation factor between this shape and the analysed DEM through scale. Furthermore, if we link this basic shape, which can be represented by a function, to frequency analysis, we might develop a rigorous and exhaustive multiscale structural analysis. Moreover, the best representation of our function in a specific scale level would illustrate which types of structures arise in this same level.

3.6 New multiscale framework in geomorphometry

De Boer (1992) suggested that scale should be used as an analytical framework to reduce the high frequencies caused by finer scale levels. The idea is to focus on the functionalities and properties of a DEM at a certain scale. As we will show in chapter 4, and if we think of frequency analysis, the Fourier transform cannot be used to perform this complex operation due to its stationary property. Thus we will explore another frequency analysis method which is the wavelet transform. It has localisation and compact support properties which fulfil our needs (see section 1.1). If we consider this fine DEM as part of another coarse DEM through scale, we might want to determine the best way to separate its corresponding high frequencies. Thus the analysis of multiscale DEMs has to link two approaches: an analytical function to describe topography, which is the link to wavelets, and a framework which

enables the decomposition of a general system in analytical sub-systems. These sub-systems are a separation of the initial information into low-pass and high-pass information (figure 3.10, results of operation A). The wavelet transform enables precisely to define specific scale intervals, thus a pyramidal representation (or the sub-systems) of terrain models using a bottom-up approach. The link between each scale is made by the functions describing the transform and the generalisation scheme has to be adaptive to local terrain variations.

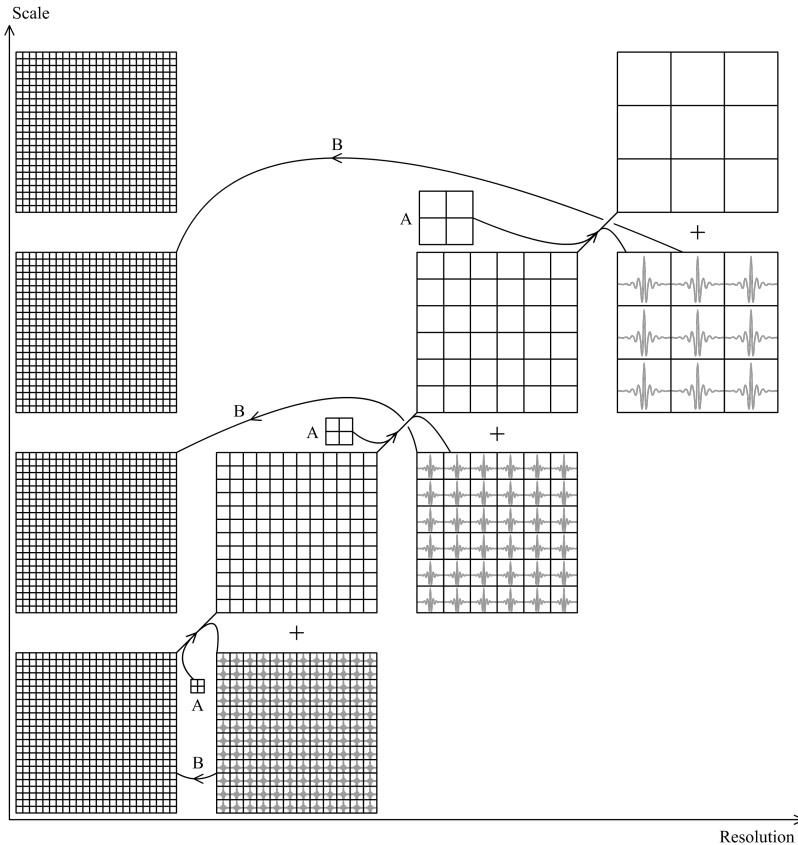


Fig. 3.10. Scale effect - Proposed framework, A is the generalisation operation (or analysis) and B is the specific scale reconstruction (or synthesis).

In our framework, we will try to define a way to rebuild multiscale structural information, but being scale selective. This case induces a complex transformation. In fact, two separate operators have to be defined (figure 3.10). The first (A) allows the generalisation of information into different low-pass and high-pass decompositions representing various scale levels. It is the first step of the wavelet analysis, respectively the wavelet transform. The second function (B) is part of the reconstruction process of information into high resolution. This is the second step of the wavelet process, which is called the synthesis procedure or the inverse wavelet transform. We will primarily explore this framework in this study.

The question is, can we define a framework which involves scale driven processes and the delimitation of scale intervals. We cannot a priori have any knowledge of the best partition and representation of the frequency space. An exploratory approach is therefore necessary to apprehend it, as well as to understand the link between structures, processes and phenomena. In this study, we try to define these spaces by interpreting and analysing a certain reality by means of multiscale representation. In interpreting these spaces, we hope to reconstruct the reality of the processes that affects a topographical phenomenon, not only regarding their formal definition, but also in the context of the structural nesting they are made of. Figure 3.11 illustrates this. Step I is the core of the study, i.e. the development of the methodology. Step II is the validation process. However, validation has only been slightly explored, partly by lack of experts and partly by lack of time. The web-based GAS survey (chapter 6) gives a few perspectives to validate the method. It does not go deeply into a validation process, but it is a first attempt to disseminate the implemented methodology .

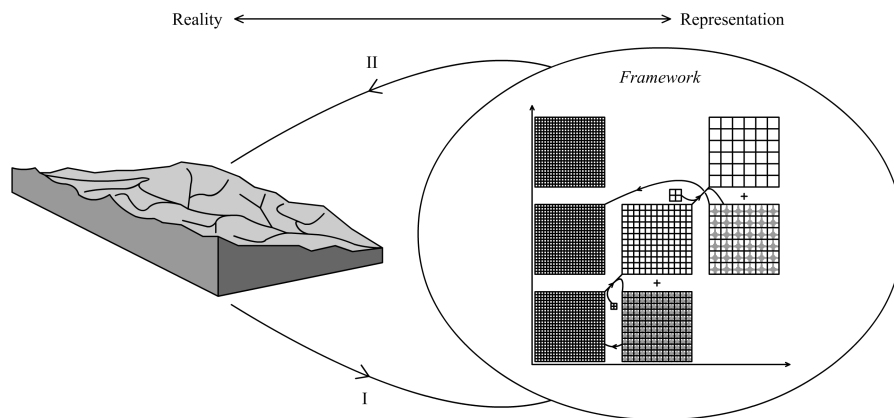


Fig. 3.11. New multiscale framework - Transition between reality and the appropriated representation of it. Step I is the development of a methodology to understand and decompose the complex reality. Step II is the validation process. The framework is described above and illustrated in details in figure 3.10.

4. Multiscale DEM using wavelets

As seen in the previous chapter, high resolution DEMs are composed of multiscale scale information. The bottom-up approach discretizes them into several scale intervals containing relevant and specific structural information. Furthermore, frequency analysis is a promising way to apply downscaling and to analyse the underlying results of dense datasets at very fine scale. As the Fourier transform is not adapted to non-stationary and heterogeneous signals (see section 4.1.1), the wavelet transform will be used to circumvent these limitations. Through conceptual considerations, it creates frequency discrete spaces, or partitions of the global frequency space. The implicit link between frequency space and spatial space is hard to make, but using statistical analysis and visual interpretation of the wavelet transform (WT) results, we will try to give an explicit scale definition of the new created spatial spaces.

First, we will introduce the wavelet transform with some theoretical elements and formulation (section 4.1) and then express our approach in using it for DEM generalisation and analysis purposes (section 4.2).

4.1 Wavelet for generalisation

Human vision uses simple cell in the visual cortex to perceive our environment. The representation our brain makes of this information is a discretization of spatial variables and frequencies (Marcelja, 1980). Wavelets, through their spatial and frequency definition, fit very well the particular statistical structure of our visual environment (Field, 1999; Gaudart *et al.*, 1993); they are spatially localised and defined in the spatial frequency domain (Mallat, 2000). The wavelet transform is a mathematical tool for spectral analysis and simplification, and it is strongly related to the Fourier transform (Polikar, 1995).

Conceptually, the Fourier transform is a combination of harmonic waves designed to reconstruct an almost random signal (like the elevation profile in figure 4.1). Wavelet transforms are similar to the Fourier transform, but they are locally adaptive to the signal. Therefore, they are not inducing an infinite continuity as a sine or cosine wave does. The next two sections describe these differences.

4.1.1 Fourier transform

A signal $f(x)$ is defined through its period $T = \frac{1}{f_0}$ where f_0 is the reference frequency (base frequency). Every periodic signal can be decomposed into a infinite sum of sine and cosine functions. If we take a 2-periodic function $f(x)$ (Zwillinger, 2003):

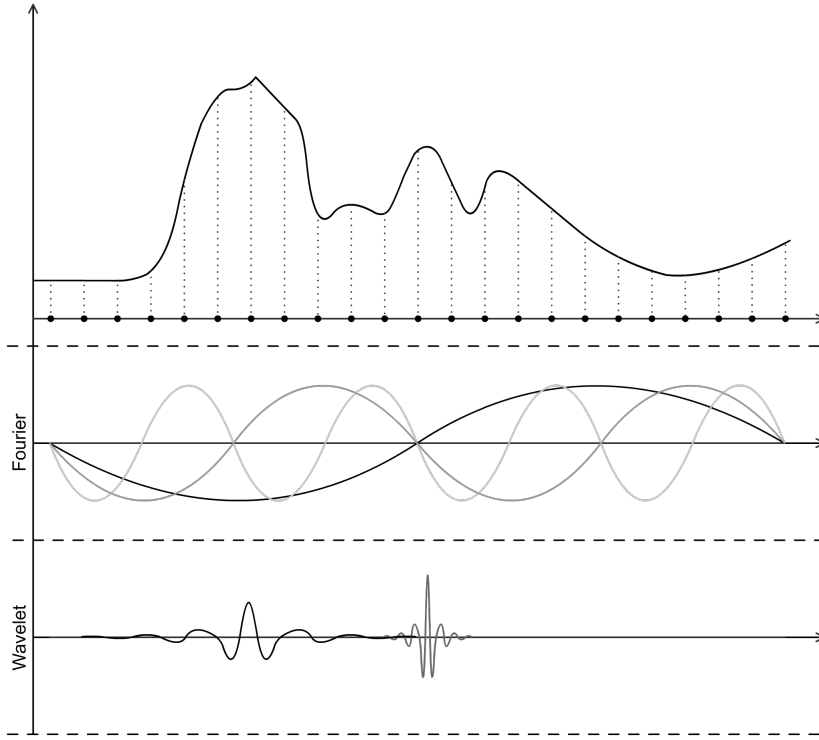


Fig. 4.1. Fourier versus wavelets

$$f(x) = \frac{A_0}{2} + \sum_{n=1}^{\infty} (A_n \cos(2\pi n f_0 x)) + B_n \sin(2\pi n f_0 x) \quad (4.1)$$

If we use complex notation to describe this series, we can show that

$$f(x) = \sum_{n=-\infty}^{\infty} D_n e^{2\pi j n f_0 x} \quad (4.2)$$

with $D_n = \frac{1}{2}(A_n - j \cdot B_n)$.

In equation 4.2, D_n are defined as the Fourier coefficients. The Fourier transform decomposes a signal into two components: the magnitude and the phase of the coefficients in the complex domain. Thus, if we interpret the signal as continuous, the Fourier transform is a signal decomposition into frequencies composing it and defined in equation 4.3.

$$\mathcal{F}[f(x)] = F(\omega) = \int_{-\infty}^{+\infty} f(x) e^{-2\pi j \omega x} dx \quad (4.3)$$

If we consider a terrain profile and we apply to it a Fourier transform, the results will give the frequencies composing the signal, but not the localisation of those frequencies in the profile space. Indeed, the Fourier transform is well defined for stationary signals, but it can hardly be used for non-stationary signals, like terrains or terrain profiles. The differences between stationary and non-stationary signals are:

1. Stationary: the statistics of these signals are constant over time. The signal repeats itself over time (like a sine or cosine wave) and can be predicted using a sum of sine and cosine waves.
2. Non-stationary: non-redundant signals. The signal cannot be predicted.

Natural phenomena signals are often non-stationary. Intuitively, it is easy to understand that an integral which covers a complete spatial domain has not the same properties as natural phenomena. This is similar to the link between our visual system (see Gaudart *et al.* (1993) for details) and the identification of localised natural phenomena. If we take a terrain profile, the probability that the signal repeats itself is almost equal to zero. Many authors have applied the Fourier transform to terrain models or shown that it was not adapted to terrain data (Pike and Rozema, 1975; Amgaa, 2003; Gallant and Hutchinson, 1996; Mahler, 2001; Martinoni, 2002). However, as Amgaa (2003) stated: *a signal simply cannot be represented as a point in the time-frequency space* and Mahler (2001) concluded that: *For analysing non-stationary or transient phenomena with the occurrence of signal changes at a particular location, such as a terrain, the space-invariant Fourier transform is not suitable*. Rao (1995) stated that the Fourier transform is well localised in the frequency domain, but poorly in the space (or time) domain.

The Fourier transform cannot be used to perform this complex operation because its properties assume that the signal (the topography) is stationary and not local. Moreover, sine functions cannot represent basic topographical features in an appropriate way (Gallant and Hutchinson, 1996), because spatial data is generally autocorrelated, non-stationary, non-normal, irregularly spaced and discontinuous (Meentemeyer and Box, 1987). However, an approach based on frequency analysis can be implemented (Bjorke and Nilsen, 2003).

4.1.2 Wavelet transform

Wavelets appeared because of the lacks of the Fourier transform in describing local properties of signals (Cohen, 1992). In the 1930s, the Haar function was used to study Brownian motion (Graps, 1995). Multiple research fields therefore used wavelet-like algorithms (see Meyer (1992) for an overview). Then, in 1946, D. Gabor introduced the first time-frequency wavelet, even if his development could only be used on a continuous system, the wavelet transform was in development. The present wavelet transform was defined and developed by Mallat (1989). He highlights the next relations between following elements:

- Conjugate quadrature filters. A wavelet ψ defining a conjugate quadrature filter generates an orthonormal basis of $L_2(\mathbb{R})^1$. A conjugate quadrature filter decomposes a discrete signal into two downsampled signals (double filtering and downsampling (Mallat, 2000) , see figure 4.4). In the Fourier domain, $\hat{\psi}$ can be interpreted as the impulse response of a high-pass filter (G).
- Pyramidal algorithms (in image processing). Some structures have to disappear from one resolution to another and other structures have to be maintained. These algorithms enable to generate a 2^{i+1} resolution image

¹ L_2 is a space where the defined functions are of finite energy, thus $\int |f(x)|^2 dx < +\infty$ (Mallat, 2000), where L stands for Lebesgue.

from a 2^i resolution original image, where i is the decomposition level (Meyer, 1992).

- Orthonormal basis. Mallat (2000) showed that every signal $f \in L_2(\mathbb{R})$ can be decomposed on an orthonormal basis $\{\psi_{i,k}\}_{(i,k) \in \mathbb{Z}^2}$, equation 4.4.

$$f = \sum_{i=-\infty}^{+\infty} \sum_{k=-\infty}^{+\infty} \langle f, \psi_{i,k} \rangle \psi_{i,k} \quad (4.4)$$

Starting from these elements, Mallat (1989) developed the multiresolution approximation of $L_2(\mathbb{R})$ and defined the continuous wavelet transform. We will replace the time-frequency concept by position-frequency, because we are not processing a temporal signal, but a terrestrial localized signal (a DEM). Using wavelets having variable sizes on the position axis, Mallat (2000) defined the wavelet transform as the transform of a signal in a family of shifted and dilated wavelets, and he developed the transform for 2D signal.

Definition 4.1.1 (Mallat, continuous wavelet transform). *A wavelet is a function $\psi \in L_2(\mathbb{R})$ with zero mean:*

$$\int_{-\infty}^{\infty} \psi(x) dx = 0 \quad (4.5)$$

If the wavelet ψ is dilated by a factor i and translated by k , we obtain:

$$\left\{ \psi_{i,k}(x) = \frac{1}{\sqrt{2^i}} \psi \left(\frac{x - 2^i k}{2^i} \right) \right\}_{(i,k) \in \mathbb{Z}} \quad (4.6)$$

Thus, the wavelet transform of $f \in L_2(\mathbb{R})$ at position k and scale i is:

$$Wf(i, k) = \langle f, \psi_{i,k} \rangle = \int_{-\infty}^{\infty} f(x) \frac{1}{\sqrt{2^i}} \psi^* \left(\frac{x - 2^i k}{2^i} \right) dx \quad (4.7)$$

where ψ^* is the complex conjugate of ψ .

The dilation factor implies that at each decomposition level i , the wavelet spectra is divided by 2 (dyadic transform). Mallat (2000) thus introduced a complementary function in order to avoid redundancy and enable perfect reconstruction (no information loss) by the inverse transform. This is shown by relation 4.8, the wavelet subspace being defined by $W_i = \{\psi_{i,k}(x)\}_{(i,k) \in \mathbb{Z}}$.

$$\{f(x)\}_{L_2(\mathbb{R})} \in W_1 \cup W_2 \cup \dots \cup W_i \cup \dots \cup W_n, \quad n = \infty \quad (4.8)$$

If we define $V_0 = \{f(x)\}$ and a fine-to-coarse sequence of subspaces $V_i \subset \dots \subset V_0 \subset L_2(\mathbb{R})$, to avoid an infinite series of wavelet subspaces W_i , we can then express:

$$\{f(x)\}_{L_2(\mathbb{R})} = W_1 \cup W_2 \cup \dots \cup W_i \cup V_i \quad (4.9)$$

Orthogonality ensures the no-redundancy property between W_i and V_i . Hence a new function, complementary to ψ , is defined (see equation 4.10), called the scaling function $\varphi(x)$ ($V_i = \{\varphi_{i,k}(x)\}_{(i,k) \in \mathbb{Z}}$).

$$\langle \varphi(x), \psi(x - k) \rangle = 0 \quad (4.10)$$

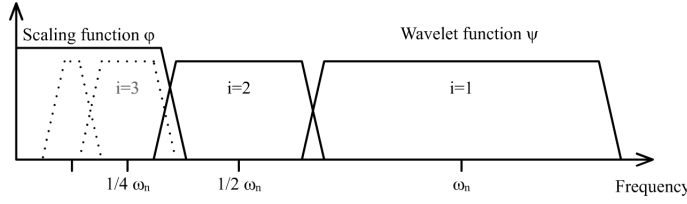


Fig. 4.2. Spectral coverage of the wavelet and scaling functions

Equation 4.10 makes sure that the whole spectrum of $f(x)$ is covered by the analysis (figure 4.2). Unser and Blu (2003) showed that the scaling function φ can be defined using two ways. Either it is given explicitly or it is derived from the refinement filter $H(\mathbf{z})$ (itself derived from the wavelet function).

In other words, we use two functions ψ and φ , which have a two-scale relation, and which can decompose a signal into two distinctive subspaces W_i and V_i . The first, related to ψ , represents at each decomposition step i the half of the analysed frequency space and the second, related to φ the other half. On this latter, the same process can be applied again (figure 4.3).

As we are using discrete sampled signals (DEM), we use the discrete wavelet transform. To ensure a good interpolation of the DEM generalisation process, a B-spline basis is chosen as scaling function (see section 4.2.3 for a detailed description). For a complete description of the mathematics and the derived filters refer to appendix A.

Wavelet discrete transform.

The discrete transform, as shown in appendix A, defines two quadrature conjugate filters² ($H(\mathbf{z})$ and $G(\mathbf{z})$). The first one is the impulse response of the scaling function φ and the second one is the impulse response of the wavelet function ψ . In fact, they are a low-pass filter and a high-pass filter. Their conjugate filters allow a perfect reconstruction of the signal (see equation A.29, appendix A) and they are separable because of the separability of their impulse response (Mallat, 2000); thus the separability of the two basis functions (Unser, 2001):

$$\begin{aligned}\varphi_{m,n}(k,l) &= \varphi_m(k) \cdot \varphi_n(l) \\ \psi_{m,n}(k,l) &= \psi_m(k) \cdot \psi_n(l)\end{aligned}\tag{4.11}$$

where m and n are respectively the row and column dimensions and k and l respectively the size of the image (k =number of rows and l =number of columns).

This defines a bi-dimensional convolution by dividing the problem into two parts: a first unidimensional convolution on the image rows followed by an unidimensional convolution on the image columns (Mallat, 2000). At each step, the convolution is followed by a dyadic subsampling (2^i) over the convoluted dimensions. Intuitively, by considering all combinations of these filter, four results will be obtained using the wavelet transform: a low-pass image ($c[2\mathbf{k}]_{i+1}$), a high-pass horizontal image ($d[2\mathbf{k}]_{h,i+1}$), a high-pass vertical image ($d[2\mathbf{k}]_{v,i+1}$) and a high-pass diagonal image ($d[2\mathbf{k}]_{d,i+1}$). The high-pass

² Quadrature filters implement the filter bank. They split the input signal into two dyadic subsampled resulting signals: a high-pass and a low-pass.

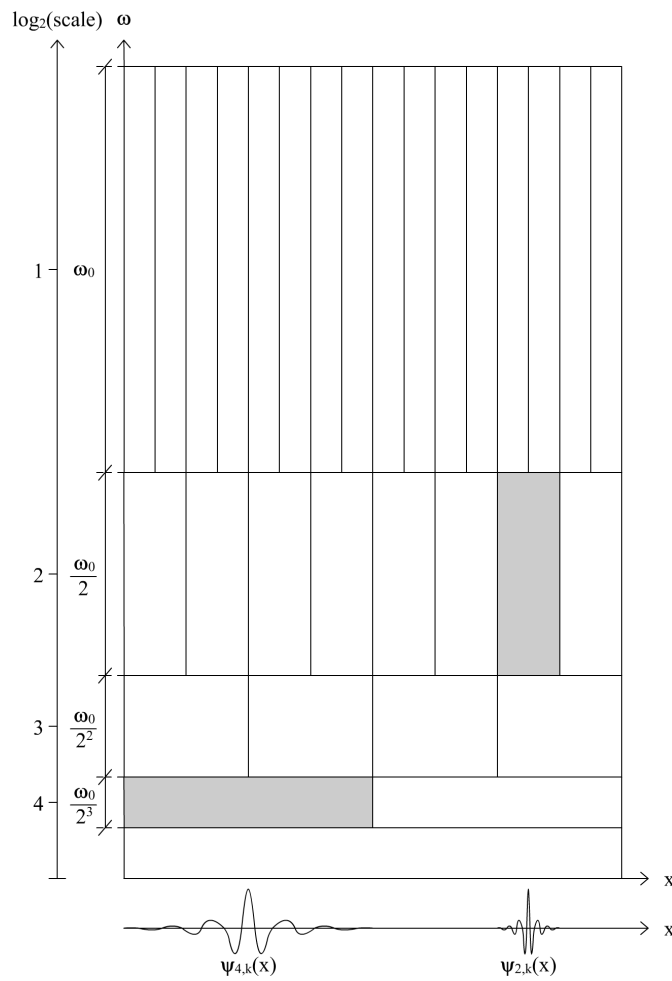


Fig. 4.3. Idealized representation of how the space-frequency plane is tiled by the wavelet basis functions. At high frequencies (e.g., box related to $\psi_{2,k}(x)$), spatial localisation is high while spectral localisation is less precise. On the contrary, at lower frequency (e.g., box related to $\psi_{4,k}(x)$), spectral localisation increases at the expense of spatial localisation according to Heisenberg's uncertainty principle.

results are usually called the detail coefficients. Figure 4.4 shows the filter bank of the wavelet transform, represented in the figure by the analysis. The inverse transform (synthesis) is presented in the next section.

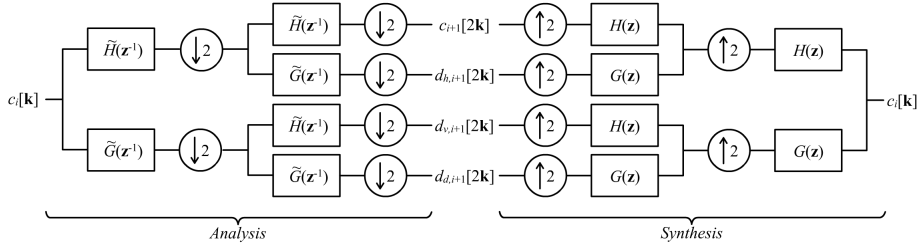


Fig. 4.4. Conjugate quadrature filter bank

Considering two dimensions, Mallat (2000) defined the wavelet basis (equation 4.12). In the spectral domain (Fourier), the energy of the decomposition can be defined as shown in figure 4.5. Thus, at each decomposition level and for each basis, a specific part of the original signal frequency spectrum is extracted by the corresponding basis. Regarding a decomposition level i , the low-pass coefficients $c[\mathbf{k}]_i$ correspond to the signal frequency spectrum covered by $\hat{\varphi}_i$, the horizontal high-pass coefficients $d[\mathbf{k}]_{h,i}$ to $\hat{\psi}_{h,i}$, the vertical high-pass coefficients $d[\mathbf{k}]_{v,i}$ to $\hat{\psi}_{v,i}$ and the diagonal high-pass coefficients $d[\mathbf{k}]_{d,i}$ to $\hat{\psi}_{d,i}$.

Theorem 4.1.1 (Mallat). *A scaling function φ and the corresponding wavelet ψ generate an orthonormal wavelet basis $\mathbf{L}_2(\mathbb{R})$. Three wavelets are defined:*

$$\psi_h = \varphi(x)\psi(y), \quad \psi_v = \psi(x)\varphi(y), \quad \psi_d = \psi(x)\psi(y) \quad (4.12)$$

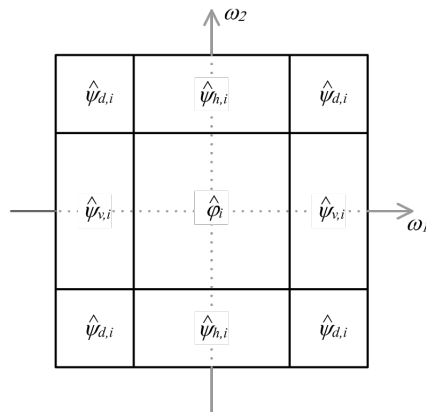


Fig. 4.5. Dyadic rectangles indicating the energy concentration of $\hat{\psi}_{k,i}$, adapted from Mallat (2000)

Mallat (2000) gave a synthetic view of the wavelet transform results (figure 4.6). The original scale of the image is divided by the dyadic subsampling, thus the resolution is reduced by a 2^i factor (i being the decomposition level). Figure 4.6 shows the result for the first decomposition level ($i = 1$). To obtain the next levels, the transform is applied to the $c_{i+1}[2\mathbf{k}]$ coefficients until the level of interest is reached.

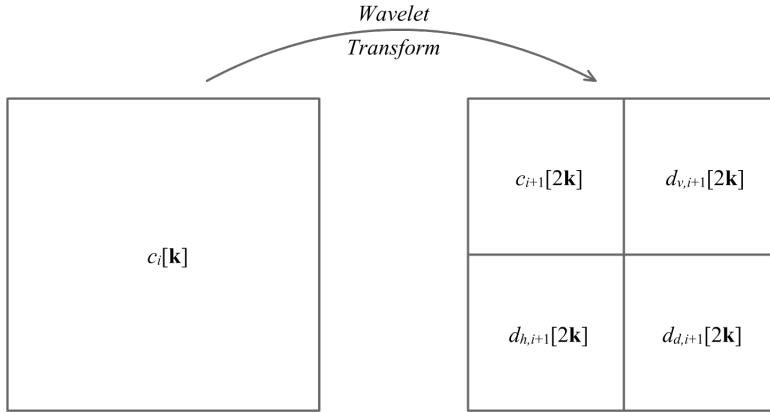


Fig. 4.6. Original signal $c_i[\mathbf{k}]$ resulting in one low-pass image $c_{i+1}[2\mathbf{k}]$ and three high-pass images $d_{h,i+1}[2\mathbf{k}]$, $d_{v,i+1}[2\mathbf{k}]$ and $d_{d,i+1}[2\mathbf{k}]$.

4.1.3 Inverse wavelet discrete transform

The perfect reconstruction conditions (Vetterli, 1986) define the relations between the analysis and synthesis filters (see equation A.29 in appendix A for details). Figure 4.4 shows that the synthesis is just an inversion of the analysis; the downsampling steps correspond to upsampling and the filters are reverted translated versions by pairs of the impulse response of the analysis filters (dual basis³).

4.2 Generalisation of high resolution DEMs

4.2.1 DEMs and wavelet

As seen, few attempts were made to use the wavelet transform on DEMs (Bjorke and Nilsen, 2003; Pike, 2000). Since the emergence and dissemination of this image transform techniques, only few researchers (Gallant and Hutchinson, 1996; Mahler, 2001; Martinoni, 2002; Amgaa, 2003; Bjorke and Nilsen, 2003) have tried to apply wavelets and their effects on DEMs. Even in prior years to the 2D wavelet transform development, researchers (Weibel, 1989b) have shown that there is a need to have different spatial DEM resolutions, this in order to be able to apprehend this huge amount of information. Both approaches, visual and computational, are subject to this fact.

³ A dual basis is defined following: $\tilde{H} = [\tilde{u}_1 \ \tilde{u}_2 \ \dots \ \tilde{u}_n] = (U^{-1})^H$ where $()^H$ is the hermitian transpose ($A^H = (A^T)^* = (A^*)^T$), $()^*$ is the complex conjugate (Unser, 2001). This basis is defined in an Hilbert space (scalar field $\in \mathbb{C}$) (Zwillinger, 2003)

Wavelet applications on DEMs are divided into several application fields. A non-exhaustive list of previous work is proposed hereunder:

- Feature extraction. The wavelet transform can be used for feature extraction. Studies (Grewe and Brooks, 1997; Amgaa, 2003) have shown that the considered feature has to be of high gradient limit. In DTMs, most of the geomorphologic features are nested one in another and gradient limits are considerably harder to identify, probably due to the higher autocorrelation than in usual images. Amgaa (2003) and Vu and Tokunaga (2002) applied wavelets to the extraction and segmentation of DSMs containing building information. In this context, wavelets are efficient because of the sharp and clean building limits. The transposition of this work to DTMs and natural phenomena seems impossible and inefficient for such structures.
- DEM filtering: Mahler (2001) and Martinoni (2002) filtered the wavelet coefficients. Results were filtered versions of the original DEM. They also gave some hints of isolating specific scale information. Since the used wavelets (Haar and Daubechies) are not symmetric (Daubechies) or complex enough for terrain representation (Haar), the generalisation and filtering process induces artificial structures (see appendix B where the 0.5 degree wavelet is almost similar to the Haar wavelet). BJORKE and NILSEN (2003) tried almost the same approach. They also used the Haar wavelet. As long as there is no need for a generalised representation or extraction of morphometric indicators - only a visual analysis of the DEM or of the different coefficients - the Haar wavelet can be used. However, in quantitative approaches, the Haar wavelet is problematic because of the square structure it induces.

4.2.2 Validating the wavelet approach

As seen above, wavelets were used for multiple purposes. In our study, we will use them to fulfil a geomorphological multiscale description of a high resolution (1 m) DEM containing a landslide. In order to understand what the effects and issues of the WT are applied to such a structure, we create a virtual landslide on a regular plane, to which the WT is applied until the eighth decomposition level ($i = 8$).

In order to assess that the generalisation scheme using the WT is adapted to DEMs, the generalised low-pass results are analysed regarding the following indicators:

- Global surface analysis: statistical indicators (mean, median, maximum, minimum and standard deviation) computed over the whole generalised DEMs and regarding all the decomposition levels.
- Profiles: some 1D profiles are visually analysed regarding the zone of interest. The same statistical indicators, as for the global analysis, are computed for the elevations composing each profile.
- Slope to elevation distribution: it gives us a synthetic view of the maxima attenuation in the different decomposition levels. It is strongly related to scale and shows how fast the generalisation process tends to create an inclined plane.
- Local fractal analysis: the local Hurst coefficient shows how, locally, the relations between the DEM pixels evolve regarding their specific scale interval.

- Global spatial autocorrelation: as we analyse the local relations in the pixel distribution, we want to know how it globally evolves regarding the elevation distribution. In order to do so, we use autocorrelation indicators (Moran’s coefficient and Geary’s ratio).

4.2.3 Wavelet function choice

There are plenty of functions which can be used as wavelets. In fact, a function has to be continuous, tend to zero when x tends to infinity and have vanishing moments. Most wavelets were designed for a specific task in a specific application. Thus, by choosing a wavelet transform, the main issue is to choose either a scaling function or either a wavelet family that satisfies specific needs. Almost any function could be applied (Reza, 1999) as long as it meets the wavelet transform conditions.

We choose to explore the fractional B-spline wavelet family. Unser and Blu (2000) wrote that they appeared to have the smallest approximation error, i.e. the scale decomposition is true to the original signal. Another property is that splines are a well recognized interpolation basis for DEMs (Gachet, 2005; Mitasova and Hofierka, 1993), and B-splines are a special case of splines. Indeed, they are the basic atoms of polynomial splines (Unser, 1999; Schoenberg, 1946). A lot of wavelets are constructed on splines (for example Haar, Battle-Lemarié, B-spline). They allow construction of linear space decomposition and reconstruction schemes (Stadt *et al.*, 1998).

B-spline wavelets have the following properties (Unser, 2001):

- Symmetric and positive - Because of the base definition of B-splines, convolution products of elementary B-splines are always positive and symmetric.
- Compact support - A B-spline of degree n has a compact support over $[-\frac{n+1}{2}, \frac{n+1}{2}]$, thus the B-spline basis value is equal to zero elsewhere.
- Differentiable - Regarding the degree of the B-spline, it can be derivated $n - 1$ time.
- Optimally localized in position and frequency.

In terms of DEM equivalents, these four properties are expressed as follows:

- Symmetric and positive - DEM structures approach symmetry, but are rarely symmetric. Moreover, a lot of phenomena represented by DEMs have some symmetric structures (or approach symmetry). The property of positivity gives us positive coefficients where the terrain is convex (thus positive) and negative coefficients where it is concave⁴. This property, as we will see in the next sections, is significant for our analytical method applied to terrain analysis.
- Compact support - Every structure in a DEM, even the largest, has a compact support. Topography is not infinite. For example, a hill is a 2D compact supported structure: it has a peak and is delimited by its base boundary.
- Differentiable - In this study, this property will be not be explored, but it could be linked to geomorphometry indicators, like the first and second derivatives (see section 2.4).

⁴ Concave and convex are used as defined in section 2.4.1.

- Optimally localized in position and frequency - If we cannot localize structures in DEMs, the result analysis and visual interpretation are hard to undertake. As already mentioned at the beginning of this chapter, non-localized frequency analysis is not optimal for DEMs.

In order to see the effect of the wavelet transform on structures, a SNR analysis is undertaken and linear profiles are used (see appendix B). For each wavelet degree ($n = 0.5, 1.0, \dots, 5$), the same profile was computed on compared to original DEM profiles. These were chosen because of their specific shape.

Results on the profiles (figure B.7 in appendix B, and figure 4.7) confirm the first conclusion about the smoothing effects. Using a fractional degree lower than 1.0 induces a stepwise bias. It may either be positive, thus increase the elevation, or negative and induce a pit. For higher degrees, as visible on the figures, the higher the degree the more averaging the resulting elevation seems to be. The correspondence with the original DEM increases as the B-spline degree is increased. But it is not a linear process and the profiles of the different degrees seem to converge. Regarding the SNR analysis (see appendix B) and the profile analysis, our choice is the B-spline basis of degree 3.

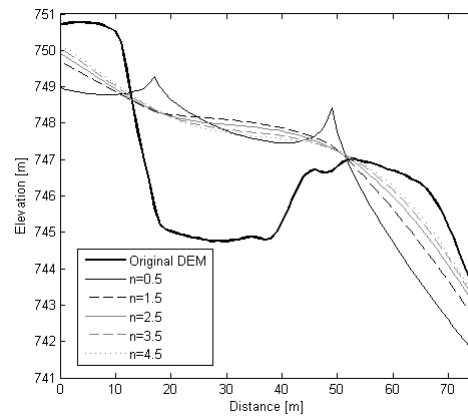


Fig. 4.7. Wavelet effect on profile 2

Thus, our choice of wavelet is not based on the wavelet function, but on the scaling function (B-spline). As shown in appendix A, B-splines of degree n are convolutions of the basis function β_0 . The family of wavelets is then defined by the perfect reconstruction conditions (Vetterli, 1986).

Unser and Blu (2000) developed the so-called fractional splines and wavelets (see appendix A for theoretical details). For generalisation purposes, hypothesis was made that a B-spline of degree 3 is the best interpolation basis for DEM generalisation (regarding B-spline basis of other degrees). The associated scaling and wavelet functions are shown in figure 4.8. A small study comparing wavelet analysis using different degrees is given in appendix B.

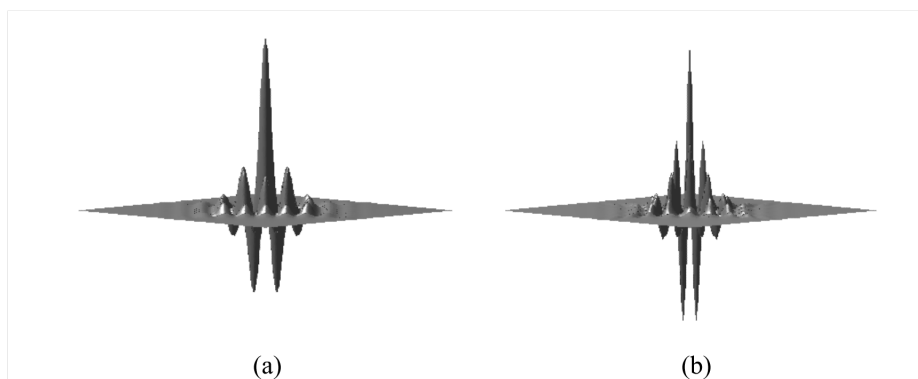


Fig. 4.8. Illustrations of the scaling function (B-spline of degree 3)(a) and the wavelet function (symmetric dual wavelet)(b)

4.2.4 Wavelet transform effect - A simple model

As shown in section 4.2.3, we chose a B-spline scaling function of degree 3. To apprehend and describe the effect of this transform on a DEM, a simple virtual landslide model was created on a regular plane. A small introduction to the shape features of this landslide is therefore given below. This virtual DEM has following properties (see figure 4.9 for localisation of elements):

- Plane slope: 18.4°
- Scarp zone: 14 ha
- Head zone: 26 ha
- Main body zone: 10 ha
- Accumulation zone: 25 ha

The minimum elevation value is 0 and the maximum elevation value 254.33 and so the range.

Each of these zones has specific properties, e.g. small structural variations. The whole landslide was combined to a plane of constant slope. In the scarp zone, strong elevation variations were made, modelling the material destruction. The head zone is in the continuity of the scarp zone, the included features are modelling the unstructured material resulting from the scarp zone. Mass movement is then shown in the main body, but therein the shape of moved material is smoother. This was done in order to see if these small features had an impact on the wavelet transform and could be seen in the high-pass coefficients. Downhill the main body, the accumulation zone is a convex hill with, at its end, a steep slope showing the strong mass movement of the landslide toe. A profile, going from the scarp zone to the accumulation zone and being centred in the landslide, is shown in figure 4.10 on which this different elements can be retrieved.

The aim of creating such a DEM was to reproduce a typical landslide. Indeed, the aim is to understand the theoretical behaviour of the wavelet transform applied to DEMs and to the shapes it contains. These have to be enough consistent and easy to understand in a morphological point of view, and using simple (but realistic) shapes is a good generic approach.

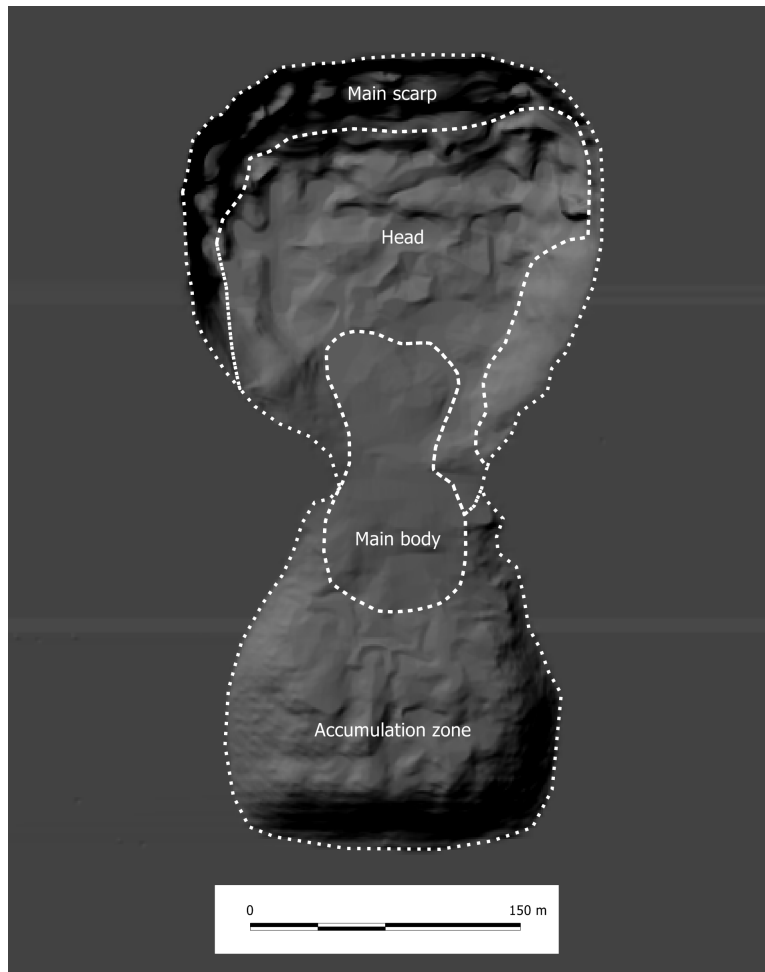


Fig. 4.9. Shaded virtual landslide

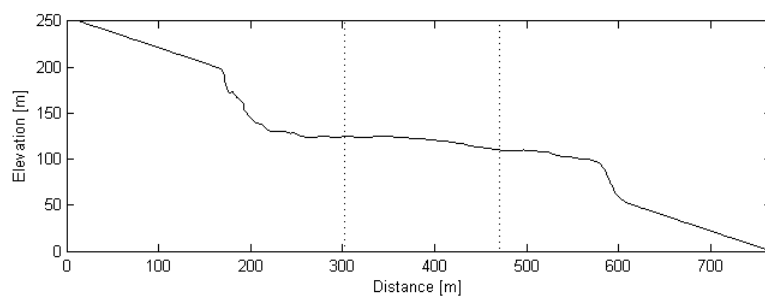


Fig. 4.10. Centred profile of the virtual landslide - The dashed vertical lines show the upper and lower limits of the main body.

Pyramidal decompositions.

Visual analysis of the low-pass surfaces (or generalised DEMs) shows that, as expected, less and less details are visible in the successive decompositions. Figure 4.11 shows the five first levels, but decompositions were computed until the eighth level. Assuming that the original DEM had a 1 *m* resolution, at the eighth level, the resulting surface has a 256 *m* resolution. Visually, the landslide (in its global shape) disappears from the decomposed DEM at the seventh level, thus all the information concerning the landslide was transmitted to the high-pass coefficients and only the regular plane is remaining in the low-pass resulting surfaces. The size of the original DEM is 768×768 pixels. Thus, in the pyramidal decomposition, the size of the resulting low-pass surfaces is for $i = 1 \Rightarrow 384 \times 384$, $i = 2 \Rightarrow 192 \times 192$, $i = 3 \Rightarrow 96 \times 96$, $i = 4 \Rightarrow 48 \times 48$, $i = 5 \Rightarrow 24 \times 24$, $i = 6 \Rightarrow 12 \times 12$, $i = 7 \Rightarrow 6 \times 6$ and $i = 8 \Rightarrow 3 \times 3$.

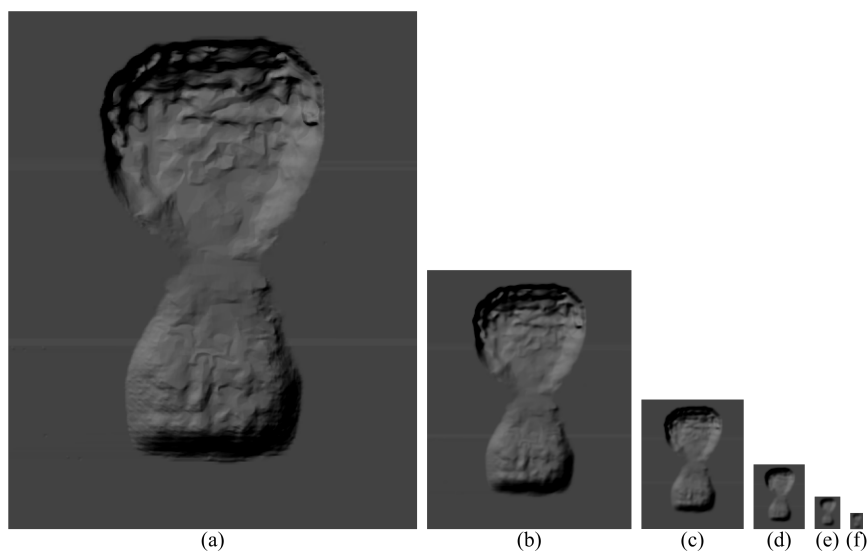


Fig. 4.11. Low-pass decomposition pyramid; (a) original DEM, (b) first decomposition level, ..., (f) fifth decomposition level

The pyramidal representation is the generalisation result (or low-pass) of the WT. The elements not retrieved in the different low-pass surfaces are contained in the high-pass coefficients, depending on the frequency scale. The so-called details will be sent by the transform in one of the high-pass images. It is the “orientation” or preferential direction of the wavelet adjustment over the elements that determines in which high-pass image (horizontal, vertical or diagonal) the element is sent. Indeed it is always a combination of low-pass and high-pass filters which determines which value will be in which resulting image. The geomorphological analysis and interpretation of three high-pass images is complex and disturbing for non-specialists of the WT. This partition of the space domain, or in our case, the territorial domain, is the main limitation of the usual wavelet transform. In chapter 7, we will illustrate how to get rid of this limitation and give a complex definition to the high-pass coefficients.

A wavelet coefficient (the pixel value in the high-pass images) has two characteristics: a magnitude and a direction. The latter was explained in the previous paragraph. The former is the local energy needed by the wavelet to have the best correlation with the local structure or element, thus the local scale versatility. The higher the magnitude is, the more (vertically) stretched to fit the structure the wavelet is. Inversion of the wavelet shape is given by a negative coefficient (e.g. figure 4.12). Section 4.3.1 will give more details about detail coefficient values and analysis.

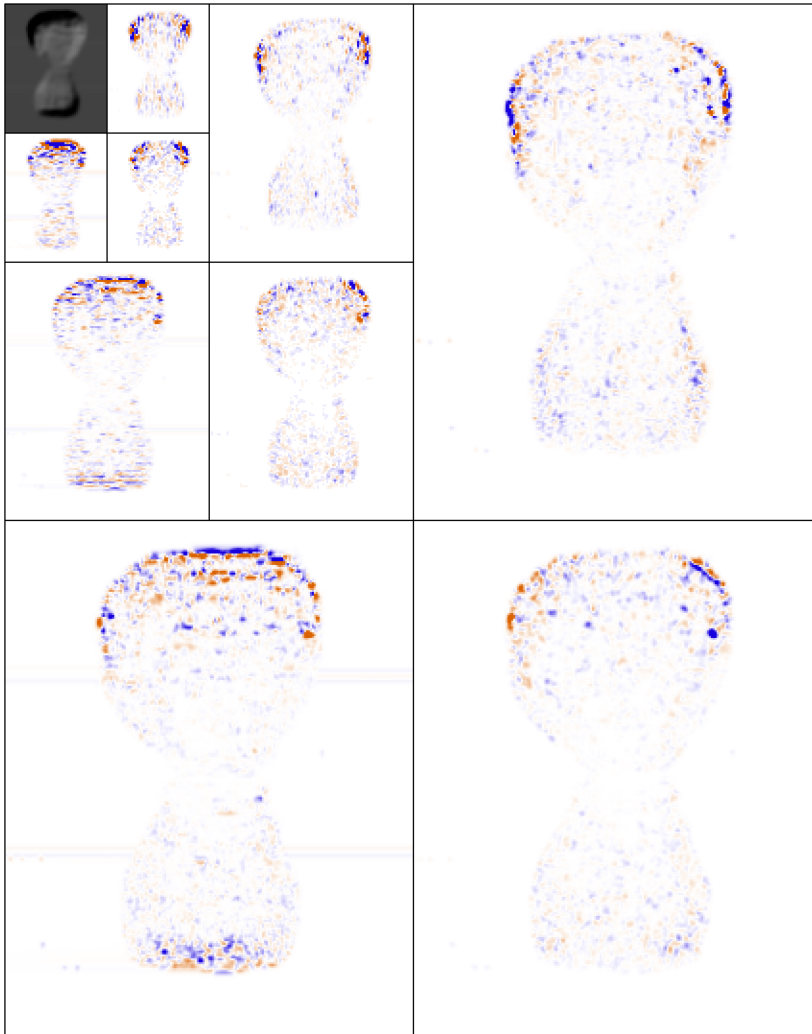


Fig. 4.12. Mallat's decomposition scheme applied until the third decomposition level. Positive coefficients are in red and negative coefficients in blue.

4.2.5 Global surface statistics

To understand the behaviour of the WT and to ensure that the low-pass result corresponds to the original DEM regarding their resolution, a few simple statistical indicators were computed (figure 4.13). The convergence of these to about 150 *m* is explained by the fact that at a specific scale (eighth decomposition level), almost all structures defining the virtual landslide have disappeared from the low-pass, and thus, the remaining structure is the regular plan. Its mean elevation is about 150 *m*.

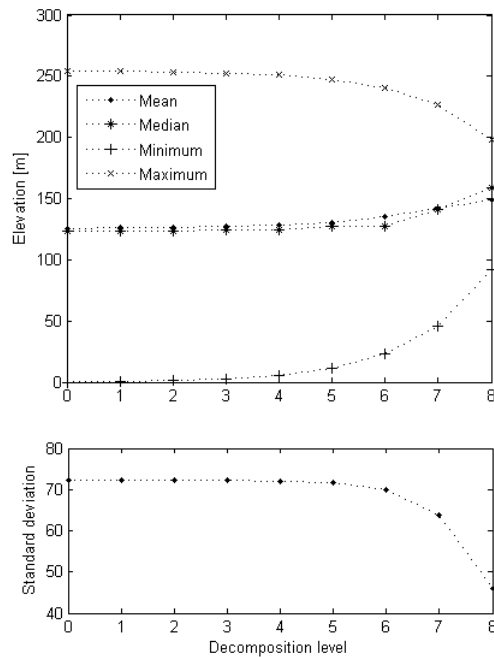


Fig. 4.13. Statistical indicators of elevation variation through the decomposition levels

An interesting fact is that the minimum and maximum also tend to the mean. This can be explained by the averaging properties of pixel generalisation. The further the surface is generalised, the more the values of the generalised pixels tend to the global mean value of the surface; and thus the generalisation smoothes the minimum and maximum (see section 4.2.7 for more details). Moreover, the standard deviation starts to decrease at the same levels as the other indicators, and it is the result of the mean convergence. The homogenization of the pixel values causes a decrease of the standard deviation. It is also noteworthy that, statistically and from the sixth level, the number of pixels is low, thus probably not any more representative. Finally, the standard deviation shows us when the number of pixels begins to be critical in combination with the structural composition tending to a plane.

4.2.6 Profiles on generalisations

Profiles on the low-pass results (the generalised DEMs) are used to monitor the trends of generalisation by following a one dimensional signal. The evolution of this one has the advantage of simplifying the visual interpretation of physical morphology modifications in a 2.5 dimensional surface. Three profiles (figure 4.14) were defined on the virtual DEM. First, they were analysed on the original DEM ($i = 0$), then on the different generalised DEMs ($i = 1, \dots, 8$). Only low-pass results are illustrated (see section 5.7.2 for high-pass filtered profiles).

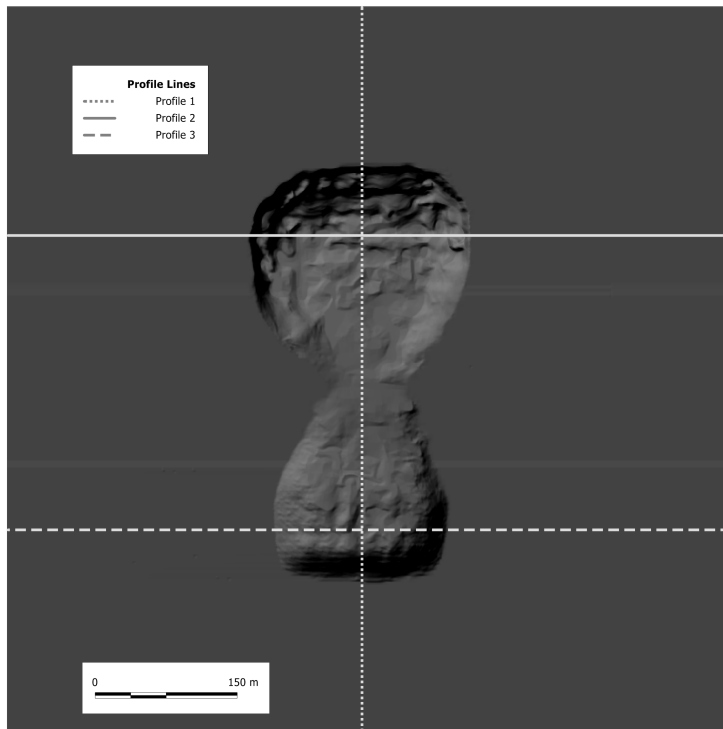


Fig. 4.14. Profiles on virtual landslide

The first profile goes through the landslide from the top to the bottom. This area is very disturbed and multiple folds are visible. The second profile is going through the scarp zone and the head zone. Finally, the third profile goes through the accumulation zone.

The results for profile 1 are given in figures 4.15 to 4.17 and, for profiles 2 and 3, they are given in appendix C.

The first profile illustrates perfectly the WT effect. As the decomposition level increases, the details remaining on the resulting surface diminish. There is a direct link between the generalisation process and the scale of features. Indeed, from level 0 to level 3, the effect does not seem apparent, but this is only due to the size of features transferred by the WT to the high-pass images. At the seventh level, even the biggest structures of the landslide have been filtered and there are only some traces of a feature located on the

former landslide structure. All seventh level profiles (figures 4.16, C.2 and C.5) illustrate this. At the next level, the resulting low-pass surface is the regular plane which was defined.

Global variance values on the profile (figure 4.17) show almost the same behaviour than global variance values computed over the whole surface (figure 4.13), but local scale-dependent structures modify slightly the median value. Because the profile follows the direction of the slope and goes through the landslide, the convergence value of the different indicators is also 150 *m*. This is logically different for the other profiles (appendix C, figures C.3 and C.6). For profile 2 convergence value tends to the maximum because the underlying structure is concave and suppressed at the seventh and eighth level. For profile 3, the inverse should happen, but because of the pixel averaging effect (see section 4.2.7), it is attenuated. Interestingly, the standard deviation remains stable longer than for the whole surface. If we refer to the profile's illustrations (figures 4.15 to 4.16), the overall landslide structure is present in the low-pass surface until the seventh level, exactly the level at which the standard deviation decreases.

The global statistics, as seen in figure 4.13 for the whole DEM and in figures 4.17, C.3 and C.6 for the profiles, show a break of linearity in their evolution through the decomposition levels: for the whole DEM, this break occurs at the 4-5 levels, for profiles 1 and 2 at level 4, and for profile 3 at level 3. These breaks are due to the suppression of all high-pass information which is included in the global shape of the analysed elements (DEM or profiles). Thus, the wavelet transform begins, at the next level and regarding these breaks, to have an effect on the global structures, therefore the transfer to the high-pass images of the global shape included in each type of element (DEM or profile). This induces a global flattening, thus an attenuation of the maximum or the minimum, regarding the type of shape (concave or convex) represented. An interesting observation in profiles 2 and 3 is the much more nuanced reduction of the standard deviation, while the other indicators are evolving in a less coherent way (figures C.3 and C.6). This is due to attenuation throughout the decomposition of the concavity and convexity in the respective profiles. Even if the structures are reversed in the profiles, the attenuation remains the same.

4.2.7 Slope to elevation distribution

In order to determine the effect of the wavelet transform on terrain smoothing, slope attenuation can be analysed according to the decomposition levels. A bi-variated representation (scattergram) is used to visualise slope attenuation regarding terrain elevation (Sulebak, 1999). Slopes were computed using the usual morphometric algorithms using a 3×3 window (Evans, 1979; Zevenbergen and Thorne, 1987).

Every data generalisation implies a data smoothing whatever its kind is, sound, image or, as in our case, a DEM. Figure 4.18 shows the smoothing effect of an average (or mean) filter applied to a simulated profile. In this case, the extreme value (local maximum) tends to diminish due to the smoothing effect of the average filter. In contrast to this simple method, the wavelet transform will tend to maintain structures until the frequency of this element matches to the decomposition level and, thus, the elimination (transition to the high-pass images) thereof. Moreover scale-specific structures should be retrieved in the high-pass images of each level.

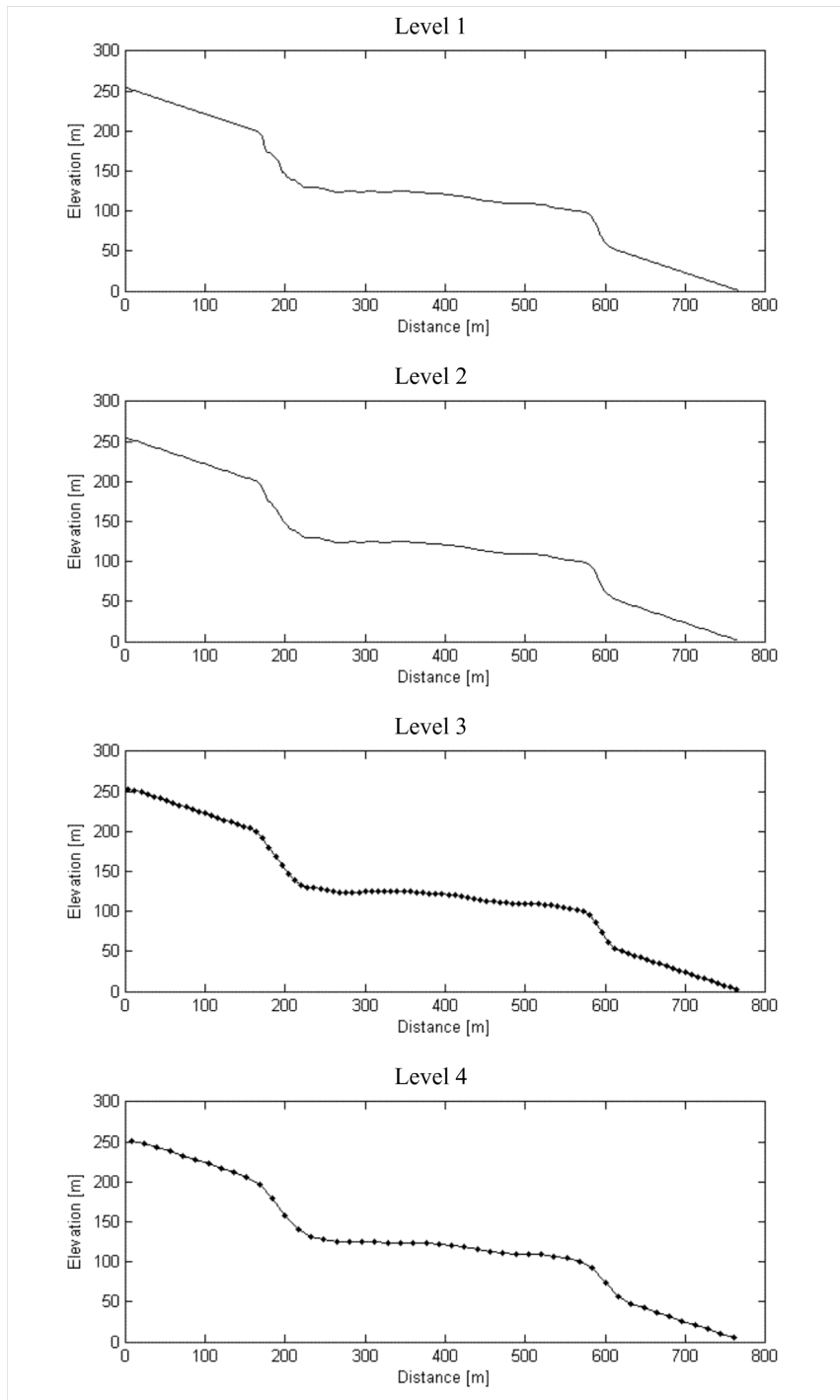


Fig. 4.15. Profiles 1, decomposition level 1-4 (Left side is the northern end of the profile and right side is the southern end of the profile.)

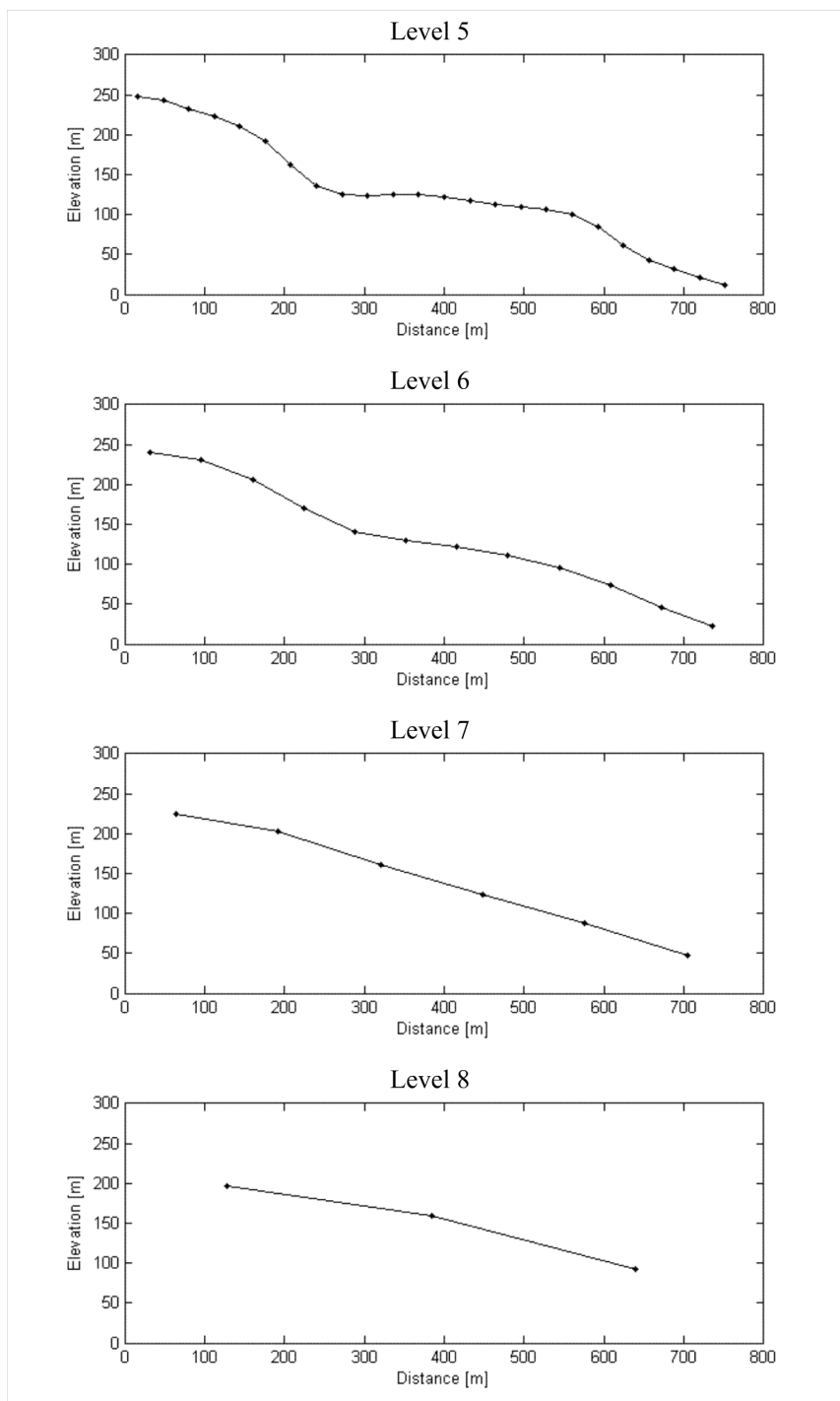


Fig. 4.16. Profiles 1, decomposition level 5-8 (Left side is the northern end of the profile and right side is the southern end of the profile.)

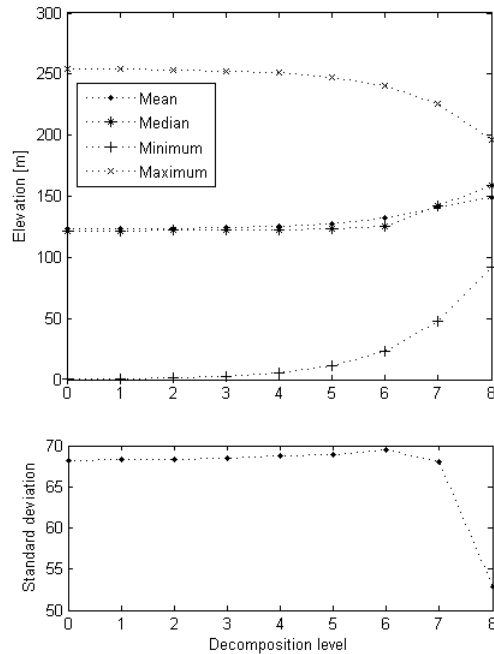


Fig. 4.17. Statistical indicators of elevation variation through the decomposition levels over profile 1

In figure 4.18, by taking the average filter, it is clear that the attenuation will not depend on the frequency (or the spatial distribution) of the extreme value, but only on the generalisation operator (the average).

The slope to elevation distributions were computed by using the original virtual DEM and its generalised low-pass results. Figure 4.19 shows only the results regarding visual context. the legends are different from one scattergram to another. This is due to the fact that the number of used occurrences diminishes when proceeding through the decomposition levels, because the DEMs are composed of less and less pixels.

The original DEM is composed of 768×768 pixels (589 824 pixels) and the first decomposition of 384×384 pixels (147 456 pixels). At each level, the number of pixels is divided by four. At the eighth level, only 3×3 pixels (9 pixels) remain for the analysis. Thus, there are not enough pixels left to make a bi-variated analysis at this level.

In figure 4.19, the results show two distinct facts: the inclined regular plane and the other structures composing the virtual landslide. The plane is represented by the horizontal lines in the scattergrams. Indeed, at each elevation, a certain number of pixels represent the plane. The rest of the values of the scattergrams represent the distribution of pixels forming the virtual landslide, and therefore its internal structures. The disappearance of the horizontal lines through the decomposition levels does not reflect the suppression of the plane, but it only indicates that the plane is represented by less and less pixels. Moreover, at each decomposition level, the regular inclined plane

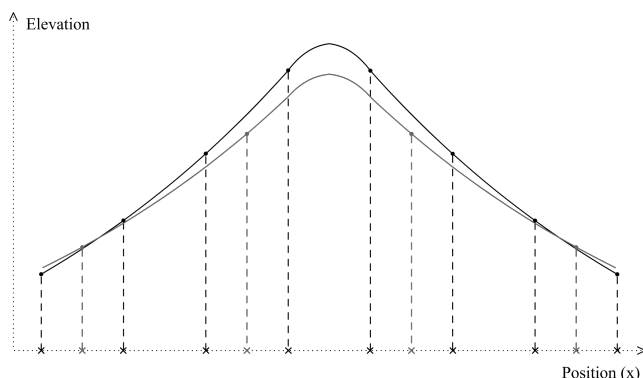


Fig. 4.18. Attenuation of the extreme value using average generalisation - Example on a regular profile. The black profile is the original shape of the structure and the gray profile is the dyadic downsampled result using an average filter.

is represented by specific elevations having a slope of 22° , but there are less and less values representing the plane, thus less and less values in the scattergrams. A general decline of slopes can also be identified. The suppression of steep slopes is due to the elimination of morphological structures at high scale, because these elements induce high gradients regarding their nature (high structural variability, and so, steep slopes). The appearance of higher slope values in levels 4 and 5 shows that the WT maintains extreme values and in combination with the reduction of local slope, thus more global slope, the gradients increase. Two high resolution pixels will usually have a lower slope gradient than two lower resolution pixels representing the same feature. If we would have used a increased convolution window size, this local slope effect would have been absorbed by this extending of the spatial window size.

To verify the stability between slope and elevation, a linear regression, weighted by the number of occurrences, was computed for each scattergram. By stability, we mean that the slope to elevation distribution should remain identical through all decomposition levels. The results are given in table 4.1 and figure 4.20. The latter does not take into account all the results for clarity. The regression (table 4.1) shows that the slope - elevation relation is quite stable and this despite the drastic reduction of the resolution. At the sixth decomposition level, the trend line begins to vary a lot (visual result, figure 4.20). One has to remember that the resolution of this decomposition level is $64 m$.

The seventh level shows that the plane's slope is also attenuated through the WT process. Thus the transform is not completely free from global terrain attenuation. One could ask if the generalisation should take into account a larger data set in order to avoid the effects of global structures. We nevertheless have to remember that for the seventh level and the eighth level, the resolution is very low (respectively $r = 128 m$ and $r = 256 m$).

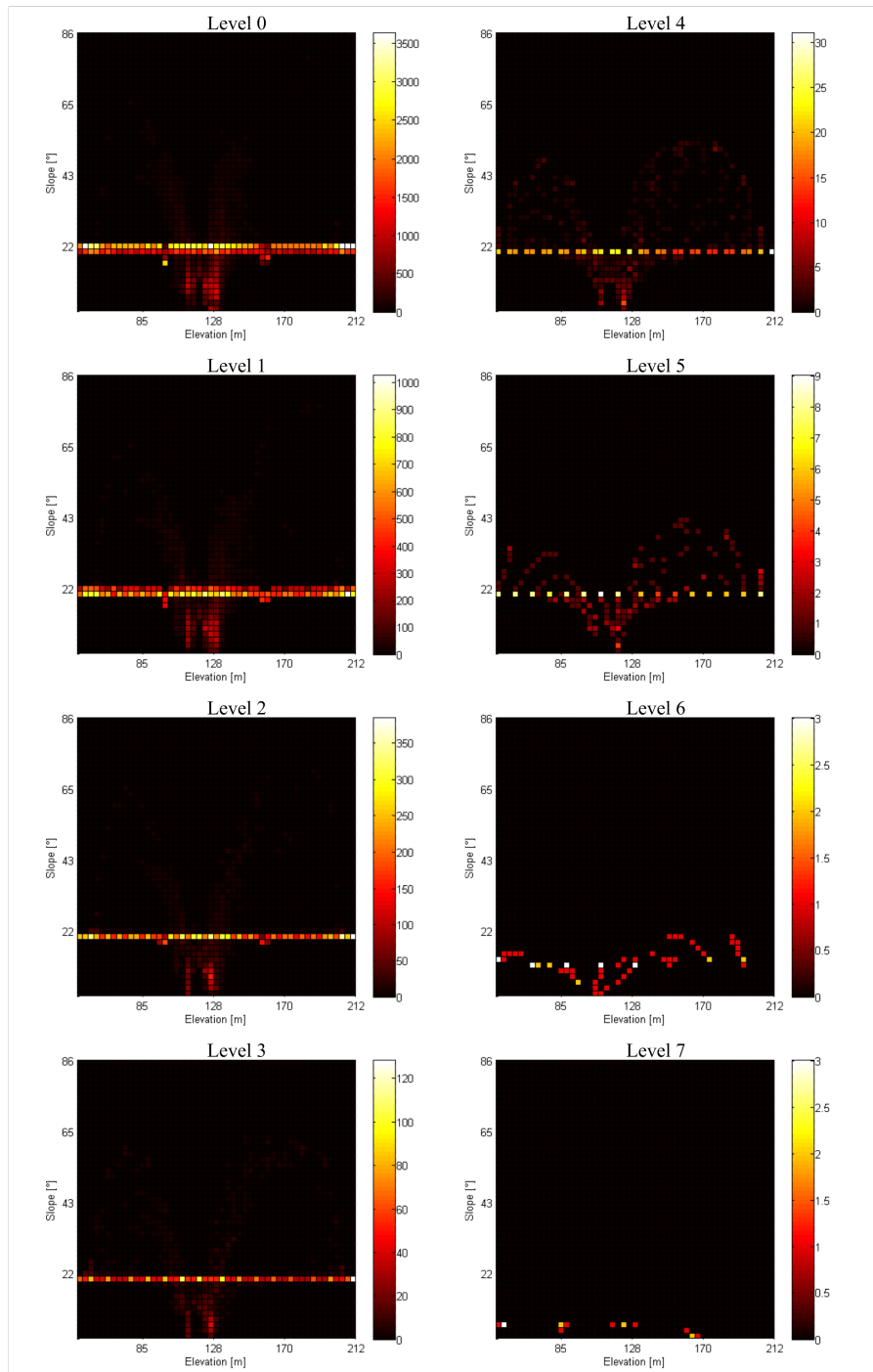


Fig. 4.19. Elevation - slope scattergrams for the different decomposition levels of the virtual landslide (The colour scheme goes from black (no value) to red, from red to yellow and from yellow to white. The colours represent the number of pixels in the 2D distribution.)

Decomposition level	β	$\arctan(\beta)$ [deg]	α
0	0.008	0.49	21.04
1	0.011	0.61	20.46
2	0.015	0.86	19.62
3	0.019	1.09	19.30
4	0.022	1.27	18.69
5	0.029	1.64	17.34
6	0.034	1.94	8.51
7	-0.024	-1.35	5.74

Table 4.1. Weighted linear regression on the scattergrams $Slope = \beta \cdot Elevation + \alpha$

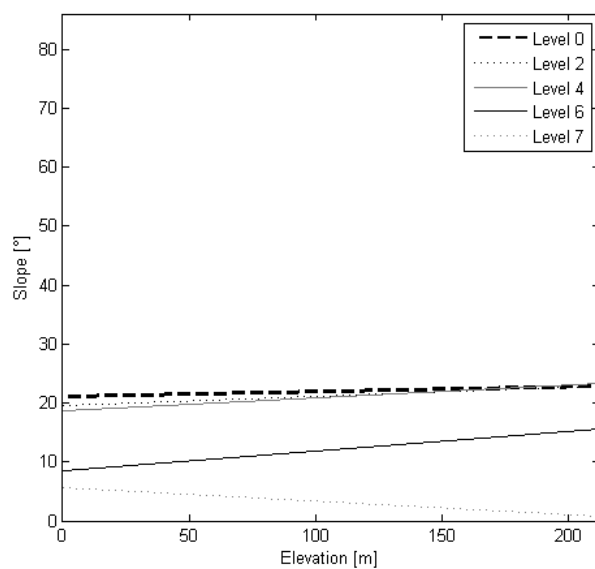


Fig. 4.20. Elevation - slope scattergrams regressions for the different decomposition levels. The x and y axis limits correspond to the limits of the scattergrams.

4.2.8 Local fractal validation

Spectral and fractal methods were used to characterize the kind of topography included in DEMs. Pike and Rozema (1975) and later Tate (1998) developed these methods in order to characterize the spectrum and fractal dimension of DEM profiles and DEMs. All encountered some methodological problems in the computation of either the power spectrum or of the fractal dimension. Some similar problems were mentioned by Braun (2002) in his attempt to do a spectral analysis over profiles. These problems are essentially due to the fact that topography is non-fractal (Sulebak, 1999). Related to this fact, Klinkenberg and Goodchild (1992) wanted to answer a fundamental question: “*Is the land a self-similar fractal?*” Their answer was actually partial, the value of the fractal dimension depending more on the used fractal-like model than on the type of surface.

Our analysis will not implement a direct spectral analysis of our surface generalisations, as the reduction of the power spectrum is completely linked to the definition of the WT filters, thus the wavelet and scaling functions. We chose to implement a local fractal indicator, the Hurst coefficient (Parker, 1997; Russ, 1994, 1990)(see appendix D for details). This is a local fractal-like method. It is a measure of the surface roughness. Through the generalisation process, we expect a reduction of the fractal dimension (or the Hurst coefficient), because our surface is a plane, on which local structures were applied. And therefore, these structures are removed by the WT, and the complexity of the resulting surface diminishes to tend to the original plane.

The larger the Hurst coefficient is, the smoother local variations are. In absolute, we would like to have the same global roughness for all decomposition levels, but different local roughness variations. The global variations were measured as a statistical analysis of the Hurst coefficients computed on the different decomposition levels of the virtual landslide (see table 4.2 and figure 4.21).

Decomposition level	Mean	Minimum	Maximum	Standard deviation	Number of values
0	1.05	0.00	3.60	0.12	568516
1	1.06	0.14	8.82	0.16	136900
2	1.07	0.21	3.38	0.16	31684
3	1.08	0.37	3.38	0.20	6724
4	1.09	0.42	2.55	0.27	1156
5	1.17	0.54	2.21	0.33	100
6	0.85	0.45	1.46	0.22	64
7	0.45	0.35	0.61	0.08	16

Table 4.2. Hurst coefficient results

As expected (table 4.2), the mean of the Hurst coefficients is stable throughout the decomposition levels. From the sixth level on, the mean seems to diminish. This indicates a less smooth surface. It may be induced by the reduction of the maximum starting at the fourth level (see figure 4.21). The maximum has an extremum at the first level due to undefined Hurst coefficients of the previous level (original image, see figure D.4 in appendix D for details). Due to the generalisation, it is normal that the minimum and maximum converge to the mean value, thus analysis seems to have a bias at these high levels: not enough pixels. A constant slope is an indicator of roughness stability throughout the decomposition levels, thus an indicator of the fractal composition of a multiscale surface analysis.

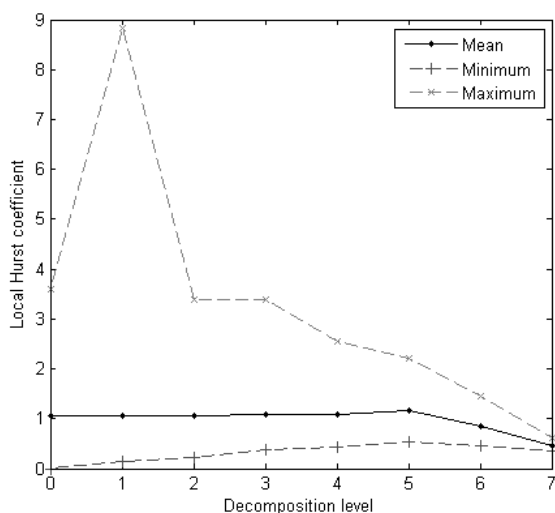


Fig. 4.21. Evolution of the Hurst coefficient through the decomposition levels

Remark concerning the local fractal indicator

As we use a multiscale space computed using the WT, we could directly analyse the energy of the wavelet coefficients in order to calculate the decrease of the wavelet energy spectra. This was developed on the basis of fractional Brownian motion⁵(Flandrin, 1989, 1992). Thus, the method, which we apply, is linked to fractals, but it is an analysis of the local variations in a circular 7×7 window around each pixel. It does not analyse the global energy decrease of the WT coefficients like Flandrin's methodology does. This could show us the decrease of the energy through the decomposition levels and show us when our model is not self-similar any more.

⁵ Fractional Brownian motion is a model for modelling self-similar phenomena (Nicolis *et al.*, 2006). Brownian motion is a mathematical description for the modelling of a random movement of a particle. The fractional Brownian motion is represented by a self-similarity indicator called the Hurst exponent.

4.2.9 Global spatial autocorrelation

For the analysis of the WT generalisation effect, Moran's coefficient and Geary's ratio⁶ were used (Anselin, 1995, 2005). These are spatial autocorrelation indicators. According to Goodchild (1986), the definition of spatial correlation is: “the degree to which objects or activities at some place on the earth's surface are similar to other objects or activities located nearby”. It is related to Tobler's first law of geography (Tobler, 1970; De Smith *et al.*, 2008). In the present study, we are going to compare variables which are the pixel values of a regular grid. For this purpose, the present work is inspired by Qi and Wu (1996). They generalised elevation models using an average function and computed spatial autocorrelation over these different scales. We will do the same, but use the WT instead of an averaging function.

Moran's coefficient values are defined between -1 and 1 . Where negative values indicate negative spatial autocorrelation and positive values indicate positive spatial autocorrelation. For Moran's coefficient, a zero coefficient indicates that the analysed surface is completely random.

Geary's ratio is not defined on the same interval. It is defined between 0 and 2 . Zero means that data is completely positively spatially autocorrelated. At 1 , the analysed surface is completely random and at 2 , completely negatively autocorrelated.

Looking at the values of Moran's coefficient (figure 4.22) shows that the results are extremely good, although the results may seem confusing. Indeed, it is not the wavelet smoothing effect which is illustrated here, but the reduction of the number of pixels. It induces more pronounced direct neighbouring effects (queen contiguity). Thus, two neighbouring pixels will have less similar elevations, but a greater spatial extent (lower resolution). In this case, Moran's coefficient does not illustrate a smoothing effect, but the increase of elevation differences between neighbouring pixels. As expected, they indicate that the high original spatial autocorrelation is reduced through the decomposition. This clearly indicates the generalisation process. However this reduction of spatial autocorrelation is not linear (like the resolutions of the decomposition levels). Thus level 0 is not so different from level 1 , but level 6 is a lot more different from level 7 . At level 8 , only the inclined plane is left on the surface, thus the spatial autocorrelation tends to zero (due to the definition of Moran's coefficient, i.e. $x_i - \bar{x}$ tends to zero). Unlike Moran's coefficient, Geary's ratio is less sensitive to the information reduction and does not indicate the generalisation process well. Therefore, it does not seem appropriate for the verification of the generalisation process. Geary's ratio is more sensitive to local autocorrelation unlike Moran's coefficient which is more sensitive globally. In fact, these indicators show exactly what was expected: a transform which globally reduces the resolution, but regarding the reduction of the frequency space and not the spatial one.

⁶ Moran's coefficient and Geary's ratio were computed using their definition in Qi and Wu (1996): $Moran = \left(\frac{n}{\sum_{i=1}^n \sum_{j=1}^n c_{ij}} \right) \frac{\sum_{i=1}^n \sum_{j=1}^n c_{ij} (x_i - \bar{x})(x_j - \bar{x})}{\sum_{i=1}^n (x_i - \bar{x})^2}$, $Geary = \left(\frac{n-1}{2 \sum_{i=1}^n \sum_{j=1}^n c_{ij}} \right) \frac{\sum_{i=1}^n \sum_{j=1}^n c_{ij} (x_i - x_j)^2}{\sum_{i=1}^n (x_i - \bar{x})^2}$, where n is the total number of pixels, x_i and x_j are the values of pixels i and j . \bar{x} is the mean value of all pixels and c_{ij} is the connectivity of pixels i and j . If these are adjacent, the connectivity has value 1 , else 0 . We used the queen contiguity (all eight neighbours) scheme for the connectivity. Thus, the eight pixels surrounding the analysed pixels have a connectivity of 1 with this one.

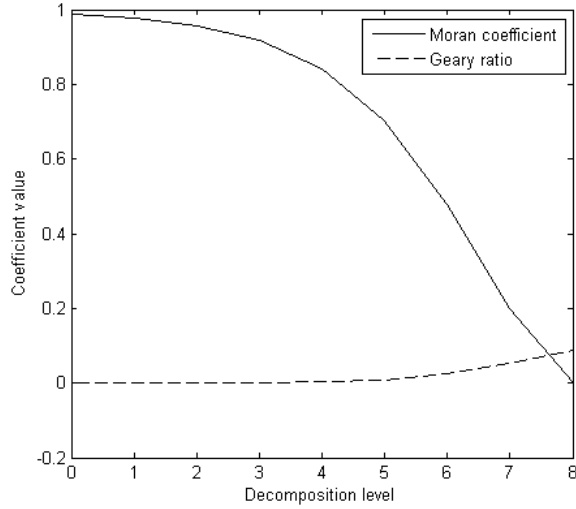


Fig. 4.22. Evolution of Moran's coefficient and Geary's ratio through the decomposition levels

4.3 Wavelet coefficients

As seen in previous sections and using Mallat's algorithm (Mallat, 2000), a wavelet analysis gives four images out of the original one (figures 4.4 and 4.6). Until now, we have analysed the low-pass results of our decomposition scheme. From one level to another, some information is transferred to the next low-pass DEM, but part of this information is transferred to the so-called high-pass coefficients.

For DEM multiscale analysis, we always use the low-pass filtering result, corresponding to $c_{i+1}[2\mathbf{k}]$ in figure 4.4. Likewise, all the analysis were done regarding this information. This is the main piece of information retained for the proceeding of the next iteration in the decomposition process. Also, we know that the wavelet decomposition is one of the most adaptive way to decompose a signal. It will always exclude a part of the initial information contained in the signal. If we analyse the information contained in the three parts $d_{h,i+1}[2\mathbf{k}]$, $d_{v,i+1}[2\mathbf{k}]$ and $d_{d,i+1}[2\mathbf{k}]$, we hope to find the scale corresponding features. The detail coefficients surely contain information of the used decomposition resolution. It seems logical that a detail coefficient at a low resolution cannot contain specific high resolution information. The contrary is not as explicit as that, because of the pyramidal effect of the wavelet transform.

4.3.1 Coefficient filtering

All elements of the wavelet transform ($c_{i+1}[2\mathbf{k}]$, $d_{h,i+1}[2\mathbf{k}]$, $d_{v,i+1}[2\mathbf{k}]$ and $d_{d,i+1}[2\mathbf{k}]$) can be transformed before the wavelet synthesis. As examples, the transformation may consist of: suppression of one or more of the resulting surfaces, enhancement of specific coefficients, soft and hard coefficient thresholding. In imagery, most of those transformations are noise reduction operations.

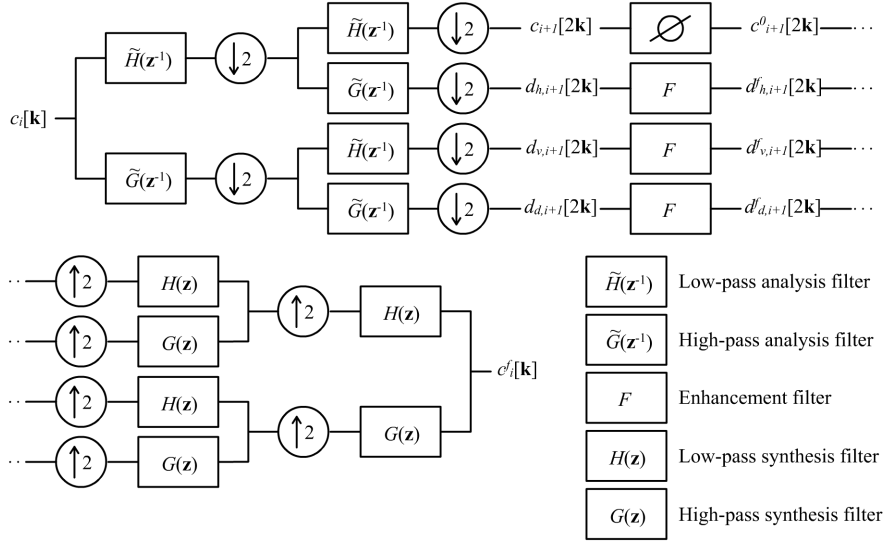


Fig. 4.23. Filter bank for wavelet coefficients filtering for one decomposition level, adapted from Unser (2001).

The following elements compose the proposed filter bank (figure 4.23):

- $c_i[\mathbf{k}]$: low-pass surface, i^{th} decomposition level
- $c_{i+1}[2\mathbf{k}]$: low-pass surface, $i + 1^{th}$ decomposition level
- $d_{h,i+1}[2\mathbf{k}]$: high-pass surface, horizontal coefficients, $i + 1^{th}$ decomposition level
- $d_{v,i+1}[2\mathbf{k}]$: high-pass surface, vertical coefficients, $i + 1^{th}$ decomposition level
- $d_{d,i+1}[2\mathbf{k}]$: high-pass surface, diagonal coefficients, $i + 1^{th}$ decomposition level
- $\tilde{H}(\mathbf{z}^{-1})$: low-pass analysis filter (given by the third order B-spline base function)
- $\tilde{G}(\mathbf{z}^{-1})$: high-pass analysis filter (given by the symmetric dual wavelet)
- $H(\mathbf{z})$: low-pass synthesis filter (complementary of $\tilde{H}(\mathbf{z}^{-1})$, see section 4.1.2)
- $G(\mathbf{z})$: high-pass synthesis filter (complementary of $\tilde{G}(\mathbf{z}^{-1})$, see section 4.1.2)
- $c_{i+1}^0[2\mathbf{k}]$: low-pass surface, $i + 1^{th}$ decomposition level, all coefficients are set to zero
- $d_{h,i+1}^f[2\mathbf{k}]$: high-pass surface, horizontal filtered coefficients, $i + 1^{th}$ decomposition level
- $d_{v,i+1}^f[2\mathbf{k}]$: high-pass surface, vertical filtered coefficients, $i + 1^{th}$ decomposition level
- $d_{d,i+1}^f[2\mathbf{k}]$: high-pass surface, diagonal filtered coefficients, $i + 1^{th}$ decomposition level
- $c_i^f[\mathbf{k}]$: low-pass surface reconstructed by the inverse wavelet transform, i^{th} decomposition level
- F : filter applied to the $i + 1^{th}$ decomposition level high-pass coefficients.

Mallat (2000) defined this filter bank for images (or 2D surfaces). In figure 4.24 is illustrated, as example, a two level wavelet filtering transform on a DEM. The operational steps are:

- WT: the DEM is analysed using the wavelet transform until the second decomposition level ($i = 2$). Seven new surfaces are computed, two horizontal high-pass surfaces, two vertical high-pass surfaces, two diagonal surfaces and one low-pass surface.
- F: all the low-pass surface coefficients are set to zero, the six high-pass surfaces filtered using the value of F for the i^{th} decomposition level.
- IWT: using the inverse wavelet transform (IWT), a new surface is computed, containing only the filtered high-pass information, but at the original DEM resolution.

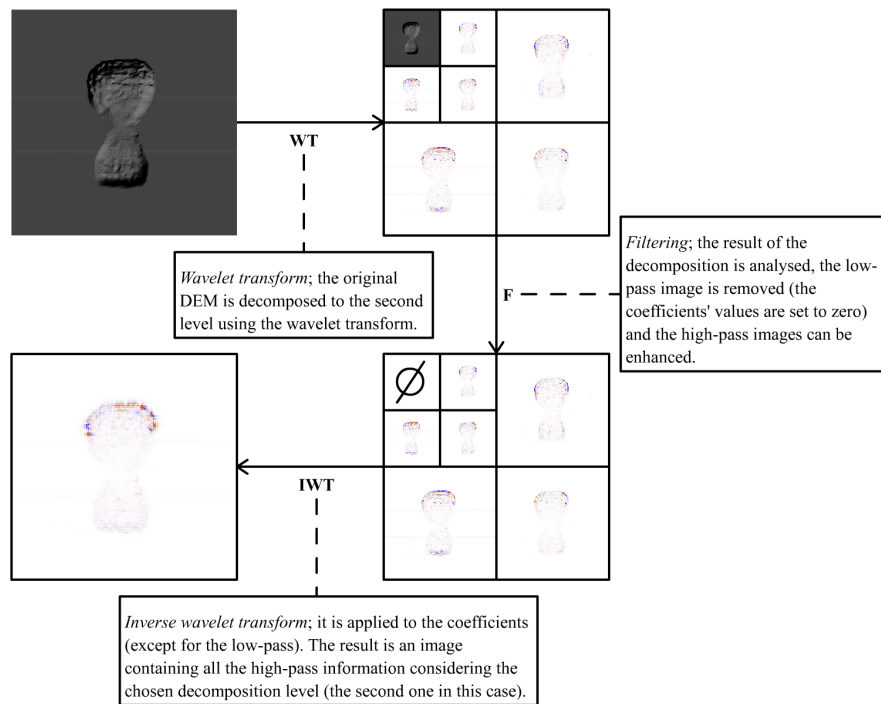


Fig. 4.24. Wavelet transform (analysis), enhancement by coefficient filtering, inverse wavelet transform (synthesis) - example using a two level decomposition

Given three different spectral reconstructions, three filters were applied to the high-pass coefficients of each decomposition levels. As we do not want to enhance the levels regarding main directions (east-west and north-south), all the detail coefficients (by detailed coefficients, we mean the three high-pass images given by $d_{v,i}[\mathbf{k}]$, $d_{d,i}[\mathbf{k}]$ and $d_{h,i}[\mathbf{k}]$) of one level have been enhanced using the same factor (see figure 4.25 for specific factors). The first filter is set to one, thus no enhancement is undertaken. The second one is an attempt of enhancing linear breaks in the DEMs, thus high frequency information. It is determined by trying different combinations of filter parameters. It shows that high structural importance is given to the second level. The last filter is determined using a wavelet filter⁷.

⁷ $F_i = 1/(0.75^{-i})$ where i is the decomposition level. This is a high frequency enhancing filter, which is largely used in the image processing community.

These filters are used to highlight the structural nesting, i.e. to highlight certain types of structures throughout the decomposition levels. Their specificities were developed to illustrate the following features of the DEM:

1. The first filter is not really one. It is simply the reconstruction of high resolution images using the high-pass coefficients. This allows us illustration of the separation of structures that occurs using the WT.
2. The second filter sets all the coefficients of the first decomposition level to zero. By hypothesis, we suggest that this level contains only noise or terrain micro-structures which are not interesting. A lot of importance (or energy) is given by the filter to the two next levels. For the five last levels, the filter values decrease progressively. Consequently, the structures induced by the landslide will be enhanced. The landslide dynamic has indeed induced a series of cracks, tractions and materials flows, which we hope to illustrate by giving them more importance through the filter values.
3. This filter should allow us to see if the DEM acts as an image using the WT or whether, given its characteristics, it can be compared to a grayscale image. The filter values are decreasing regarding the decomposition levels. Thus, they give less and less importance to the information contained in the successive levels. This filter is designed similarly as the second filter, but the differences between the levels are less abrupt.

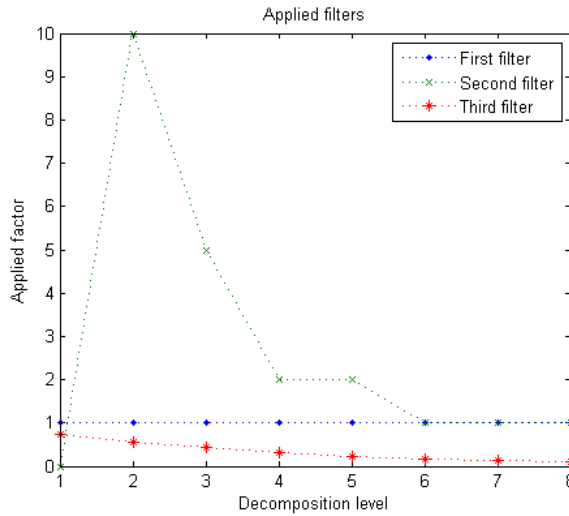


Fig. 4.25. Factor F_i applied to the high-pass coefficients before synthesis

The analysis of the signal-to-noise ratio⁸ (SNR)(figure 4.26) on the decomposition levels shows the proportion of the original signal (or DEM) reproduced

⁸ Independent Signal-to-Noise ratio:

$$SNR = 20 \cdot \log_{10} \left(\frac{\sqrt{\frac{1}{(n \cdot m - 1)} \cdot \sum_{i=1}^n \sum_{j=1}^m (I_{original,i,j} - I_{original})^2}}{\sqrt{\frac{1}{(n \cdot m - 1)} \cdot \sum_{i=1}^n \sum_{j=1}^m (I_{noise,i,j} - I_{noise})^2}} \right)$$
, where $I_{original}$ is the original DEM, I_{noise} are the synthesised coefficients, n and m are respectively the height and width of the DEM.

by the coefficient images of the different decomposition levels. As long as the SNR is not equal to zero (0 dB⁹), the original DEM is not entirely reproduced. Indeed, the wavelet transform reproduces only partially the frequency space at each decomposition level (figure 4.2). The remaining frequencies are within the frequency space of the low-pass image, represented by its base function φ (figure 4.2).

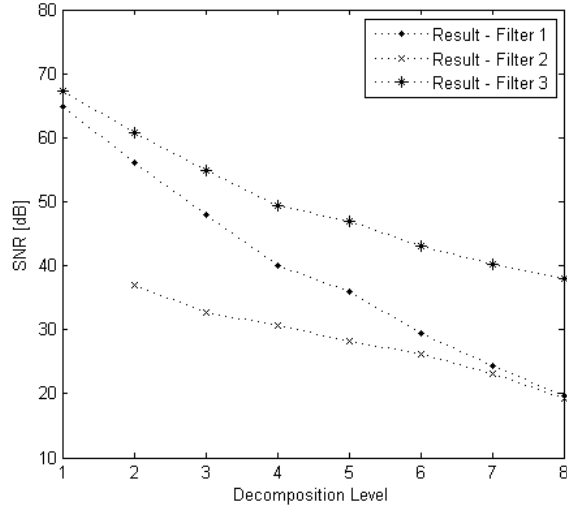


Fig. 4.26. SNR of the decomposition levels for the applied enhancement filters on the virtual landslide

For the second enhancement filter, the first decomposition level is not represented because the first filter factor F_1 is equal to zero. Therefore, the first high-pass synthesised image is composed of zeros which would correspond to an infinite noise. The slope of the second filter factors (figure 4.26) is less steep near the last decomposition levels as the base transform (first filter). This is due to the filter's definition which enhances more the high frequencies than the low frequencies.

As seen, the wavelet transform creates multiscale surfaces whose pixels values are the wavelet coefficients. The adjustment of the wavelet on the local frequencies of the terrain is reflected by these values. Eight decompositions were computed with following resolutions: 2 m, 4 m, 8 m, 16 m, 32 m, 64 m, 128 m and 256 m. All decomposition levels were filtered using the filter coefficients defined previously (see section 4.3.1).

All enhancement and filtering results are illustrated in appendix E. In the higher levels (6-8), the enhancement filter effect becomes visible, high frequency details become visible in the more general structures. As the usual detail reconstructions (Filter 1) give a good overall result, the filtered versions

⁹ Usually, the SNR ratio is given in decibels (dB), because it is mainly used in sound frequency analysis, but this unit does not make sense in our case. Consequently, the SNR shall be used as a dimensionless indicator and only relative values will be compared.

of these reconstructions give additional information on the internal micro-structures of more global structures. Again, the definition of global structures versus micro-structures is completely dependent on the decomposition level taken into account. Thus, what are called global structures are the biggest structures one can visually determine looking at the filtered or raw coefficient reconstructions.

Looking at the defined filters (Filter 2 and 3), it seems that the most effective one is not the usual image processing filter (Filter 3), but the filter defined empirically (Filter 2). The values of this filter strongly enhance high frequencies, regarding the values of the filter for higher levels. As the figures illustrate (figures E.5 to E.8, appendix E), high frequency information is a very good indicator in understanding how global structures (or low frequency information) are formed and what are their inherent relations.

5. Case study

5.1 Introduction to the case study

All elements, information and indicators computed and analysed in the previous sections are valid for the virtual landslide which was defined. In order to analyse and compare the effect of the WT filtering, the process was applied on a “real” DEM. The analysis includes the following indicators: global statistical indicators, profiles analysis, slope to elevation distribution, local fractal indicator, global spatial autocorrelation and wavelet coefficient analysis and filtering. A DEM, including a recent landslide located in the Val de Travers - Canton of Neuchâtel - Switzerland, in the village of Travers, is used for this purpose. For a complete geological and data description of the used DEM, refer to appendix F.

Local analysis should highlight the links between the wavelet transform and the results of a visual expert morphological analysis using the next elements: a phenomenon map (Krähenbühl, 2007), the 1 *m* DEM, the geological map and an aerial photography. The DEM has a 1 *m* original resolution and a size of 768×1280 pixels. Global indicators were computed, profiles analysed and different kinds of wavelet filtering applied. This was done in order to assess the multiscale capabilities of wavelet transforms in DEM analysis.

The validation of the applied methodology and of the WT is done by comparison with the results obtained using the virtual landslide, as we do not have any other comparison material or method. Indeed, we have to validate the recognised structural elements and variations through, either expert geological knowledge¹, or through terrain observations (like the work done by Krähenbühl (2007)). The virtual landslide gives us a first approach to understand the complex structural modifications induced by the WT and the underlying transform.

5.2 Global statistical indicators

Using the same indicators as for the virtual landslide (see section 4.2.5) will help to understand the effect of WT process on the Travers DEM.

Global indicators of this DEM show a strong decrease in the surface maximum through the decomposition levels (figure 5.1). Surprisingly, the mean, median and minimum do not seem to be influenced by this decrease. The only explanation is that this decreasing effect is due to the attenuation explained

¹ The expert geological analysis and critics are done in collaboration with Dr. P. Turberg from the laboratory of engineering and environmental geology (GE-OLEP) at the École Polytechnique Fédérale de Lausanne - Switzerland.

in section 4.2.7. Indeed, the minimum is not converging to the mean as much as for the virtual landslide. This is certainly due to the fact that the DEM mainly contains a flat region which has almost the minimum elevation. That is also why the median is smaller than the mean. The standard deviation has the same behaviour as for the virtual DEM. Thus, even on a DEM, which was produced using measures of the topographical elevation, the standard deviation behaves about the same way as for an artificial one.

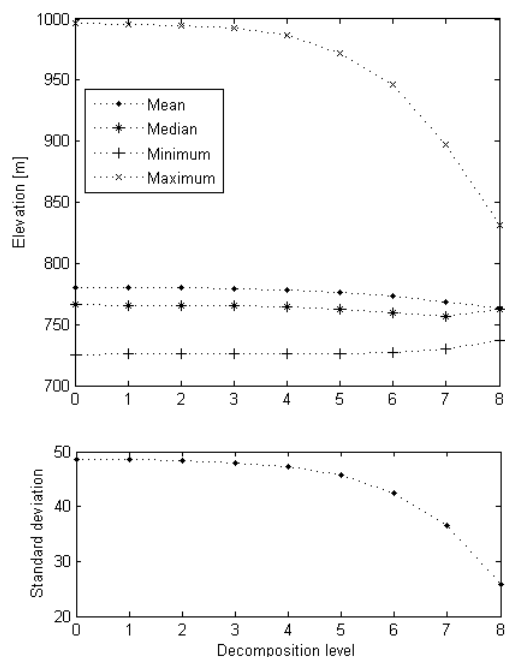


Fig. 5.1. Statistical indicators of elevation variation through the decomposition levels

5.3 Profiles on generalisation

The first profile (figure 5.2) goes through the landslide which is part of the case study. This area is very disturbed and multiple folds are visible. On the contrary, the second profile is on a fairly homogeneous meadow area, constituted of a hill. The last one is located on a mound on which there is an artificial gravel-pit. This one was chosen to see at which scale - or decomposition level - it will be “absorbed” by the wavelet and transferred to the high-pass images, thus the disappearance from the low-pass image or the DEM.

Profile 1

This profile (figure 5.3), despite its location through the landslide, is quite homogeneous. One has to take into account that the variations are at a finer



Fig. 5.2. Three profiles used for the analysis, DEM©SITN

Profile	Azimet $^{\circ}$	Length m
1	312	455
2	324	358
3	90	460

Table 5.1. Profile specifications

scale than the scale of representation (1 m resolution on 455 m). Global variations on the profiles show a general reduction of elevation (uphill to downhill). In figure 5.4, the mean, median, minimum and maximum variations through the decomposition levels are illustrated. All these values tend to tail off. The minimum and maximum values tend to converge to the mean. We will try to assess this in the other profiles.

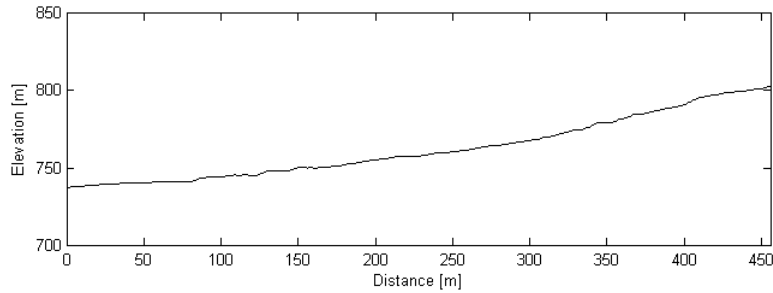


Fig. 5.3. Profile 1, original DEM ($r = 1 m$), (Left side is the north-western end of the profile and right side is the south-eastern end of the profile.)

Illustrations of the same profile on the generalised surfaces are in appendix G (figures G.1 and G.2). As in the virtual landslide, there is an evident attenuation of the maximum, but on this profile, the minimum stays stable. Because this profile is very regular, even if it is going through the landslide, the wavelet effects still remain hard to apprehend.

Overall, the statistical indicators of profile 1 are similar to the general statistical indicators of the DEM.

Profile 2

Figure 5.6 shows mean and median values with a tendency to lower from the sixth level on. By verifying the shape of the profiles (figure 5.5), the transition from the sixth to the seventh level corresponds to the suppression of the hill in the DEM, and thus lower elevations. The profile tends to be a line (see figures G.3 and G.4 in appendix G). As before, the mean, median, minimum and maximum values converge. The standard deviation begins to decrease at the same level at which the hill suppression occurs.

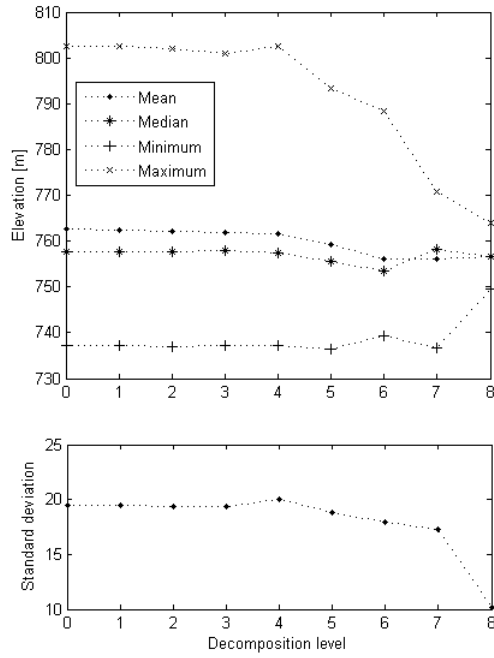


Fig. 5.4. Statistical indicators, profile 1

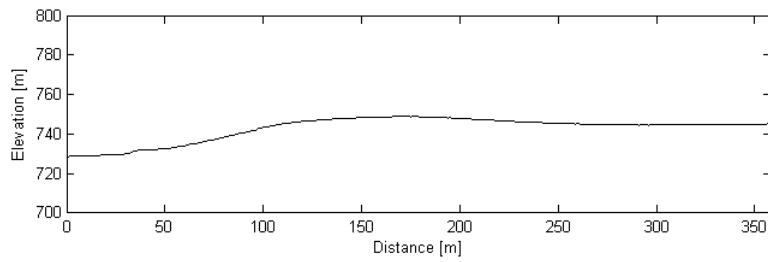


Fig. 5.5. Profile 2, original DEM ($r = 1 m$), (Left side is the north-western end of the profile and right side is the south-eastern end of the profile.)

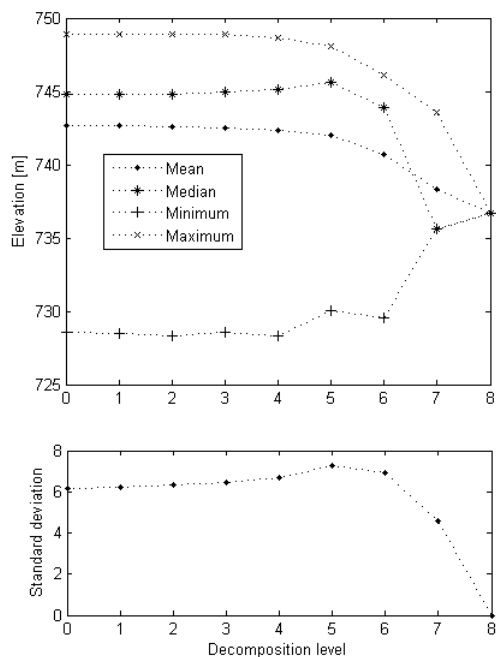


Fig. 5.6. Statistical indicators, profile 2

Profile 3

This last profile contains the highest elevation variations (figure 5.7). The figure shows that the gravel-pit is visible until the third decomposition level, and the mound, containing this gravel-pit, disappears from the low-pass at the seventh decomposition level (figures G.5 and G.6 in appendix G).

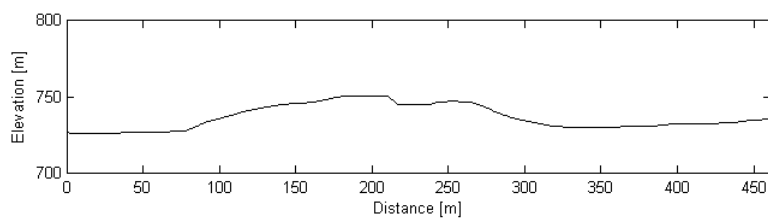


Fig. 5.7. Profile 3, original DEM ($r = 1\text{ m}$), (Left side is the western end of the profile and right side is the eastern end of the profile.)

In figure 5.8, the variations (mean, median, minimum and maximum) do not illustrate these structural suppressions. The maximum value begins to diminish effectively at the third level, but it is difficult to see the real impact

of the subsidence on these values. Similarly, the strong increasing of the maximum at the seventh level is difficult to explain. A possible explanation is that the wavelet was adjusted to a morphological element at a bigger scale than the profile 3, thus it is invisible on it. The standard deviation decrease shows clearly the mound suppression, and it increases at the eighth level because of the adjustment of the WT to the general slope. Thus, the range of the elevation values is larger.

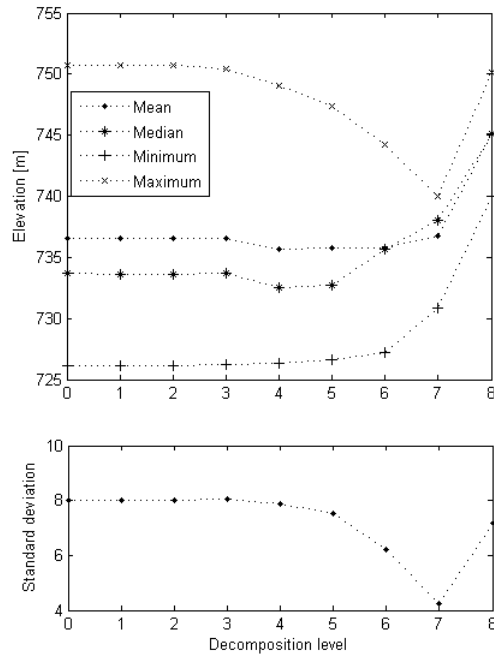


Fig. 5.8. Statistical indicators, profile 3

General remarks concerning profiles

The three analysed profiles show that landforms are space dependent and that the WT is a selective process, regarding the frequency domain, of terrain generalisation and simplification. Indeed, it is the analysis of the remaining detail coefficients which will give the frequency domain discretization and, thus, the extracted feature of a specific scale interval.

As we have already seen in section 4.2.6 for the virtual DEM, statistical indicators for the Travers DEM, which are calculated from the whole DEM or in profiles, show again the same type of behaviour. The local maxima of the DEM are indeed reduced from the third decomposition level, that is to say from a resolution of eight meters. In the first profile as well as in the second, it only begins at the fifth level. Moreover, it appears that the indicators are much less stable in the second profile than as in the others. A priori, nothing in the shape of the profile suggests that behaviour. It is in fact the level at which the hill (located between 75 *m* and 175 *m* in figure

5.5) is removed from the low-pass resulting DEM. In the low-pass of the next level, the profile represents only an inclined plane and not any more the hill (figure G.4, appendix G). Almost the same behaviour is visible in the third profile. However, the linearity break occurs more rapidly due to the progressive elimination of the gravel-pit through the levels. The instability of the indicators from the sixth level indicates the total suppression of the hill.

The indicator analysis shows that it is possible, using simple indicators, to detect the suppression of *anomalies* related to a scale. By *anomaly*, we mean that at some levels, certain morphological types are removed from the low-pass resulting DEMs. This suppression is completely dependent on the scale of the morphological element, and thus, in a perspective related to wavelets, on the frequency space in which these elements make sense and are defined.

5.4 Slope to elevation distribution

Compared to the virtual landslide, the Travers DEM is not composed of a regular inclined plane. Thus, the slope to elevation distribution does not illustrate a horizontal trend like the virtual landslide. The aim is rather to verify that the main slope of the distribution's regression is not attenuated too much. Indeed, there is a much better slope to elevation stability (table 5.2) for this DEM than for the virtual landslide (figures 4.19 and table 4.1). The regression α parameter indicates that the general elevation is still attenuated, but less than for the virtual landslide. Mainly because of the structural differences, there is no regular plane in the Travers DEM and, thus, the WT does not induce as much bias as on the virtual landslide. The plane of the virtual landslide was influenced by the shape of the wavelet at strong break limits, like the transition from a regular plane to the virtual landslide.

Decomposition level	β	$\arctan(\beta)$ [deg]	α
0	0.13	7.24	6.36
1	0.12	7.02	6.28
2	0.12	6.89	6.19
3	0.12	6.83	5.83
4	0.12	6.85	5.51
5	0.12	7.00	4.73
6	0.14	7.87	3.96
7	0.16	9.04	1.54

Table 5.2. Weighted linear regression on the scattergrams $Slope = \beta \cdot Elevation + \alpha$ for the Travers DEM

Similarly to the virtual landslide, the number of different values in the scattergrams is reduced by increasing the decomposition level. Thus, from

a heterogeneous surface, the decompositions tend to a regular surface. The scattergram values are more and more distributed around the linear regression values, consequently the residuals of the linear regression are becoming smaller and smaller. This information shows that the surface complexity and roughness decrease through the WT process, thus we go from high-detailed information to more and more generalised morphologies. In fact, this effect is also observed in the previous section (section 5.3), but it has not been clearly distinguished until now.

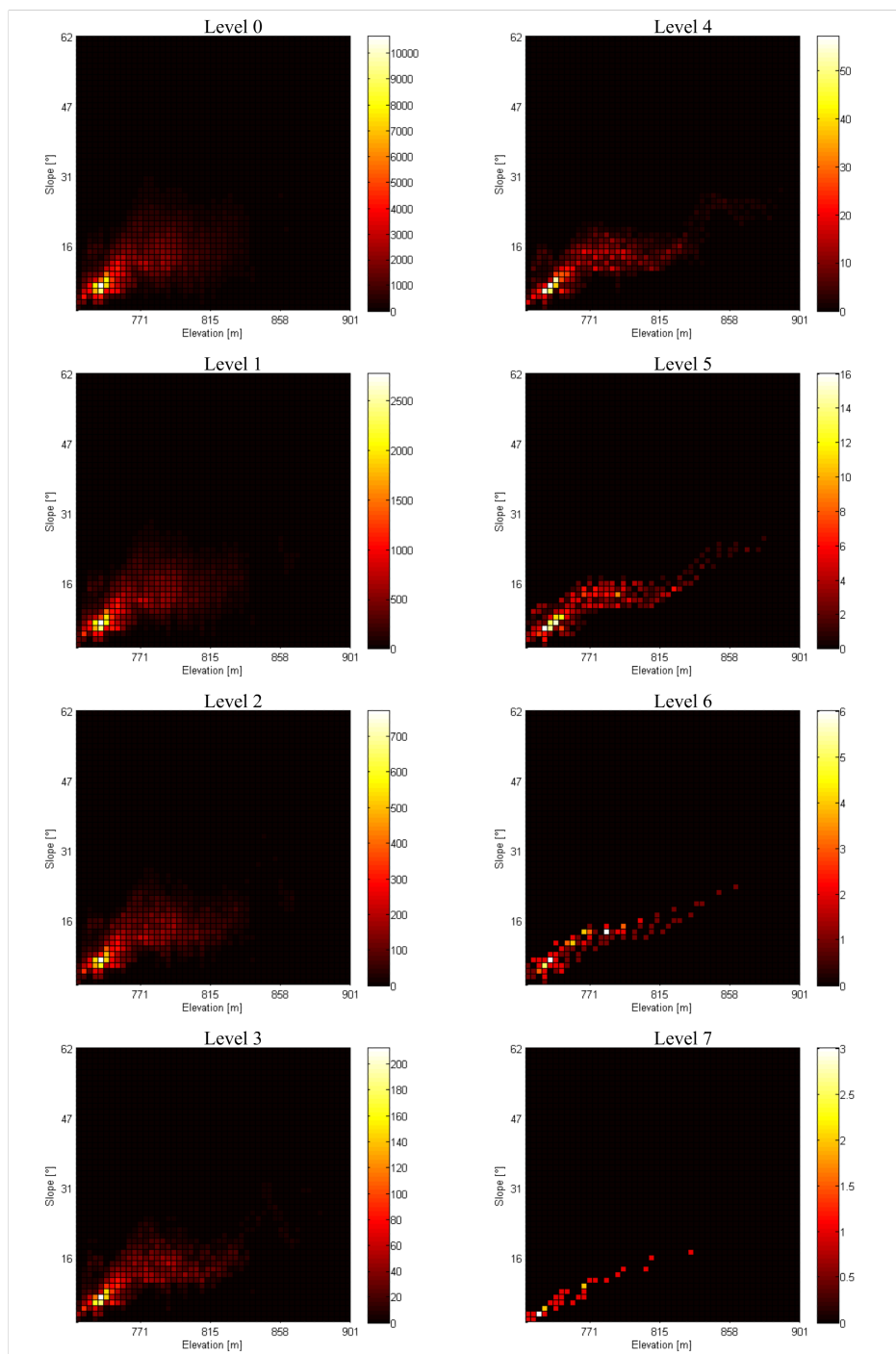


Fig. 5.9. Elevation - slope scattergrams for the different decomposition levels for the Travers DEM

5.5 Local fractal indicator

Again, the Hurst coefficient (see appendix D) was computed for the Travers DEM. Visual results are given in figure 5.11. There were some undetermined pixels in the northern part of the DEM due to the flat neighbouring effect induced by filtering buildings. The global DEM coverage was reduced in order to take into account border effects.

The statistical analysis of the Hurst coefficient (table 5.3) shows that there is a strong reduction of the maximums by increasing the decomposition levels. These are divided by a factor of two from the original DEM (level 0) to level 8. Likewise, the minimums are not so much influenced and the means stay almost constant. Explanation for this is, again, the roughness reduction through the decomposition level as we saw for the analysis of the virtual landslide.

Decomposition level	Mean	Minimum	Maximum	Standard deviation	Number of values
0	1.07	0.00	3.57	0.18	524288
1	1.07	0.15	3.06	0.18	131072
2	1.07	0.19	3.05	0.17	32768
3	1.07	0.58	2.24	0.15	8192
4	1.07	0.54	2.19	0.17	2048
5	1.05	0.41	1.77	0.18	512
6	1.03	0.58	1.69	0.20	128
7	0.93	0.38	1.63	0.32	32

Table 5.3. Hurst results for the Travers DEM

The stepwise statistics effect (figure 5.10) shows clearly the reduction of structural diversity and landforms standardization due to the WT process. The wavelet seems to be more adapted to the natural or “real” DEM than to the virtual landslide, because of the increased complexity (no regular plane) and a structural roughness having a shape which matches more to the wavelet shape.

If we compare the standard deviation evolution between the virtual landslide and the Travers DEM result (figure 5.12), we see that for both types of surface, it tends first to increase. However, for the virtual landslide, it decreases strongly as the decomposition level begins to represent the scale level at which the DEM tends increasingly to represent a regular inclined plane. It would have been interesting to continue the successive WT on the Travers DEM to see if it had the same behaviour. Nevertheless, because of the DEM’s size and lack of time, this was not undertaken. This break in the standard deviation could tell us at which the scale all geomorphological elements are removed from the DEM and, finally, to leave in the resulting low-pass only a simple inclined plane.

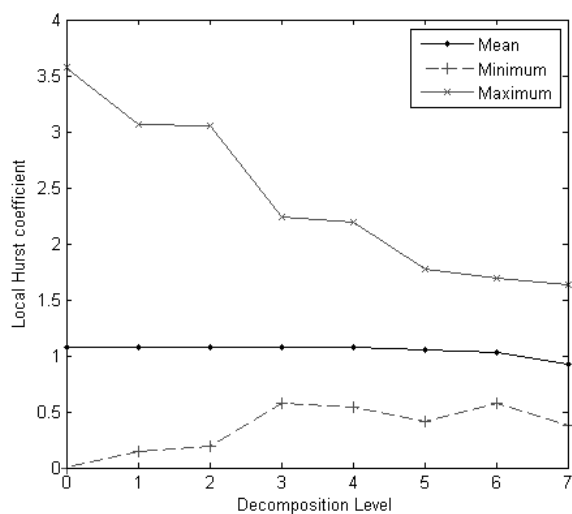


Fig. 5.10. Evolution of the Hurst coefficient through the decomposition levels on the Travers DEM

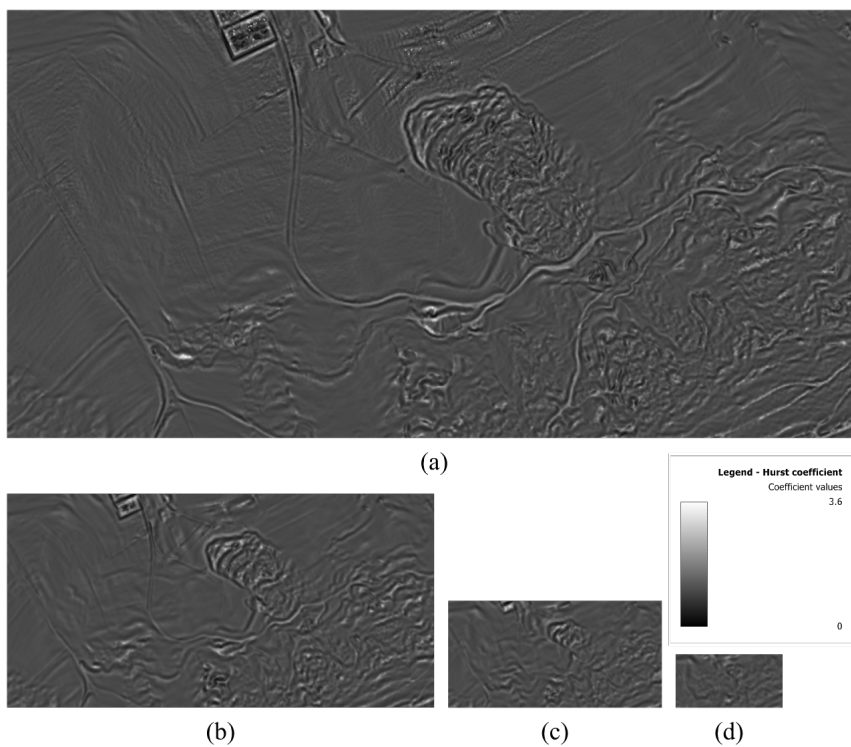


Fig. 5.11. Standard deviation of the Hurst coefficient, (a) decomposition level 0 ($r = 1 m$), (b) decomposition level 1 ($r = 2 m$), ..., (d) decomposition level 3 ($r = 8 m$)

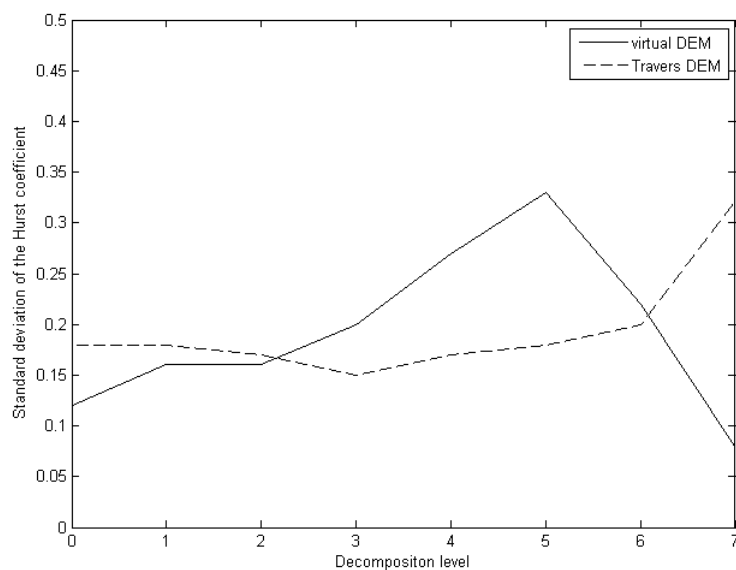


Fig. 5.12. Standard deviation of the Hurst coefficient, (a) decomposition level 0 ($r = 1 m$), (b) decomposition level 1 ($r = 2 m$), ..., (d) decomposition level 3 ($r = 8 m$)

5.6 Global spatial autocorrelation

The WT filters ($\tilde{H}(\mathbf{z}^{-1})$ and $\tilde{G}(\mathbf{z}^{-1})$) are determined using autocorrelation in the frequency domain. Thus, their effect on the DEM is inherent to the autocorrelation (in the frequency domain). An important observation is that the mean of Moran's spatial autocorrelation, which is measured and computed in the spatial domain, is almost equal for the virtual landslide (figure 4.22) and for the Travers DEM (figure 5.13). Thus, whatever the DEM, the definition of the WT filters in the frequency domain has the same effect in the spatial domain, according to Moran's spatial autocorrelation. Geary's ratio, which is more a local measure of spatial autocorrelation, is more increasing than for the virtual DEM. This shows a slightly faster reduction of the local spatial autocorrelation. But, as a reminder, there is positive autocorrelation when Geary's ratio is equal to zero and at the eighth decomposition, the values are still equal to less than 0.2, which still indicates a high positive autocorrelation.

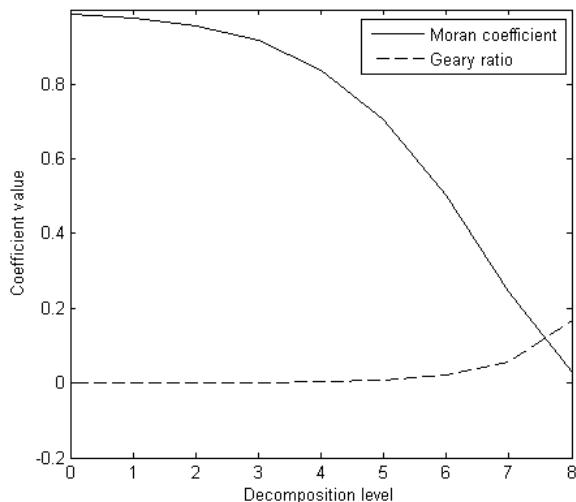


Fig. 5.13. Evolution of Moran's coefficient and Geary's ratio through the decomposition levels, Travers DEM

5.7 Wavelet coefficient analysis and filtering

Using the same enhancement filters as for the virtual landslide (for more details see section 4.3.1), the high-pass coefficients were enhanced and the IWT applied. All high resolution images can be found in appendix H. Four distinct analyses were done. The first is a global analysis of the landslide context using the filtered coefficients. The second illustrates one-dimensional frequency modifications induced by the WT in the landslide zone and the last two are landslide areal analysis of the WT filtering effect.

5.7.1 Global landslide context analysis

In order to understand the global geomorphological context of the landslide, a general analysis of the filtered and reconstructed coefficients was undertaken. Finally these results were compared to Gocht's geological map (appendix F, figure F.5). Thus, all the figures of appendix H were used to do this analysis. Going through the scale levels gave the following results:

Decomposition level 1 (figure H.1, appendix H)

The roughness of the images shows that, contrarily to the pasture area, the landslide and its hillside are less homogeneous. The landslide is an active structure and, north-east to it, there is a similar structural element (this will be analysed in detail in the next levels). Moreover, the hillside indicates exactly the same structural perturbations. Note that this area is in forest, therefore roughness might be due to the land cover.

Decomposition levels 1-2 (figure H.2, appendix H)

The first recognizable structures appear. Except the artificial structures (roads, house basement and gravel-pit), the high roughness zones show again structural heterogeneity. The north-south oriented linear structure which is located at the south of the landslide scarp zone is a forestry road. These can be found in various areas of the hillside. It is therefore likely that these heterogeneous zones are rougher due to terrain variations, and not due to the forest cover. Therefore the DEM is representative of terrain features.

Decomposition levels 1-3 (figure H.3, appendix H)

In the landslide global context, decomposition level 3 confirms the previous assumptions. At this scale and for the descriptive typology, it is still hard to make conclusions.

Decomposition levels 1-4 (figure H.4, appendix H)

Uphill the landslide, some south-west - north-east oriented structural elements appear. These are not directly adjacent to the landslide (figure 5.14, “Linear structures”), but separated by a very heterogeneous zone (figure 5.14, “Deconstructed zone”). A first bed strike was drawn on the map and regarding the geology, the uphill linear structures are the terrace levels of the limestone subsidence. The bed strike illustrates the limit between these limestone formations and the deconstructed zone composed of molasses and fallen rocks (figure 5.15). The drawn geological profile is clearly very similar to the one which was drawn using in situ observations and measurements (figure F.7, appendix F). The analysis of the next levels will confirm and refine these observations.

Decomposition levels 1-5 (figure H.5, appendix H)

The linear structural elements (called “Linear structures” in figure 5.14) seem to be subjects to areal generalisation through the scale intervals. Thus, no exact deformation scheme of the limestone can be drawn or made. Moreover the generalisation process gives us a scale decomposed vision of these limestone terraces, but it is impossible to give an exact description of the morphological imbrication and interaction only by visual interpretation of the coefficients.

Decomposition levels 1-6 (figure H.6, appendix H)

At this level and using the filtered version (filter 2) of the coefficient reconstruction, the deconstructed zone could be delimited with more precision (figure 5.16). Again, a generalised version of the linear elements could be recognized. Some new elements also appeared (described as S1 to S4 in figure 5.16). These are mostly due to older settlements and erosion in the morainic zone. It is almost sure that S3 was induced by a landslide, but traces of it have disappeared through the ages. A good indicator of such unstable zones is the absence of human agriculture, more precisely of pasture. These zones were not deforested because they have this unstable property.

Decomposition levels 1-7 (figure H.7, appendix H)

The limit between the uphill limestones and the molasse is visible (figure H.7, Filter 2). Structurally the scale interval is representative of elements which begin to cover the whole uphill region. The hills which are located in the valley on the moraine formation are made more and more visible through the analysed frequency space.

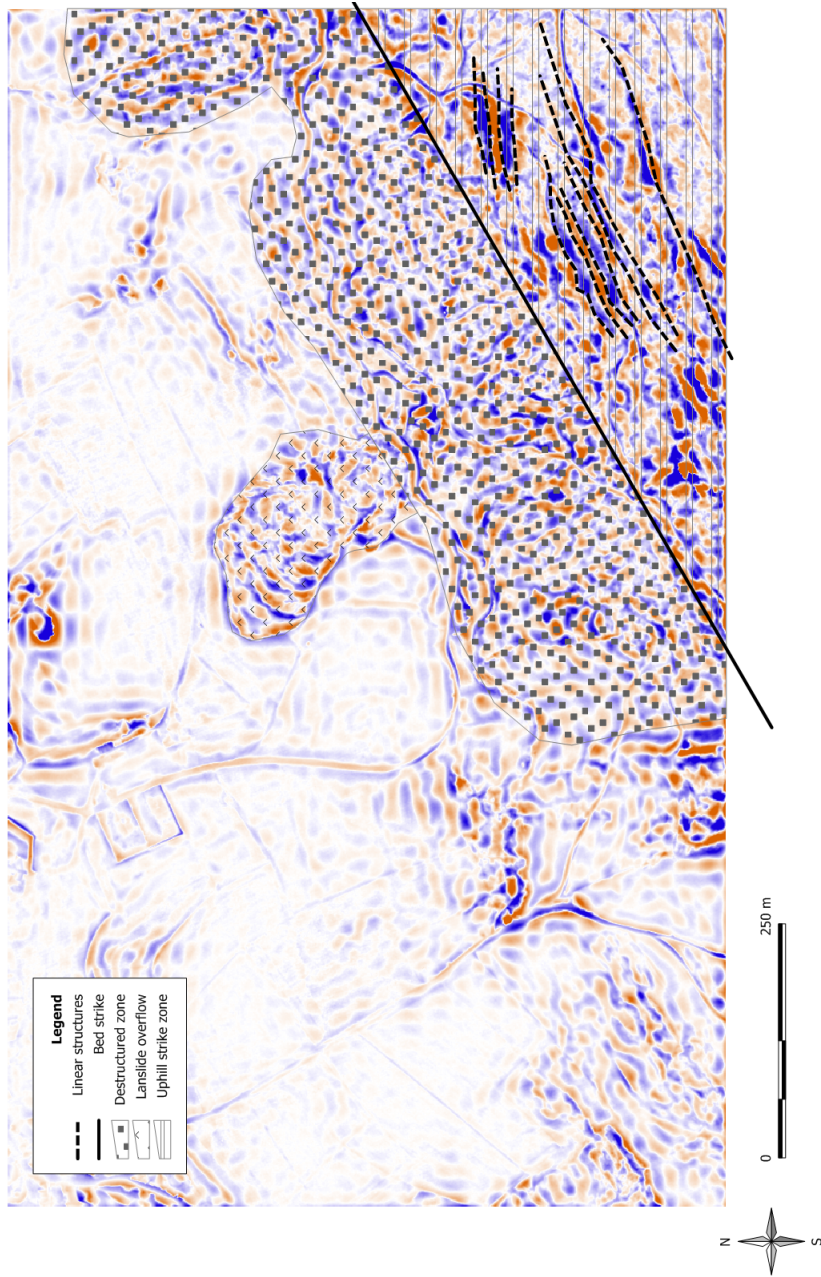


Fig. 5.14. Context analysis, decomposition levels 1-4, filter 1

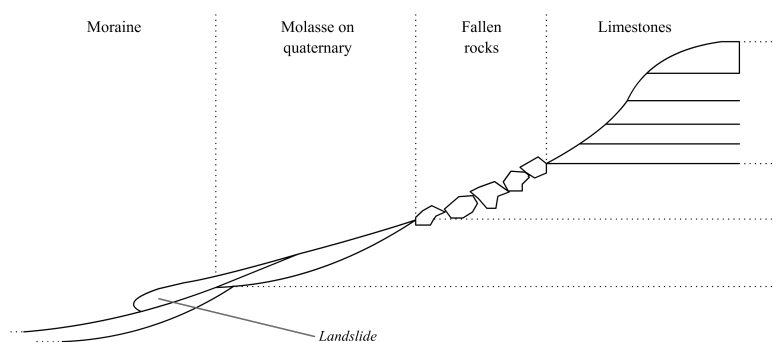


Fig. 5.15. Illustration of the successive geological formation along the landslide hill

Decomposition levels 1-8 (figure H.8, appendix H)

At this level, the scale interval is clearly showing local geological structures of the hillside and of the valley. Some interesting structural elements are highlighted in this level (zones Z1 to Z4 in figure 5.17). For Z1 and Z4 it is the limestone subsidence which appear (see overlay with geological map, figure 5.18). But for Z2 and Z3, it is less clear. There is a convex hilly formation included in these zones, but it is hard to define them as limestone subsidences, as the geological map does not show them. Through the quaternary period and deposit of the moraine, the limestone formations were eroded, thus some convex hilly formations appeared. This is exactly what happened with zones Z1 and Z4. To prove and analyse in detail if this is the case with zones Z2 and Z3, we should enlarge the processed DEM, but as this is not the issue and goals of the present study, this will not be undertaken.

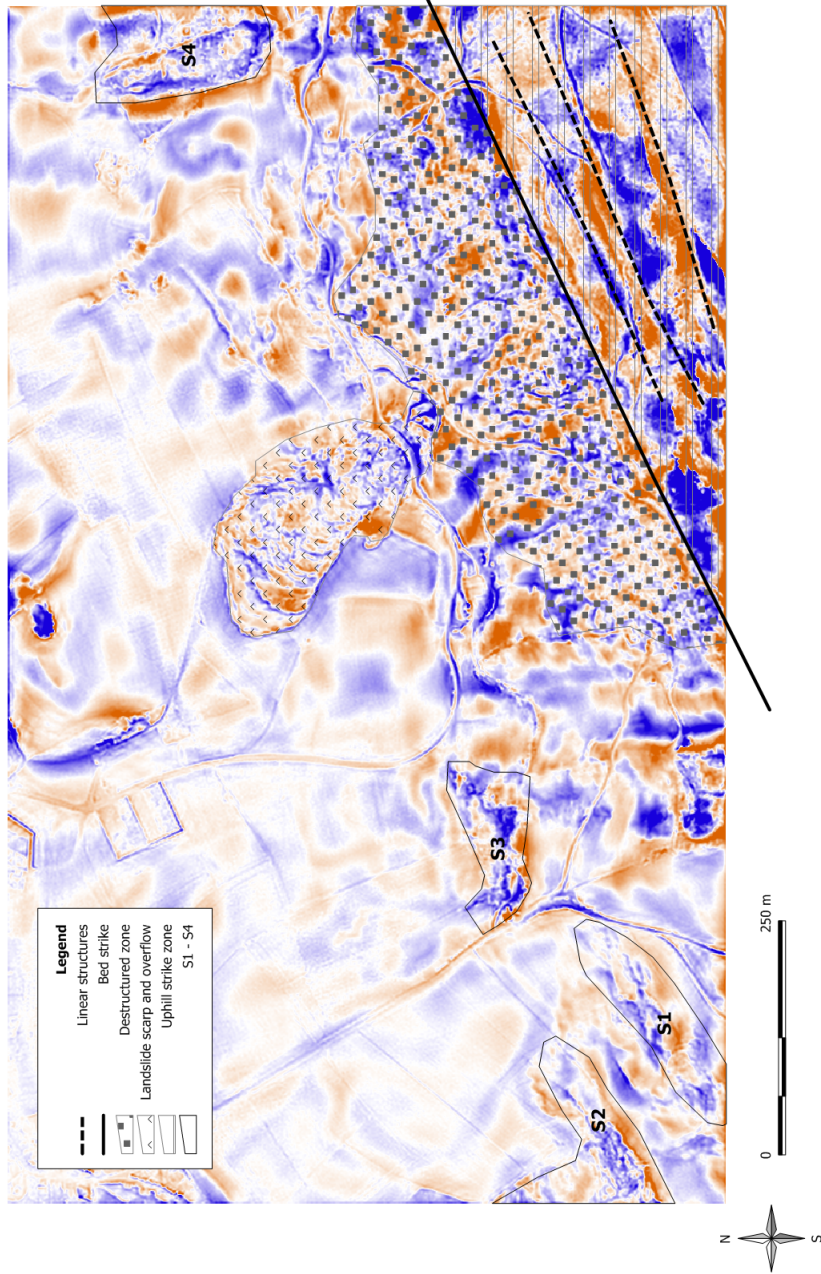


Fig. 5.16. Context analysis, decomposition levels 1-6, filter 2

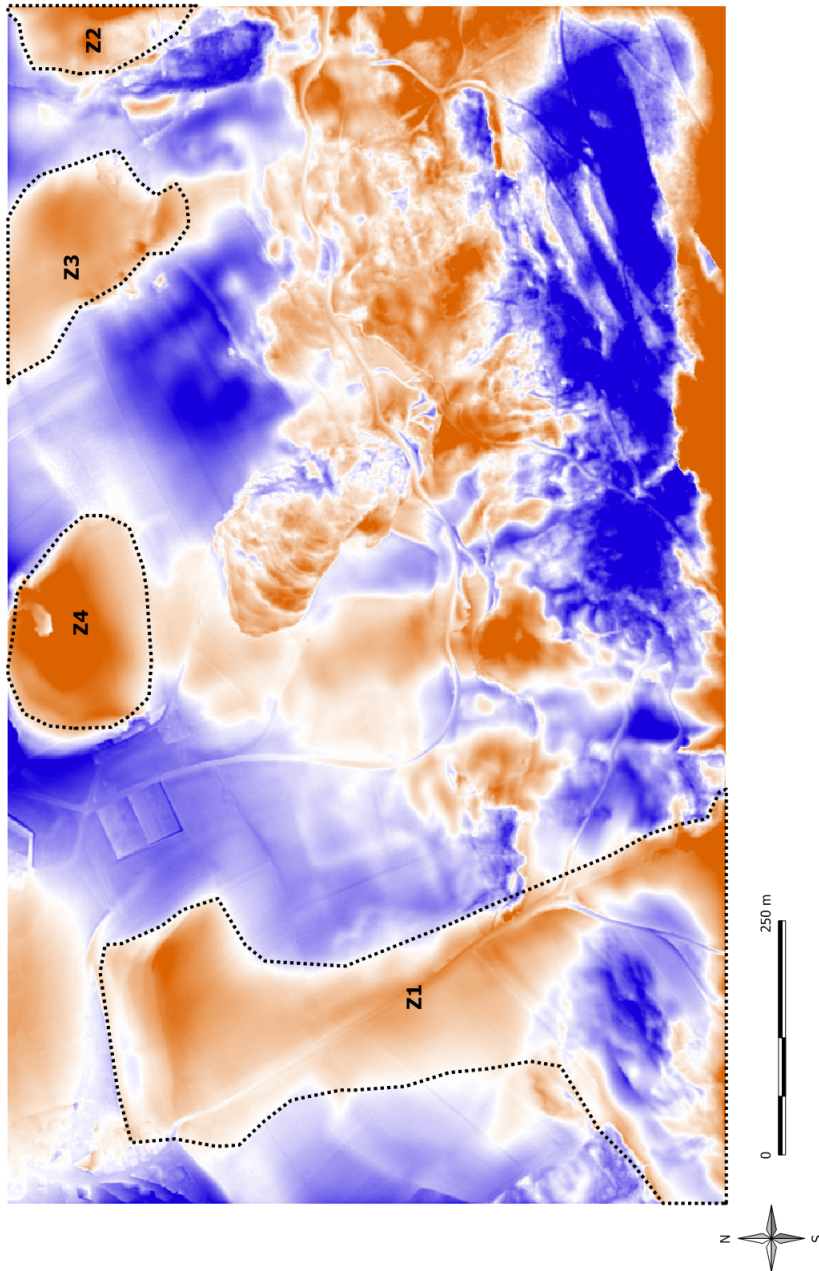


Fig. 5.17. Context analysis, decomposition levels 1-8, filter 3

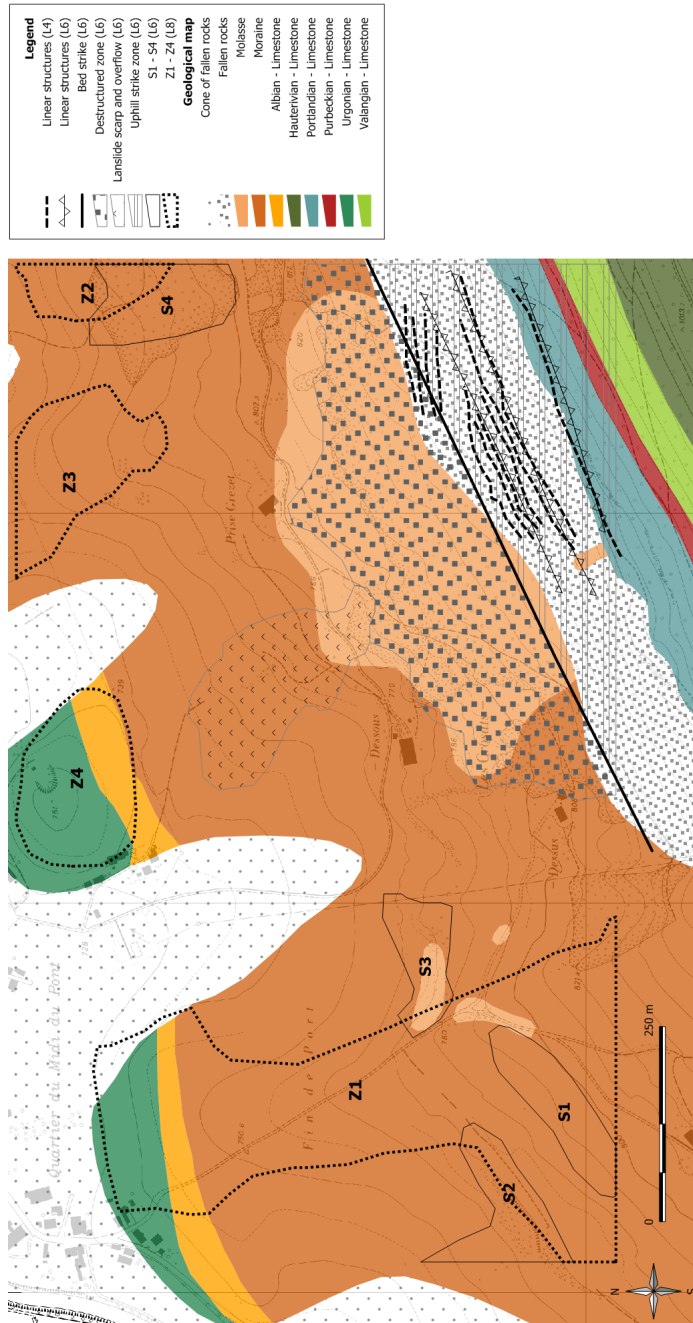


Fig. 5.18. Global context analysis with geological map (Gocht, 1961), plan d'ensemble 1 : 10 000 ©SITN

5.7.2 Profile on the accumulation zone

The accumulation zone (compressed material) begins at the former road, and it is composed of series of folds in which undulatory micro-structural elements can be found. The profile and its analysis on the folds (figures 5.19 to 5.21) clearly show these big folds (spaced out by $\sim 20\text{ m}$) composed of micro folds. The frequency of these micro elements is higher and the wavelength is estimated between 2 to 8 meters (figure 5.21).

The profile on the accumulation zone (figure 5.19) was applied to all high-pass images (8 decomposition levels and 3 types of filter). Figure 5.22 shows the value of the wavelet coefficients of the first decomposition level. For this level only this result is shown, because, for the second filter (Filter 2) the coefficients are null (value of the filter) and for the third filter (Filter 3), the results do not give significant differences because the effect of the enhancement parameters is not strong enough at this level.

These folds have a homogeneous distribution regarding their frequencies (see figure 5.19). Indeed, it is a frequency imbrication of terrain folds. The lowest has an approximately 40 m wavelength with shorter wavelength (2 – 4 m) superpositions. This can be seen in figures 5.20 and 5.21 which are a projection of a profile (located in figure 5.19) through the folds. The residuals of a linear regression on the profile show the low and high frequency folds.

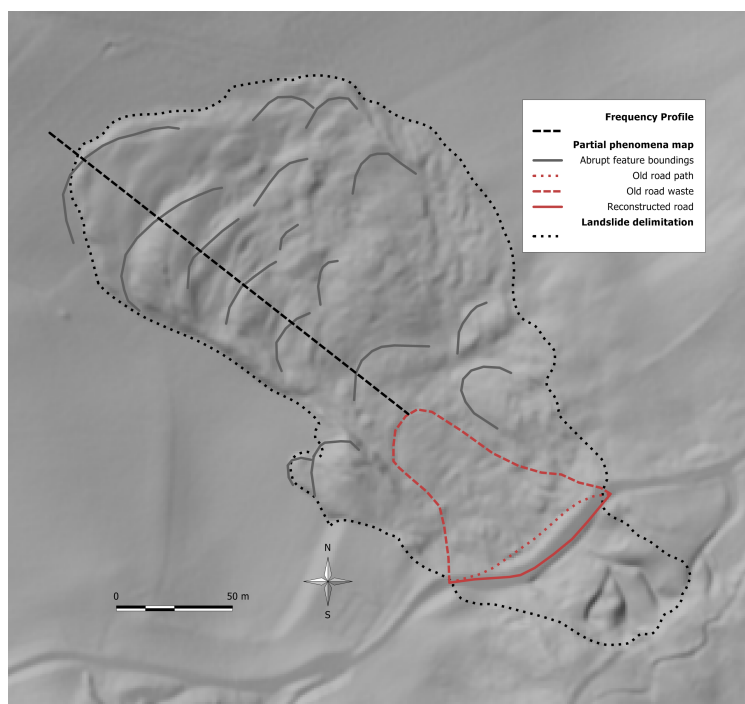


Fig. 5.19. Profile definition over the folds (in map as “Abrupt feature boundaries”), DEM©SITN

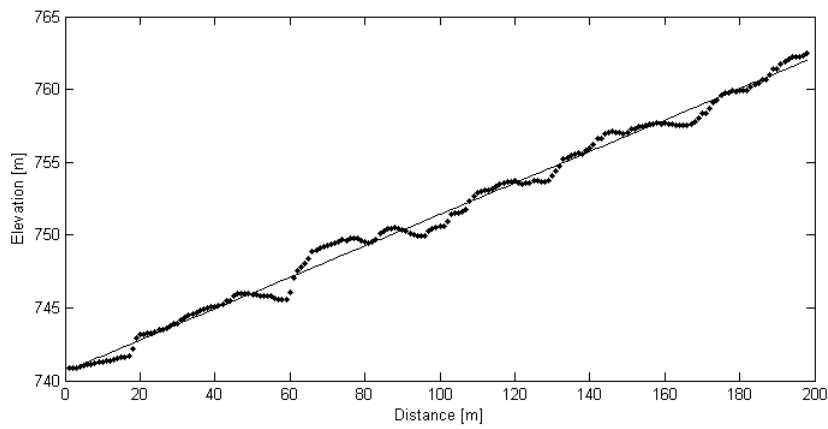


Fig. 5.20. Profile with linear regression, (Left side is the north-western end of the profile and right side is the south-eastern end of the profile.)

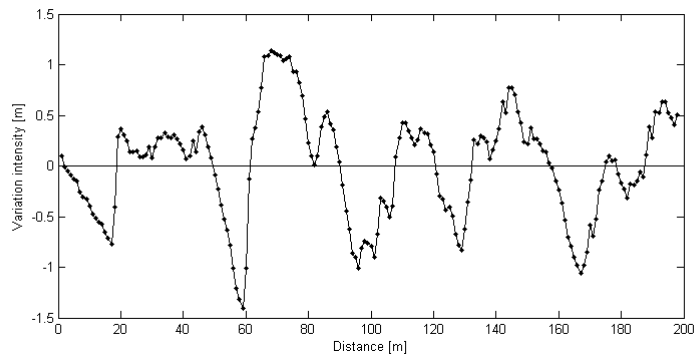


Fig. 5.21. Residuals of linear regression

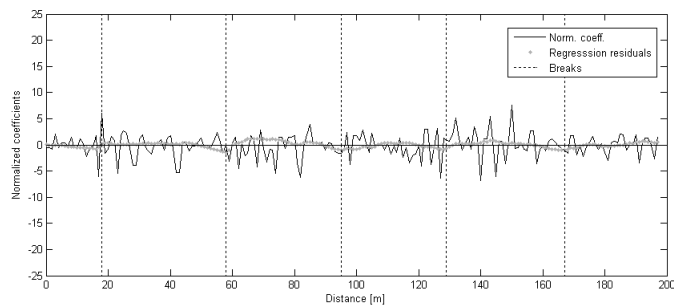


Fig. 5.22. Values of normalized coefficients, decomposition level 1, filter 1

The profiles are illustrated following:

- Normalized coefficient values: the coefficients were normalised over a range of $[-100, 100]$.
- Regression residual: adjusted on the values of the original surface (figures 5.19 to 5.21)
- Breaks: “main” folds identified visually on the original DEM. The location of these ones is approximate.

Figure 5.22 shows the terrain high frequency variations (wavelength 2 to 8 meters) of the micro folds. However, on the high-pass image, these are not visible, because the noise (very high frequency variations) is still pre-dominant. The next figure (figure 5.23) shows the profiles given all enhancement filters of the second decomposition level. Little differences are visible between enhancement filter 1 to 3, but they are not significant. Filter 2 only slightly smooths the structures of the profile, because it does not take into account the first decomposition level (enhancement parameter equal to zero).

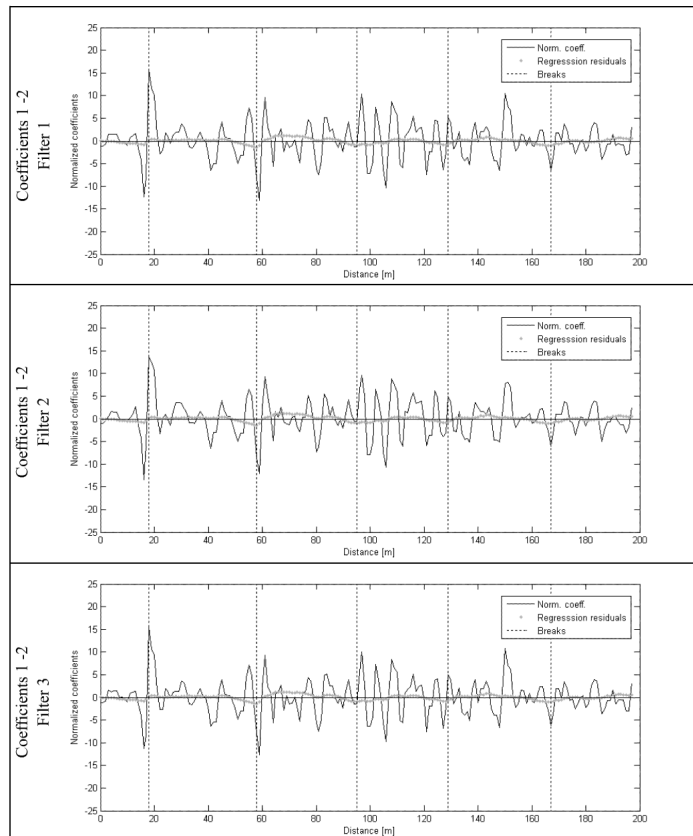


Fig. 5.23. Values of normalized coefficients, decomposition levels 1-2, filters 1-3

Not all decomposition levels will be illustrated, but only those which best illustrate, in our opinion, the multiscale effect of structural feature imbrications. Figure 5.24 illustrates the fifth decomposition level. The “main” folds

limits begin to become obvious and easy to establish. Local minimums appear, defining a structural transition. In the same figure and for the profile concerning the second type of filter (filter 2), the micro-structures resulting from the first levels are better conserved than for the two others filters. These have a smoothing effect on these types of strong structures. The profiles for the sixth decomposition level (figure 5.25) show this even better. The local minimums tend to get smoother, because this level takes into account frequencies having a longer spatial wavelength than the “main” folds.

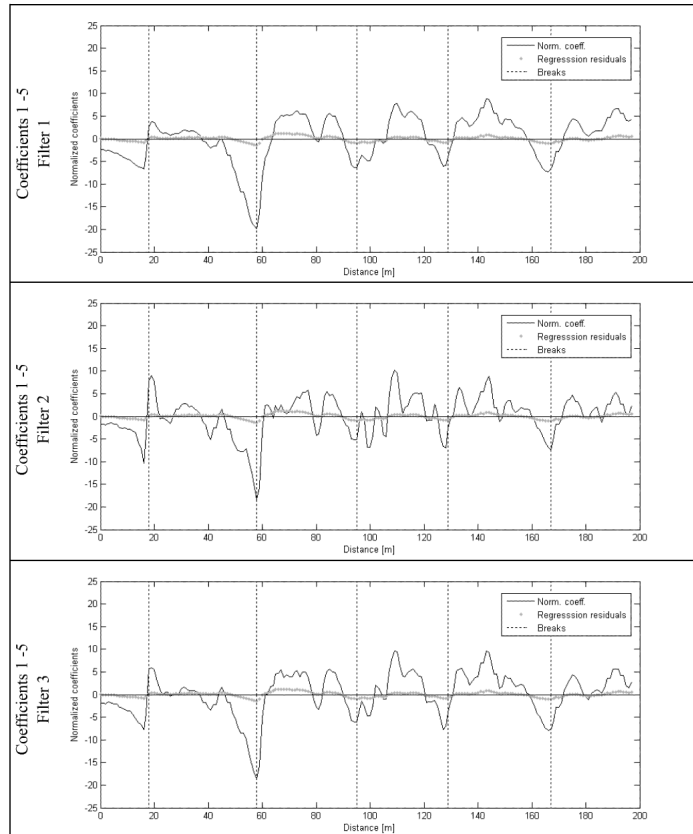


Fig. 5.24. Values of normalized coefficients, decomposition levels 1-5, filters 1-3

For higher levels (see appendix I, figures I.1 to I.4), the second filter (filter 2) seems to conserve better the micro-structures than the two other filters. The parameters of this filter were established empirically and they show that if an enhancement has to be done, the values of the filter for the first decomposition levels have to be much bigger than for the other levels.

Knowing the internal structure of the landslide enabled to establish the multiscale capabilities of the WT used to process a DEM. The scale imbrication of differential settling is shown by the multiscale approach. The one dimensional analysis illustrates better this fact, but the comparison between the visual expert analysis and the filtered versions of the detail coefficient should give the same results.

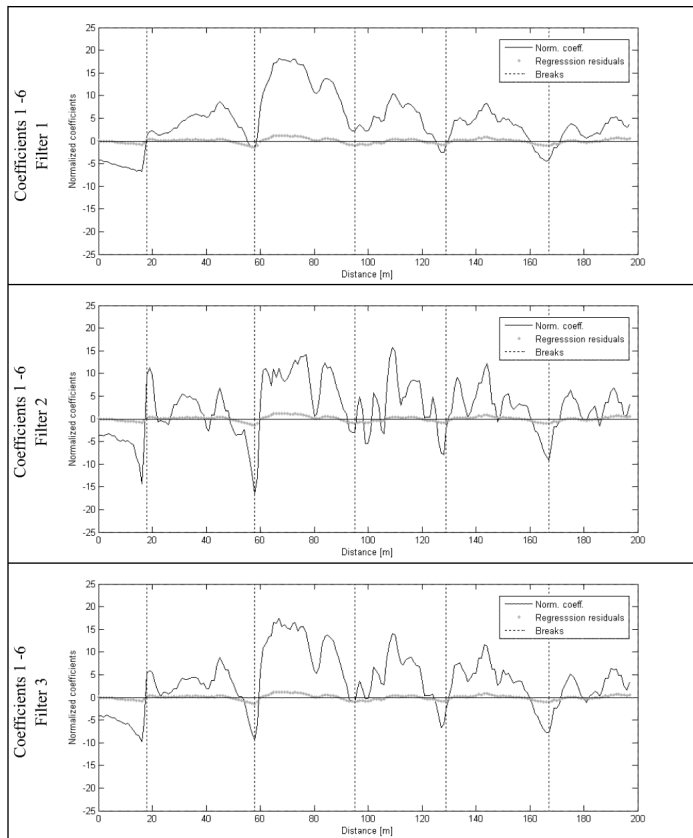


Fig. 5.25. Values of normalized coefficients, decomposition levels 1-6, filters 1-3

5.7.3 Geomorphological visual analysis

Three types of morphological features were identified:

1. Linear structural elements
2. Areal structural elements
3. Areal detailed elements

The same analyses were undertaken as on the shaded DEM analysis (section 5.7.1).

Linear structural elements

A delimitation of linear elements was undertaken by the geological expert² using aerial photography, terrain knowledge and observations. From the WT results point of view, linear elements are difficult to interpret (figure J.1 and J.2, appendix J), because they represent mainly ruptures and traction faults of small sizes. Thus the differentiation between them and DEM noise is hard in the first decomposition levels. Detection of such elements is difficult without more precision. The longest and most intense of these appear on the high-pass images of the four first decomposition levels, but there is no distinct difference between the enhancement filters. Contextually, the first and second decomposition levels give the best rendering of linear elements, but these are the noisiest levels (in a model precision matter), suchlike linear elements do not distinctively appear.

In the higher levels, the second enhancement filter (filter 2) preserves better these linear elements. The filter enables to identify high frequency information in the general context. For the other filters, there is a tendency for these elements to be suppressed, thus being replaced by ones at a coarser scale.

Through this analysis and using this methodology, linear structural elements seem difficult to detect: some are visible, but the resolution does not make it possible to recognise them clearly. As a reminder, empirically, remote sensing specialists have established that a feature (or element) should cover at least three pixels (thus these pixels should approximately have the same values) in order to be detected; covering less than three pixels, the element is assimilated to noise (as long as its context is not clearly defined, see section 3.2). Perhaps by computing gradients on the coefficient images and using edge detectors, such as the Canny edge connectors (Parker, 1997), multiscale linear elements would be easier to identify. At first, a threshold should be applied to the coefficients. As we will see in the next chapter and using the present proposed methodology, some information about their orientation can be retrieved visually, but clearly not their perfect delimitation.

Areal structural elements

A zonal delimitation was undertaken by the geological expert using the aerial photography, terrain knowledge and observations. This analysis resulted in the definition of seven different zones (figure 5.26):

- Zone I: this zone corresponds to the plastic and solid deformations at the downstream of the landslide. Laterally it is surrounded by more destructive zones (zone II and V).

² The expert geological analysis and critics are done in collaboration with Dr. P. Turberg from the laboratory of engineering and environmental geology (GE-OLEP) at the École Polytechnique Fédérale de Lausanne - Switzerland.

- Zone II: this is where the scarp material flowed to. It was mainly liquefied by the water resurgences.
- Zone III: this is the main scarp zone. Regarding the accumulation zone, the scarp is very little and material flowed downhill.
- Zone IV: transition zone between the liquefied material of zone II and the almost flat meadow surrounding the landslide. It is composed of a lot of little folds due to material differential displacement.
- Zone V: like zone IV, this is the transition between the side of zone I and the meadow.
- Zone VI: this zone could be linked to zone I, because it is not part of the liquefaction process, but the material submitted a plastic settlement.
- zone VII: this little zone was influenced by the nearby material displacement, showing some little folds and discontinuities.

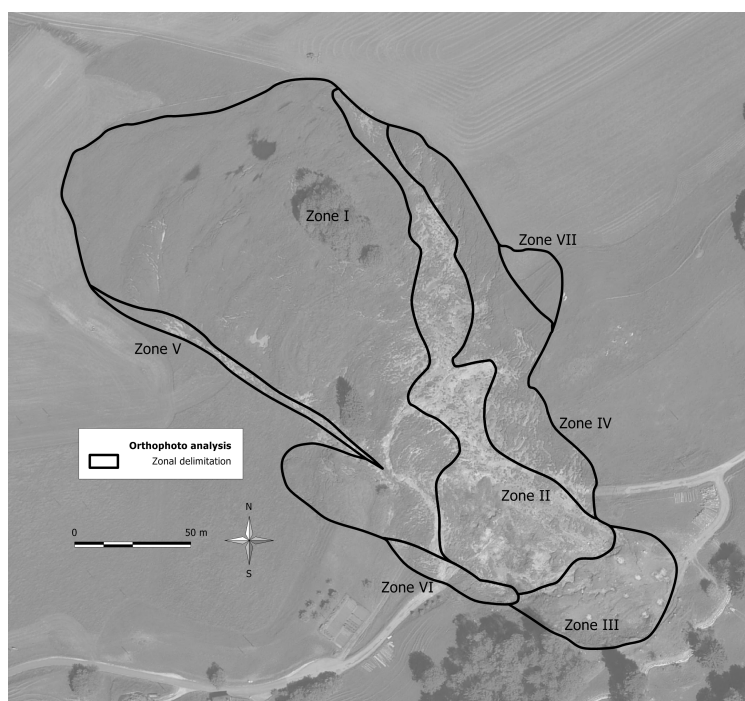


Fig. 5.26. Visual delimitation of structural elements using aerial photography, aerial photography©SITN

The results of the wavelet filtering are given in figures 5.27 and 5.28. Looking at the size of the zone, there is no chance for them to appear in the four first decomposition levels. In figure 5.28, the end of the accumulation, at the southwest of zone I, appears clearly. Again, it is interesting to see that the internal structures are better conserved by using a strong enhancement filter (filter 2). Zone II and III show similar behaviour.

At the seventh and eighth levels, some of the defined zones do not respect the delimitation of the wavelet spatial recognition. As example, zone IV is not as rectilinear as drawn by the expert, but it intersects a depression (blue

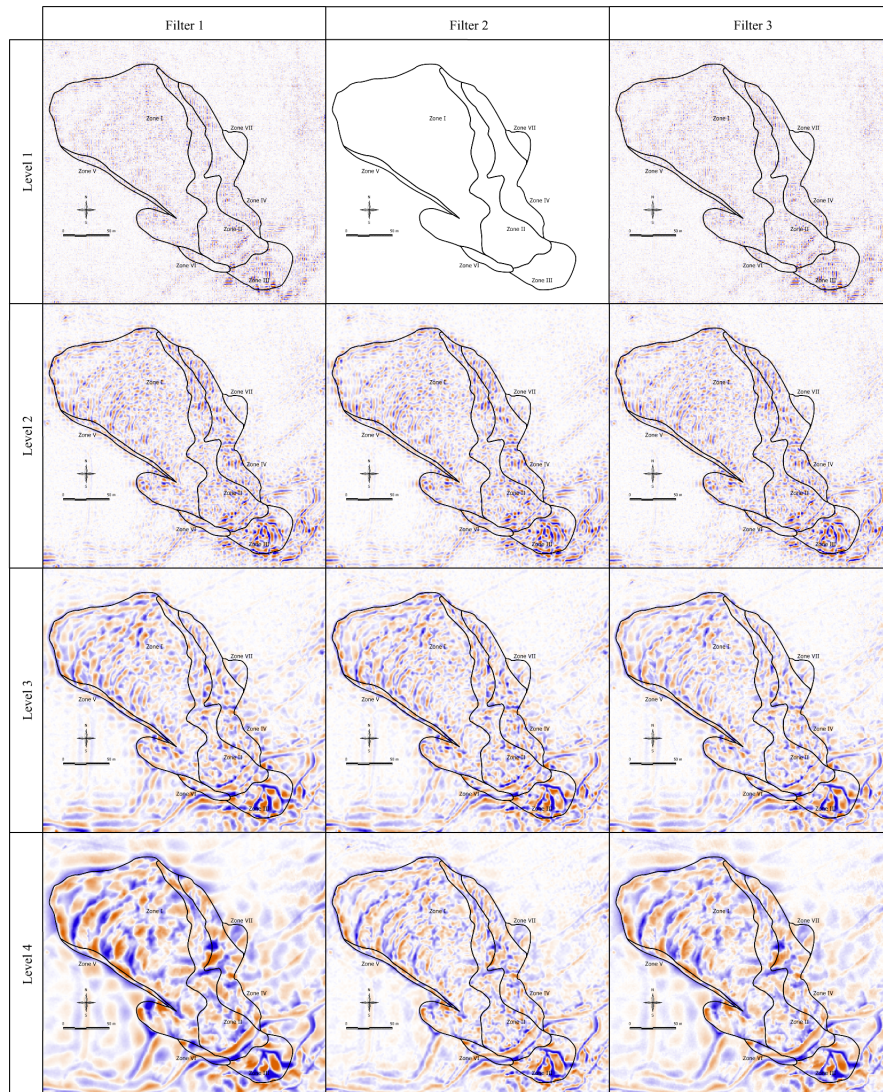


Fig. 5.27. High-pass results for areal elements using the three filters, for decomposition levels 1 to 4

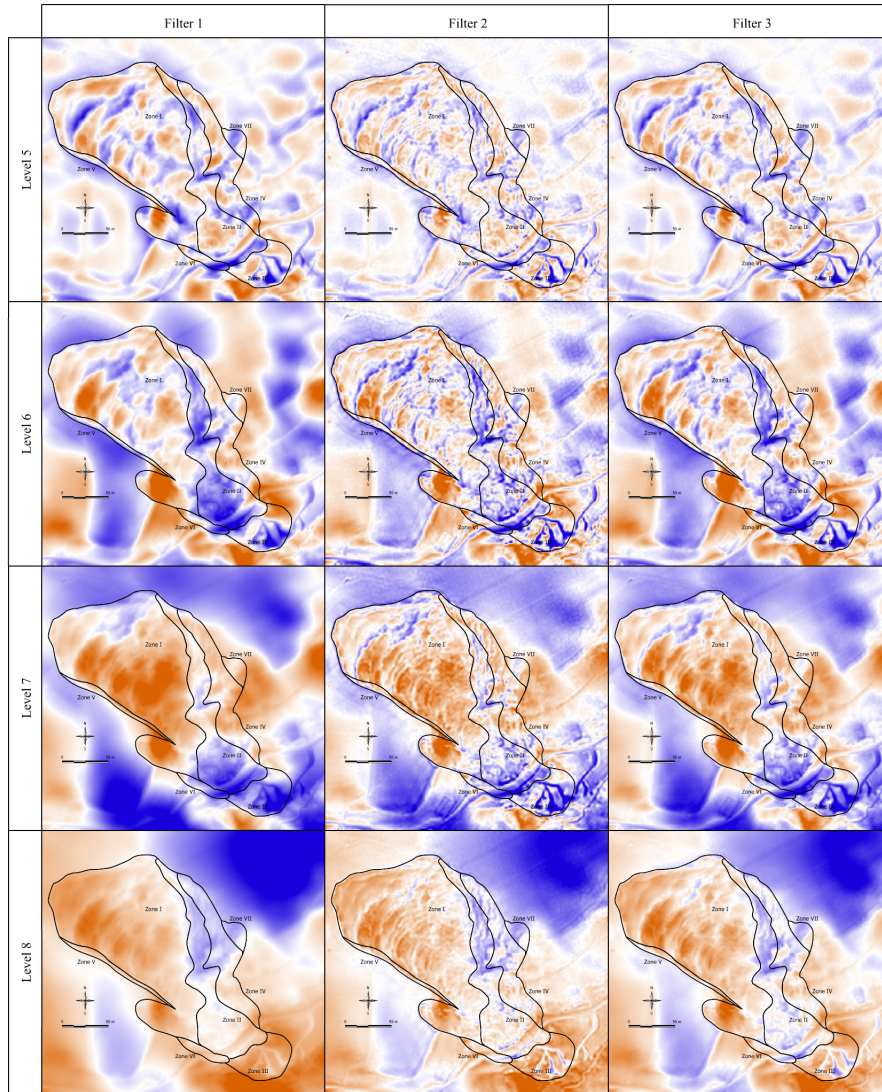


Fig. 5.28. High-pass results for linear elements using the three filters, for decomposition levels 5 to 8

on the images) which is a continuity of zone II. Zone V is the only one which cannot be identified (even partially). Indeed, on the aerial photography it can hardly be seen as an entity.

Areal detailed elements

Based on what we have seen and identified in the previous section, we can now identify three areas in order to make a more detailed analysis of their different scale components. They are described as follows:

- Zone I is located in the toe of the landslide, thus in the settlement of the accumulation zone. It mainly contains wave-like structures due to the plastic behaviour of the phenomenon. The settlement is inherent to the uphill mass movement. The surface of zone I is $5\,360\text{ m}^2$.
- Zone II is the continuity of the material flow which occurred downhill from the scarp zone. The material consists mainly of clay and sandy liquefied molasse. It is therefore revealing the fluid material mass movement of the landslide. Its surface is $2\,720\text{ m}^2$.
- Zone III is simply the whole scarp zone ($1\,810\text{ m}^2$). It is the smallest of the three zones. It is crucial to note that this area was reshaped and reorganised by the authorities to ensure the drainage of surface water to the spillway. Thus the structures composing it are very acute. There are three surface channels which intersect at the bottom of the scarp zone towards the spillway.



Fig. 5.29. Visual delimitation of structural elements of the DEM - zones I to III, 1 m resolution shaded DEM, DEM©SITN

Identification of landforms is never unique and dissimilarities may appear when comparing results of different experts. Rather than probing a geological expert, it is the scale imbrication of structures that we want to demonstrate and its impact on the phenomena. Moreover, using smaller areas would certainly give results, but because of their size, the structural elements inside would be hard to describe from a geological point of view. It was decided that the zones would be distributed to cover spatially all main structural elements of landslide (scarp zone, settlement in accumulation zone and fluid accumulation zone).

Zone I

The overlays between zone I and the high-pass reconstructed images are given in figures 5.31 and 5.32.

In the first decomposition levels (1 to 3) and for all types of filters, it is noteworthy that the linear structure types are bent in the direction of the mass movement (north-west). Moreover, there is a low roughness area between the north-west and south-west of this zone, as if the structures had a lower amplitude in the centre of the zone. This effect however disappears when going to decomposition level 4. From this level on, the effects of the filters become visible, but the differences between the results using filters 1 and 3 are still difficult to identify visually. However, filter 2 gives significant different results. Indeed, the enhancement of the high frequency spaces highlights the micro-structures contained in the zone. In the three images of decomposition level 4, the separation of the zone into two distinct convex areas is visible. These are separated by a sharp concavity shown by the coefficient amplitude (i.e. the saturation of the blue colour) visible in the image. As for these two sub-zones, they are composed of micro-structures of lower magnitude.

The separation of zone I into two sub-zones is visually effective in levels 5 and 6. It clearly identifies the landslide toe and another uphill area (the two red zones in zone I). There is a terrace-like effect where the toe (filter 2) is disturbed by micro-folds. Schematically (figure 5.30), zone I represents the toe and a secondary settlement area. This latter is less perturbed by micro-folds, which is probably due to the differential settlement. Indeed, the forces (weight of materials) are extreme at the bottom of the mass movement.

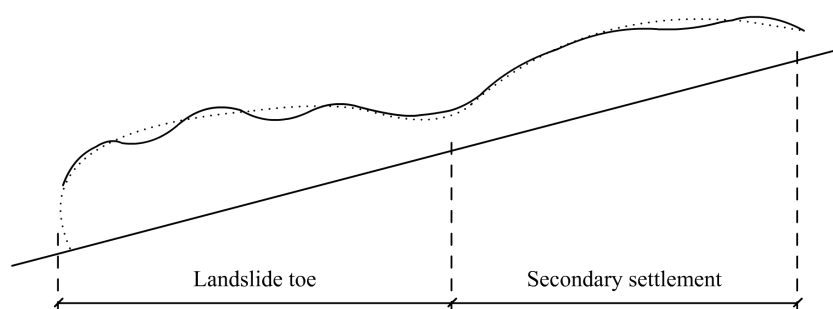


Fig. 5.30. Profile schema of the toe structures - The dashed points show the global profile tendency, whereas the full line the local structures

Finally, decomposition levels 7 and 8 show clearly that the represented scale intervals are larger than the zone, and therefore the frequency spaces are of lower wavelength, than those composing the structures of the zone. For the last level (8), it is interesting to note that the second filter preserves more detail structures composing the terrain.

Zone II

The same figures 5.31 and 5.32 show the overlay between zone II and the high-pass reconstructed images.

Again, in the first decomposition levels (1 to 3), structural elements show, in the northern area of the zone, the preferential direction of mass movements. The second level shows distinctly the fluid flows to which this area was subjected by the fact that the linear structures are oriented south-north. As before, the effects of filters are not visible at these levels.

From level 4, the linear structures tend to disappear in the benefit of areal structural elements. Enhancing the high frequency space using filter 2 seems however to stabilise these a longer time in the frequency space than by using the two other filters. In addition and for this level, the defined zone seems less consistent compared to zone I. Namely, it is more difficult to recognize this zone through the visual analysis of the images.

Decomposition levels 5 and 6 show a subdivision of the zone into two separate areas. The first is a sort of bump of rather low convexity south of the zone and the second a concave hollow in the north. As for zone I, the micro-structures of the lower levels are best preserved using filter 2.

The higher levels (7 and 8) give no more or little information about the structural elements of the zone. However, in level 8 and for filter 2, the flow lines are still preserved north of the zone due to the filter effect.

Zone III

Zone III is illustrated in figures 5.33 and 5.34.

For this zone and because of the structural configuration of the scarp zone (artificial alteration), the first two levels are different. Level 1 shows the intense reaction of the wavelets to the drainage canals dug by the authorities. There are high magnitude oriented structures in two dimensions (x and y) of the zone. In the second, it is already possible to guess the reconstructed shape of the canals; they have very acute shapes, which correspond to the wavelets of the second frequency space.

The next two levels (3 and 4) do not give any additional information for this zone. Actually, it is likely that structural elements of the scarp zone are well represented by the first two levels, and therefore, there is less influence of the third and fourth frequency spaces, thus levels 3 and 4.

In the fifth level and for the image of the filter 2, the location of the spillway becomes very obvious. There is, however, no more additional information concerning the zone until level 6. From this one, the scarp zone is aggregated to the rest of the flow zone, including the new road (north-west area). Moreover, at higher levels, the scarp zone is completely absorbed by hillside phenomena, which scale exceeds by far the size and structure of the zone. Note that the filters tend to maintain high frequencies, which highlights the canal dug in the images of the eighth level using filters 2 and 3.

To sum up this short analysis of the zones, we have seen that the high-pass images improve human visual capabilities by applying selective filtering to the so-called raw data. Enhancement of specific structural information improves our comprehension of the phenomena.

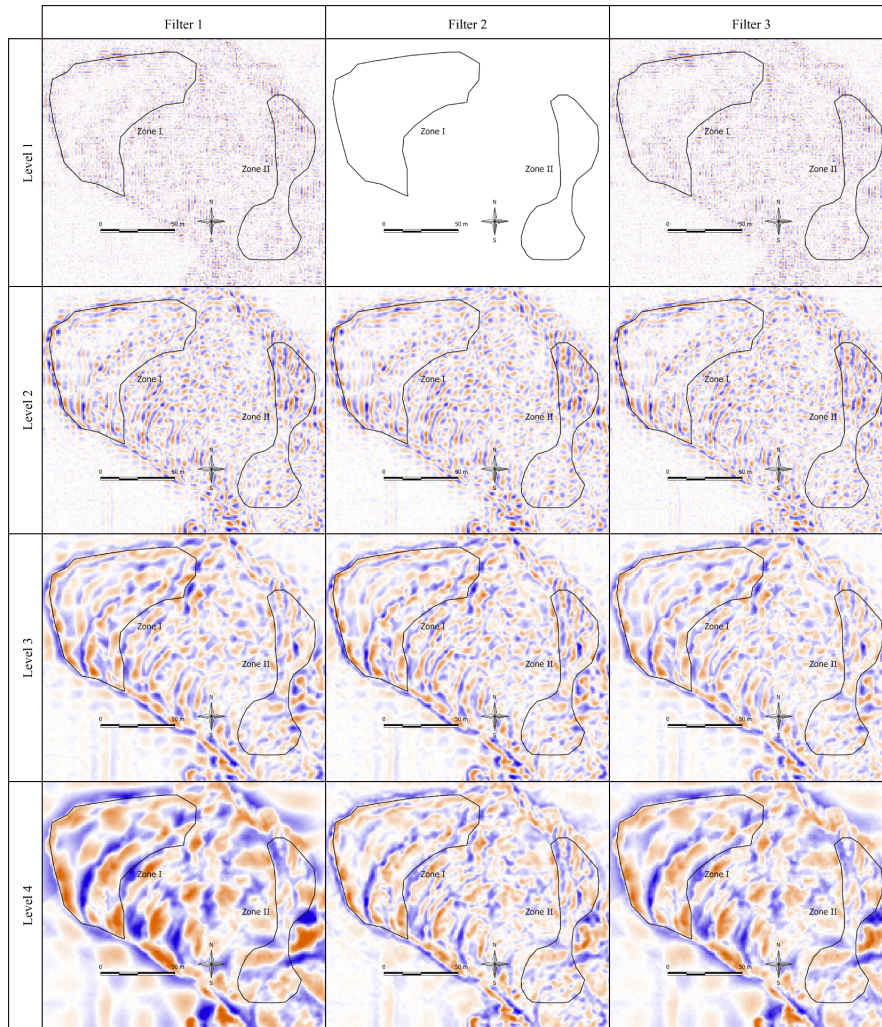


Fig. 5.31. High-pass results for zones I & II using the three filters, for decomposition levels 1 to 4

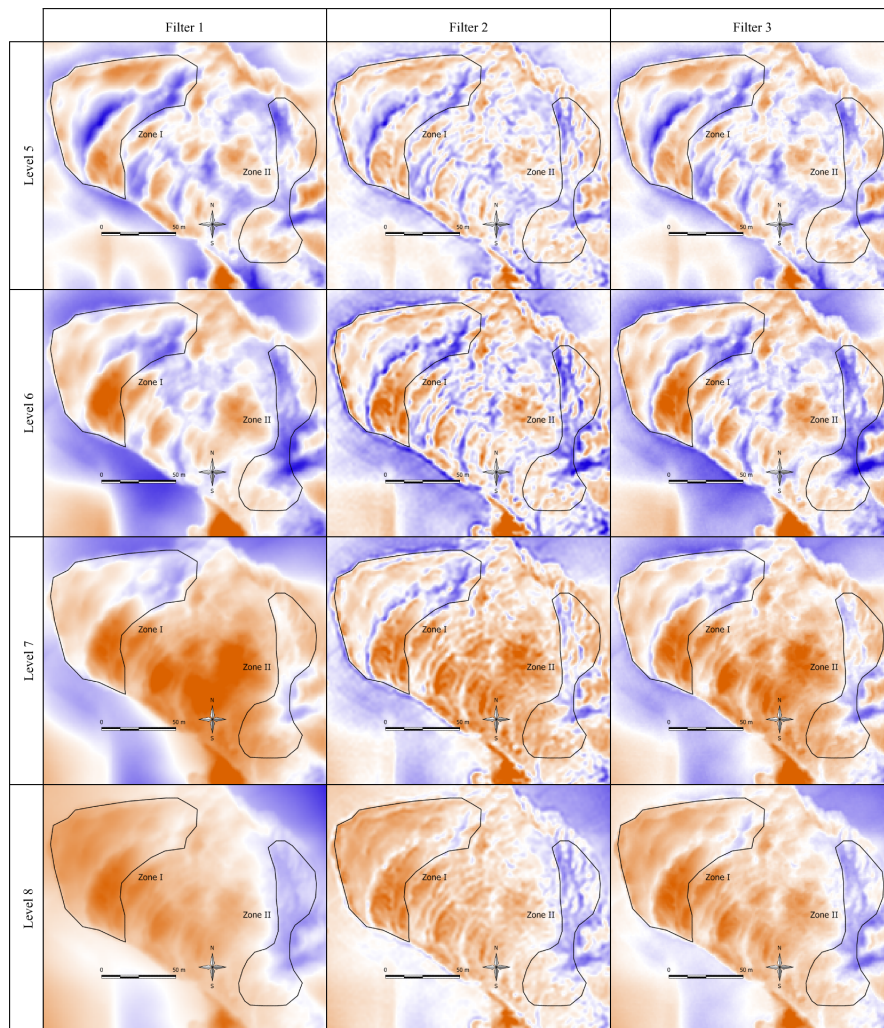


Fig. 5.32. High-pass results for zones I & II using the three filters, for decomposition levels 5 to 8

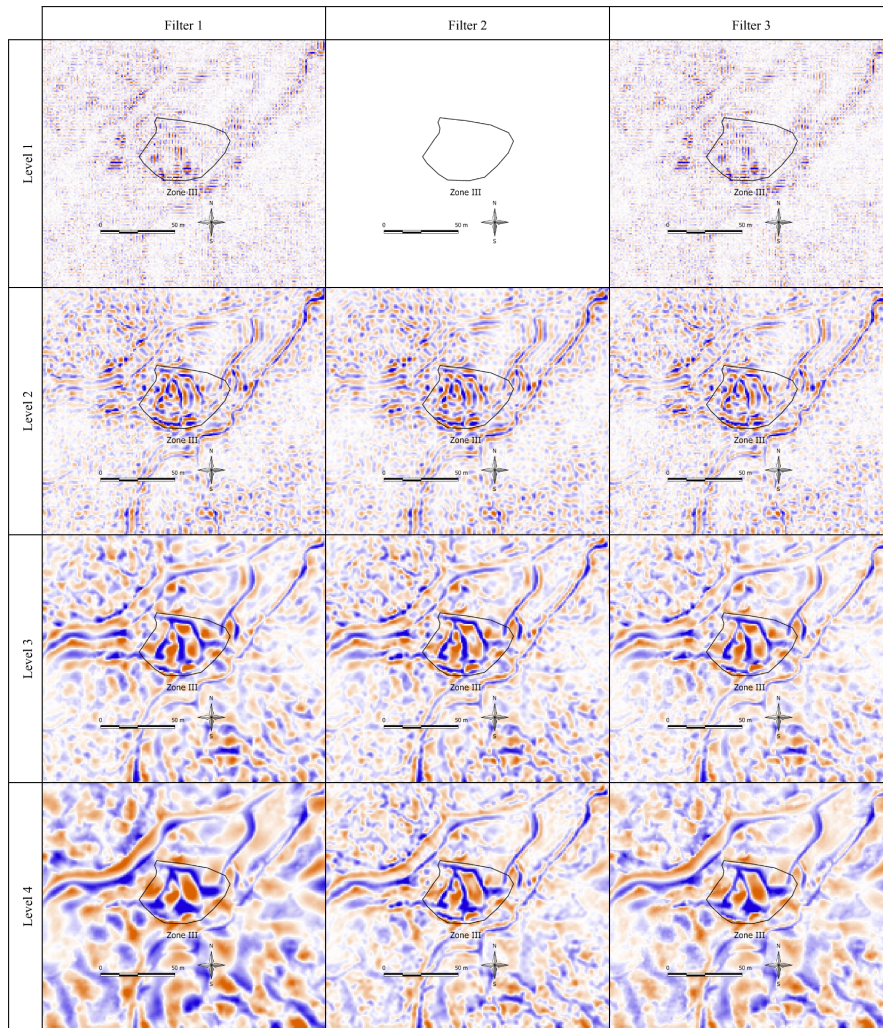


Fig. 5.33. High-pass results for zone III using the three filters, for decomposition levels 1 to 4

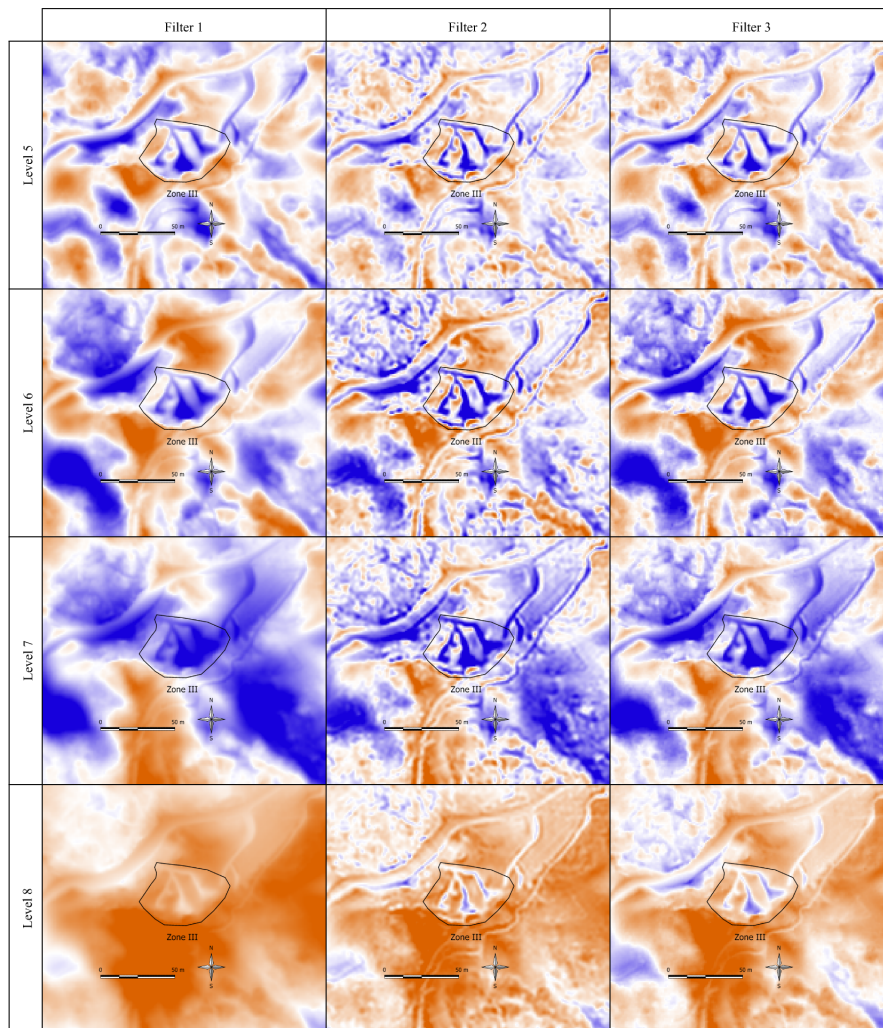


Fig. 5.34. High-pass results for zone III using the three filters, for decomposition levels 5 to 8

5.8 Conclusion on the case study

The performed analyses and interpretations of the WT results are purely visual and contextual, which means that they are determined according to our analytical capabilities, and not using any deterministic or stochastic indicators. However, the wavelet transform and the associated enhancement filters give good results necessary to the morphological interpretation of geological physical phenomena. However, the values of the enhancement filters are purely exploratory and strongly depend on what type of scaled structures have to be highlighted. The structural analysis shows that the high-pass images give a lot of indications regarding geomorphological elements contained in DEMs. The multiscale approach gives a nested vision of morphological features.

More than the generalisation process, it is the localised scalable frequency transfer which is important. Being able to enhance specific spectral information enables to understand better the topographical structural system and its interactions with others systems at other scales. Understanding processes and interaction showed a better understanding of the morphological process which induces the landslide.

As first draft, and valid only for this study, we tried to characterize the elements we analysed (figure 5.35). In three different analyses that we carried out (see the previous three sections), we identified four types of phenomena that span scale. Starting with the micro-scale and going to the macro-scale, the structural hierarchy through the scale intervals is a function of the DEM resolution and can to be organised as follows:

1. The domain of terrain roughness analysis is defined from levels 1 to 3.
2. The domain of internal individual structures is defined from levels 3 to 5.
3. The domain of internal general structures is defined from levels 5 to 8.
4. The domain of local geological structures is defined from levels 8 to the upper ones.

This partition is a first attempt to highlight the scale intervals of interest for the Travers DEM and it should be admitted with precaution. But it gives an overview of structural organisation and is a help for the multiscale characterization of the different structural elements.

The discretization of space scales illustrates which structural elements can be found in which partition. It also shows that a geomorphological phenomenon always consist of structural elements of different scales. Throughout this analysis, it must be emphasized that the space partition, that each of the four defined typology covers, is roughly comparable to the number of dyadic spaces, i.e. to say that each typology covers about 2 frequency spaces (from the dyadic WT). These conclusions refer of course to the present analysis of the Travers landslide.

Remark concerning predictive capabilities of the wavelet transform

Some researchers asked us if the wavelet transform had any predictive capabilities for geological phenomena, like landslide or rock fall. At the present state of the study, there is no evidence of such skills. The introduced methodology and technique only answer an opened question, but does not rethink

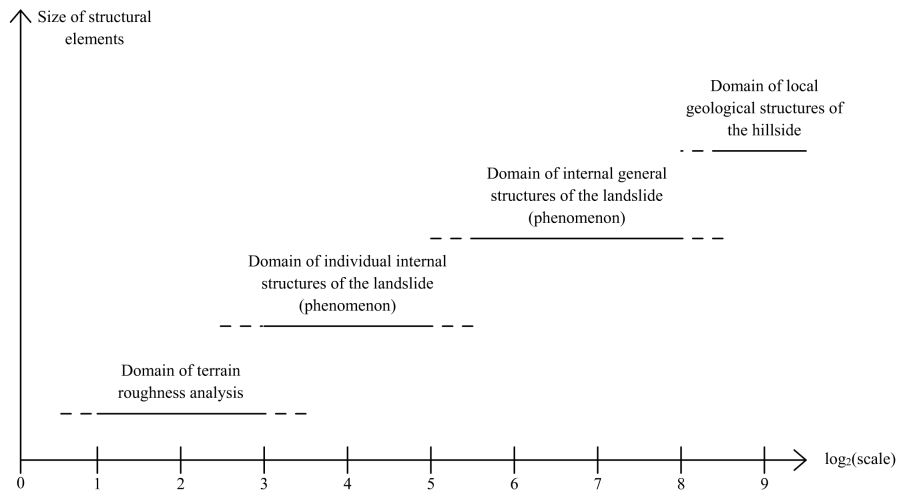


Fig. 5.35. Scale interval typologies - a \log_2 is applied on the scale axis in order to reduce the axis length. The different scales are represented by the decomposition levels and they are representative of the associated resolution.

the current practice. The method is a geomorphological tool for the analysis of roughness and structural composition of high resolution DEMs. Although some geomorphometric evidence may predict some geological behaviour, as long as these predictors have not been described and visually recognised on the results, the method does not give any predictive indications. As we saw on the Travers DEM, some areas, located laterally to the landslide (north-east and south-west) on the hillside, show some similar roughness (compared to the landslide) in the first decomposition level. Indeed, the south-western area is an older landslide which was eroded and stabilised through the years, and the second zone might be a similar bedrock strike as the one located in the landslide. It might have induced the same kind of phenomenon as the one which already occurred.

6. Methodological validation

6.1 Introduction

Following the experimental case study, analysis and interpretation of the Travers DEM, we decided to validate our methods using two different approaches:

- GAS: we proposed to an expert audience to do the same analysis using a web-based system called Geomorphometric Analysis System (GAS). Firstly, we wanted to know if an analysis performed by someone external to the study with no a priori knowledge of wavelets was possible and secondly, if it could be better or worse to a usual geomorphometric analysis, or even complementary to it. We therefore submitted the reconstructed coefficients to the scientific community using the web-based GAS survey. After a short introduction to the landslide phenomenon and in a first cartographic exercise, the participants had to make a geomorphological analysis of the Travers DEM using usual geomorphometric indicators (computed using a 3×3 convolution window). In the second exercise, they had to do the same task again with only the reconstructed wavelet coefficients at hands.
- Multiscale pattern analysis: often, researchers of the geomorphometric community create classifications using geomorphometric indicators. The present attempt tries to understand how these classification schemes can be applied in a multiscale point of view and how the resulting patterns are evolving through scale.

6.2 GAS - Geomorphometric Analysis System

6.2.1 Purpose and objectives

The purpose of the Geomorphometric Analysis System was to analyse how researchers specialised in geomorphometry, geology, geographic information systems and cartography use data derived from DEMs for the analysis and cartography of landforms. Usual geomorphometry (see section 2.4) is defined by the quantitative analysis of DEMs and by its underlying indicators. Geomorphologists use them to identify, delineate and understand geomorphological features.

The wavelet approach, developed in chapter 4, analyses DEMs in the perspective of a scale specific analysis and therefore visually interpretable through scale. These results also enable to make a geomorphological quantitative analysis, similarly to what was done in chapter 5.

The goal of GAS was to compare the two approaches in order to determine if both of them are exclusive, complementary, or if the wavelet approach is not suitable for geomorphological analysis.

As hypothesis we state that the localised approach (i.e. the wavelet approach) is complementary to usual geomorphometry. GAS's purpose was thereby to verify the pertinence of the subband selective reconstruction of the wavelet high-pass coefficients by comparison with usual geomorphometry.

GAS was conceived as an online platform that enables the user to visualise different geospatial data-layers. Moreover the interface offered the functionality to digitize and specify spatial features (using points, lines and polygons) on top of the data-layers that the user chose to visualise. Figures 6.1 and 6.2 show two screenshots of the GAS user interface.

The mapping system was developed using the open Scalable Vector Graphics¹ (SVG) standard. The static SVG visualisation capabilities were enhanced with dynamic JavaScript functionality, for instance to enable the user to switch between layers or to digitize features. The system uses a spatially enabled database called PostgreSQL/PostGIS² to store features digitized by the users.

6.2.2 The survey

In order to test the proposed hypothesis we integrated the GAS-digitizing interfaces (figures 6.1 and 6.2) in an online survey system which consisted of seven different steps (figure 6.3):

- (i) An introduction about the landslide represented by the Travers DEM from a phenomenological and geological point of view.
- (ii) The user has to answer some questions about himself and about his knowledge regarding GIS and DEMs (see table K.4, appendix K).
- (iii) The user has to perform a first cartography. He is asked to draw (point, line or polygon) the features he is able to identify. Following data is available: a shaded DEM, slope, aspect profile curvature, plan curvature and wetness index.
- (iv) A second set of questions is asked regarding the first cartography (see table K.5, appendix K).
- (v) An introduction of the wavelet transform and its underlying data production is given.
- (vi) The user has to perform a second cartography. He is again asked to specify the features he is able to identify. Following data is available: a shaded DEM and subband selective reconstructions of the wavelet high-pass coefficients (see section 4.3).
- (vii) A third set of questions is asked regarding the second cartography (see table K.6, appendix K).

Due to the fact that prior knowledge of the terrain, phenomena and methods are susceptible to induce a bias in the analysis we carefully selected the people for this survey. Once selected, participants were invited by email. The GAS-survey was conducted between June 2009 and the end of September 2009.

¹ <http://www.w3.org/Graphics/SVG>, accessed 15 February 2010

² <http://postgis.refractory.net/>, accessed 15 February 2010

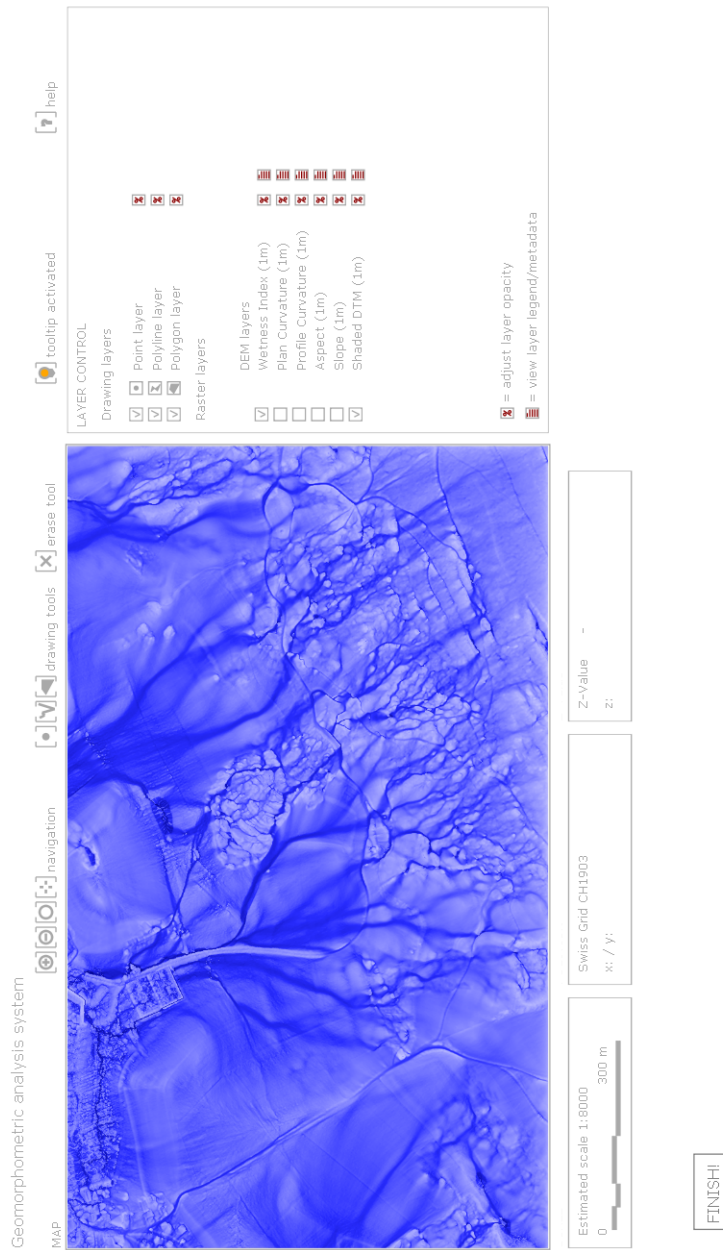


Fig. 6.1. Screenshot of the Geomorphometric Analysis System (GAS) - Digitization of features using high resolution DTM data

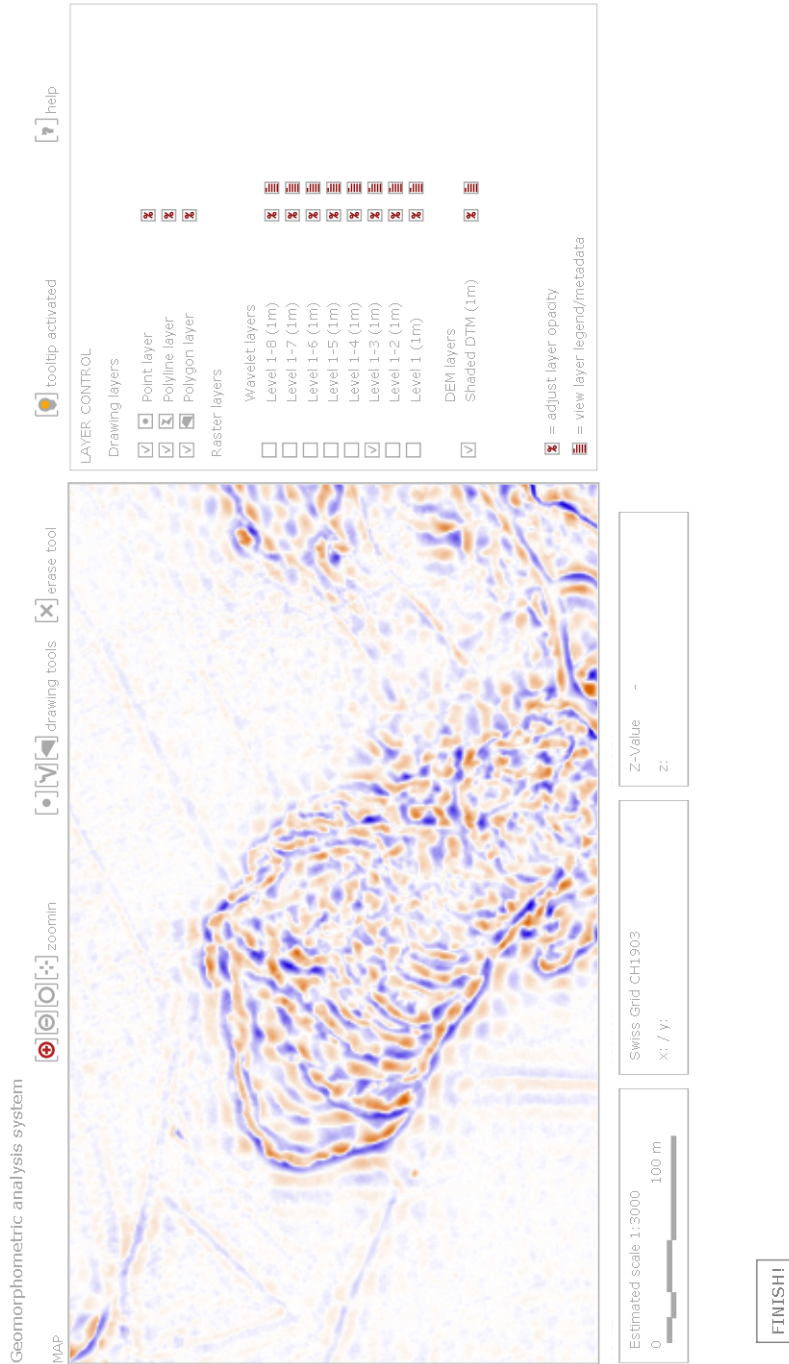


Fig. 6.2. Screenshot of the Geomorphometric Analysis System (GAS) - Digitization of features using wavelet data

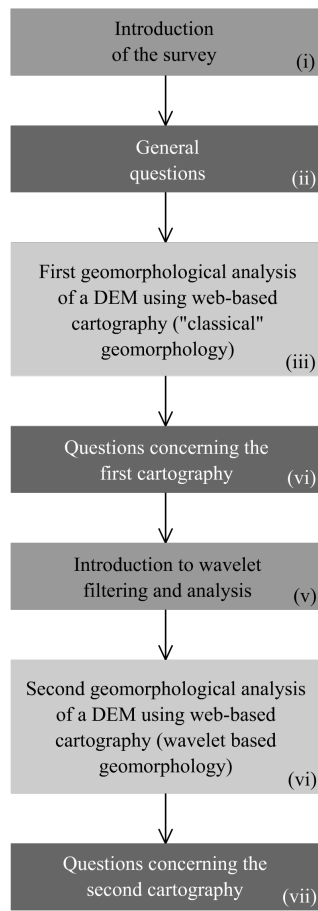


Fig. 6.3. GAS framework

We were able to gather fourteen people for this survey. Four of them were younger than 30 years. These users were possibly PhD students or young engineers. The users older than 30 were scientific adjuncts or professors. All of the participants had some GIS skills and knew what a DEM is. Only two participants did not know what DEM derivatives are. One did not have any knowledge of ALS data. (details about the participants are summarised in table K.1, appendix K.)

Although some of our participants had intermediate skills for the survey, we can state that the general knowledge of GIS and DEM analysis was good.

6.2.3 Results

As suggested by our hypothesis, users were not satisfied with the first analysis using only geomorphometric indicators. We argue that this fact might be related to a lack of qualitative information in the system such as a description of the geological context or an aerial overview. This is also reflected by the participant's comments (see table K.2, appendix K). One participant for instance stated that he *"needed derivatives to be computed at multiple window sizes and grid resolutions to better assess larger features and provide context"*. This comment suggests that the participant was a geomorphologist who is used to LandSerf³, a software tool developed by Wood (1996). Landserf enables the use of multiple window sizes to compute geomorphometric indicators, this in order to analyse context effects linked to scale.

Regarding the contribution of wavelet data to terrain analysis we analysed the comments given by the participants after the second digitization (for details, see table K.3, appendix K). One important result was a considerable number of users who found the wavelet reconstructions useful for their analysis. However the global satisfaction did not increase (only one user was more satisfied). Most participants found the analysis easy to do using these new layers.

One participant stated that he found the explanatory power of wavelet analysis somewhat limited, but he was surprised about the fact how well larger landforms were captured by the low-passed filtered images. Furthermore he stated that high-pass images show artefacts. (see comment C in appendix K). The user apparently had some knowledge about wavelets, but the wavelet results which are given in GAS were already a restricting factor for him and he would probably have liked less constrained wavelet results.

The positive fact is the two answers to questions 2 and 4 (table K.3, appendix K). This tells us that wavelets bring complementary information and understanding in the analysis.

Regarding the users' general comments, we can conclude that wavelet layers contributed with complementary information to the terrain analysis but without being exclusive. One comment also showed that it is difficult to interpret data that is only available visually and that it is important to understand what the data represents in order to be able to do the analysis.

³ <http://www.landserf.org>

Cartography.

It was decided to illustrate the results of the mapping process for only 3 sessions. They are representative of the users' perception of the structures contained in the DEM. Session 3 illustrates how people (or different visual systems) perceive DEM and the shading effect. Although the shading parameters (azimuth and sun angle) were indicated in the first GAS description, the user of session 3 inverted the scarp and accumulation zones (figure 6.4). She/he actually saw a convex deposit zone where the transition zone is located, and a concave scarp zone where the accumulation (or deposit) zone is located. This illustrates the need to have an independent system which is more user-friendly, this was however not the purpose of this survey.

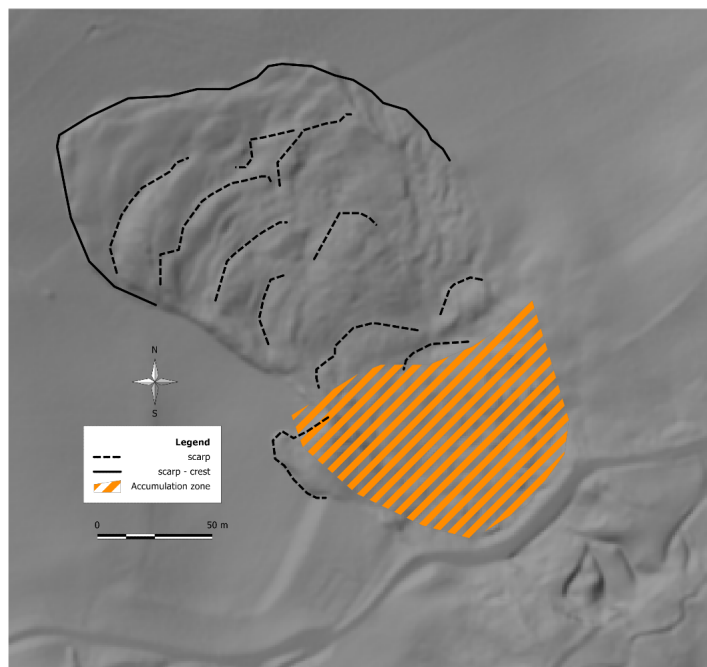
The second analysed session (session 7) shows clearly the difference of terrain perception using both type of information. In the second exercise (figure K.1 (b), appendix K), the user saw something that he actually was not able to identify, but which confused him regarding the first exercise. In fact, he identified the zone where the liquefied material flow, or the real deposit zone of the material which flowed down from the scarp zone. The navy blue and orange stripped zones (figure K.1 (b), appendix K) are settlement zones and not deposit zones. This fact clearly illustrates that wavelets tools and products may be used as complement to usual geomorphometry.

The last analysed session (session 9, figure 6.5) shows about the same as session 7. The wavelet analysis enabled the user to perform a further analysis than using only usual geomorphometry. Some elements, like the lateral flow (figure 6.5 (b)), were identified only in the second exercise.

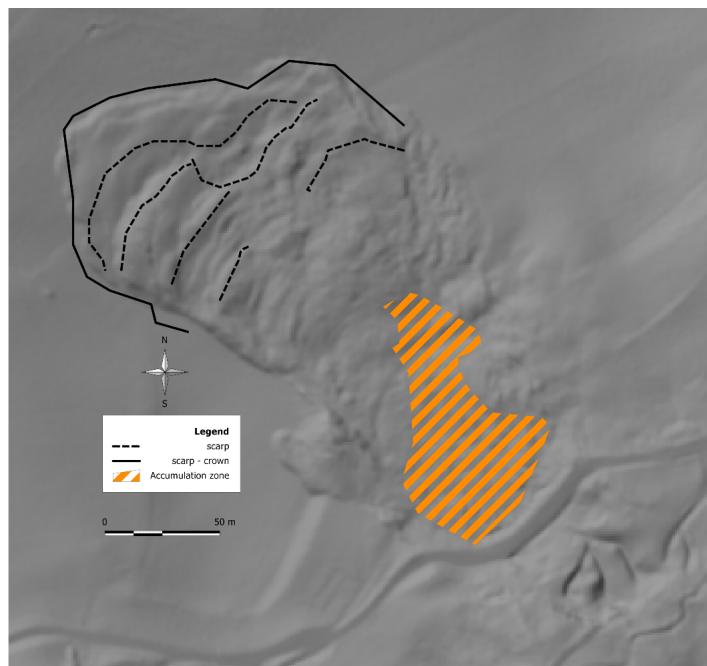
6.2.4 Conclusions

As we have seen, people found the wavelet approach useful and complementary to usual geomorphometry, but the result analysis showed that they were confused by the new data, because:

1. Wavelet analysis and synthesis is not a geometrical analysis, as usual geomorphometric indicators are. Geomorphometry has a short common history with frequency analysis. The first attempts used the Fourier transform, which is not really suitable in this case and induces a general rejection of methods which use scale analysis and frequency partitioning (user comment: *I am not sure if this frequency filtering is good here except for detecting wave-like patterns in the landslide body*).
2. The resolution, using subband high-pass reconstruction, does not decrease. Users with little geomorphometric skills have problems understanding how different sized elements can be retrieved in layers (or images) which have the same resolution. This issue is common to multiscale geomorphometry. In the GAS survey, only one participant gave a reference to multiscale geomorphometry in the way that Wood (1996) developed it.
3. Geomorphometry, in its present application, is an "old" methodology. Its general definition was given by Evans (1972). Since then, technological developments and computational power have incredibly increased, but the applied techniques are still the same; geomorphometry specialist and GIS users still use the well-known 3×3 convolution window. Most of them do not even have a thought on what multiscale geomorphometry



(a)

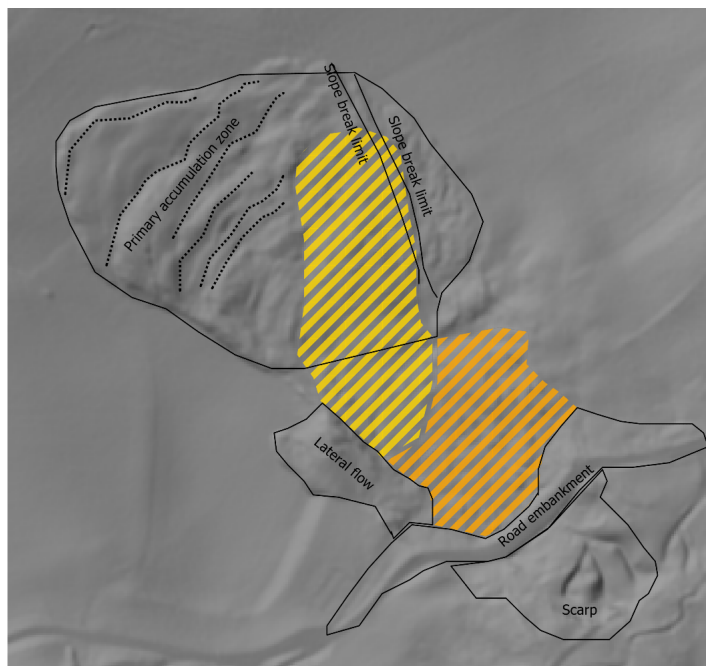


(b)

Fig. 6.4. GAS mapping - session 3, (a) exercise 1 and (b) exercise 2



(a)



(b)

Fig. 6.5. GAS mapping - session 9, (a) exercise 1 and (b) exercise 2

is. This behaviour induces a strong refusal of methods and techniques, which certainly are not completely innovative, but which give an impulse to scale analysis in geomorphometry.

Some criticism has to be expressed regarding GAS. Firstly, the geomorphometric indicators were computed using a 3×3 window. The users had no access to enlarged convolution windows (Wood, 1996). The choice of the window size could have given the users access to indicators (like curvature) which approach quite well the wavelet reconstruction levels. Secondly, the users had to do the same analysis in two different exercises and it is very likely that users have been influenced by a learning effect. The first exercise gave them the first raw overview of the landslide and the second exercise enabled them to improve their learning of the phenomenon's description.

Regarding the structure of the GAS interface, some criticism was also revealed by the users' remarks. The WT explanations did not seem to convince some users. Some of them did not really understand what the WT was and how it dealt with the structures contained in the DEM. Some people understand the WT as a frequency transform using some kind of localized sine and cosine waves (which it is not!).

Regarding the criticisms above, the following improvements should be implemented in GAS:

- Give a better explanation of the WT. Perhaps should it be less detailed than at the present.
- Inverse the exercise and find some new participants to do the survey. It could reveal how pronounced the learning effect is.
- Give access to the users to multiscale information regarding usual geomorphometry.
- Reduce the spent time. The exercise should focus on a less general analysis and give some hints to the users. A lot of them were confused, because they had not clue on how to do the exercise and on what they had to look for.

In conclusion, most users found the approach very interesting and complementary to usual geomorphometry. Of course, we did not give too much guidance information to the users on how to interpret the coefficient images, because we wanted to test their raw analysis capabilities. However, it appears that the lack of understanding of the algorithms and methods were a major limiting factor. All users were able to identify different structures at different scales, although sometimes their definition was completely wrong regarding reality. Following the analysis of the drawn structures (see figure 6.4 and 6.5, and figure K.1, appendix K), it is interesting to notice that no user identified the same elements regarding which information she/he used: usual geomorphometric indicators or the reconstructed wavelet coefficients. Therefore, we may conclude that wavelet analysis is complementary to geomorphometry.

6.3 Multiscale pattern analysis

DEMs and the underlying geomorphometry produce a great quantity of information and indicators. Some of these are highly correlated and some are independent of each other. This may be compared to the spectral bands of satellite imaging and like this, classification may be undertaken. There are many classification frameworks, for a complete review, refer to Caloz and Collet (2001) for imagery and to MacMillan and Shary (2009) for specific landform classification.

By having multiple indicators resulting from geomorphometry, we shall use a multi-dimensional classification method. In addition, as we do not have any a priori knowledge of the classification scheme, we will explore only unsupervised classification. Thus, we shall determine patterns using the low-pass results from the multiscale decomposition levels (chapter 4), proposing a multiscale pattern description of landforms. We will concentrate this section on the following questions:

- For each type of landform, is there a relevant number of multi-resolution clusters?
- For each clustering level (resolution) are the multiscale patterns nested one in another?
- Does the spatial distribution of patterns inform us about the geological and geomorphological features?
- Is multiscale clustering an effective way to characterize the evolution of landscape pattern through scale and to assess the primary aims of this study?

6.3.1 Unsupervised classification of geomorphometric indicators

In order to avoid any a priori determination of classes or categories, we choose to perform an unsupervised classification. As there are many possibilities for unsupervised classification, we will only skim over some to show the fundamental differences between them:

- Defined number of clusters: ISODATA and k-means (Bezdek, 1984) are two techniques which are very similar. ISODATA is only a more specialised algorithm, because it uses the intern cluster variation to accept or reject a cluster, thus, the number of cluster may be decreased by the iterative algorithm. Many authors have used either ISODATA or k-means for the classification of geomorphometric information (Irvin *et al.*, 1997; Burrough and McDonnell, 1998; De Bruin and Stein, 1998; Burrough *et al.*, 2000, 2001; Arrell *et al.*, 2007).
- Defined scale analysis: the mean shift algorithm (Comaniciu and Meer, 2002) differs from the two others, because it is not the number of clusters that is pre-defined, but the spatial boundary (radius) in which a cluster has to be confined. Because we are not using spectral information (like the red-green-blue bands), it is hard to define which is the bandwidth threshold to use. In addition, we are not using normalised data like images which are normalised between [0, 255].

Regarding the above descriptions, we will focus on the fuzzy k-means algorithm. The fuzziness is defined by the pixel's membership to a cluster, which is never absolute. Indeed, the pixel has a membership to each cluster. Usually, it is only the hard cluster which is illustrated, or, in other words, the highest membership to a cluster defines the pixel's attribution to a cluster. The issue using this kind of classification algorithm is that it does not take into account any spatial neighbourhood relation. Each pixel is classified regarding its position in the multi-dimensional space of the used variables, but not regarding its spatial location and thus its surrounding pixels.

6.3.2 Fuzzy k-means

Fuzzy k-means classification has already been applied with success on various DEMs with various resolutions (De Bruin and Stein, 1998; Hanesch *et al.*, 2001; Irvin *et al.*, 1997; Arrell *et al.*, 2007). But each author focuses on the direct geological patterns obtained and not on the nature of the primary data. In this part, we are interested in the relevance and relations of partitions of the landscape using several scales and not in the geological definition of the obtained patterns.

The purpose is to analyse the nesting of patterns (or clusters) one in another through different scales as defined by the wavelet transform. The Travers DEM was used to do this classification.

Fuzzy k-means is a clustering method. Using several variables a multi-dimensional space is created (see 2D example in figure 6.6). Then an arbitrary number of random positioned cluster centres is initiated. Through iterations, the distance⁴ between the centres and the data point of the multi-dimensional space is minimised using generalised least-squares. At each iteration, the cluster centres are repositioned using the results of the estimated new centres. For a complete review of the algorithm, refer to Bezdek (1984). The fuzziness is originated by the membership of each data point to each cluster. Thus, the iterations stop once a certain threshold of membership has been reached for the minimized distances (Hanesch *et al.*, 2001). The mathematical description of the fuzzy k-means classification is described in appendix L.

The quality of the fuzzy k-means classification may be analysed using some statistical indicators. First, correlation between the used variables shows how these are independent one of each other. Ideally there should not be any correlation between them. But this is hardly achievable as we will use derived variable from a DEM (see next section). We also used the confusion index which indicates how good the classification of each observation is. Finally, two coefficients (the F_{scaled} partition coefficient and the H_{scaled} classification entropy) are overall indicators of the classification. All these indicators are described more thoroughly in appendix L.

6.3.3 Application to DEM pixel classification

To be able to apply a multiscale cluster analysis, the high resolution DEM was first resampled using the wavelet transform. This preprocessing produced a DEM with a 2^i resolution (i being the decomposition level, $i = 0, 1, 2, 3, 4$) compared to the original DEM. The wavelet transform was applied four times

⁴ The distance may be the Euclidean distance or the Mahalanobis distance.

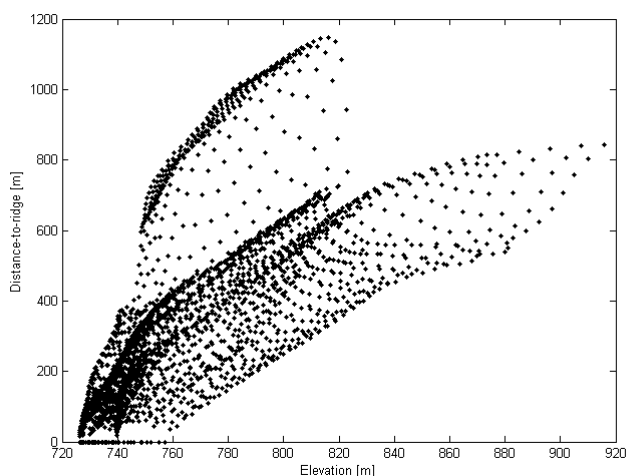


Fig. 6.6. Plot of the elevation versus the distance-to-ridge. This defines a 2D space in which the cluster could be positioned.

which resulted in five DEMs with five different resolutions: 1 *m* for the original DEM, 2 *m* for the first level DEM, 4 *m* for the second level DEM and so on until the fourth level which gave a 16 *m* resolution DEM. For details about the wavelet transform, see chapter 4.

The following geomorphometric indicators were computed for each of these DEMs:

- Slope
- Solar radiation
- Profile curvature
- Plan curvature
- Wetness Index
- Distance to ridges

To these six variables was added the raw DEM and the fuzzy k-means were applied to the seven dimensional space defined by these variables. For each DEM, the k-means were applied using 2, 3, ..., 9 clusters. This produced 36 different classifications.

The choice of these variables was made regarding previous studies (Irvin *et al.*, 1997; Burrough and McDonnell, 1998; De Bruin and Stein, 1998; Burrough *et al.*, 2000, 2001; Arrell *et al.*, 2007). It is clearly an arbitrary choice. Besides, these variables should be independent, what they clearly are not. Each geomorphometric indicator is computed using the original elevation, and most of times, they are a combination of the first or second DEM derivative. Correlations between the indicators should show if it is pertinent to use them for the clustering. If there is a high correlation between two of them, the information will be redundant and will not bring any new information to the clustering.

Correlation

As shown in table L.1 (appendix L), the highest (negative) correlation occurs between the slope and the wetness index. This high correlation is explained by the fact that the wetness index is computed using the slope (see section 2.4.2, equation 2.9) and increasing the decomposition level, (negatively) increases the correlation. The same is visible between the distance to ridge and the wetness index. Again, they both are dependent of specific catchment area.

The correlation between the slope and the solar radiation is more due to the specific topography of the DEM. This one covers one hillside and its downhill valley. Thus the hillside has a preferential solar radiation with a very regular slope and the downhill region has a smooth slope with another preferential solar radiation due to the river which is passing across. Authors (Burrough and McDonnell, 1998) who used the same method for pattern classification showed that usually slope is more or less highly correlated to annual irradiation.

F_{scaled} & H_{scaled} coefficients

The combination of the partition coefficient and the entropy coefficient give the next (but not exhaustive) property:

$F_{scaled} = 1 \Leftrightarrow H_{scaled} = 0 \Leftrightarrow \forall maxfuzz1$, “the associated cluster k is a hard cluster”. ($maxfuzz1$ is the first dominant membership.)

Usually, the best classification is considered to be a combination of large values F_{scaled} and small values of H_{scaled} .

The F_{scaled} and H_{scaled} coefficients show a reduction of the hard classification while increasing the number of classes. Only in the second level, these coefficients show that four classes would be an appropriated classification scheme (see figure 6.7). For all the other levels, the two classes choice would statistically be the most appropriated.

Nevertheless, the F_{scaled} is a combination of the variance of each class and the variance between classes. The F_{scaled} is a global clustering statistical indicator (Bezdek, 1984). On the other hand, the H_{scaled} entropy ratio is more sensitive to local changes.

So, why do these indicators degrade when increasing the number of classes?

Burrough *et al.* (2000) used two DEMs with different resolutions (5 m and 75 m). Thus we should obtain about the same correlation results for the second level ($r = 4 m$) as Burrough. Correlations show a high similarity with his results and the results concerning the assessing of the classification (F_{scaled} and H_{scaled} coefficients), but for all other levels the results are not as expected. The ratios are not showing any best class. In other words, the best class is the two classes and increasing the number of classes makes the ratios only decrease (F_{scaled}) and increase (H_{scaled}), thus the quality of the classification decreases.

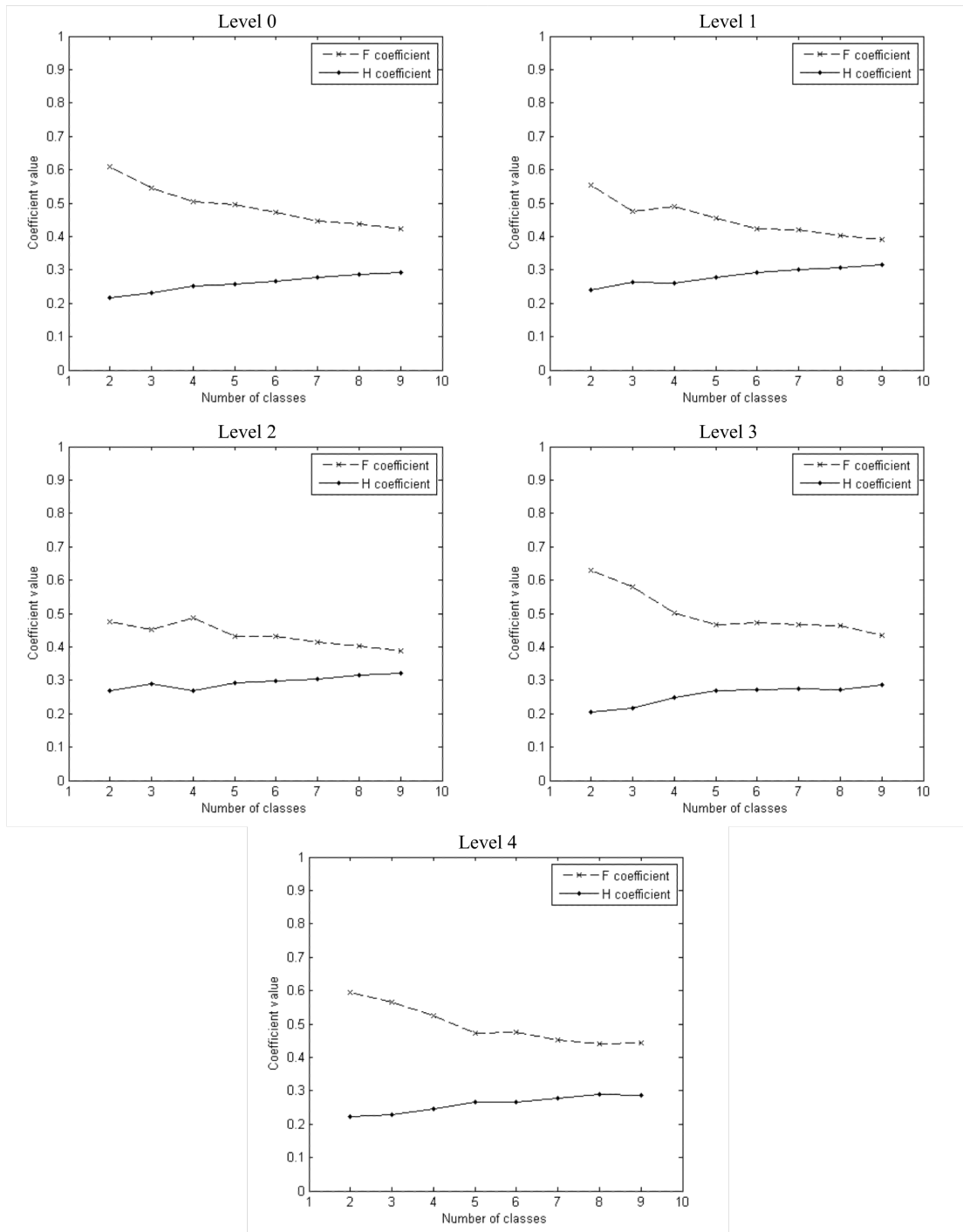


Fig. 6.7. F_{scaled} & H_{scaled} coefficients

Pattern distribution analysis.

The pattern distribution analysis has to be understood as the analysis of specific relief configuration in a 64×64 meter area or window. It was defined to be representative of the studied area. For each number of clusters and each decomposition level, indicators of density were computed. On this basis, the evolution of the patterns through the different scales is analysed, thus the evolution of the signal frequency embedded in the patterns. We hope to illustrate the evolution of the unstable high frequency superficial morphology of the topography into superficial morphology which is more stable, at lower frequency. In this context, the patterns give a more synthetic view of the generalisation effects and the geological definition of these patterns. Namely, if there is a variability of the unstable patterns across scales, and which there relevance to a specific phenomenon is.

For each decomposition level, a 64×64 window means:

Level	Window size	Number of pixels
Level 0 (1 <i>m</i> resolution)	64×64	4096
Level 1 (2 <i>m</i> resolution)	32×32	1024
Level 2 (4 <i>m</i> resolution)	16×16	256
Level 3 (8 <i>m</i> resolution)	8×8	64
Level 4 (16 <i>m</i> resolution)	4×4	16

Table 6.1. Size of the pattern analysis window for each decomposition level

Four zones were defined for the pattern density analysis (figure 6.8). These will be described regarding their geology by using two elements: the DEM (figure 6.9) and a geological map (figure 6.10) based on the work of Gocht (1961).



Fig. 6.8. Location of the four zones, aerial photography©SITN

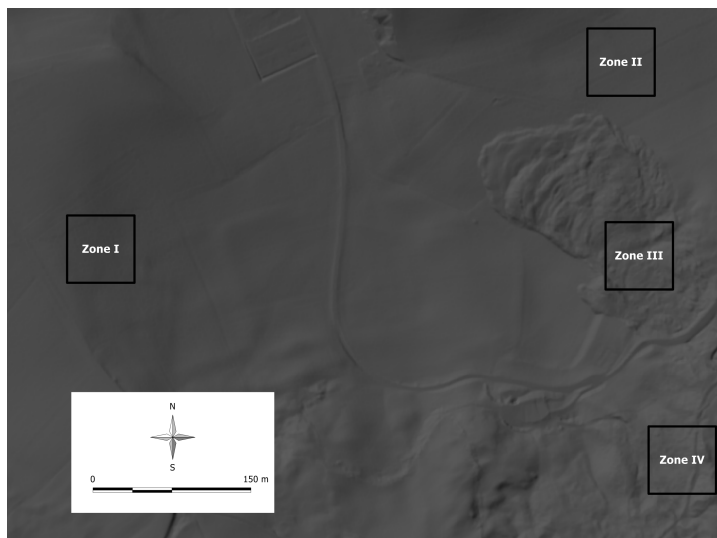


Fig. 6.9. DEM and the four zones, DEM©SITN

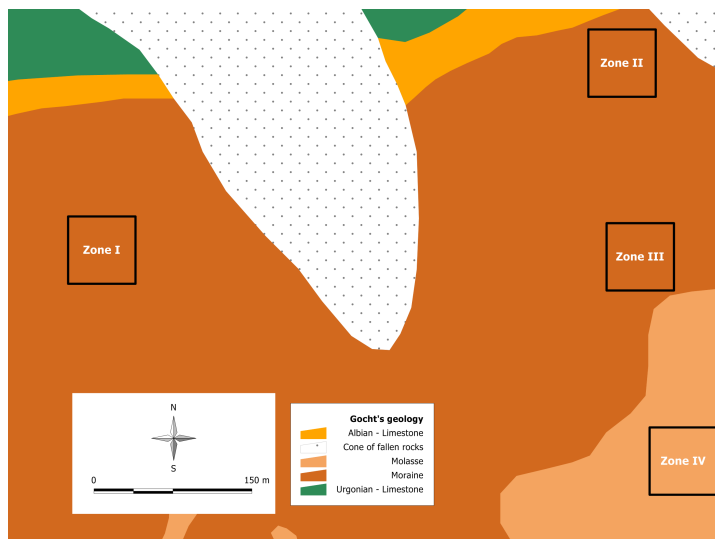


Fig. 6.10. Gocht's geology and the four zones, (Gocht, 1961)

The following geological descriptions are based on Gocht's map (figure 6.10).

Zone I

We are dealing with a limestone zone having a quaternary morainic outcrop, thus a fairly stable zone in a geomorphological point of view. However, morainic formations have rather a low electrical resistivity and, thus, rather a high water permeability:

- Location: at the west of the landslide on the side of a hill. It is located on an agricultural pasture area. In a geomorphological point of view, it is not located on a lowland formation, but on the extension of a formation coming downhill from the Jura.
- Geology: it is completely contained in a substratum composed of limestone from the albian-aptian geological period, thus a more or less stable formation. This is recovered by moraine from the quaternary period.

Zone II

As for zone I, it is a limestone zone with a morainic outcrop, thus a stable zone in a geomorphological point of view. As remainder, morainic formations have a rather low electrical resistivity and, thus, a rather high water permeability.

- Location: at the north of the landslide on a very flat meadow. Geomorphologically, it is located on a lowland formation (valley of Val de Travers).
- Geology: it is straddling on two limestone substratum formations from the albian - aptian and urgonian periods, thus a more or less stable substratum. As for zone I, these are covered by moraine from the quaternary period. There is a limestone outcrop just at the north of zone II.

Zone III

In zone III, the geological context before the landslide seems irrelevant, because the materials which are now located on it come from the scarp zone. The liquefaction of the material and their flow created an extremely heterogeneous geological area. It might be a mix of moraine and sandstone with a matrix of clay-sandstones.

- Location: inside the transition zone of the landslide, it is surely in a unstable formation. After the landslide, it is located in an area of sandstone which is a mixture of clays and sandstones.
- Geology: before the landslide and looking at the substratum, this zone was in a transition zone between the uphill sandstone and the limestone outcrop downhill. The quaternary period deposited a morainic formation on the top of this substratum.

Zone IV

Regarding Krähenbühl (2007), this zone is located in a strongly disturbed area with blocky limestone and covered by a thin morainic layer. This implies strong water flows and infiltration, thus screes. Regarding the forest coverage, most of them are more or less stabilised.

- Location: south of the landslide on the north hill of the Jura. The slope of this anticlinal is steep for the Jura. On the DTM, the zone is located on a disturbed morphological area with a high roughness.
- Geology: the coverage is of sandstone. Furthermore, the sandstone-moraine interface is located downhill.

Spatial density indicators

For each classification result and each decomposition level, two density indicators were computed in order to verify if specific frequencies or scales react preferentially to the type of topographical coverage, thus the suggested geology or geomorphology.

The *Shannon*⁵ and the *Simpson*⁶ diversity indicators were calculated for each zone at each scale and for each classification (number of clusters).

The *Shannon* and *Simpson* indicators are not significantly different in this case. The behaviour of these indicators is identical for our four zones (see figures 6.11 and 6.12). Thus, we will only use the *Shannon* indicator to do the analysis.

⁵ $Shannon = -\sum_{i=1}^m (P_i \ln(P_i))$, $Shannon \in [0, \infty)$, where P_i is the proportion of area occupied by each cluster. When $Shannon = 0$, than the analysed zone contains only one cluster. *Shannon* increases as the number of contained clusters increases (Anonymous, 1995)

⁶ $Simpson = 1 - \sum_{i=1}^m P_i^2$, $Simpson \in [0, 1]$, where P_i is the proportion of area occupied by each cluster. When $Simpson = 0$, than the analysed zone contains only one cluster. *Simpson* increases as the number of contained clusters increases. *Simpson* is more sensitive to the presence of “rare” (or poorly represented) clusters than *Shannon* (Anonymous, 1995).

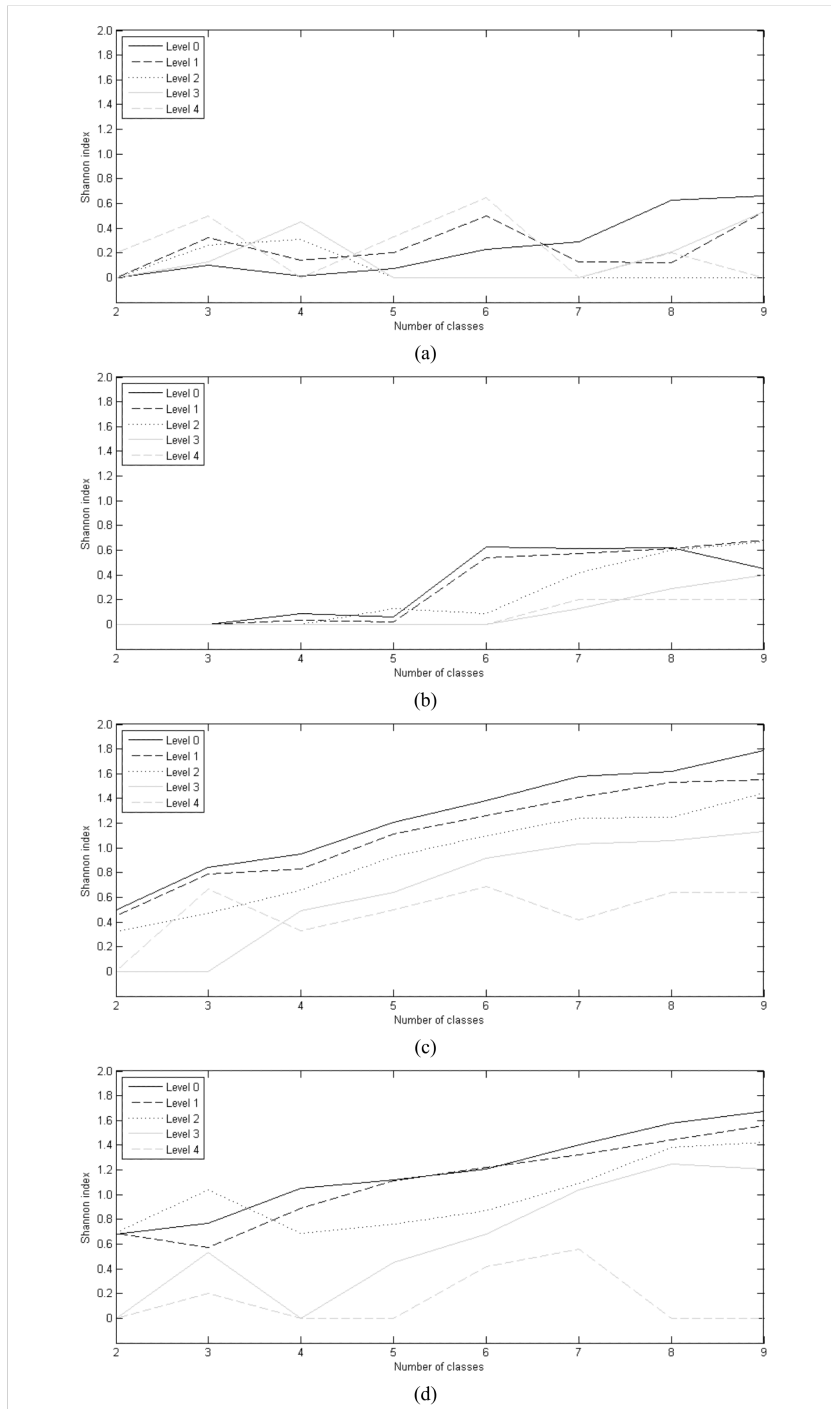


Fig. 6.11. Shannon indicator, (a) Zone I, (b) Zone II, (c) Zone III and (d) Zone IV

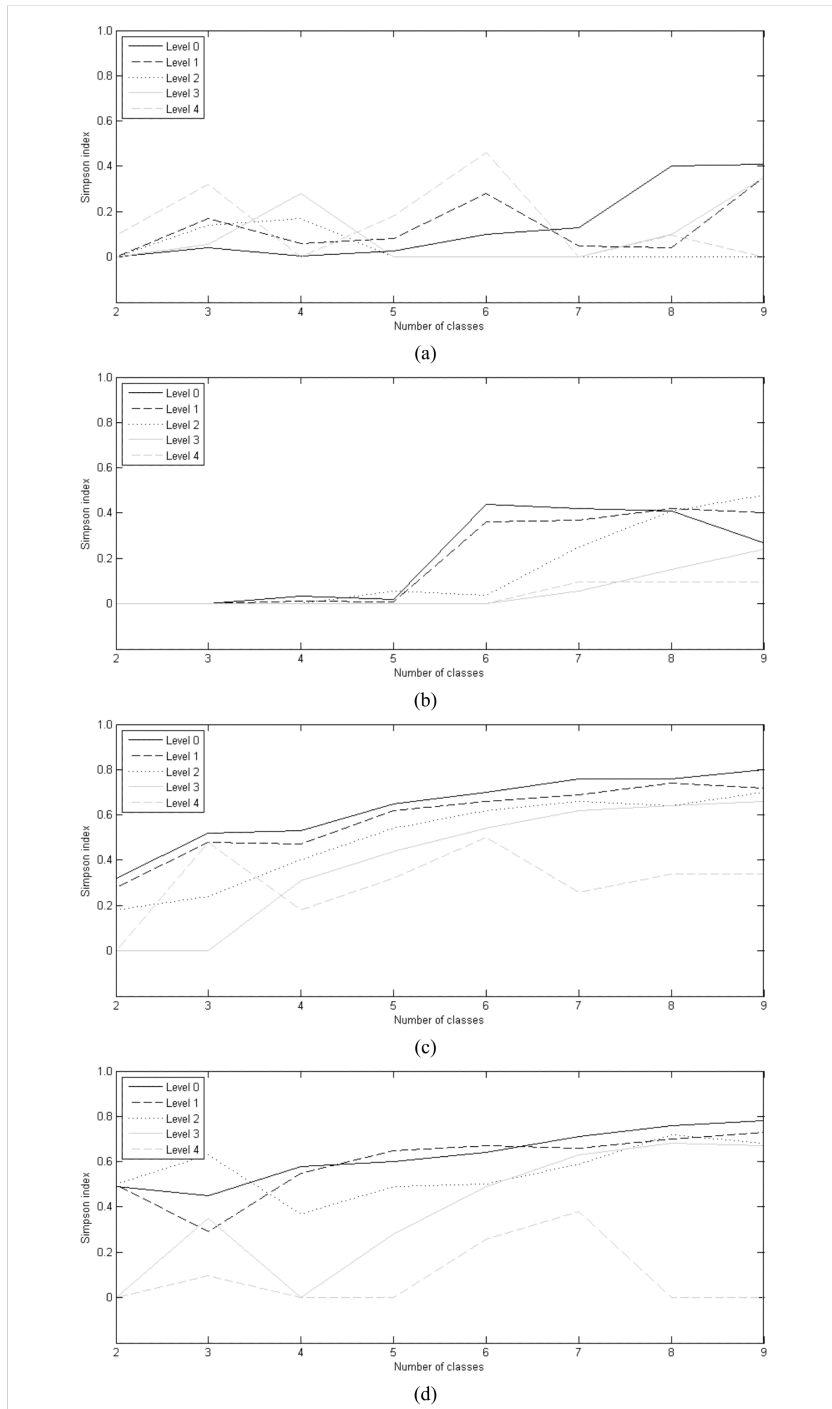


Fig. 6.12. Simpson indicator, (a) Zone I, (b) Zone II, (c) Zone III and (d) Zone IV

Regarding the geological description and the position of the zones, following assumptions can be made:

- Zone I & II are similar. They are located on similar geological substratum. There are positioned on a homogeneous morphological area, thus they should be members of the same clusters and the evolution of the *Shannon* indicator should be about the same.
- Zone III is located in a very perturbed area, the landslide. But we have to notice that even if the morphological roughness is high, the zone is still located in a heterogeneous area, the size of the landslide structures is very little, thus rather a very high frequency area.
- Zone IV is located in a fallen rock area. Thus, the geomorphological elements are of bigger sizes than for zone III. The frequency composition of the geomorphological elements is lower.

Inherently to its definition, we expect the *Shannon* indicator to increase as the number of clusters increases. Indeed, when the number of cluster increases, statistically, the diversity should increase within our areas. It is interesting to note that:

- There is a clear difference in the behaviour of the indicator between Zones I & II and III & IV. The less disturbed areas, and therefore more homogeneous, have indicator values which are much smaller and their evolution, gradually as the number of clusters increases, is much less linear.
- The fourth level of decomposition is highly variable and unstable. The resolution of this level (16 m) and the size of the analysis window (64 × 64) are the factors influencing these variations, mainly because the *Shannon* indicator was calculated using only 4 × 4 pixels. This level is not appropriate to the size of the window, because the frequency space that it represents is of much lower frequency than the structural elements included in the window.
- The linear progressions of the indicator in Zone III & IV are ordinary. The pixels included in these areas are extreme at all levels. Their values are surely not near the average values of the different predictors (elevation, slope, etc.). Their membership values related to a specific cluster are much higher than for zones I & II. These latter are in areas of medium fluctuations of the predictors, and so the distances to each cluster centre are less differentiated.

In conclusion, we found that uniformity of surface makes the classification less constant through scale. Namely, that these low frequencies structures are more prone to organisational variations of the clusters. Thus, the number of clusters within the area is not constant compared to the total number of classification clusters. In zones III & IV, the indicator is much more constant, therefore the increase of the cluster number within the zones, compared to the increasing number of classification clusters, is constant. The high frequency structural elements, thus high roughness, are more stable even if the indicator tends to decrease through scale, which is due to the reduction of the number of pixels. By applying a moving window, it is possible to find stabilities (frequency stabilities and not geological) of terrain across scale.

7. A vision for multiscale DEM analysis

7.1 From wavelets to Marr's vision theory

As seen in chapter 4, wavelet decompositions are a powerful tool for multiscale image analysis. Wavelet analysis of high resolution DEMs (Lassueur *et al.*, 2006) is highly complementary to geomorphometric indicators (Wood, 1996) and includes, for instance, multiscale filtering and enhancement. Geomorphological phenomena are clearly multiscale (Schmidt and Andrew, 2005). Thus, the identification and delimitation of these are not easy due, on one hand, to their complexity across scales and, on the other hand, to the inherent geological or geomorphological interactions.

The wavelet transform gives us a partitioned vision of our environment and of its scale intervals following the dyadic subsampling. As we have seen, our analysis has mainly been carried out on the detail coefficients and, more importantly, on their selective reconstruction. However, when we analyse a landscape and its DEM decompositions into a four component 2D signal (low-pass, horizontal high-pass, vertical high-pass and diagonal high-pass), we hardly ever focus separately on the details of the scene using the horizontal (east-west), vertical (north-south) and diagonal (north west - south east or north east - south west) directions. Classical wavelet transforms (Mallat, 1996, 2000) (see chapter 4) act like a smoothed multiscale derivative operator when applied to the data, but in a two directional manner. Our visual system concentrates on the directional continuum. In addition, the landscape and geomorphological forms are focused on a directional field covering the whole azimuth (from 0° to 360°), and not just on the three directions described by the wavelet transform. Thus, we have an interpretative issue. Basically, multidimensional data are processed in a separable way, i.e. dimension-by-dimension, which leads to multiple wavelets at each scale making the interpretation difficult. What we want now is to go one step further in the characterization of scale intervals and their representation than what we have done with the classic wavelet transform.

7.2 Marr's theory of vision

Marr's theory (Marr, 1982) suggests that vision (or human visual capabilities) is linked to information cells tuned into different spatial frequencies, thus making it possible to do multiscale analysis (Glennerster, 2007). The connection with the wavelet transform is immediate, because that is exactly what they do. Whether the dyadic subsampling is the proper way to create the scale partition of a high resolution is debatable, but the analysis undertaken in chapter 4 demonstrates that it is useful at least. Ideally, the system should

reproduce a multiscale analysis, function that the wavelet transform has, but in a multi-directional and continuous way, and not only bi-dimensional as we actually have seen.

Marr developed his theory of human vision using three distinct levels (Francescotti, 1991; Marr, 1982; Poggio, 1981):

- The computational level is constrained by the properties of the visible world.
- The algorithmic level is the set of rules to carry out the computation level and its inherent function(s).
- The implementation level is the architecture and realisation of the system.

Marr developed the computational level most thoroughly, which is the one we are most interested in. As Francescotti (1991) suggested, “*The computational level will involve the specification of certain facts about a human’s relation to his external environment which are powerful enough to ensure that the visual system successfully and reliably performs its designed function*”. As we mentioned in the previous chapter, high resolution DEMs contain a huge quantity of information. Geomorphological methods and the underlying quantitative geomorphometry are mostly univariate in scale. Thus, proposing multiscale analysis methods gives a better overview of topographical elements represented by DEMs. Furthermore, offering a multiscale approach where the experts do not have the choice of scale intervals, but where the approach gives them the most pertinent scale related information -regarding a given partition of scale - greatly simplifies the decision support process.

We now introduce various methods using Laplace-gradient wavelets and structure tensors in order to highlight the multiscale nesting of landscape features. The method was applied on the Travers DEM including the landslide (for a complete geological and phenomenological description, refer to appendix F) in order to make a first exploratory cartography of the phenomenon. The aim is to show the potential of this method and to give hints for further development of such tools in terrain analysis systems. Thus, we will only aim the study at the structural elements composing the landslide and not at the global context.

7.3 Marr’s decomposition

The recently introduced “Marr wavelet pyramid” (Van De Ville and Unser, 2008; Unser *et al.*, 2009) is an intrinsic 2-D wavelet design inspired by David Marr’s theory of the primates’ vision (Marr, 1982) that circumvents the limitations of the classic wavelet transform. Each scale is characterized by a single wavelet that acts like a Laplace-complex gradient operator. Consequently, the wavelet coefficients are complex-valued. The phase provides directional information and the magnitude indicates the wavelet deformation energy. This links this methodology directly to the implementation of Marr’s theory (Poggio, 1981) by detecting gradients and directions at all scales.

The Marr wavelet pyramid (figure 7.1), as developed by Van De Ville *et al.* (2008), is a method approaching the goal and issues of Marr’s theory. Applying it on high resolution DEMs brings us closer to the view of the structural composition of landforms, similarly to what our visual system would ideally do, according to Marr’s assumptions and theory.

The great difference with the classical wavelet transform (figure 4.6) is, there is only one resulting high-pass image, but this one is of complex form and we have some redundant information due to the first non-dyadic transform of the Laplacian operator (figure 7.1).

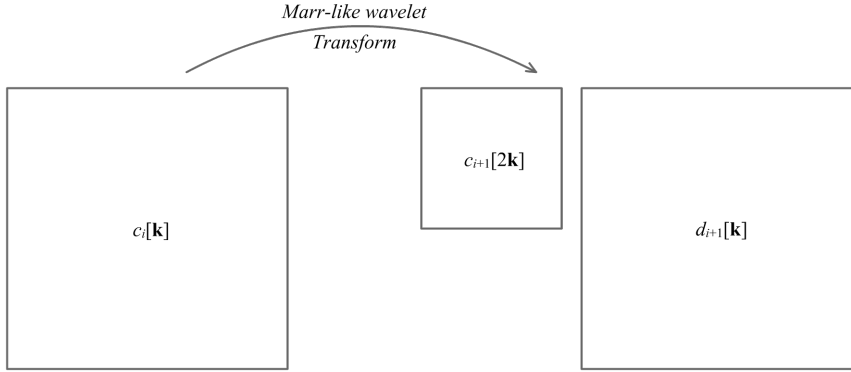


Fig. 7.1. Marr-like wavelet pyramid for one level

All the mathematical description and development are given in appendix M. Hereunder, we shall only discuss the result of the transform.

Applying the transform to each decomposition level i , the low-pass or generalised DEM will have a 2^{i+1} meter resolution and the high-pass or the detail coefficients will have a 2^i meter resolution (assuming that the original resolution is 1 meter), hence the redundancy. If the complex coefficients are separated using the real and imaginary parts (figure 7.2), we will retrieve the partial derivatives regarding the x and y directions.

7.3.1 Magnitude and phase of the complex wavelet subbands

If we combine the two components (real and imaginary) using a polar transform¹, we can isolate the magnitude and phase of the operator for each pixel at each scale (figure 7.3).

We will then observe that the magnitude reveals interesting structural features and the phase their underlying azimuth, depending on the decomposition level (thus the equivalent resolution of the shape). Both these indicators may be used for multiscale Canny edge detection (Parker, 1997), but this is not the purpose of this study.

For the first decomposition levels, phase represents phenomena of smaller sizes than the one which were already mapped (identified in chapter 4). This is also visible on the associated magnitude. Those are actually micro-folds which are linked to the large folds. The compacted materials did not withstand the pressure created by these large folds, and micro-folds were formed. Absence of roughness shows that the materials of the settlement zone are rather homogeneous and plastic. Indeed, pressure was roughly constant over the duration of the landslide, because the spacing of these folds appears to be constant (between 2 and 10 m).

¹ $Magnitude = \sqrt{\Re(d_i)^2 + \Im(d_i)^2}$ and $Phase = \arctan(\Im(d_i)/\Re(d_i))$

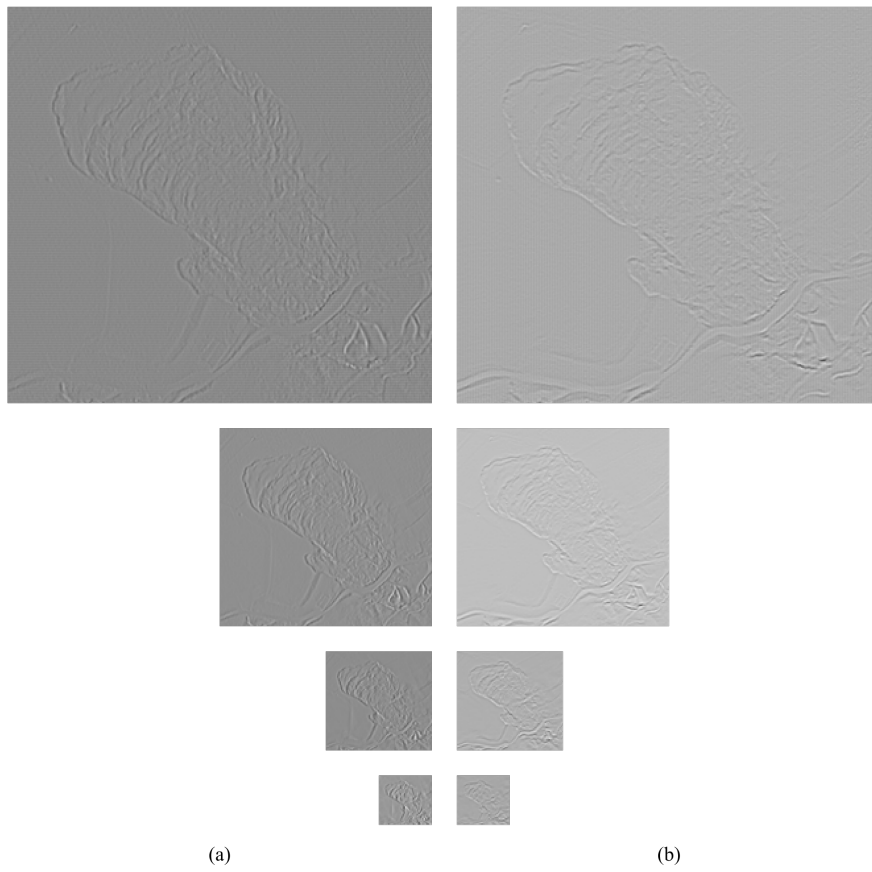


Fig. 7.2. Marr wavelet pyramid for the Travers DEM, respectively the real part $\partial/\partial x$ (a) and the imaginary part $\partial/\partial y$ (b) of the complex $d_i[\mathbf{k}]$ coefficients for levels 1 to 4.

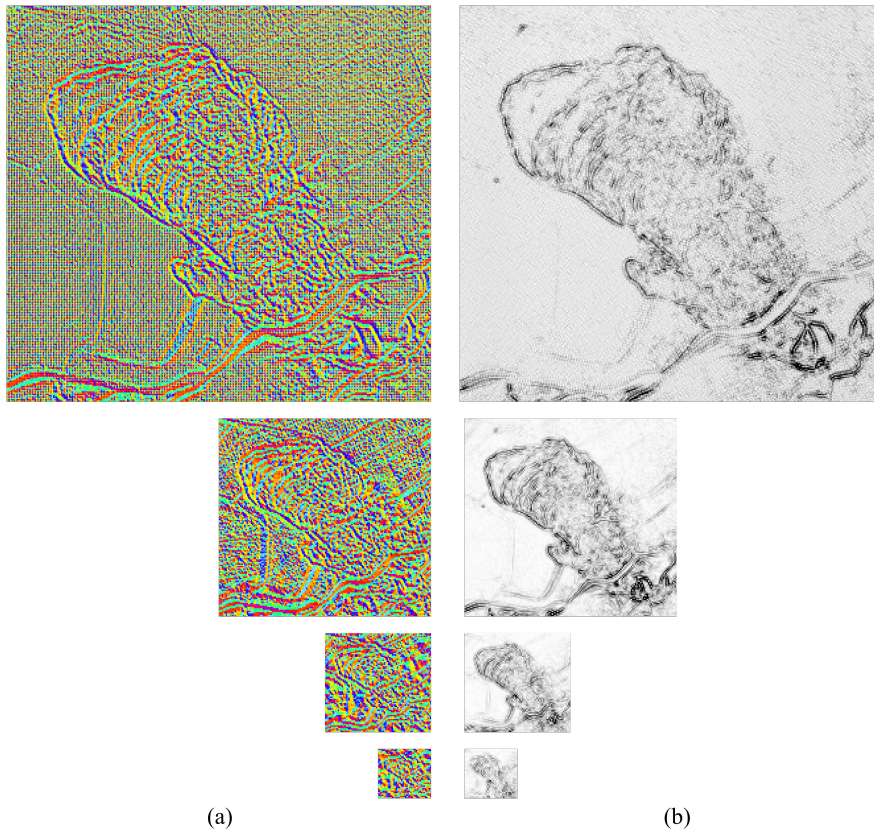


Fig. 7.3. Phase (a) and magnitude (b) results on the landslide area for the first four decomposition levels (i.e. resolutions of 1, 2, 4 and 8 meters)

The macro-folds can be already retrieved in the 3rd level magnitude map. However, the magnitude clearly indicates other type of folds. We can interestingly point out that these folds are not spaced out at regular intervals and that they correspond to micro-folds.

In the scarp zone, the first level of magnitude and phase clearly show the drainage area the authorities have built in direct response to the landslide. We must underline that artificial elements and interventions are those that stand out best, because they often are most acute. The large gap south of the accumulation zone, between the large landslide foot and the smaller foot is clearly visible. Its linearity indicates the direction of material flows.



Fig. 7.4. Magnitude of the first level and the digitized micro-folds

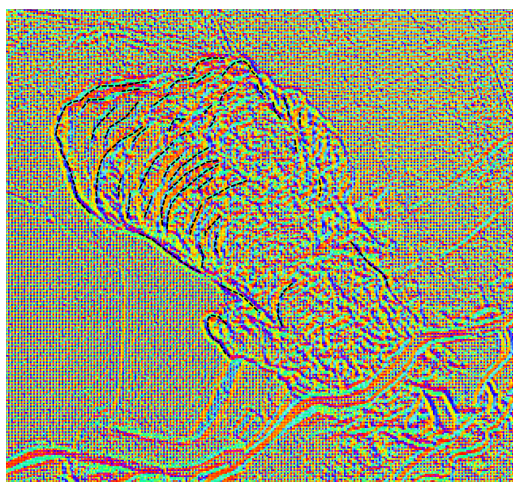


Fig. 7.5. Phase of the first level and the corrected digitized micro-folds

7.3.2 Subband-selective reconstruction

The selective reconstruction enables us to visualize information at the original high resolution, but the contained information is specific to one decomposition level and to one kind of information (the low-pass or high-pass information). Therefore, this is linked to a selective scaling filtering process. It is equivalent to the wavelet coefficient filtering which was introduced in section 4.3.

Low-pass coefficient reconstruction.

The low-pass results of the filtering process show the scale discretization which is obtained using the dyadic subsampling. Each decomposition level has a defined low-pass result complementary to the high-pass coefficients. The next steps are applied to the low-pass reconstructions:

1. The high resolution DEM is analysed until the n^{th} level.
2. The resulting high-pass coefficients are suppressed.
3. The Marr pyramid is reconstructed using the subband regression (SR) (figure 7.6).

The results show clearly the reduction of the frequency space following the decomposition (figure 7.6). However, as with the so-called classic wavelet transform, the low-pass information visual analysis is difficult. The model is certainly generalised, but the resulting information loses its context and the identification of structural elements is made more difficult. Again, it seems that the bottom-up approach, developed in section 4.3, can provide a better support to the visual interpretation by adding context to a specific decomposition level. As a matter of fact, this time, we will not analyse the direct effects of generalisation, but rather the remains, or high-pass coefficients of the transform. Because we are less constrained by the processing scheme, the multi-directional analysis will be added to the multiscale analysis. Nevertheless, an additional issue is revealed through this process:

- Each decomposition level gives a subjective view of the considered scale space.
- Each decomposition level produces two components: phase and magnitude

The low-pass results of the filtering process show the scale discretization which is obtained using the dyadic subsampling. Each decomposition level has a defined low-pass result deduced from the combination of the magnitude and the phase. In the geomorphological analysis, level 5 (figure 7.6 (d)) was used to digitize the main zones of the landslide phenomenon. This level showed the best partition of the landslide elements, thus this level is, for our own visual system, representative of the scale of these elements.

Some topographical elements clearly belong to a scale interval, as micro-elements to the 2nd level and macro-folds to the 4th level (figure 7.6 (a) and(c)), but there is no representation of scale imbrications. Most topographical elements have relations with others in scale, thus we will use a scale combination method in the next section to overcome this limitation.

As a consequence, if we use 8 levels of decomposition in our model, this results in the creation of 16 new surfaces. There is therefore a serious representation issue regarding this new information. No one is currently able to manage visually so much information and to analyse it in a selective and relevant manner. That is the reason why we will analyse the same bottom-up approach as in the previous chapter.

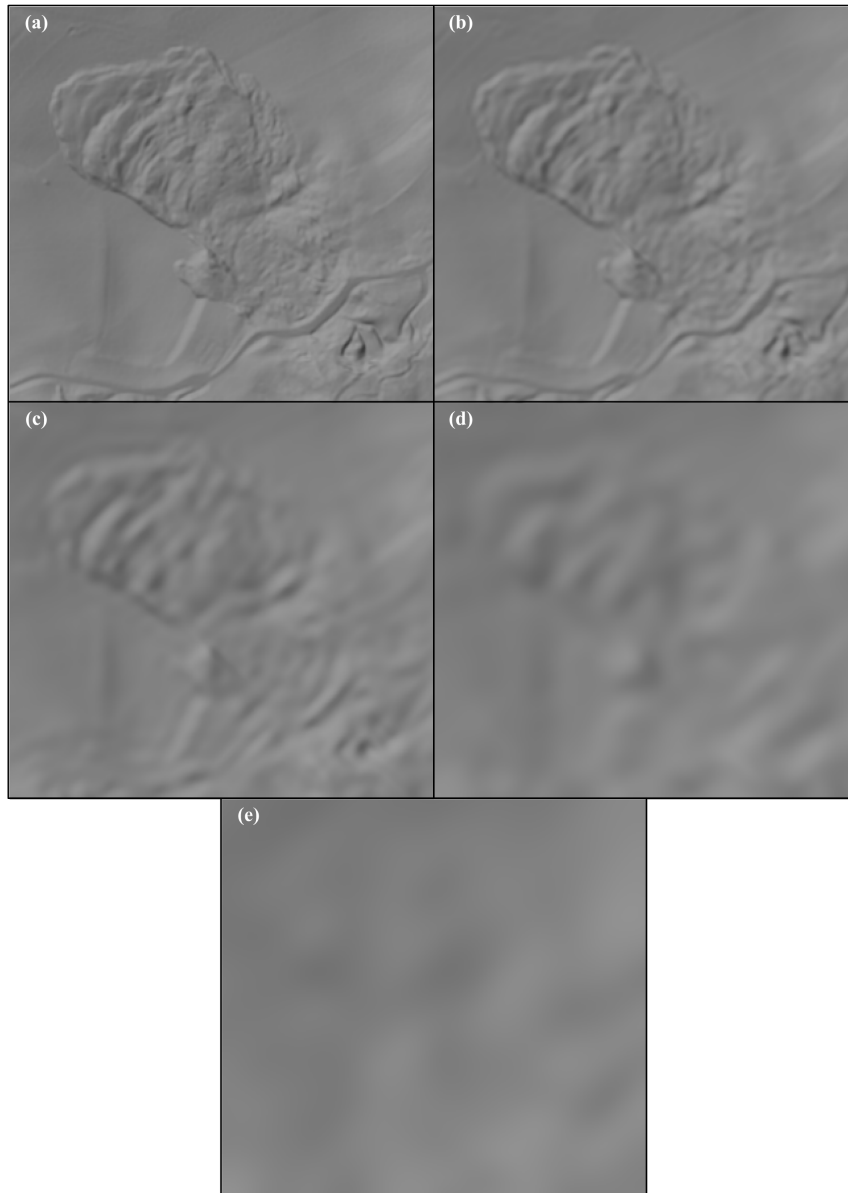


Fig. 7.6. Low-pass filtering and SR reconstruction of the Travers landslide DEM for the following decomposition levels: (a) 2nd level, (b) 3rd level, (c) 4th level, (d) 5th level and (e) 6th level.

Detail coefficient reconstruction.

Using only each level specific high-pass information does not allow a synthetic view of the topographical evolution through scale (see figure 7.7); i.e. the high frequency information which is specific to each decomposition level is too abstract for our visual cognitive system. There is a complete loss of context, as for example in the 4th level high-pass coefficients (figure 7.7). This is similar to what we have discussed in the previous section. The specific scale interval of this level is not relevant without its relation(s) to other scale intervals. To create the link between scale intervals, we reconstructed to the finest scale (1 *m* resolution) specific subbands by choosing which elements, based on their resolution (i.e. decomposition level), have to be included in the reconstruction process. Figure 7.8 shows the combination results of the different decomposition levels. It is similar to what was done in chapter 4. The following procedure was used to create these images:

1. The high resolution DEM was analysed until the n^{th} level.
2. The resulting low-pass grid was suppressed.
3. The Marr pyramid was reconstructed using the subband regression.

The images in figures 7.7 and 7.8 are normalised ($[-100, 100]$) coefficients with a colour saturation level at $[-20, 20]$. Negative values are given in blue and positive values in orange. The coefficients of the different levels were not enhanced (frequency boosting), but this could be done easily, depending on the interest of the geomorphologist.

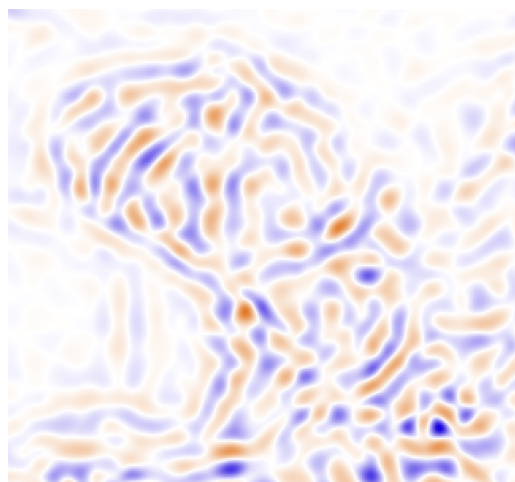


Fig. 7.7. Specific high-pass coefficients for decomposition level 4.

Thus, combining the high frequency information of each level with the others using a bottom-up approach gives context to the lowest level that we add at each iteration (figure 7.8). For example, figure 7.8 (d) is the synthesis (or SR reconstruction) of the high-pass information of levels $0, 1, \dots, 5$. Indeed, we deliberately omit all the information which is transferred to the $i+1^{\text{th}}$ level. For figure 7.8 (d), this would be the information transferred by the filtering process to the 6th decomposition level (figure 7.8 (e)).

If we continue our geomorphological analysis using figure 7.8, we will concentrate on the levels of interest regarding the elements that we want to analyse. As we have already had a global partition of the landslide component zones, we will first try to correct this one. The lower levels (2, 3, 4) give us information about the surface water flow. In this case the multiscale approach enables us to understand the high complexity of these regarding the morphological arrangement of the topography. Thus we are able to construct a geomorphological map, only regarding surface elements, which is then compared to the phenomena map established by Krähenbühl (2007) (figure F.6, appendix F). We used the lower levels to visually determine the main earth flows which occurred in the landslide. The higher levels were used to correct the main zones we already delimited using the low-pass information. The final result is illustrated in figure 7.12.

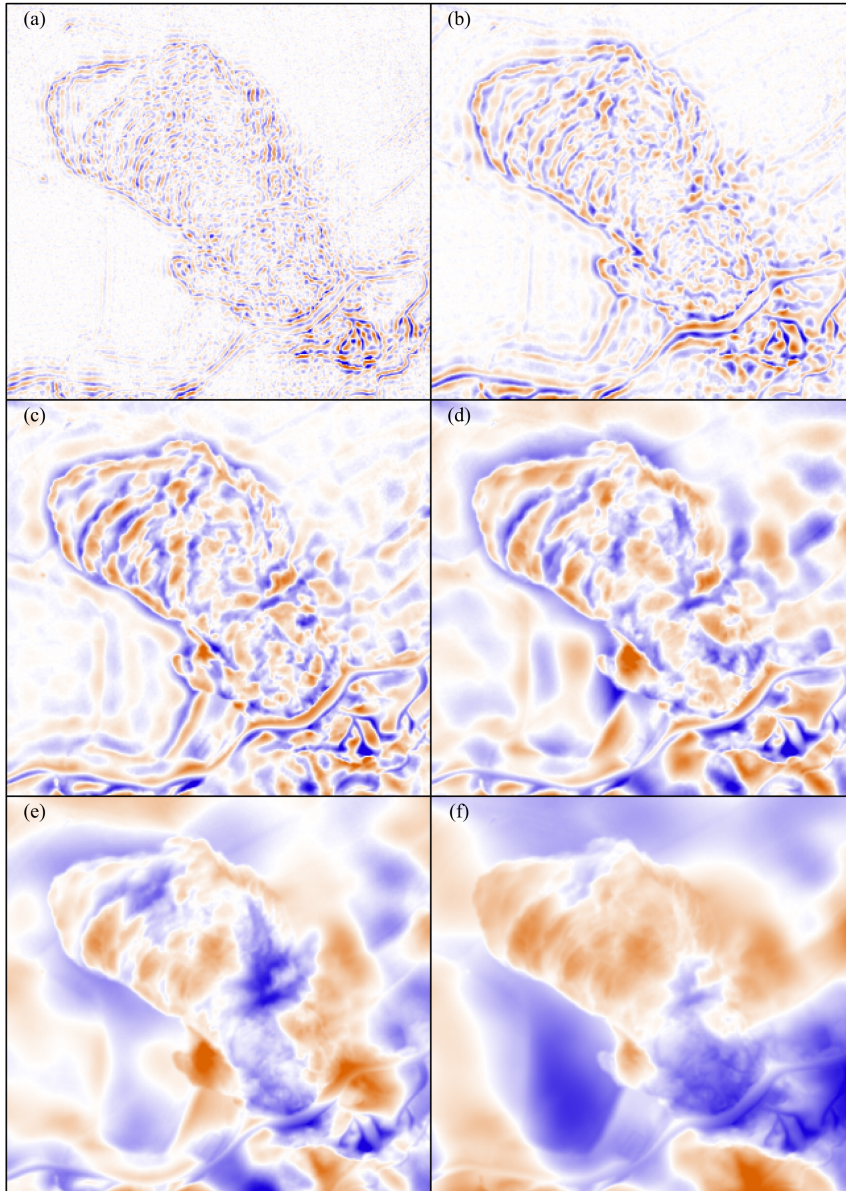


Fig. 7.8. Cumulated high-pass coefficients for levels 2 (a) to 7 (f)

7.4 Structure tensors

Structure tensors are a representation of pixel value changes in a local neighbourhood. The complex-valued wavelet coefficients can be interpreted directly as the gradient of a Laplace-filtered and multiscale smoothed version of the data. All the mathematical developments are given in appendix M.2. Regarding the wavelet coefficients, the structure tensors take into account the local neighbourhood of these by using a 3×3 Gaussian window ($\sigma = 1.5$). We chose this window size, because we want to analyse the direct neighbourhood of each pixel in each scale and we already have multiscale information through the Marr-like transform. Thus, the pixel dependency at each scale regarding structural elements should be highlighted. Through the multiple products of the structure tensors, three new variables can be computed: the coherency of the analysed pixel regarding its neighbourhood, the energy of the pixel, and its local orientation. This can be achieved by using the eigenvectors and eigenvalues of the structure tensor, which provide robust and essential information about the signal variation at a given scale. Specifically, the three new variables obtained from the tensor (Van De Ville *et al.*, 2008) describe:

- *Orientation*: orientation shows the dominant direction of the local structures. It is less prone to noise than the coefficient-wise orientation. Since the tensor is a second-order descriptor, there is no difference between a “positive” and a “negative” edge; i.e. gradients pointing in opposite directions are considered equally ($orientation \in [-\pi/2, \pi/2]$).
- *Energy*: energy of the the local gradient.
- *Coherency*: the ratio between the mean square magnitude of the gradient and the magnitude of the orientation vector gives an indicator called coherency ($coherency \in [0, 1]$). Large coherency shows that there is a dominant orientation in the local neighbourhood (depending on the Gaussian window’s size) whereas small coherency indicates isotropy (Van De Ville *et al.*, 2008; Jähne, 2005).

The different measures obtained from the structure tensor at multiple scales provide characterization of landscape elements. Figure 7.9 illustrates the results for the first decomposition level. As expected, coherency shows the isotropic behaviour of the structures represented by this level (whitest pixels) whereas energy the local energy of the coefficients. Through coherency and for each decomposition level, thus at each scale, we see what the relevant elements are. Coherency gives us an overview of related pixels.

In order to have a comprehensive visualization of these measures, the three components are combined in a composite HSB (hue-saturation-brightness) image. The orientation was coded in the hue level (colour tint), the coherency in the saturation level and the energy in the brightness level. We applied histogram equalization to the energy component, since some initial adjacent pixels (elevations) have markedly different values. These ones induce much higher energy values than most of the other pixels. A root function (3rd or 4th order, depending on the decomposition level) was used to soften this effect. As a result, the images show more and more generalized structures as we go through the different levels of scale.

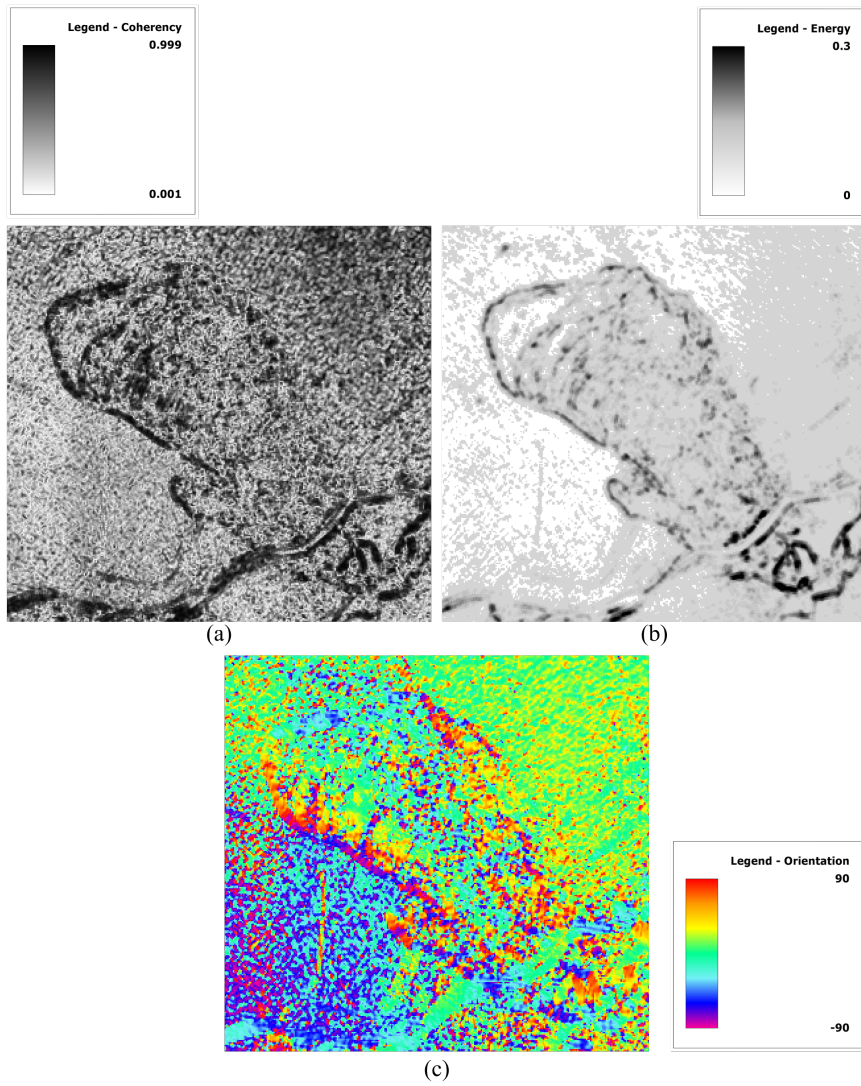


Fig. 7.9. Structure tensor results for the first decomposition level, (a) coherency, (b) energy and (c) orientation

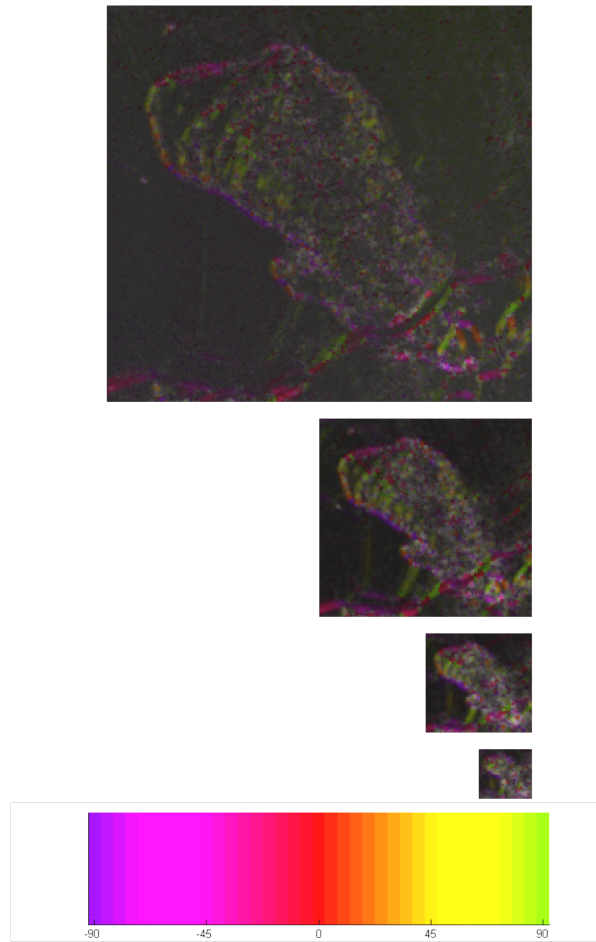


Fig. 7.10. HSB images of structure tensor results for the first four decomposition levels. The colormap shows which colour represents which orientation.

We see that at the fourth level, the saturation of the HSB image (figure 7.10) is very low, thus the coherency rather low. This means that we are in an isotropic zone, where there is no preferential direction; even the energy is quite low. This clearly defines the depleted material deposit zone. By progression through the other levels, this unstructured zone is also visible.

Undeniably, the HSB representation is hard to interpret. It is a three component representation and creating the abstraction levels between these components is hard, thus “less is sometimes more”. We therefore chose a point representation which illustrates only 2 dimensions and which omits the orientation. The point size is proportional to the energy and so is the darkness of the colour to coherency. This enables to study the evolution of topographical isotropy in relation to scale. For each level, the results differ due to the multiscale effect; e.g. the new road is not a coherent entity at a specific scale (figure 7.11 (a)), but at another scale it is coherent, thus anisotropy appears, with a high energy. The same kind of effect is visible for the hydrological network in the scarp zone.

This clearly shows the scale partition in which specific topographical elements are mostly represented or to which scale interval they are related. Relations between different elements which have the same location, but not the same scale, can also be identified. For instance, the scarp zone is identified in the 3rd level, not as a coherent element, but with a high energy (figure 7.11 (b)). And the hydrological network, contained in it, is identified in the first level with high coherency and energy (figure 7.11 (d)).

7.5 Exploratory geomorphological mapping

Using the different methods and techniques, the following elements appeared as relevant to the exploratory approach:

- *Low-pass result*: nevertheless, using only the low-pass results is difficult, because the different decomposition levels are only represented by their scale interval, thus the inter-dependence of the decomposition levels is not represented and the context analysis is hard.
- *Subband-selective reconstruction*: with this scale partition, it is possible to conceptualise the hierarchical imbrications of topographical elements. Each decomposition level gives an indication about the topographical elements composing its frequency space, and this, in relation to the higher frequency spaces. So, the two first levels illustrate the folds and faults, the roadsides and the hydrological network, thus linear elements of the topography. At the third level, little hills and hollows appear and, at the fourth level, we identify a generalisation and grouping of these same elements. In our example, the last shown level, namely the seventh, shows that the underlying frequency space is greater than the size of the topographical elements contained in the landslide. It links, however, the landslide to the general topography of the slope.
- *Phase and magnitude*: in terms of perception scales, the magnitude shows clearly that above the 6th level, scale or frequency analysis exceeds the phenomenological size (or scale) of the landslide, i.e. the topographical elements analysed are of bigger size and lower frequency. For micro-elements, phase is often very heterogeneous, thus hard to interpret.

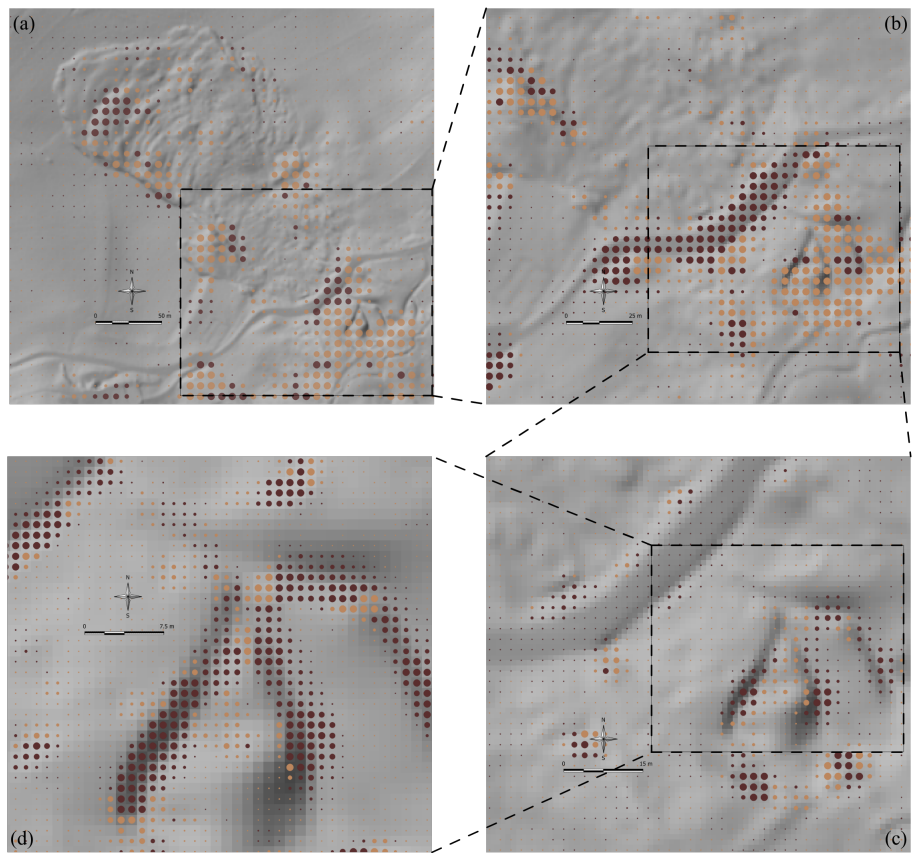


Fig. 7.11. Multiscale energy and coherency analysis; the point size indicates the energy (the bigger the size, the higher the energy) and the colour shows the coherency: brown indicates coherency higher than 0.8, beige indicates coherency between 0.2 and 0.8, and points with a lower coherency are not represented. Subfigure (a) is the coherency-energy representation of level 4, (b) of level 3, (c) of level 2 and (d) of level (1).

- *Structure tensor*: the HSB is not easy to interpret regarding the size of the analysed elements. A last approach is to simplify the cognitive difficulty and represents only two variables out of the three resulting from the tensor structure. Thus, using the discrete frequency spaces, the point representation illustrates the nesting of structural elements in order to understand the multiscale phenomenological effects. The interpretation of nested phenomena is thus simplified.

By using these different methods and techniques, we established a structural map of the landslide. That one is only structural, because it does not take into account any geological issues; neither does it represent a phenomenological reconstruction of the landslide. However, as a first approach, it helps us to identify elements of interest which we will then analyse using terrain observation and geological information (figure 7.12).

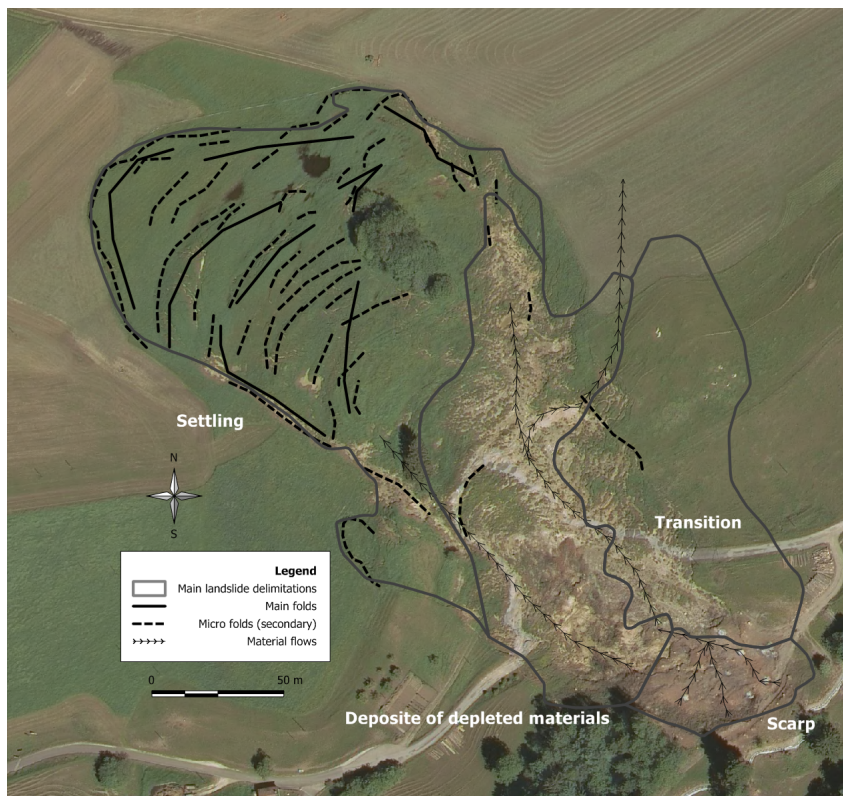


Fig. 7.12. Map of the digitized elements using the Marr pyramid and structure tensors, aerial photography©SITN

8. Discussion

The definition of our framework introduced in section 3.6 has been attested and validated by the visual interpretation and the quantitative analysis of chapters 4 to 7. We have seen that they allowed us the definition of scale intervals (figure 5.35) at which typical structures appeared and were identifiable. However, this recognition is impossible without the illustration of the structural multiscale interconnections. This was done using the bottom-up approach and by combining the multiscale structural elements. Subsequently, we believe that we have digitally represented and processed information nearby the same way that we would analyse it using our visual system (see chapter 7 for some perspectives).

8.1 Wavelets and DEMs

As seen in chapter 4, wavelets and the underlying transform are highly relevant analytical tools for multiresolution analysis. The scale partition is clearly pre-defined, because of the dyadic subsampling. The spectral localised investigation of the wavelet transform identifies frequency properties of terrain features. If we think of partitioning scale through frequency, we might think of the Fourier transform, which in this case is not applicable, because not localised. Thus, if we suppress or filter some frequencies in the Fourier domain, we do not know what exactly will be the implications in the spatial domain. As seen, wavelets are ideal to get rid of this limitation. The filter bank simplicity allows us creation of multiple frequency subspaces in the spatial domain, thus the analysis of specific and combined scale intervals by subband suppression.

The main issue using the wavelet transform is to choose a wavelet family which corresponds to the structural features of a DEM. As we applied the transform to a DEM countryside region, the spatial breaks are not as sharp as they would be in a DSM representing a city. The first tentative of analysing the wavelet effect showed us that a B-spline basis as scaling function was appropriated for our goals. But it might be completely different for other types of territorial coverages.

The application of the WT on DEMs and its basic minimalistic parametrisation enable the replica of the methodology on other DEMs. Currently, the only controlling factor is the size of the original DEM, but nowadays computer memory is powerful enough, such as a $20\,000 \times 20\,000$ pixel DEM can be processed without major issue. Obviously, the scaling function and its related wavelet family are the main parameters to choose. By having a good scaling interpolation function, we make sure to have *appropriate* high frequency coefficients thereafter. By *appropriate*, we mean that no artefacts, noise or

wavelet specific structures were injected in the model by the WT. A good and appropriate generalisation model ensures that, and the analysis of the detailed coefficients may consequently be undertaken. This is what we verified by the different analysis regarding the low-pass results. On both of the surfaces (virtual landslide and Travers DEM), the wavelet transform gave a well-interpolated result. As accredited by the visual interpretation and statistical analysis, the transform had the reaction we expected: a generalisation process with few artefacts and noise injection.

Reconstruction of scale relevant information

The bottom-up approach of combining high-pass coefficients has emerged from the lack of context resulting from the visual analysis of the high-pass coefficients of each level. The whole frequency domain is partitioned in different levels, but these ones, taken as a unity, do not give relevant information for the geomorphological analysis, because the geomorphological context is lost. Indeed, the nesting of structural information is decomposed, which induces this “loss of context”. This is the main limitation of this analysis. Without explicitly wanting to prove this nesting through the analysis of the high-pass coefficients, we have shown that a one scale analysis is not relevant for geomorphometric analysis (regarding high resolution). But to counter this “loss of context”, we have developed the bottom-up approach. High frequencies give context to scale, thus the nesting of structural information is assured and illustrated. Filtering the high-pass coefficient levels is only a way to exaggerate or threshold specific frequency information. It is clear that this can only be undertaken once we know which structural elements are represented by the different levels. Even if we are able to analyse a DEM using the wavelet transform, there is clearly a lack of scale interval specification.

Wavelet effect on geomorphological features

As shown in figure 5.35 (chapter 4), the defined scale intervals provide an identification range for various structural types which may be experienced in reality. However, it is significantly harder to determine at what scale which elements will be transferred from a low-pass image at decomposition level i to a high-pass image at decomposition level $i + 1$. In fact, any natural feature is a composition of certain frequency spaces, which are a priori unknown. The wavelet transform does not analyse directly structural elements, but the frequencies that compose them. The decisive step is thus the identification - by the wavelet - of the main frequency components, or rather the frequency combinations, which then are transferred; that is to say, from the lowest to the highest frequency composing the feature. It therefore becomes obvious that the decisive step is the lowest frequency that composes the feature. If we look at the defined spaces (figure 5.35), we have focused our discretization on the lower frequencies composing the feature.

Visualisation and interactive exploration

In chapters 4 and 5, the geomorphological analysis, in its quantitative approach, is enhanced by the coefficient filters, consequently a huge amount of information is created. The illustration of the results may be disconcerting for non-specialists, because we have multiple views of the same spatial area but containing different and discrete information. Thus, being able to represent all this information in a synthetic view is still an issue for which we have no practical answer. Perhaps, as Wood (2009) suggested, we should find a way

to reduce this visual complexity and even visualize data in another way than a 2D projected image. Ideally, it would mean to implement the following two principles:

1. Complex analytical visualisation solves the problem of information multiplicity.
2. User interaction should provide access to information in a simple and easy way, e.g. find a way to navigate through the different scales.

8.2 Wavelet transform applied to geomorphological characterization

8.2.1 Geomorphological scale and the wavelet transform

If we look at the scale definition of Tobler (1987) (see table 3.1), there is always a relation between the spatial resolution and the spatial size of the structural components of a DEM. Nevertheless, the relation between a scale interval, which is linked to a well-defined sub-space of the frequency domain, and the size of a structure is less explicit. Highlighting the link between the size of structural components and the frequency domain would give us a good methodology to extract and analyse scale-specific structures. But as seen in this study, we are only able to make a link between the resolution of the decomposition level and the size of shapes, or the landforms structure represented therein. Moreover, this link is empirical, because it emerged from afterthoughts following discussions with the expert. Using the results of the case study (section 5) and approximately, the ratio may be set at: $2 \text{ pixels} \cdot \text{resolution} = \text{shape size}$. For example, this would mean that at the fourth level ($r = 16 \text{ m}$), structures having a size of about 32 m should be highlighted by the WT and its enhancement. Indeed, this relation matches Tobler's statements.

By visual interpretation of the subband reconstructions (reconstructed high-pass coefficients) of the Travers DEM and throughout its global context, we were able to construct empirical geological spaces which correspond to the decomposition levels (figure 5.35, section 5.8). But these are based on our single analysis of the Travers DEM and, therefore, cannot be taken as any kind of absolute definition. The defined spaces have a local meaning. They could lead us to a scale based typology of geomorphological structures.

As we are able to interpret scale effects on geomorphological structures, we might ask ourselves which are the element we do not recognise or identify. Indeed, and compared the usual geomorphometry, topographical context is not possible as no slope or even slope flow accumulation indicator are computed. Only topographical structures are enhanced and extracted using the wavelet transform.

So, if we state that wavelets are intuitive, can easily be applied on DEMs and give pertinent results by showing structural scale nesting, we can ask the question why the geomorphological community does not use them?

Although we are not dealing with this question throughout this study, we assume that the methodological approaches might be the reason of this lack of usage. A premise of answer can be given by the experimental design approaches used by the geomorphometric community: it is essentially an approach using processes. That is to say, geomorphometry tries to characterize a process by carrying out structural analysis (using geomorphometric indicators). In contrast, image analysts are often primarily interested in feature detection and in its characterization to define the involved processes. Furthermore, Marr's approach and the underlying structure tensors bring us clearly closer to geomorphometry. It defines indicators that describe the process. Although Marr's approach brings us some of the methodological elements related to geomorphometry through the definition of structural indicators, this question remains open. The elements above are only assumptions sustaining the debate.

8.2.2 Patterns & multiscale DEMs

Since the end of the 20th century, more and more publications have been written on classification of geomorphometric indicators for geomorphological characterization purposes (refer to section 6.3 for a review). As a first attempt to determine multiscale patterns using k-means, we tried to classify our low-pass results - the generalised DEMs - regarding geomorphometry indicators (elevation, slope, plan and profile curvature, solar radiation, topographical wetness index and distance-to-ridge) (see section 6.3 for the detailed study). The results, given the classification statistical indicators (confusion index, F-coefficient and H-coefficient) showed us that only two clusters were statistically pertinent for most of the decomposition levels, which is not satisfactory for a classification using seven variables. Only for the second level ($r = 4 m$) the indicators identified the 4 clusters solution as the best one. Moreover, the correlations between the input variables (geomorphometric indicators) were too high to expect an independent multi-dimensional space. An additional pattern diversity study is undertaken. The evolution of diversity in some pre-defined zones shows the behaviour of the wavelet interpolation scheme through the levels.

The question is why do we have no positive results where others have succeeded? Several factors may interfere. The first might be the spatial coverage of the Travers DEM. This one contains a hillside (south-eastern part of the DEM) which flows down to an almost flat valley. If we compare our results to the studies which were already undertaken, the structural configuration of our DEM does perhaps not contain enough different morphological typologies for the classification of the last decomposition levels (thus the low resolutions, which correspond to the resolution of the previous studies). But we are unable to give an explanation for the first levels ($r=1 m, 2 m, 8 m$).

As conclusion of this classification attempt, patterns analysis using k-means is not appropriate in our case. The statistics (correlation, confusion index, F-coefficient and H-coefficient) of almost all levels show that k-means are not appropriate. Moreover the result interpretation is almost impossible, due to their diversity. Conceptually and regarding Tobler's definition (equation 3.1), it is hard to define the parameters for natural phenomena. There is no way to define the *Domain* or the *Number of observations*, thus a unclear definition of the equation component. A priori, these two parameters

are unknown in the classification scheme. We might guess them, but there is no definite answer to the number of elements composing a phenomenon. Furthermore, the sensitivity to describe natural phenomena and processes is specific to each person. A lot of studies, which deal with the classification of geomorphometric indicators, use a high number of operating parameters. Undeniably, this excessive setting of parameters, factors and variables cuts out almost any replica possibility of the methodology. As example, reproducing a geological map, using classification of geomorphometric indicators, does not bring anything, since the map is anyway already existent.

Geomorphometric information contains a huge amount of information and as Goudie *et al.* (1990) noticed, "*The nature of relationships identified between variables depends on the scale of an investigation*" or Turner (1989): "*Because landscapes are spatially heterogeneous areas ..., the structure, function, and change of landscapes are themselves scale-dependent. The measurement of spatial pattern and heterogeneity is dependent upon the scale at which the measurements are made.*". The developments of this study enlarge the scope of a single scale analysis by adding the multiscale dimension. It ensues that the classification framework is hard to define using a priori categories or classes, thresholds and data are different for each scale level.

As remark, and further development, this kind of classification does not allow taking into account the fact that we have multiscale data. Each classification for each decomposition level is an independent realisation. I.e., for each level we create a new classification space, but the method does not take into account the relations between the different levels. It induces a lack of coherence between the classifications of the different levels. From our point of view and to be more consistent in multiscale classification, the inter-relations between the different scale levels should be explored more thoroughly in all further developments of a classification scheme using multiscale DEMs.

8.3 Marr's vision and DEMs

In chapter 4, the wavelet transform was analysed and used for the geomorphological characterization of a geological phenomenon. As we already know, the reconstruction of the detail coefficients result in scale-dependent images. Their values are wavelet magnitudes, and the orientation of the high-pass coefficients is given by the three high-pass subbands (horizontal, vertical and diagonal). Chapter 7 is a tentative to go a step further in the representation of DEM multiscale filtering. Using Marr's vision theory (Marr, 1982) and latest developments in its application to image processing (Van De Ville *et al.*, 2008), we tried to give a more synthetic view of coefficient phase and magnitude, describing a novel DEM multiscale analysis approach. Combined to weighted structure tensor, the results give one synthetic image (figure 7.10) of the analysis.

The phase and magnitude are embedded in complex wavelet coefficients, which provide a unique representation of multiscale nested features. The combination of coefficients from distinct decomposition levels permits to obtain scale dependent structures. This localised and oriented multi-structural information, as well as structure tensors, provide additional analytical elements. The multiscale analysis contributes to an improved understanding of the elements that compose a topographical phenomenon. Like what was done using

the classic wavelet transform, the implementation of pyramidal decomposition techniques simplifies the combination of frequency spaces resulting from the discretization of continuous scale. With the case study and the analysis of surface effects, we improve the comprehension of the landslide dynamics. The identified and digitized elements should help to apprehend the mass movement and flows of the landslide area. Therefore, mapping them gives a first overview of the main topographical factors that characterize the phenomenon (figure 7.12).

As we have seen in chapter 7, phase and magnitude give good results in the first levels. We were able to analyse high frequency structural linear elements (micro-folds), which were not identified using the classic wavelet transform. It is mostly the phase which gives the best overview of these structures, because their linearity gives context to phase in the two first decomposition levels. It is similar to the highway on a satellite image example in section 3.2. As we progress through the levels, phase becomes nevertheless less evident to interpret visually. These upper decomposition levels are clearly not any more representative of linear structures, but of areal structures. For such structures, phase represents a kind of “generalised” aspect, but with almost no relation to its neighbouring values at this stage. It is the structure tensor analysis which gives a synthetic local weighted solution to this issue. The values of phase and magnitude reflect structural information through scale. However, we are not able, except for micro-structures, to identify fundamentally different or new information compared to the classic transform.

As we have seen we use a Laplacian operator. If we adjust the orders of the isotropic Laplacian (γ) and of the complex gradient (N) (equation M.3, appendix M), we can compute the second derivative in a multiscale framework. This would approach us to the methods developed by Wood (1996). But instead of using a quadratic surface (equation 2.4, section 2.4), our derivation basis would be the complex polyharmonic B-spline. It enables us to propose a clean and nice approach to compute multiscale first and second derivatives of the DEM using the wavelet transform. This approach would bring us nearer to the current methods used in geomorphometry.

Marr’s scope of analysis is to bring us nearer to human vision by the synthetic view of scale. This issue is clearly reached regarding the structures we are able to recognise. Finally, the analysis of the structure tensor (coherency, orientation and energy) is, in our opinion and regarding our goals, the most interesting result. According to three geologists and from a geomorphological point of view, the combined images (HSB image) is hard to interpret. For them, it looks like “art” on terrain, mainly because the three represented dimensions (coherency, orientation and energy) are hard to distinguish. Consequently, we proposed the coherency and energy composition, dropping the orientation.

Coherency & Energy

As stated in chapter 3, a feature has to cover at least two pixels, which was enlarged to three in our study, in order not to be assimilated to noise in an image or a DEM. If coherency takes into account the phase and magnitude of each pixel regarding its neighbouring pixels (3×3 convolution window), than we actually are trying to identify structural elements using neighbouring analysis tools. Furthermore, if we add to that the multiscale component, we have an overview of which scale interval (or frequency space) represents which

type of structure (e.g. the scarp zone in figure 7.11). Indeed, we could make an inventory of structural elements regarding their scale, but this is only correct as long as the defined structures are not too scale-complex.

8.4 Framework benchmark

The framework used in this study is composed of two main steps: I (methodology) and II (validation) (figure 3.11). Following the above discussion and remarks, we are able to provide consistent and coherent analysis as well as multiscale interpretations of high resolution DEMs. Chapters 4 to 7 have shown that scale analysis on a heterogeneous and non-stationary signal is possible by using local and compact-supported techniques (wavelets). The wavelets synthesis capacities have also shown that it was possible to combine structural elements from different scales.

However, we still need to ask ourselves what the consequences on the side of geomorphology and its experts are. These new methods can be used provided that experts validate and accept them. Although the web-based GAS survey (chapter 6) partially fulfilled and verified these methods, GAS remains predominantly non-dynamic. That is to say, some very specific results are presented to an audience, and they can neither be altered nor can other types of synthesis be applied. Notably, the type of coefficient filter cannot be modified, neither can scale specific reconstructions be undertaken. This lack will be introduced as a perspective in the next chapter.

9. Conclusion

Scale exploration in geomorphometry is possible using multiple methods. As we have seen, most of them are confined to the geometric analysis of a gridded elevation model. Using the wavelet transform, we add a new approach to exploratory geomorphometry. This allows us implementation of any potential structural combinations at different scales. Although the approach is defined in the frequency domain, the localisation properties of the transform is a significant advantage compared to the Fourier transform. Consequently, we are able to analyse non-stationary and irregular signals such as an elevation model. Moreover, we combine wavelet coefficients using different decomposition levels. These results are enhanced by the sign of each spatially localised wavelet coefficient. Using these reconstructed generalisations, it is possible to specify and isolate features and structures of a specific phenomenon.

However, the multiplicity of information reveals a representation problem. This includes a way to interpret multiple views and structural combinations that cover the same phenomenon. A first approach is given by recent algorithmic developments in the field of wavelet analysis. The different analysis and interpretations show that all applied wavelet tools are well suited to geomorphological analysis.

9.1 Review of the goals

Each defined goal (see section 1.1) will now be taken in review and commented regarding what has been analysed and expressed in this study.

To define a good scaling method for elevation models and, if possible, to implement multiscale analysis approaches

This first goal was clearly achieved. We have shown that it was possible to generalise DEMs using the wavelet transform. The generalisation process is validated by the statistical indicators, the visual interpretation and the profile analysis. In the continuity of the generalisation filter bank, the wavelet transform gives us a unique way to represent specific scale spaces by reconstructing specific subbands. The multiscale information can be reconstructed using almost infinite possibilities of combination and coefficient filtering. The second methodology (chapter 7) enlarges the scope of multiscale analysis by the identification of specific scale (or frequency) intervals related to simple structures, throughout the coherency-energy analysis.

To transfer information from fine scale to broad scale and keep the best structural geometry

The information transfer is carried out by the wavelet transform in a dyadic scale interval. It was shown that this process creates a generalised model of the original without bias or artefacts. Thus, structures are maintained in the model as long as they correspond to the underlying scale interval. Although there is no absolute quantitative method or technique to verify it, we used multiple methods to prove the adequacy between the generalisation steps.

Conserving the best structural geometry is complicated in the natural phenomena representation (the model). What is “the best structural geometry” in relation to natural structures? How is that defined? If we had a modelled structure or feature with well-defined edges and borders, then we could try to analyse the conservation and quality of geometry through scale. Furthermore, if we take a second feature geomorphologically similar to the first one, but with a slightly different shape, we cannot be sure that its scale interval will correspond to the one of the first feature.

Using a scale analysis to generalise and simplify information by retaining only the essential data for multiscale geomorphological analysis

We are looking for geomorphological features whose structure cannot be pre-defined. It is the analysis and interpretation, which will define the structural hierarchy and thus the feature of interest. As we have seen, its determination is crucial for the characterization and understanding of a phenomenon. Nevertheless, its theoretical definition depends completely on the geomorphological context in which it is located. Thus, there is no universal solution. The wavelet analysis of the frequency domain aims at providing the best structural combinations regarding a feature for geomorphologists. It does not provide direct recognition of the feature, but suggests scale combinations - or frequency combinations, given the interdependence of scale and frequency - at which the feature can visually be identified. In certain circumstances and context, we can expect a repetitive behaviour of the wavelet analysis regarding a structural typology; that is to say, to give relevant scales for a type of phenomenon. Nevertheless it is not a quantitative indicator, but a scale interval. Our methodology fulfils this goal, but the recognition and identification of features can only be supported, not automated.

To interface scales of interest by combining data at different scales

This goal is partially fulfilled, because we show how to do it and we give examples. But multiple combinations can be made, and for each new one, a new layer is created, increasing at the same time the number of layers to analyse. As stated above, we are able to create a lot of combinations, but our visual system cannot link an infinite number of them. Thus, we have to concentrate on a specific number of such combinations.

To produce and recognise geomorphological features through these scale levels

The only mapped features are digitized through visual interpretation of the different methodologies. There is, at the present, nothing in this study which automates pattern and/or structure recognition. Section 9.3 gives some hints on what could be undertaken to try to achieve this goal. But again, our spatial domain is made of heterogeneous natural features, each of which has its own shape. Thus, there is almost no chance to be able to define a normalised methodology to do such recognitions.

To identify specific scale domains and scale thresholds regarding geomorphological phenomenology

An attempt (figure 5.35) to fulfil this goal has been made. However, we should continue the wavelet transform further than the eighth level to be able to give a clear partition of scale into domains. However, the size of the original DEM is a first limitation. More importantly and as an essential condition, the defined domains must be validated using another DEM which contains other features at other scales.

9.2 Final outcome

The technical elements presented clearly do not replace terrain observations, geological mapping, geomorphology, and expertise. They simply give additional analytical techniques and methods that allow the expert to focus directly on topographic remarkable elements. Moreover, methodologically, it is necessary to define an implementation framework, because these techniques are certainly not time-consuming regarding the processing, but they provide a large number of new surfaces and images. This means for the experts that they will have to choose the best data combinations for their purposes. Therefore, it requires a good knowledge of the process and its underlying effects.

We believe that we have introduced innovative analysis techniques to help experts to characterize a phenomenon better in its topographical aspects. Moreover, the multiscale approach extends the analysis by simplifying the complex hierarchy of topographical elements. Although the approach is still exploratory, we can now partition the spatial domain using its spectral components and identify scale-specific features. Moreover, we believe that the convergence of geomorphology with image analysis and processing can only be beneficial to these disciplines and enrich them.

9.3 Perspectives

9.3.1 Energy of wavelet coefficients

In chapter 4, we used a local fractal indicator to analyse local self-similarities. In the wavelet application field, the log plot of the wavelet energy spectrum versus the scale interval is used to analyse the fractal properties of each decomposition level on the whole image (Flandrin, 1989, 1992; Nicolis *et al.*, 2006). This plot shows the variation of the high-pass coefficients' energy throughout the decomposition levels. At a specific level, this energy will be so low that the wavelet transform does not give us any useful information any more.

The slope break of the plot gives an indication of non-fractal images versus fractal-like images. It is certainly interesting to do such analysis on DEMs and to specify what implication the multiscale approach has on the fractal dimension of the generalised DEMs. Perhaps, this could also be an approach to specify until which level the wavelet transform is pertinent. Thus, regarding the original DEM, it should show us when the image is not self-similar any more and, consequently, inform us about the wavelet transform reliability.

9.3.2 Vision for geomorphometry

Marr's vision theory is a link between our visual perception and the interpretation we make of the world surrounding us. As we attempt to connect the wavelet pyramid to his theory, it opens up the field of visualisation of our new data. We have seen that we are able to produce a huge quantity of data, using little time and limited efforts. It is however surely not appropriate to transmit all this information as it is. We have to find a way to synthesize the information, similarly to what the Marr-like wavelet pyramid does, and imagine new visualisation methods for information and its underlying analysis. Data complexity has to be interpreted by specialists, but if we manage to synthesize information to make it usable and interpretable for the Earth science community, the dissemination of such methods and techniques will be enlarged.

Another exploratory field is to continue in direction of Marr's theory and to apply the latest developments of Van De Ville and Unser (2008), especially the Marr primal sketch of the structural information in an image. This sketch uses the complex coefficient resulting from the transform and is an iterative process to create a scale consistent sketch. However, this approach was not addressed in this study.

9.3.3 Linking geological space and decomposition levels

Links between geological scale intervals and decomposition levels can be created by analysing a much larger DEM, in order to reach less detailed scales. The problem now is that we have used a rather small DEM (1280×768 pixels), which limits our assessment and our interpretation of micro- and meso-geology. The response of larger geological formations to the wavelet transform would be the next step. This extension should allow us classification of hierarchically geomorphological features better, including bigger geological formations. Moreover, also to understand the effect of filters used on larger structures, and therefore, be able to understand the structural nesting in a bigger spatial extend than at present.

It is a scale specification issue. If we are able to specify at which resolution which structure arises, we could give to geomorphologists the scale interval at which the elements are isolated by the transform. Therefore give them the best view of a geomorphological feature and of its composing features.

9.3.4 Dissemination of the wavelet transform applied to DEM analysis

As the GAS survey illustrates (chapter 6), most participants found that the wavelet approach was complementary to usual geomorphometric indicators. In their actual form, the algorithms can however hardly be disseminated. The whole concept should be analysed in order to distinguish which features are important to non-experts (of the wavelet transform). More tools should be given, and visualisation efforts undertaken to diffuse the method. Simple analytical features should be added to the tool panel, such as representing the frequency space of the decomposition levels, filtering using pre-defined filters, soft and hard thresholding of the coefficients, etc.

If the method and approach are to be communicated to a wide audience, presenting it in a user-friendly manner is essential. It could be a step toward the reconciliation of geomorphologists and frequency analysis. It is necessary to ask ourselves whether the proposed interface should give the user the know-how or the understanding of the scientific method. By know-how, it is suggested to provide geomorphologists with analysis capabilities using frequency analysis. As a first introduction, the GAS web-survey (chapter 6) gives us a first glimpse of what the interface should be. Moreover, from our point of view, it is important that the know-how is developed and not the complete knowledge of the mathematical background. Most GIS users do not know exactly the scientific development of the methods or tools they use. For example, most GIS users do not have any idea of the strict definition of the slope that they calculate using a DEM. However, they calculate it and use it.

Bibliography

- Amgaa, T. (2003). *Wavelet-based analysis for object separation from laser altimetry data*. Master's thesis, International Institute for Geo-Information Science and Earth Observation, Enschede, Netherlands.
- Anonymous (1995). *FRAGSTATS - Documentation*. Department of Natural Resources Conservation, University of Massachusetts.
- Anselin, L. (1995). Local indicators of spatial association - LISA. *Geographical Analysis*, **27**(2), 93–115.
- Anselin, L. (2005). *Exploring Spatial Data with GeoDa (TM): A Workbook*. Spatial Analysis Laboratory, Departement of Geography, University of Illinois, revised version edition.
- Arrell, K. E., Fisher, P. F., Tate, N. J., and Bastin, L. (2007). A fuzzy c-means classification of elevation derivatives to extract the morphometric classification of landforms in Snowdonia, Wales. *Computer & Geosciences*, **33**(10), 1366–1381.
- Baltsavias, E. (1999a). Airborne laser scanning: basic relations and formulas. *ISPRS Journal of Photogrammetry & Remote Sensing*, **54**(2-3), 199–214.
- Baltsavias, E. (1999b). Airborne laser scanning: existing systems and firms and other ressources. *ISPRS Journal of Photogrammetry & Remote Sensing*, **54**(2-3), 164–198.
- Batson, R., Edwards, K., and Eliason, E. (1975). Computer-generated shaded-relief images. *Jour. Research U.S. Geol. Survey*, **3**(4), 401–408.
- Bernard, C. (2001). *Ondelettes et problèmes mal posés: la mesure du flot optique et l'interpolation irrégulière*. Ph.D. thesis, École Polytechnique, Paris, France.
- Beven, K. J. and Kirkby, M. J. (1979). A physically based, variable contributing area model of basin hydrology. *Hydrological Sciences - Bulletin des Sciences Hydrologiques*, **24**(1), 43–69.
- Bezdek, J. C. (1984). Fcm: The fuzzy c-means clustering algorithm. *Computers & Geosciences*, **10**(2-3), 191–203.
- BGS (2002). *Klassifikation der Böden der Schweiz: Bodenprofileuntersuchung, Klassifikationssystem, Definitionen der Begriffe, Anwendungsbeispiele*. Technical report, Eidgenössische Forschungsanstalt für Agrarökologie und Landbau, FAL, Zürich, Switzerland.
- Bian, L. (1997). Multiscale nature of spatial data in scaling up environmental models. In D. A. Quattrochi and M. F. Goodchild, editors, *Scale in Remote Sensing and GIS*, pages 13–26. CRC Press.
- Bigun, J., Bigun, T., and Nilsson, K. (2004). Recognition by symmetry derivatives and the generalized structure tensor. *Pattern Analysis and Machine Intelligence, IEEE Transactions on*, **26**(12), 1590–1605.
- Bishop, M. P. and Shroder Jr, J. F. (2004). *Geographic Information Science and Mountain Geomorphology*. Springer and Praxis Publishing, UK.

- Bjorke, J. and Nilsen, S. (2003). Wavelets applied to simplification of digital terrain models. *Int. J. Geographical Information Science*, **17**(7), 601–621.
- Blu, T. and Unser, M. (2000). The fractional spline wavelet transform: Definition and implementation. In *Proceedings of the Twenty-Fifth IEEE International Conference on Acoustics, Speech, and Signal Processing (ICASSP'00)*, volume I, pages 512–515, Istanbul, Turkey.
- Braun, J. (2002). Estimating exhumation rate and relief evolution by spectral analysis of age-elevation datasets. *Terra Nova*, **14**(3), 210–214.
- Brennan, R. and Webster, T. L. (2006). Object-oriented land cover classification of lidar-derived surfaces. *Can. J. Remote Sensing*, **32**(2), 162–172.
- Buckley, A., Hurni, L., Kriz, K., Patterson, T., and Olsenholler, J. (2004). Cartography and visualization in mountain geomorphology. In M. P. Bishop and J. F. Schroder, editors, *Geographic Information Science and Mountain Geomorphology*, pages 253–287. Springer and Praxis Publishing, UK.
- Burrough, P. A. and McDonnell, R. A. (1998). *Principles of Geographical Information Systems*. Oxford University Press Inc., New York, USA.
- Burrough, P. A., Van Gaans, P. F. M., and MacMillan, R. A. (2000). High-resolution landform classification using fuzzy k-means. *Fuzzy Sets and Systems*, **113**(1), 37–52.
- Burrough, P. A., Wilson, J. P., Van Gaans, P. F. M., and Hansen, A. J. (2001). Fuzzy k-means classification of topo-climatic data as an aid to forest mapping in the greater yellowstone area, USA. *Landscape Ecology*, **16**(6), 523–546.
- Caloz, R. and Collet, C. (2001). *Précis de Télédétection, Volume 3, Traitements Numériques d'Images de Télédétection*. Presses de l'Université du Québec, Sainte-Foy, Québec, Canada.
- Cao, C. and Lam, N. S.-N. (1997). Understanding the scale and resolution effects in remote sensing and GIS. In D. A. Quattrochi and M. F. Goodchild, editors, *Scale in Remote Sensing and GIS*, pages 57–72. CRC Press.
- Cohen, A. (1992). *Ondelettes et traitement numérique du signal*. Recherches en Mathématiques Appliquées, Masson,.
- Comaniciu, D. and Meer, P. (2002). Mean shift: A robust approach toward feature space analysis. *Pattern Analysis and Machine Intelligence, IEEE Transactions on*, **24**(5), 603–619.
- Couclelis, H. (1992). People manipulate objects (but cultivate fields): Beyond the raster-vector debate in GIS. In A. U. Frank, I. Campari, and U. Formentini, editors, *Theories and Methods of Spatio-Temporal Reasoning in Geographic Space*, pages 65–77. Lecture Notes in Computer Science, Springer Verlag.
- Cova, T. J. and Goodchild, M. F. (2002). Extending geographic representation to include fields of spatial objects. *International Journal of Geographical Information Science*, **16**(6), 509–532.
- De Boer, D. H. (1992). Hierarchies and spatial scale in process geomorphology: a review. *Geomorphology*, **4**(5), 303–318.
- De Bruin, S. and Stein, A. (1998). Soil-landscape modelling using fuzzy c-means clustering of attribute data derived from a digital elevation model (dem). *Geoderma*, **83**(1-2), 17–33.
- De Floriani, L., Marzano, P., and Puppo, E. (1996). Multiresolution models for topographic surface description. *The Visual Computer*, **12**(7), 317–345.

- De Smith, M. J., Goodchild, M. F., and Longley, P. A. (2008). *Geospatial Analysis: A Comprehensive Guide to Principles, Techniques and Software Tools*. Troubador Publishing, UK.
- Dierckx, P. (1993). *Curve and Surface Fitting with Splines*. Oxford Science Publications.
- Dikau, R. (1989). The application of a digital relief model to landform analysis in geomorphology. In J. Raper, editor, *Three dimensional applications in Geographical Information Systems*, pages 51–77. Taylor & Francis.
- Dikau, R. (1994). Computergestützte Geomorphographie und ihre Anwendung in der Regionalisierung des Reliefs. In *Petermanns Geographische Mitteilungen*, volume 138, pages 99–114.
- Dragut, L. and Blaschke, T. (2006). Automated classification of landform elements using object-based image analysis. *Geomorphology*, **81**(3-4), 330–344.
- Evans, I. S. (1972). General geomorphometry, derivatives of altitude, and descriptive statistics. In R. J. Chorley, editor, *Spatial Analysis in Geomorphology*, pages 17–90. Methuen, London, UK.
- Evans, I. S. (1979). An integrated system of terrain analysis & slope mapping. Final report on da-ero-591-73-g0040, Dept. of Geography, University of Durham, England. In "Statistical characterization of altitude matrices by computer".
- Field, D. J. (1999). Wavelets, vision and the statistics of natural scenes. *Phil. Trans. R. Soc. Lond. A*, **357**(1760), 2543–2560.
- Fisher, P., Wood, J., and Cheng, T. (2004). Where is helvellyn? fuzziness of multi-scale landscape morphometry. *Trans Inst Br Geogr*, **29**, 106–128.
- Flandrin, P. (1989). On the spectrum of fractional brownian motions. *IEEE Trans. Inform. Theory*, **35**(1), 197–199.
- Flandrin, P. (1992). Wavelet analysis and synthesis of fractional brownian motion. *IEEE Trans. Inform. Theory*, **38**(2), 910–917.
- Francescotti, R. M. (1991). Externalism and Marr's theory of vision. *Brit. J. Phil. Sci.*, **42**(2), 227–238.
- Gachet, G. (2005). Étude comparative de différentes méthodes d'interpolation pour générer des modèles numériques d'altitude raster à partir de points bruts lidar. Technical report, LaSIG-EPFL.
- Gachet, G. (2009). *Analyse et exploitation des données de LIDAR aéroportés pour la caractérisation des milieux boisés de la Suisse*. Ph.D. thesis, École Polytechnique Fédérale de Lausanne, Switzerland.
- Gallant, J. C. and Hutchinson, M. F. (1996). Towards an understanding of landscape scale and structure. In *Third International Conference/Workshop on Integrating GIS and Environmental Modeling, Santa Fe, NM, USA*.
- Gaudart, L., Crebassa, J., and Petrakian, J. P. (1993). Wavelet transform in human visual channels. *Applied Optics*, **32**(22), 4119–4127.
- Glennerster, A. (2007). Marr's vision: Twenty-five years on. *Current Biology*, **17**(11), R397–R399.
- Gocht, W. (1961). *Geologische und hydrologische Untersuchungen südöstlich von Couvet und Travers (Kanton Neuchâtel - Schweiz)*. Master's thesis, Mathematisch-naturwissenschaftliche Fakultät der freien Universität Berlin.
- Golay, F. (1992). *Modélisation des systèmes d'information à référence spatiale et leur domaines d'utilisation spécialisés: aspects méthodologiques*,

- organisationnels et technologiques*. Ph.D. thesis, École Polytechnique Fédérale de Lausanne, Switzerland.
- Goodchild, M. F. (1986). *Spatial Autocorrelation*, volume 47. Concepts and Techniques in Modern Geography (CATMOG), GeoBooks.
- Goodchild, M. F. (1992). Geographical information science. *Int. J. Geographical Information Science*, **6**(1), 31–45.
- Goodchild, M. F. and Mark, D. M. (1987). The fractal nature of geographic phenomena. *Annals of the Association of American Geographers*, **77**(2), 265–278.
- Goudie, A., Anderson, M., Burt, T., Lewin, J., Richards, K., Whalley, B., and Worsley, P. (1990). *Geomorphological Techniques*. British Geomorphological Research Group, Taylor & Francis.
- Graps, A. (1995). An introduction to wavelets. *IEEE Computational Science & Engineering*, **2**(2), 50–61.
- Grewe, L. and Brooks, R. R. (1997). On localization in the wavelet domain. In *Proceedings of the 1997 Symposium on Computational Intelligence in Robotics and Automation, Monterey, California, USA*, pages 412–418.
- Hammond, E. H. (1964). Analysis of properties in landform geography: an application to broad scale landform mapping. *Annals of the Association of American Geographers*, **54**(1), 11–19.
- Hanesch, M., Scholger, R., and Dekkers, M. J. (2001). The application of fuzzy c-means cluster analysis and non-linear mapping to a soil data set for the detection of polluted sites. *Phys. Chem. Earth*, **26**(11-12), 885–891.
- Horn, B. K. P. (1981). Hill shading and the reflectance map. *Proceedings of the IEEE*, **69**(1), 14–47.
- Imhof, E. (2007). *Cartographic Relief Presentation*. ESRI Press, Redlands, California.
- Irvin, B. J., Ventura, S. J., and Slater, B. K. (1997). Fuzzy and isodata classification of landform elements from digital terrain data in Pleasant Valley, Wisconsin. *Geoderma*, **77**(2-4), 137–154.
- Jähne, B. (2005). *Digital Image Processing (6th revised and extended edition)*. Springer.
- Jarvis, P. G. (1995). Scaling processes and problems. *Plant, Cell and Environment*, **18**(10), 1079–1089.
- Jelinski, D. E. and Wu, J. (1996). The modifiable areal unit problem and implications for landscape ecology. *Landscape Ecology*, **11**(9), 129–140.
- Klinkenberg, B. (1992). Fractals and morphometric measures: is there a relationship? *Geomorphology*, **5**(1-2), 5–20.
- Klinkenberg, B. and Goodchild, M. F. (1992). The fractal properties of topography: A comparison of methods. *Earth Surf. Process. Landforms*, **14**(3), 217–234.
- Krähenbühl, S. (2007). *Prévision de la sensibilité locale d'un versant aux mouvements de terrain par l'analyse des indices topographiques, géologiques et hydrogéologiques - Cas du glissement de terrain de Travers (Canton de Neuchâtel, Suisse)*. Master's thesis, École polytechnique fédérale de Lausanne (EPFL).
- Lane, S., Richards, K., and Chandler, J. (1998). *Landform Monitoring, Modelling and Analysis*. John Wiley & Sons.
- Lassueur, T., Joost, S., and Randin, C. F. (2006). Very high resolution digital elevation models: do they improve models of plant species distribution. *Ecological modelling*, **198**(1-2), 139–153.

- Li, Z., Zhu, Q., and Gold, C. (2005). *Digital Terrain Modeling, Principles and Methodology*. CRC Press.
- Lloyd, C. D. and Atkinson, P. M. (1998). Scale and the spatial structure of landform: Optimising sampling strategies with geostatistics. In *Proceedings of the Third International Conference of Geocomputation, University of Bristol, UK*.
- MacMillan, R. A. and Shary, P. A. (2009). Landforms and landform elements in geomorphometry. In T. Hengl and H. I. Reuter, editors, *Geomorphometry, Concepts, Software, Applications*, pages 227–254. Elsevier.
- Madych, W. R. and Nelson, S. A. (1990). Polyharmonic cardinal splines. *Journal of Approximation Theory*, **60**(2), 141–156.
- Mahler, E. (2001). *Scale-Dependent Filtering of High Resolution Digital Terrain Models in the Wavelet Domain*. Master's thesis, Departement of Geography, University of Zurich.
- Mallat, S. (1996). Wavelets for a vision. *Proceedings of the IEEE*, **84**(4), 604–614.
- Mallat, S. (2000). *Une exploration des signaux en ondelettes*. Les éditions de l'école polytechnique, Paris, France.
- Mallat, S. G. (1989). A theory for multiresolution signal decomposition: The wavelet representation. *IEEE Transaction On Pattern Analysis and Machine Intelligence*, **11**(7), 674–693.
- Marceau, D. J. (1999). The scale issue in social and natural sciences. *Canadian Journal of Remote Sensing*, **25**(4), 347–356.
- Marceau, D. J. and Hay, G. J. (1999). Remote sensing contributions to the scale issue. *Canadian Journal of Remote Sensing*, **25**(4), 357–366.
- Marcelja, S. (1980). Mathematical description of the response of simple cortical cells. *J. Opt. Soc. Am.*, **70**(11), 1297–1300.
- Mark, D. M. and Aronson, P. B. (1984). Scale-dependent fractal dimensions of topographic surfaces: An empirical investigation, with applications in geomorphology and computer mapping. *Mathematical Geology*, **16**(7), 671–683.
- Marr, D. (1982). *Vision: a computational investigation into the human representation and processing of visual information*. W. H. Freeman and Company.
- Martinoni, D. (2002). *Models and Experiments for Quality Handling in Digital Terrain Modeling*. Ph.D. thesis, Faculty of Science, University of Zurich.
- McKean, J. and Roering, J. (2004). Objective landslide detection and surface morphology mapping using high-resolution airborne laser altimetry. *Geomorphology*, **57**(3-4), 331–351.
- Meentemeyer, V. (1989). Geographical perspectives of space, time, and scale. *Landscape Ecology*, **3**(3/4), 163–173.
- Meentemeyer, V. and Box, E. O. (1987). Scale effects in landscape studies. In M. G. Turner and D. J. Bogucki, editors, *Landscape Heterogeneity and Disturbance*, pages 15–34. Ecological Studies 64, Springer-Verlag.
- Meyer, Y. (1992). *Les Ondelettes, Algorithmes et Applications*. Armand Colin, Paris, France.
- Mitasova, H. and Hofierka, J. (1993). Interpolation regularized spline with tension. *Mathematical Geology*, **25**(6), 657–669.
- Monnier, P. (1997). *Caractérisation du terrain en vue de son traitement numérique. Application à la généralisation de l'orographie*. Ph.D. thesis, Université Louis Pasteur, Strasbourg.

- Moore, I. D., Grayson, R. B., and Ladson, A. R. (1991). Digital terrain modelling: a review of hydrological, geomorphological and biological applications. *Hydrological Processes*, **5**(1), 3–30.
- Nicolis, O., Garutti, C., and Vidakovic, B. (2006). 2-D wavelet-based spectra with application in analysis of geophysical images. Biomedical engineering technical report, Georgia Institute of Technology. <http://hdl.handle.net/1853/25838>, accessed 27 September 2009.
- Openshaw, S. (1984). *The modifiable Areal Unit Problem*, volume 38. Concepts and Techniques in Modern Geography (CATMOG), GeoBooks.
- Openshaw, S. and Abrahart, R. J. (2000). *GeoComputation*. Taylor and Francis.
- Parker, J. R. (1997). *Algorithms for Image Processing and Computer Vision*. Wiley & Sons, Inc.
- Pfaltz, J. L. (1976). Surface networks. *Geographical Analysis*, **8**(1), 77–93.
- Pike, R. J. (2000). Geomorphometry - diversity in quantitative surface analysis. *Progress in Physical Geography*, **24**(1), 1–20.
- Pike, R. J. (2002). A bibliography of terrain modeling (geomorphometry), the quantitative representation of topography, supplement 4.0. Technical report, USGS.
- Pike, R. J. and Rozema, W. J. (1975). Spectral analysis of lanforms. *Annals of the Association of American Geographers*, **65**(4), 499–516.
- Poggio, T. (1981). Marr's computational approach to vision. *Trends in NeuroSciences*, **4**(10), 258–262.
- Pointet, A. (2007). *Rencontre de la science de l'information géographique et de l'anthropologie culturelle : modélisation spatiale et représentation de phénomènes culturels*. Ph.D. thesis, École Polytechnique Fédérale de Lausanne (EPFL).
- Polikar, R. (1995). *The Wavelet Tutorial*. Iowa State University, Durham Computation Center.
- Qi, Y. and Wu, J. (1996). Effects of changing spatial resolution on the results of landscape pattern analysis using spatial autocorrelation indices. *Landscape Ecology*, **11**(1), 39–49.
- Quattrochi, D. A. and Goodchild, M. F. (1997). *Scale in Remote Sensing and GIS*. CRC Press, Inc.
- Raffy, M. (1992). Change of scale in models of remote sensing: A general method for spatialization of models. *Remote Sensing of Environment*, **40**(2), 101–112.
- Rana, S. (2004). *Topological Data Structures for Surfaces*. John Wiley & Sons Ltd, West Sussex, England.
- Rao, R. L. (1995). *Multiresolution techniques in image processing*. Ph.D. thesis, Dept. of Computer Science, Louisiana State University.
- Ratcliffe, J. H. and McCullagh, M. J. (1999). Hotbeds of crime and the search for spatial accuracy. *J. Geograph Syst*, **1**(4), 385–398.
- Reuter, H. I. and Nelson, A. (2009). Chapter 11, geomorphometry in ESRI packages. In T. Hengl and H. I. Reuter, editors, *Geomorphometry, Concepts, Software, Applications*, pages 269–291. Elsevier.
- Reza, A. M. (1999). Wavelet characteristics, what wavelet should I use? White paper, Spire Lab, UWM.
- Rottensteiner, F. and Briese, C. (2002). A new method for building extraction in urban areas from high-resolution lidar data. In *International Archives of Photogrammetry and Remote Sensing, Volume XXXIV / 4*, pages 1–10. Photogrammetric Computer Vision, ISPRS Commission III.

- Rudnicki, W. (2000). The new approach to the relief shading applied in satellite image maps. In *Proceedings of High Mountain Cartography, KB 18*, pages 105–106. TU Dresden.
- Russ, J. C. (1990). Processing image with a local hurst operator to reveal textural differences. *Journal of Computer-Assisted Microscopy*, **2**(4), 249–257.
- Russ, J. C. (1994). *Fractal Surfaces*. Springer.
- Schmidt, J. and Andrew, R. (2005). Multi-scale landform characterization. *Area*, **37**(3), 341–350.
- Schmidt, J., Evans, I. S., and Brinkmann, J. (2003). Comparison of polynomial models for land surface curvature calculation. *Int. J. Geographical Information Science*, **17**(8), 797–814.
- Schneider, B. (2003). Surface networks: Extension of the topology and extraction from bilinear surface patches. In *7th International Conference on GeoComputation, University of Southampton, UK*.
- Schoenberg, I. J. (1946). Contributions to the problem of approximation of equidistant data by analytic functions. *Quart. Appl. Math.*, **4**(1), 45–99.
- Schroeder, W. J., Zarge, J. A., and Lorensen, W. E. (1992). Decimation of triangle meshes. In *SIGGRAPH '92: Proceedings of the 19th annual conference on Computer graphics and interactive techniques*, pages 65–70, New York, NY, USA. ACM Press.
- Shary, P. A. (1995). Land surface in gravity points classification by a complete system of curvatures. *Mathematical Geology*, **27**(3), 373–390.
- Skidmore, A. K. (1989). A comparison of techniques for calculating gradient and aspect from gridded digital elevation model. *Int. J. Geographical Information Systems*, **3**(4), 323–334.
- Sorensen, R., Zinko, U., and Seibert, J. (2006). On the calculation of the topographic wetness index: Evaluation of different methods based on field observation. *Hydrology and Earth System Sciences*, **10**(1), 101–112.
- Staad, O. G., Gross, M. H., and Weber, R. (1998). Multiresolution compression and reconstruction. In *Eurographics 98*.
- Sulebak, J. R. (1999). Fractal analysis of surface topography. *Norsk. Geogr. Tidsskr.*, **53**(4), 213–225.
- swisstopo (2004). MNT25, le modèle numérique du terrain de la Suisse. Technical report, Office fédéral de topographie, swisstopo.
- Tate, N. J. (1998). Maximum entropy spectral analysis for the estimation of fractals in topography. *Earth Surf. Process. Landforms*, **23**(13), 1197–1217.
- Theler, D. and Reynard, E. (2008). Mapping sediment transfer processes using GIS applications. In *Commission on Mountain Cartography, International Cartographic Association*.
- Tobler, W. (1970). A computer movie simulating urban growth in the Detroit region. *Economic Geography*, **46**(2), 234–240.
- Tobler, W. (1987). Measuring spatial resolution. In *Proceedings of International Workshop on Geographic Information System, Beijing*.
- Toutin, T. (1998). Depth perception with remote sensing data. In P. Gudmandsen, editor, *Future Trends in Remote Sensing*, pages 401–409.
- Turner, M. G. (1989). Landscape ecology: The effect of pattern on process. *Annu. Rev. Ecol. Syst.*, **20**, 171–197.
- Unser, M. (1999). Splines, a perfect fit for signal and image processing. Technical report, IEEE Signal Processing Magazine.
- Unser, M. (2001). Traitement d'images, volume 2. EPFL.

- Unser, M. and Blu, T. (1999). Construction of fractional spline wavelet bases. In *Proceedings of the SPIE Conference on Mathematical Imaging: Wavelet Applications in Signal and Image Processing VII*, pages 551–560.
- Unser, M. and Blu, T. (2000). Fractional splines and wavelets. *SIAM Reviews*, **42**(1), 43–67.
- Unser, M. and Blu, T. (2003). Wavelet theory demystified. *IEEE Transactions on Signal Processing*, **51**(2), 470–483.
- Unser, M. and Van De Ville, D. (2008). The pairing of a wavelet basis with a mildly redundant analysis via subband regression. *IEEE Transactions on Image Processing*, **17**(11), 2040–2052.
- Unser, M., Thévenaz, P., and Aldroubi, A. (1996). Shift-orthogonal wavelet bases using splines. *IEEE Signal Processing Letters*, **3**(3), 85–88.
- Unser, M., Sage, D., and Van De Ville, D. (2009). Multiresolution monogenic signal analysis using the Riesz-Laplace wavelet transform. *IEEE Transactions on Image Processing*, **18**(11), 2402–2418.
- Van De Ville, D. and Unser, M. (2008). Complex wavelet bases, steerability, and the Marr-like pyramid. *IEEE Transactions on Image Processing*, **17**(11), 2063–2080.
- Van De Ville, D., Blu, T., and Unser, M. (2005). Isotropic polyharmonic B-Splines: Scaling functions and wavelets. *IEEE Transactions on Image Processing*, **14**(11), 1798–1813.
- Van De Ville, D., Sage, D., Balać, K., and Unser, M. (2008). The Marr wavelet pyramid and multiscale directional image analysis. In *Proceedings of the Sixteenth European Signal Processing Conference (EUSIPCO'08)*, Lausanne VD, Switzerland.
- Vetterli, M. (1986). Filter banks allowing perfect reconstruction. *Signal Processing*, **10**(3), 219–244.
- Vu, T. T. and Tokunaga, M. (2002). Designing of wavelet-based processing system for airborne laser scanner segmentation. In *Proceedings of the International Workshop on Visualization and Animation Of Landscape, Kunming, China*, volume XXX IV.
- Ware, C. (2001). Designing with a 2 1/2d attitude. *Information Design Journal*, **10**(3), 255–262.
- Ware, C. (2004). *Information Visualization, Perception for Design*. Elsevier.
- Wehr, A. and Lohr, U. (1999). Airborne laser scanning - an introduction and overview. *ISPRS Journal of Photogrammetry & Remote Sensing*, **54**(2-3), 68–82.
- Weibel, R. (1989a). Contributions to digital terrain modeling and display. Geo-Processing Series 12, Departement of Geography, University of Zurich.
- Weibel, R. (1989b). *Konzepte und Experimente zur Automatisierung des Reliefgeneralisierung*. Ph.D. thesis, Departement of Geography, University of Zurich.
- Wilson, J. P. and Gallant, J. C. (2000). *Terrain Analysis, Principles and Applications*. Wiley.
- Wong, D. (2009). The modifiable areal unit problem (MAUP). In A. S. Fotheringham and P. A. Rogerson, editors, *The SAGE Handbook of Spatial Analysis*, pages 105–124. SAGE Publications.
- Wood, J. (1996). *The Geomorphological Characterisation of Digital Elevation*. Ph.D. thesis, University of Leicester, UK.
- Wood, J. (1999). Visualisation of scale dependencies in surface models. In *International Cartographic Association*.

- Wood, J. (2000). Construction weighted surface networks for the representation and analysis of surface topology. In *5th International Conference on GeoComputation, Chatham, UK*.
- Wood, J. (2009). Visualizing geomorphometry: Lessons from information visualization. In R. Purves, S. Gruber, T. Hengl, and R. Straumann, editors, *Proceedings of Geomorphometry 2009*.
- Woodcock, C. E. and Strahler, A. H. (1987). The factor of scale in remote sensing. *Remote Sensing of Environment*, **21**(3), 311–332.
- Zevenbergen, L. W. and Thorne, C. R. (1987). Quantitative analysis of land surface topography. *Earth Surface Processes and Landforms*, **12**(1), 47–56.
- Zwillinger, D. (2003). *CRC - Standard Mathematical Tables And Formulae*. CRC Press.

Glossary

ALS	Airborne Laser Scanning
DEM	Digital Elevation Model
DGPS	Differential Global Positioning System
DHM	Digital Height Model
DSM	Digital Surface Model
DTM	Digital Terrain Model
FT	Fourier Transform
GI	Geographical Information
GIS	Geographical Information System
GISc	Geographical Information Science
GPS	Global Positioning System
HTTP	HyperText Transfer Protocol
IDW	Inverse Distance Weighting
IFT	Inverse Fourier Transform
IMU	Inertial Measurement Unit
INS	Inertial Navigation System
IWT	Inverse Wavelet Transform
ISODATA	Iterative Self-Organizing Data Analysis Technique
LASER	Light Amplification by Stimulated Emission of Radiation
LIDAR	Light Detection And Ranging
LSPs	Land Surface Parameterizations
MAUP	Modifiable Areal Unit Problem
NASA	National Aeronautics and Space Administration

PHP	Hypertext Preprocessor
PLC	PLan Curvature
PRC	PRofile Curvature
SAR	Synthetic Aperture Radars
SNR	Signal-to-Noise Ratio
SRTM	Shuttle Radar Topography Mission
SVG	Scalable Vector Graphics
SVM	Support Vector Machines
TIN	Triangular Irregular Network
WGS	World Geodetic System
WI	Wetness Index
WT	Wavelet Transform

Mathematical notations

m	Number of columns in an image or a set of pixels
n	Number of lines in an image or a set of pixels
\mathbf{x}	$\mathbf{x} = (x_1, x_2, \dots, x_n)$, vector
i	Wavelet decomposition level (usually in this study $i = 0, \dots, 8$)
j	Complex numbers, imaginary unit
ψ	Wavelet function
φ	Scale function
L	Lebesgue space
W_i	i^{th} wavelet subspace (high-pass domain)
V_i	i^{th} subspace of function $f(x)$
ω	Angular frequency (Fourier domain)
z	Complex number of the z -transform ($z = A \cdot e^{j\theta} = A(\cos \theta + j \sin \theta)$)
c_i	Low-pass coefficients of wavelet transform of the i^{th} level
$d_{h,i}$	Horizontal high-pass coefficients of wavelet transform of the i^{th} level
$d_{v,i}$	Vertical high-pass coefficients of wavelet transform of the i^{th} level
$d_{d,i}$	Diagonal high-pass coefficients of wavelet transform of the i^{th} level
H	Low-pass wavelet filter
\tilde{H}	Dual version of filter H
G	High-pass wavelet filter
\tilde{G}	Dual version of filter G
β	B-spline function
$\hat{\beta}$	Impulse response (in the Fourier domain) of β
β_+	Causal B-spline function

β_-	Anti-causal B-spline function
β_*	Symmetric B-spline function
a_φ	Autocorrelation of function $\varphi(x)$
$C(e^{j\omega})$	Fourier transform of coefficient $c[k]$
Δ	Laplace operator
∇	Gradient operator

A. Fractional B-splines and Wavelets

This appendix is a general introduction to fractional B-splines and their associated wavelets. It only shows the main formulas and developments used to understand out the wavelet transform. For a complete theoretical introduction, please refer to the given bibliography, which includes the following papers and books: Mallat (1989); Meyer (1992); Dierckx (1993); Unser (1999); Mallat (2000); Unser and Blu (2000).

A.1 B-spline Interpolation

B-spline interpolation can be defined using Schoenberg's theorem (Schoenberg, 1946). We can describe a spline as a linear combination of shifted B-splines, introducing a convolution (see section 3.3.1) in the definition and giving a polynomial form to the spline:

Theorem A.1.1 (Schoenberg).

$$s(x) = \sum_{k \in \mathbb{Z}} c(k) \beta^n(x - k) \quad (\text{A.1})$$

where $s(x)$ is a signal, $c(k)$ the B-spline coefficients and β^n the B-spline basis function of degree n .

A.1.1 B-spline basis function

If we use an uncentred causal version of the B-spline basis function and of degree 0 then:

$$\beta_+^0(x) = \begin{cases} 1 & \text{if } x \in [0, 1[\\ 0 & \text{otherwise} \end{cases} \quad (\text{A.2})$$

Using the convolution property of the B-spline basis function (recursion formula), we can compute the causal B-spline basis for a B-spline of degree n (see figure A.1 for examples):

$$\beta_+^n(x) = \underbrace{\beta_+^0(x) * \beta_+^0(x) * \dots * \beta_+^0(x)}_{n+1 \text{ times}} \quad (\text{A.3})$$

In the Fourier domain, the causal B-spline basis function of degree 0 is defined as (Unser and Blu, 2003):

$$\hat{\beta}_+^0(\omega) = \left(\frac{1 - e^{-j\omega}}{j\omega} \right) \quad (\text{A.4})$$

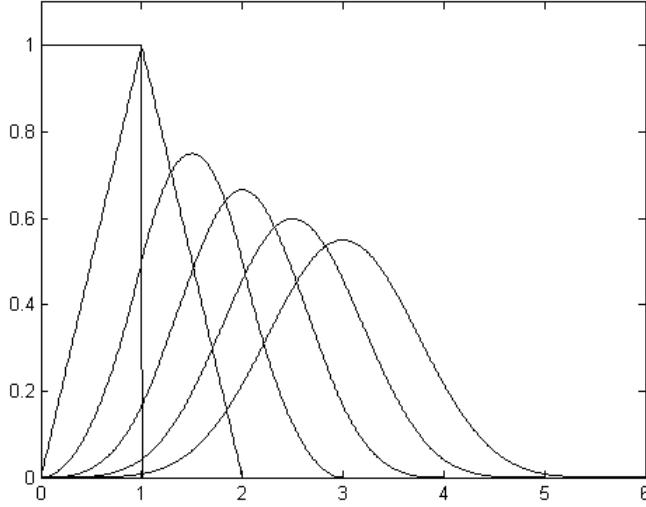


Fig. A.1. Causal B-spline basis functions, from degree 0 to 5.

By spatial convolution (equation A.3) of this function n times with itself, we obtain, in the Fourier domain, the basis function for a B-spline of degree n :

$$\hat{\beta}_+^n(\omega) = \left(\frac{1 - e^{-j\omega}}{j\omega} \right)^{n+1} \quad (\text{A.5})$$

This is the causal version of the B-spline basis function. If we want to have a symmetric function, we need to convolve the causal and anti-causal part of the function (Unser and Blu, 2000). The anti-causal part can be defined the same way we defined the causal part. Thus, the symmetric version of the B-spline basis is defined following:

$$\beta_*^n(x) = \beta_+^{\frac{n-1}{2}}(x) * \beta_-^{\frac{n-1}{2}}(x) \quad (\text{A.6})$$

What, in the Fourier domain, finally gives:

$$\hat{\beta}_*^n(\omega) = \left| \frac{1 - e^{-j\omega}}{j\omega} \right|^{n+1} \quad (\text{A.7})$$

A.1.2 B-spline coefficients

The $c(k)$ coefficients can be computed using the convolution properties in the Fourier domain of the Schoenberg Formula:

$$s(k) = \sum_{k \in \mathbb{Z}} c(k) \beta^n(x - k) = (c * b_1^n)(k) \quad (\text{A.8})$$

b_1^n are the sampled B-spline coefficients. Their definition in the Fourier domain is:

$$(b_1^n)^{-1} \stackrel{F}{\leftrightarrow} \frac{1}{B_1^n(e^{j\omega})} \quad (\text{A.9})$$

If we use equation A.8 and these sampled B-spline coefficients, we can compute the coefficients corresponding to the signal $s(k)$:

$$c(k) = ((b_1^n)^{-1} * s)(k) \quad (\text{A.10})$$

$$C(e^{j\omega}) = \frac{S(e^{j\omega})}{B(e^{j\omega})} \quad (\text{A.11})$$

Since we want to subsample our signal, we have to introduce a scaling function. In order to be a stable basis for this purpose, it has to be orthogonal. Thus, if we define our scaling function as φ , the orthogonality is reflected by:

$$\langle \tilde{\varphi}(x), \varphi(x - k) \rangle = \delta_k \quad (\text{A.12})$$

where δ_k is the discrete unit impulse and $\tilde{\varphi}(x)$ the unique dual function (Unser *et al.*, 1996). Unser and Blu (1999) defined the scaling function using the fractional B-spline autocorrelation for orthogonalisation:

$$\varphi(x) = \sum_{k \in \mathbb{Z}} (a_\varphi)^{-1/2} \beta^n(x - k) \quad (\text{A.13})$$

The Fourier transform of the autocorrelation filter is:

$$(a_\varphi)^1 \stackrel{F}{\leftrightarrow} \frac{1}{A_\varphi(e^{j\omega})} \quad (\text{A.14})$$

and finally:

$$A(e^{j\omega}) = \sum_{k=-\infty}^{+\infty} \left| \hat{\beta}^n(\omega + 2\pi k) \right|^2 = A^{\frac{n-1}{2}}(e^{j\omega}) \quad (\text{A.15})$$

$A(e^{j\omega})$ is the frequency response of the filter's autocorrelation (see section A.1.3 for computational issues). It may be computed using either the convergence of the infinite sum in the Fourier space or by computing explicitly $\hat{\beta}$.

We have now the B-spline interpolation coefficients. These will be combined to the wavelet transform.

A.1.3 Filter autocorrelation

In order to compute the $B(e^{j\omega})$ coefficient, we need to estimate the filter's autocorrelation in the Fourier domain. As shown in section A.1, either we estimate the autocorrelation, or we compute the coefficients explicitly. We choose to estimate them using the autocorrelation.

The filter autocorrelation has to be estimated at $\nu = \frac{k}{N}$, $k = 0, \dots, N - 1$ by using the equivalent Poisson expression $A^n(e^{1\pi j\nu}) \approx \sum_{n \in \mathbb{Z}} \left| \hat{\beta}_+^n(2\pi(n + \nu)) \right|^2 + \sum_{n \in \mathbb{Z}} \left| \hat{\beta}_-^n(2\pi(n - \nu)) \right|^2$. Once the filters are defined at frequency points $\nu = \frac{k}{N}$, it is not necessary to recompute them at each decomposition step i . At $i = 1$, we need H_k^n and G_k^n for $k = 0, \dots, N - 1$ and at the next step $i + 1$, we need H_{2k}^n and G_{2k}^n for $k = 0, \dots, \frac{N}{2} - 1$. This means that the filters can be precomputed before the WT only by using the degree of the B-spline (n) and the size of the signal (respectively N for the row dimension and L for the column dimension).

A.2 Wavelets

In signal processing, a wavelet analysis is a signal representation of a finite or rapidly decaying waveform. The associated transform is composed of two functions. The first is the scaling function φ , which is scaled and shifted throughout the transform to fit a signal. It is associated to a second function ψ called the wavelet function. These two functions define mirror quadrature filters, respectively filter H for the scaling function and G for the wavelet function.

Definition A.2.1 (Mallat, continuous wavelet transform). *A wavelet is a function $\psi \in L_2(\mathbb{R})$ with zero mean:*

$$\int_{-\infty}^{\infty} \psi(x) dx = 0 \quad (\text{A.16})$$

If the wavelet ψ is dilated by a factor i and translated by k , we obtain:

$$\psi_{i,k}(x) = \frac{1}{\sqrt{2^i}} \psi\left(\frac{x-k}{2^i}\right) \quad (\text{A.17})$$

Thus, the wavelet transform of $f \in L_2(\mathbb{R})$ at location k and scale i is:

$$Wf(i, k) = \langle f, \psi_{i,k} \rangle = \int_{-\infty}^{\infty} f(x) \frac{1}{\sqrt{2^i}} \psi^*\left(\frac{x-k}{2^i}\right) dx \quad (\text{A.18})$$

Definition A.2.2 (Mallat, linear filtering). *The wavelet transform can be written like a convolution:*

$$Wf(i, k) = \langle f, \psi_{i,k} \rangle = f * \bar{\psi}_i(k) \quad (\text{A.19})$$

With:

$$\bar{\psi}_i(x) = \frac{1}{\sqrt{2^i}} \psi^*\left(\frac{-x}{2^i}\right)$$

The Fourier transform of $\bar{\psi}_i(x)$ is:

$$\widehat{\bar{\psi}}_i(\omega) = \sqrt{2^i} \hat{\psi}^*(2^i \omega) \quad (\text{A.20})$$

For each wavelet, there is a scaling function φ , which can be interpreted as the impulse response of a low-pass filter:

$$\varphi_i(x) = \frac{1}{\sqrt{2^i}} \varphi\left(\frac{x}{2^i}\right) \quad (\text{A.21})$$

A.2.1 Mirror filters

If we take a scaling factor $i = 1$ (dyadic subsampling), the following decomposition can be made:

$$\varphi\left(\frac{x}{2}\right) = \sqrt{2} \sum_{n=-\infty}^{+\infty} h[n] \varphi(x-n) \quad (\text{A.22})$$

which gives in the Fourier domain:

$$\hat{\varphi}(2\omega) = \frac{1}{\sqrt{2}} \hat{h}(w) \hat{\varphi}(w) \quad (\text{A.23})$$

finally:

$$\hat{h}(w) = \sqrt{2} \frac{\hat{\varphi}(2\omega)}{\hat{\varphi}(w)} = H(e^{j\omega}) = H(z) \quad (\text{A.24})$$

Using the corresponding two-scale relation and the definition of the B-spline autocorrelation (cf. equations A.23 and A.13), the refinement filter can be computed through (Blu and Unser, 2000):

$$H(e^{j\omega}) = \sqrt{\frac{A_\varphi(e^{j\omega})}{A_\varphi(e^{j2\omega})}} \sqrt{2} \left| \frac{1 + e^{-j\omega}}{2} \right|^{n+1} \quad (\text{A.25})$$

Mallat (2000) showed that if the scaling function $\varphi(x)$ satisfies three conditions (Riesz basis criterion, refinability and partition of unity), a corresponding wavelet $\psi(x)$ exists and it is a linear combination of shifted versions of the scaling function (Unser and Blu, 2003):

$$\psi\left(\frac{x}{2}\right) = \sqrt{2} \sum_{k \in \mathbb{Z}} g(k) \varphi(x - k) \quad (\text{A.26})$$

where $g(k)$ is the impulse response of the wavelet synthesis filter.

Using Mallat (2000), we obtain the wavelet filter¹:

$$G(z) = z \cdot H(-z^{-1}) \quad (\text{A.27})$$

The decomposition of a signal using the wavelet transform boils this signal down to low-pass, high-pass filtering and down-sampling. Vetterli (Vetterli, 1986) gave the following theorem for a perfect reconstruction of the signal:

Theorem A.2.1 (Vetterli). *The conditions for a perfect reconstruction are:*

$$\tilde{H}(z^{-1})H(z) + \tilde{G}(z^{-1})G(z) = 2 \quad (\text{A.28})$$

$$\tilde{H}(z^{-1})H(-z) + \tilde{G}(z^{-1})G(-z) = 0 \quad (\text{A.29})$$

A.3 Computing the wavelet transform

First, we define the next variables and parameters (figure A.2):

- $s[k]$: discrete signal corresponding to our elevation data.
- $S(e^{j\omega})$: signal in the Fourier domain.
- i : scale index of the decomposition.
- $B(e^{j\omega})$: discrete B-spline filter in the Fourier domain.
- $C(e^{j\omega})$: spline coefficients in the Fourier domain.
- $c[k]$: B-spline coefficients in the spatial domain.

To apply the wavelet transform in the correct way, we have to inject the B-spline coefficients into the filter bank. Thus, we must first prefilter the data with the spline prefilter. Once we have computed these, we can apply the wavelet transform using Mallat's algorithm. Again, the transform results are spline coefficients which have to be post-processed to obtain elevation data again.

¹ z is the z-transform operator, which is a generalisation of the Fourier transform. It is defined by $z = e^{j\omega}$

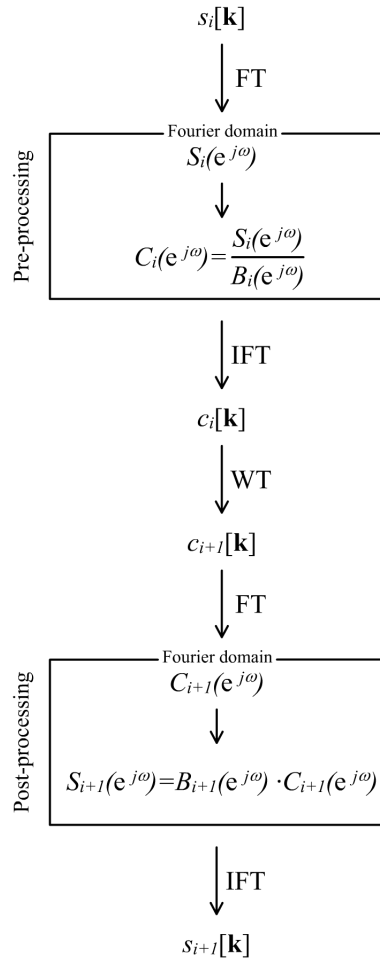


Fig. A.2. Signal pre- and post-processing

B. Fractional spline wavelet and scaling functions

As seen in appendix A, there are plenty of functions which could be used to define a wavelet family and, by deduction, the corresponding scaling function. We chose to use the fractional spline wavelets family (Unser, 1999) regarding the spline interpolation basis that may be defined as scaling function (see section B.1). If we use a B-spline basis function, the associate wavelet family will be symmetric dual¹ wavelets. In order to select an appropriate degree of B-spline basis, an empirical study using different degree is made: $n = 0.5, 1, 1.5, \dots, 5$. Scaling and wavelet function shapes are shown in figures B.8 to B.16 (except for degree 3, see figure 4.8 in chapter 4).

B.1 Fractional spline wavelets

B.2 Choice of B-spline degrees

As reminder and regarding our goals, the scaling function should:

- Give the best possible generalisation, e.g. be the best interpolation function.
- Not inject structures into the DEM due the shape of the wavelet.

B.2.1 Frequency composition of low-pass reconstructions

Using the DEM of Travers as input signal (see appendix F for details on this DEM), each basis (of degree n) was applied until the fifth decomposition level. For each level, a synthesis (reconstruction) was applied to the low-pass subsampled DEM, but with omission of all high-pass coefficients. The SNR² was then computed between each DEM and the original DEM.

The SNR gives advice on the similarity between two images. Thus the lowest it is, the more similar the two images are.

As we go through the scales, the SNR gets higher. This seems normal because the DEMs are less and less similar to the original surface as they are more and more generalised. As shown on figure B.1, at each 0.5 augmentation of the B-spline degree, the SNR gets lower. For one level, the SNR decreasing between degrees 0.5 and 1 is of factor 2.

¹ Scaling and wavelet functions φ and ψ are dual when for every i the decomposition formulae is: $f = \sum_{k \in \mathbb{Z}} \langle f, \tilde{\psi}_{jk} \rangle \psi_{jk} + \sum_{j' \geq j, k \in \mathbb{Z}} \langle f, \tilde{\varphi}_{jk} \rangle \varphi_{jk}$ (Bernard, 2001)

² Independent Signal-to-Noise ratio:

$$SNR = 20 \cdot \log_{10} \left(\frac{\sqrt{\frac{1}{(n \cdot m - 1)} \cdot \sum_{i=1}^n \sum_{j=1}^m (I_{original, i, j} - I_{original})^2}}{\sqrt{\frac{1}{(n \cdot m - 1)} \cdot \sum_{i=1}^n \sum_{j=1}^m (I_{noise, i, j} - I_{noise})^2}} \right), \text{ where } I_{original} \text{ is the original DEM, } I_{noise} \text{ are the synthesised coefficients, } n \text{ and } m \text{ are respectively the height and width of the DEM.}$$

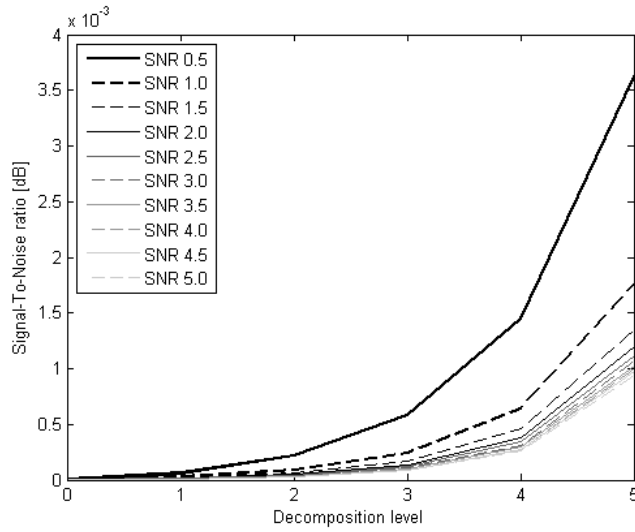


Fig. B.1. SNR of the different n degrees low-pass reconstruction (decomposition level 5) of the Travers DEM

To have a better view of the evolution at higher degree, a \log_{10} function was applied to the SNR values. It is interesting to see that since degree $n = 2$, the SNR are almost converging. Differences, looking at the SNR, are little between degrees $n = 2$ to $n = 5$.

Conceptually, degrees $n = 0.5$ to $n = 1.0$ are not appropriate as the shape of the basis function is not smooth enough and does not correspond to natural terrain shapes. This is exactly what can be seen in figure B.2. The square structures are induced by the wavelet shape, thus this degree does not respect one of our conditions.

An infinite convolution of the B-spline basis would tend to a *sinc* function, but the progression of the retrieved information in the different decomposition levels is not linear, thus it is not necessary to use higher levels. We chose to use a cubic B-spline basis ($n = 3$) as scaling function because it was already used as refinement or generalisation filter for DEM.

By visually comparing the original DEM (figure B.3) to the fifth level reconstructed DEMs (figures B.4 and B.5), low degrees surfaces ($n \leq 2$) are not appropriate because their shape injects noisy information to the model (see the square structures in figure B.3, (a), (b), (c) and (d)). From higher degrees ($n > 2$), differences between the reconstructed surfaces are hardly visible and they correspond to the generalisation process expected by going from the original DEM to the fifth decomposition.

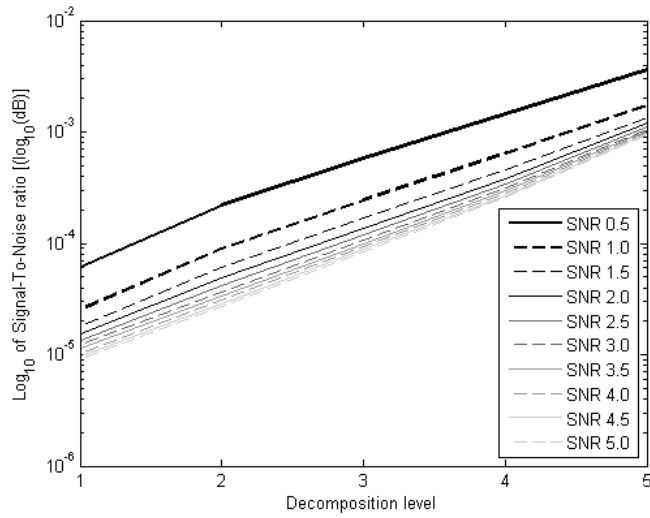


Fig. B.2. $\log_{10}(\text{SNR})$ of the different n degrees low-pass reconstructions (decomposition level 5) of the Travers DEM

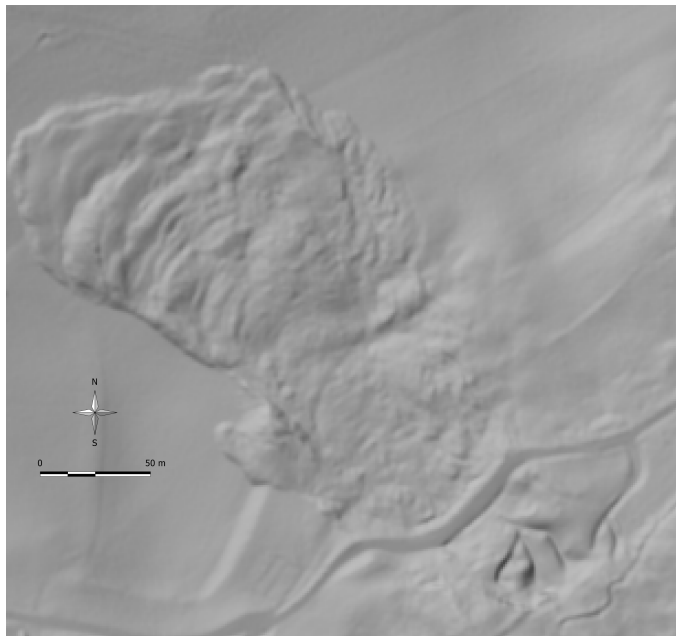


Fig. B.3. Original DEM©SITN

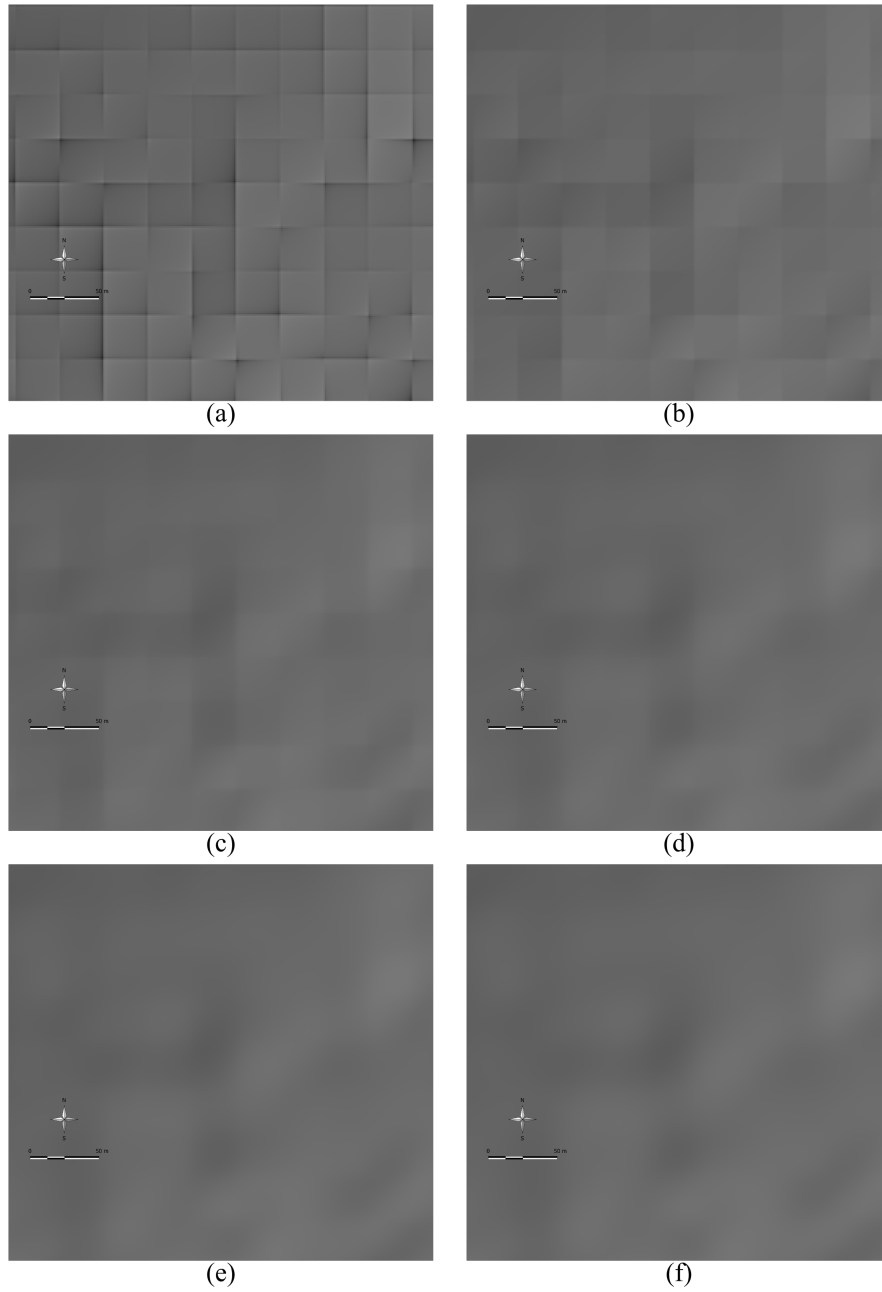


Fig. B.4. Reconstructed DEMs, degrees $n = 0.5$ (a), $n = 1.0$ (b), $n = 1.5$ (c), $n = 2.0$ (d), $n = 2.5$ (e), $n = 3.0$ (f)

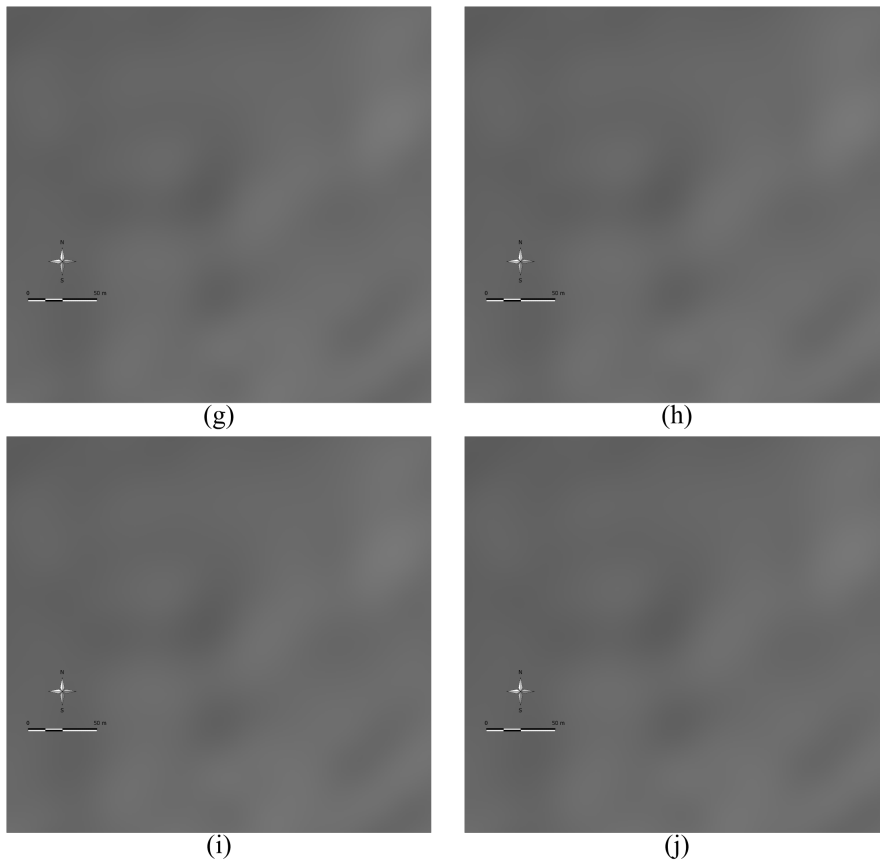


Fig. B.5. Reconstructed DEMs, degrees $n = 3.5$ (g), $n = 4.0$ (h), $n = 4.5$ (i), $n = 5.0$ (j)

B.3 Profiles on generalised DEMs

Three profiles are defined on a DEM (figure B.6). The first one (Profile 1 on figure B.6) is covering a very de-structured zone, beginning just under the new reconstructed road going through a landslide and finishing in the scarp zone. The second (Profile 2) covers a hill, but on the top of it there is a gravel-pit resulting in strong structural modifications.

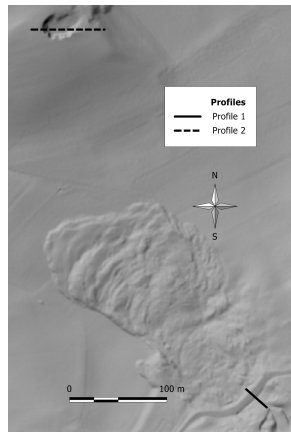


Fig. B.6. Profiles , 1 m shaded DEM©SITN

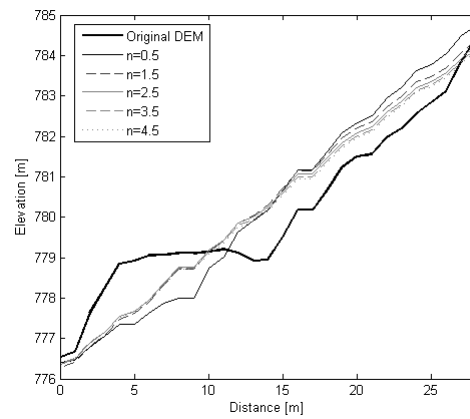


Fig. B.7. Profile 1

B.4 2D shape of fractional B-spline scaling and wavelet functions

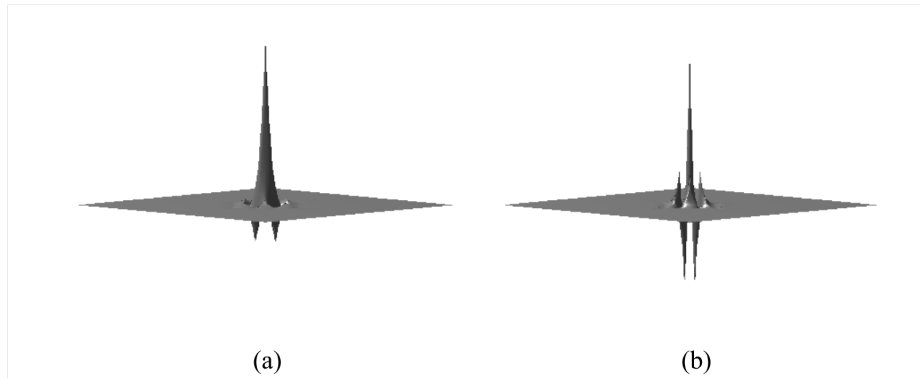


Fig. B.8. Illustrations of the scaling function (B-spline of degree 0.5)(a) and the wavelet function (symmetric dual wavelet)(b)

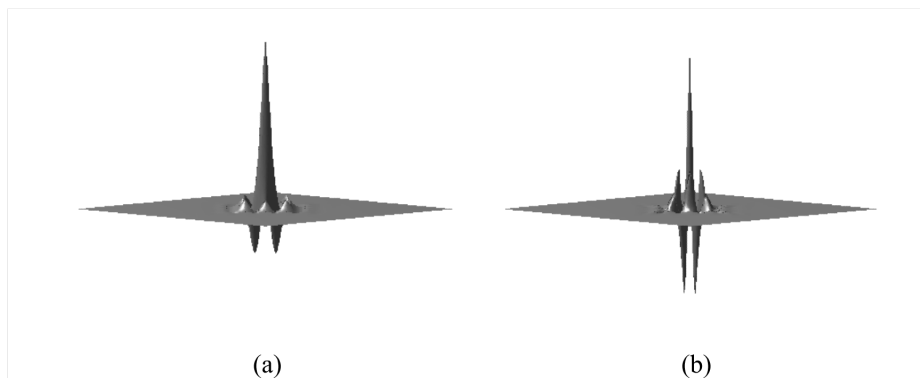


Fig. B.9. Illustrations of the scaling function (B-spline of degree 1)(a) and the wavelet function (symmetric dual wavelet)(b)

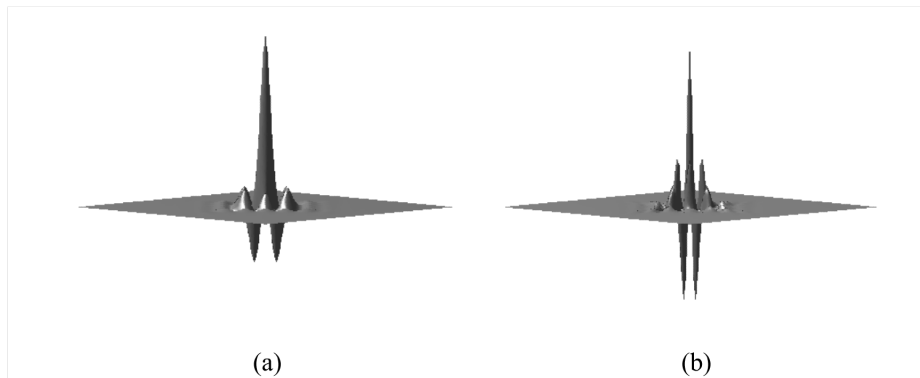


Fig. B.10. Illustrations of the scaling function (B-spline of degree 1.5)(a) and the wavelet function (symmetric dual wavelet)(b)

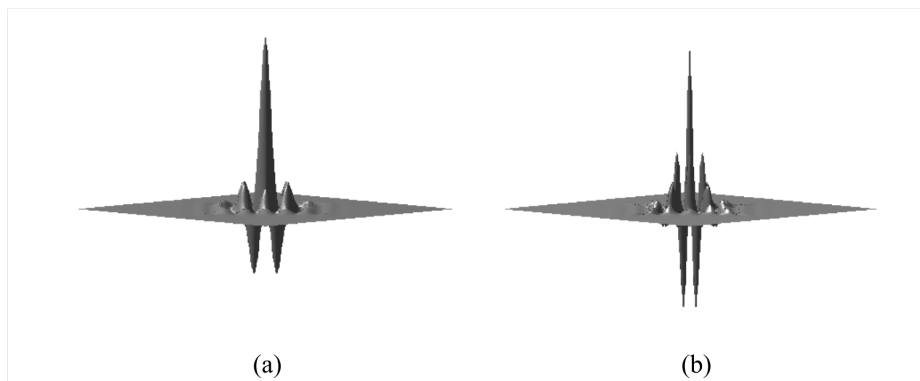


Fig. B.11. Illustrations of the scaling function (B-spline of degree 2)(a) and the wavelet function (symmetric dual wavelet)(b)

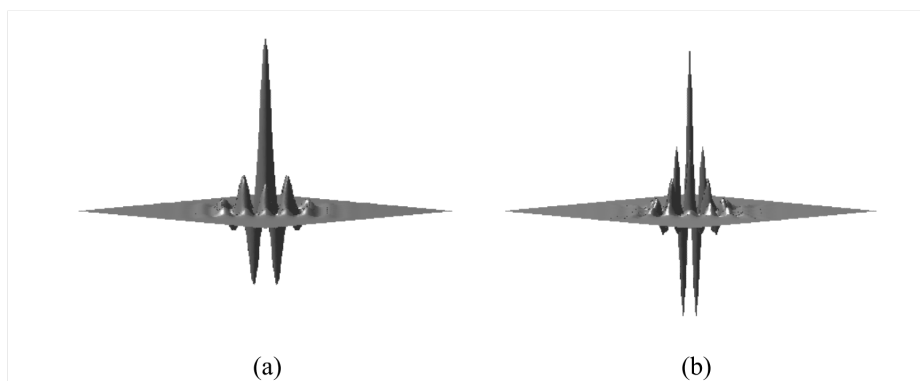


Fig. B.12. Illustrations of the scaling function (B-spline of degree 2.5)(a) and the wavelet function (symmetric dual wavelet)(b)

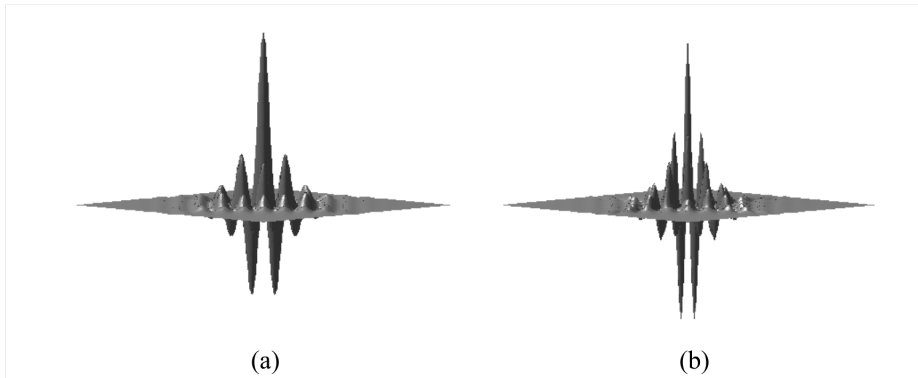


Fig. B.13. Illustrations of the scaling function (B-spline of degree 3.5)(a) and the wavelet function (symmetric dual wavelet)(b)

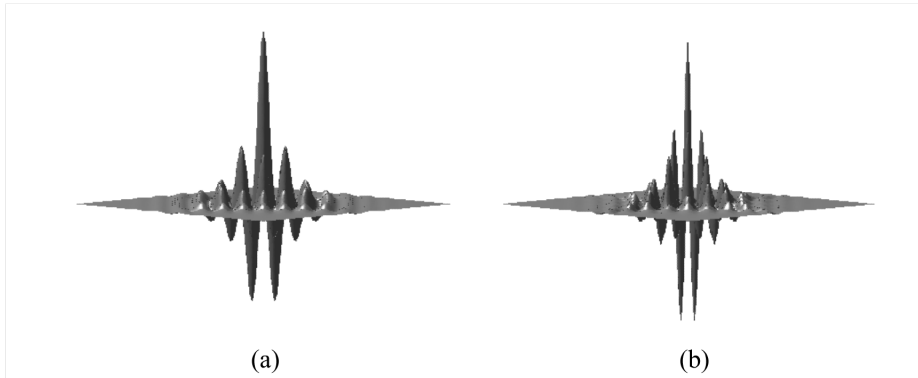


Fig. B.14. Illustrations of the scaling function (B-spline of degree 4)(a) and the wavelet function (symmetric dual wavelet)(b)

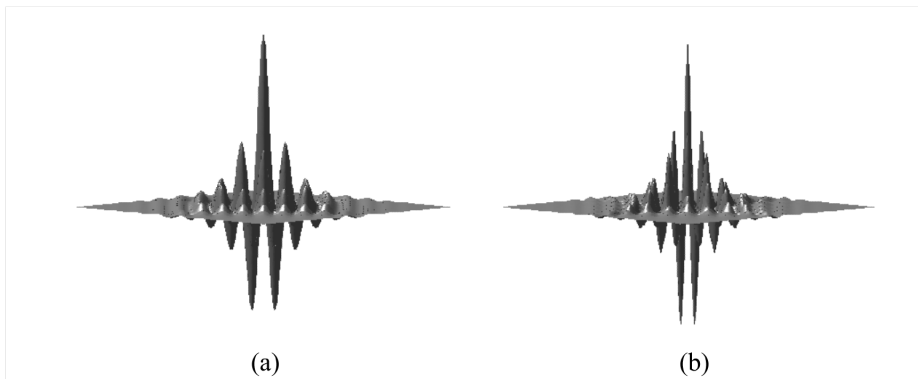


Fig. B.15. Illustrations of the scaling function (B-spline of degree 4.5)(a) and the wavelet function (symmetric dual wavelet)(b)

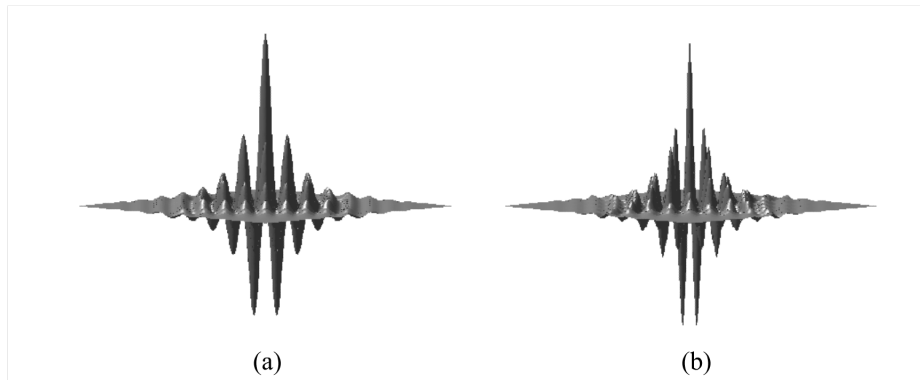


Fig. B.16. Illustrations of the scaling function (B-spline of degree 5)(a) and the wavelet function (symmetric dual wavelet)(b)

C. Profiles on generalised surface

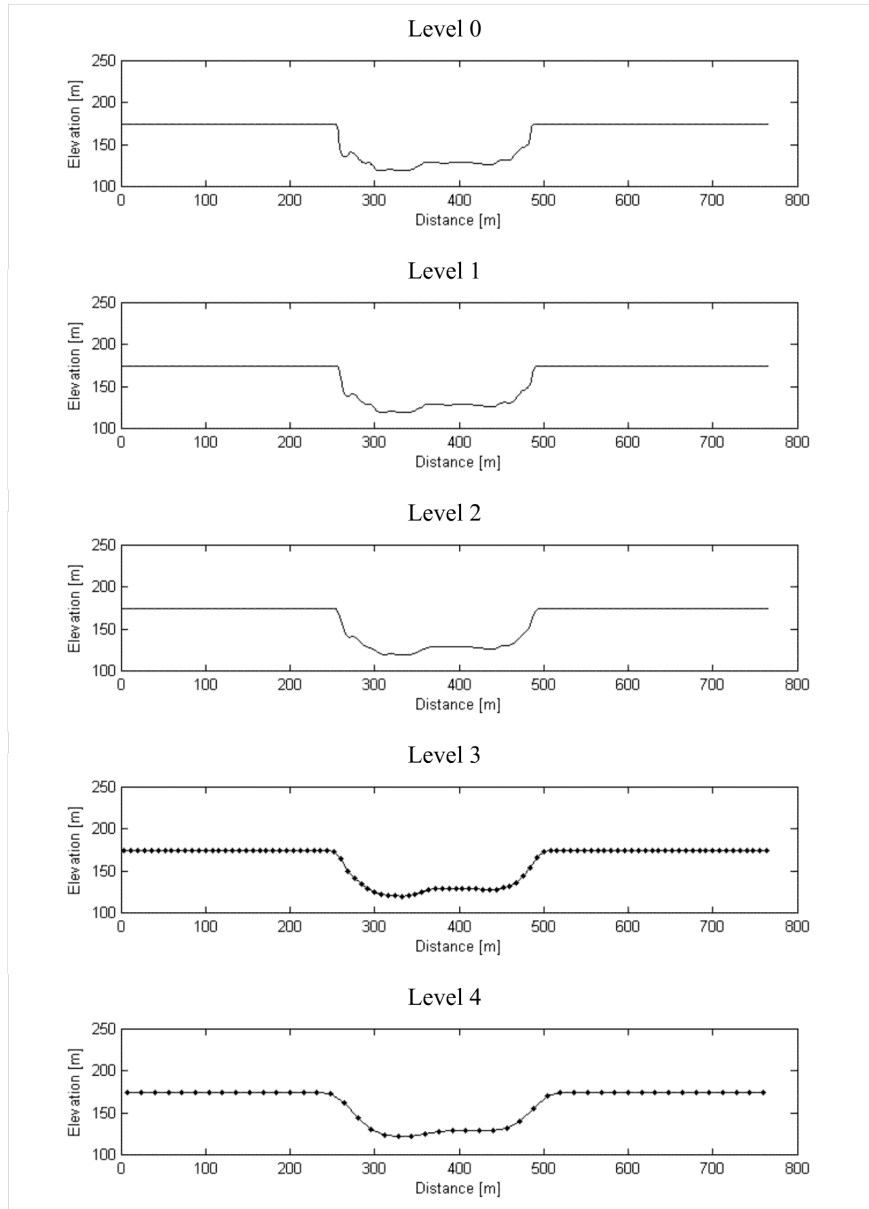


Fig. C.1. Profiles 2, decomposition levels 0-4, (Left side is the western end of the profile and right side is the eastern end of the profile.)

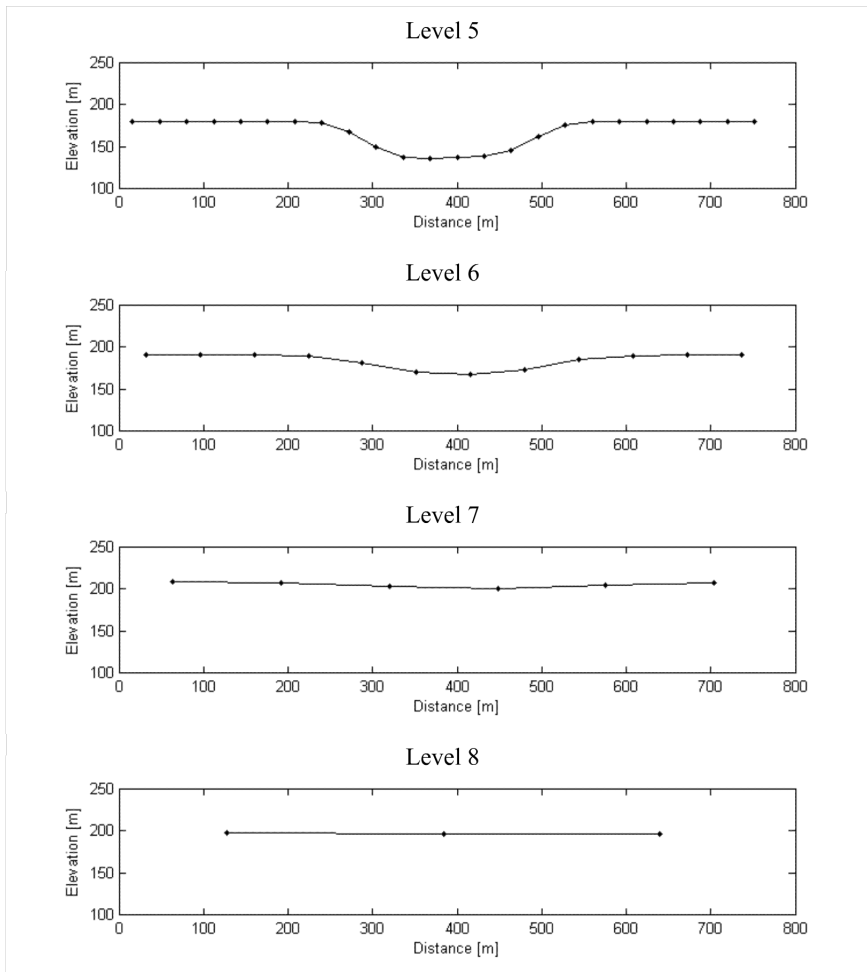


Fig. C.2. Profiles 2, decomposition levels 5-8 (Left side is the western end of the profile and right side is the eastern end of the profile.)

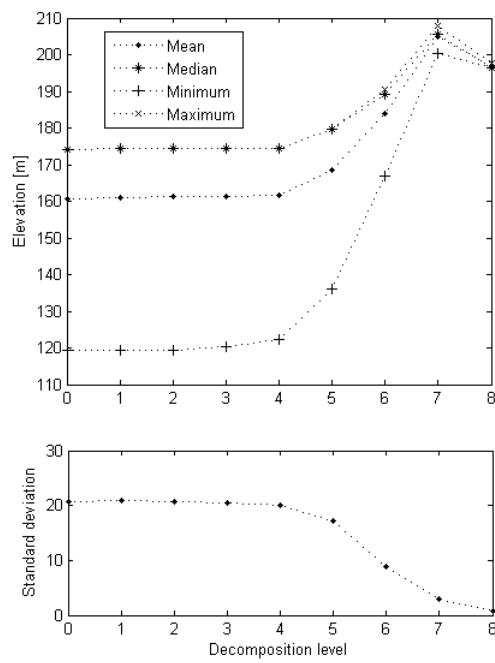


Fig. C.3. Statistical indicators of elevation variation through the decomposition levels, profile 2

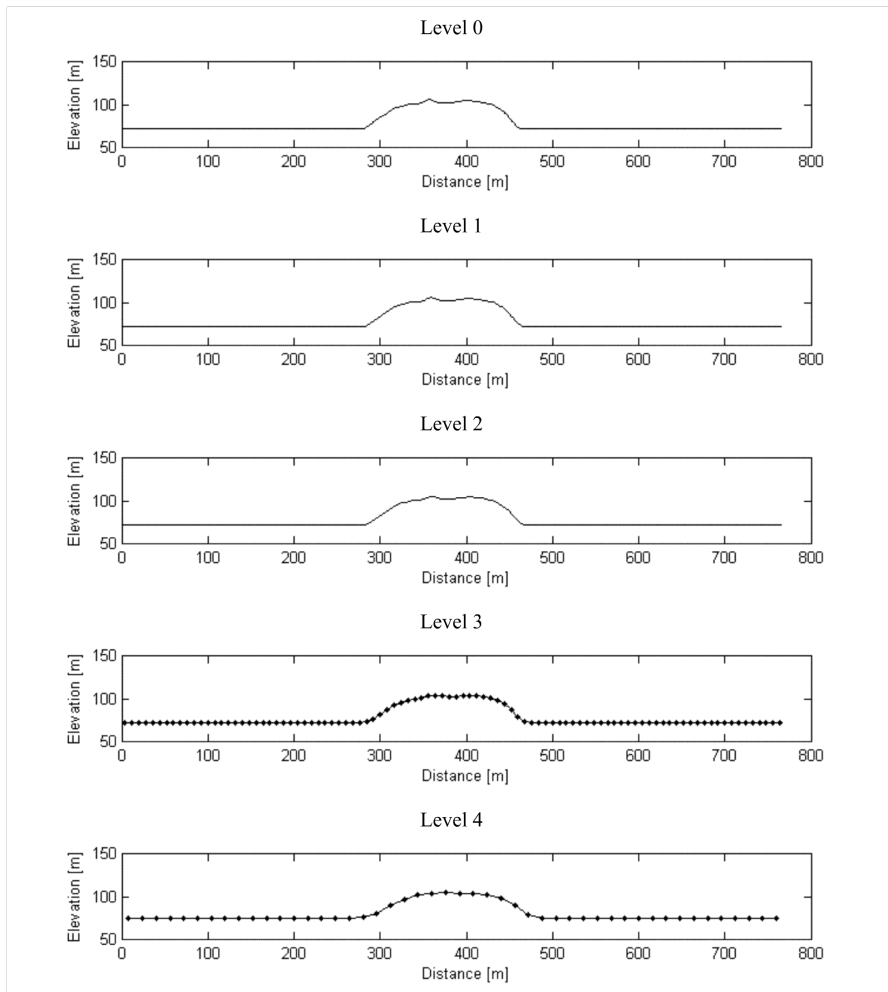


Fig. C.4. Profiles 3, decomposition levels 0-4 (Left side is the western end of the profile and right side is the eastern end of the profile.)

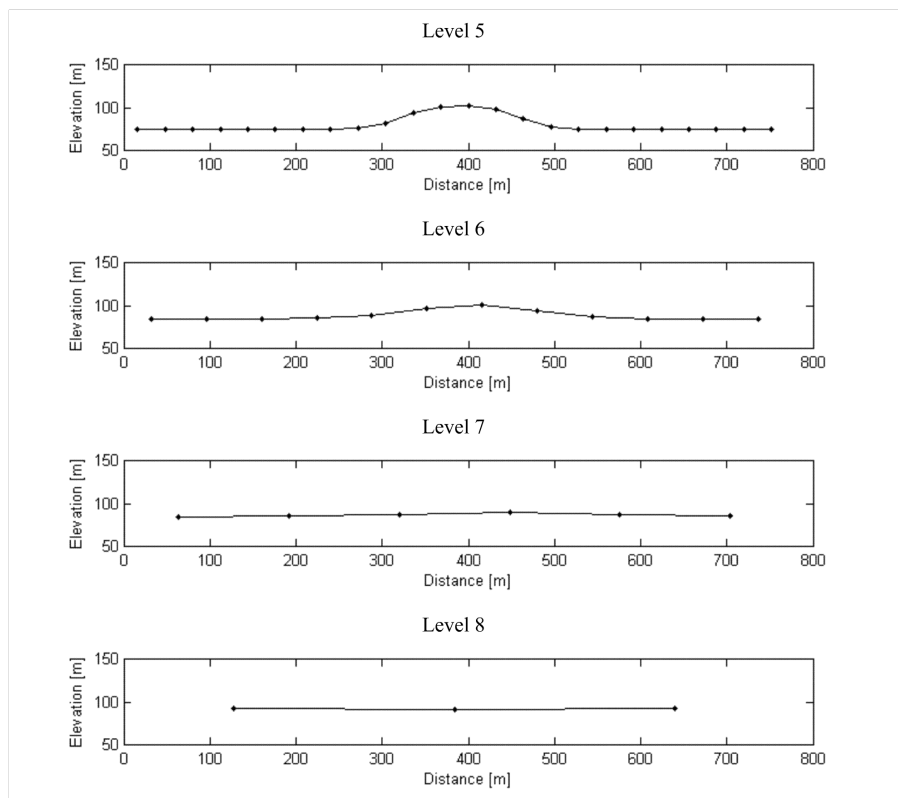


Fig. C.5. Profiles 3, decomposition levels 5-8 (Left side is the western end of the profile and right side is the eastern end of the profile.)

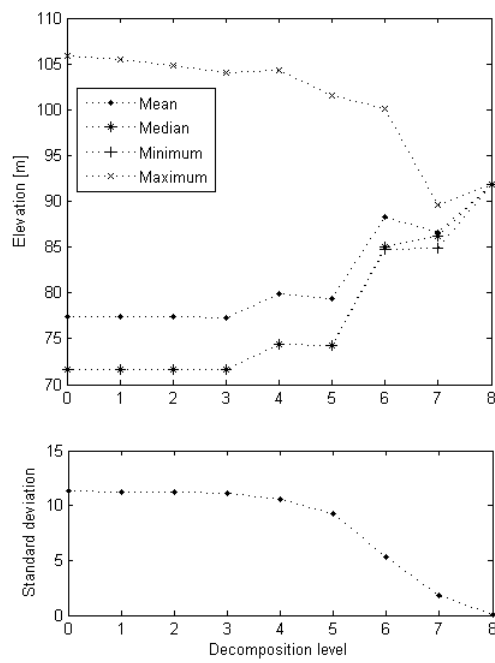


Fig. C.6. Statistical indicators of elevation variation through the decomposition levels, profile 3

D. Hurst coefficient

D.1 Hurst coefficient

We used the development described in Parker (1997); Russ (1994) and Russ (1990).

A scalable window is convoluted over the DEM. Considering the different distance classes inside this window, the elevation range is attributed to each distance class and a log – log plot is made for each convoluted pixel. Then, a linear regression is applied to the log – log plot and the slope of this regression is defined as the Hurst coefficient.

On each pixel of the DEM, the Hurst coefficient is computed using a maximum distance (d_{max}) and the resolution r of the analysed DEM. The distance threshold is simply the ratio of the maximum distance and the resolution ($threshold = ceil(d_{max}/r)$). Thus, on a convolution window of radius $threshold$, each possible distance is defined as a class. For each one, the range of the included pixel values is computed (called the elevation range). The class distances are then defined as x axis and the elevation ranges as y axis on a log – log (natural logarithm) plot. The slope of a linear regression on this plot gives the Hurst coefficient (the slope of the adjusted line). For computational purposes, the original DEM size is increased using mirror border conditions.

D.1.1 Example of Hurst coefficient computation

If we define a matrix with a $1\ m$ resolution ($r = 1$), $d_{max} = 3$ and $threshold = 3$. As example and for one pixel (see figure D.1 for the example values), the Hurst coefficient would give the following results:

- c_0 ($d_0 = 0$): is not defined as a class because the distance is equal to zero.
- c_1 ($d_1 = \sqrt{0^2 + 1^2} = 1$): the elevation range is computed using the local minimum and the local maximum of pixel in classes c_0 and c_1 , thus c_1 , $value = 770 - 738 = 32$
- c_2 ($d_2 = \sqrt{1^2 + 1^2} = \sqrt{2}$): the elevation range is computed using the local minimum and the local maximum of pixel in classes c_0, \dots, c_2 , thus c_2 , $value = 810 - 738 = 72$
- c_3 ($d_3 = \sqrt{2^2 + 0^2}$): the elevation range is computed using the local minimum and the local maximum of pixel in classes c_0, \dots, c_3 , thus c_3 , $value = 810 - 738 = 72$
- c_4 ($d = \sqrt{2^2 + 1^2} = \sqrt{5}$): this would be the next class, but because $d_4 > threshold$, this class and higher distance classes are not taken into account.

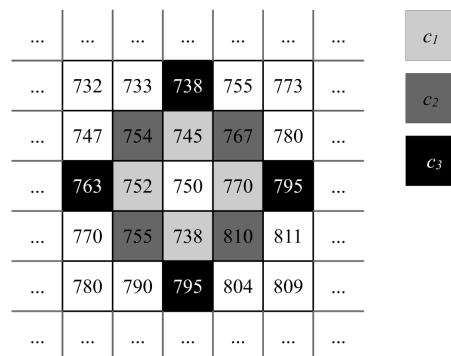


Fig. D.1. A central pixel with its local neighbouring pixels. Using $threshold = 3$, three classes (c_1, c_2, c_3) are defined.

Class	Distance	Range	$\ln(\text{distance})$	$\ln(\text{range})$
c_1	1.00	32	0.00	3.4657
c_2	1.41	72	0.35	4.2767
c_3	2.00	72	0.69	4.2767

Fig. D.2. Hurst example

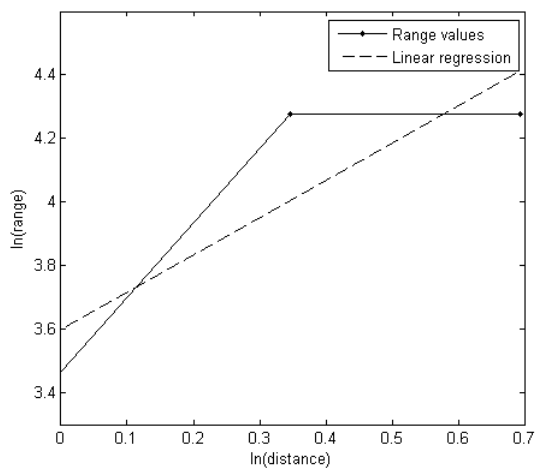


Fig. D.3. Example log – log regression

By adjusting a linear regression on the log values of the distance and range, the Hurst coefficient is defined. In this example, the equation of the linear regression is: $y = 3.6009 + 1.1699x$, thus the Hurst coefficient (slope of regression) is: 1.1699 (figure D.3).

The Hurst coefficient is similar to a measure of surface roughness, as the one defined in Li *et al.* (2005) for example. As Russ (1990) proposed, the convolution mask is usually an octagonal 7-pixel wide window.

D.2 Hurst coefficient on virtual landslide

The Hurst coefficient was computed using a 7×7 window for each image. Thus, the distance is constantly increasing with the increasing of the decomposition level. Conceptually, the distance is equal to 7 meters for the original DEM ($r = 1 m$), 14 meters for the first decomposition level ($r = 2 m$) and so on for the next levels.

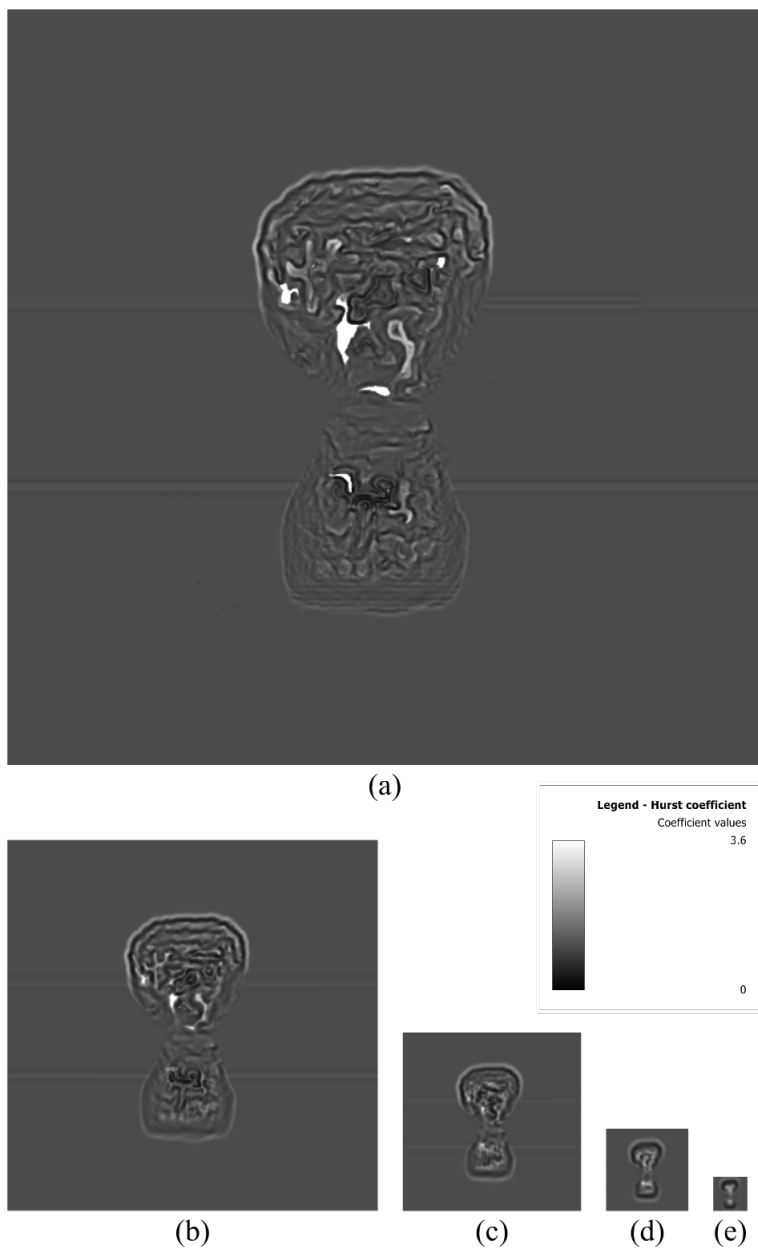


Fig. D.4. Hurst coefficient, (a) decomposition level 0 ($r = 1 m$). The white holes are flat areas. These are undetermined, because the elevation range is equal to zero, thus the natural logarithm tends to $-\infty$. As a reminder, a large Hurst coefficient indicates a smooth image. In this case, flat areas give an infinite slope, thus the smoothest image one can get. (b) decomposition level 1 ($r = 2 m$), ..., (e) decomposition level 4 ($r = 16 m$)

E. Detail coefficient of the virtual landslide

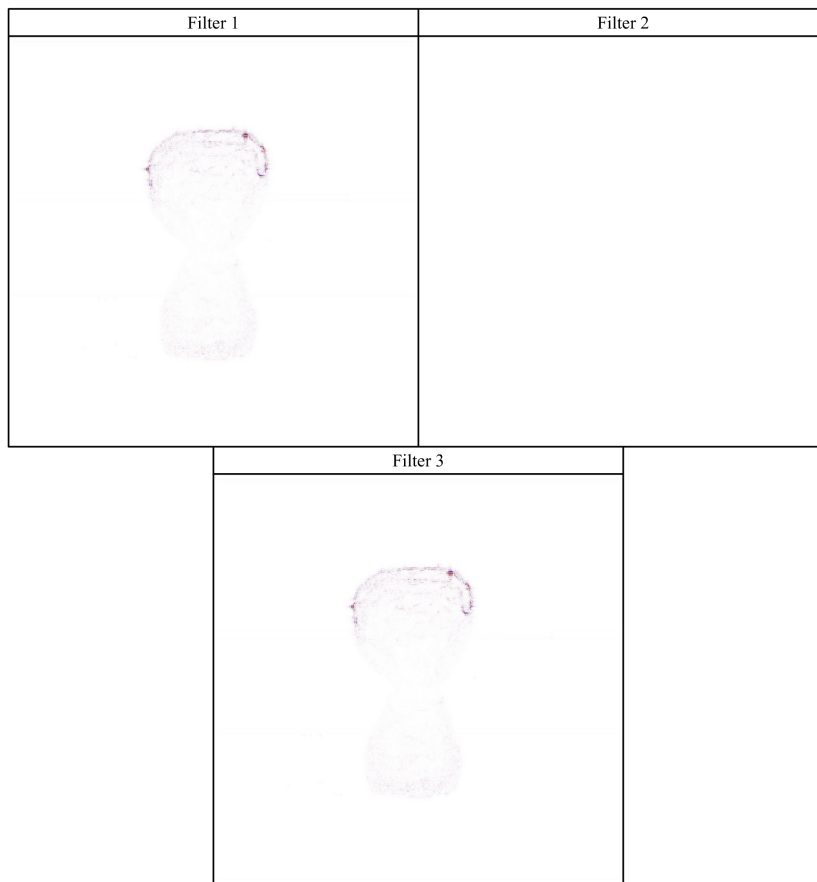


Fig. E.1. Images of normalized coefficients (normalisation at $[-100, 100]$, saturation at $[-40, 40]$), decomposition level 1, filters 1-3

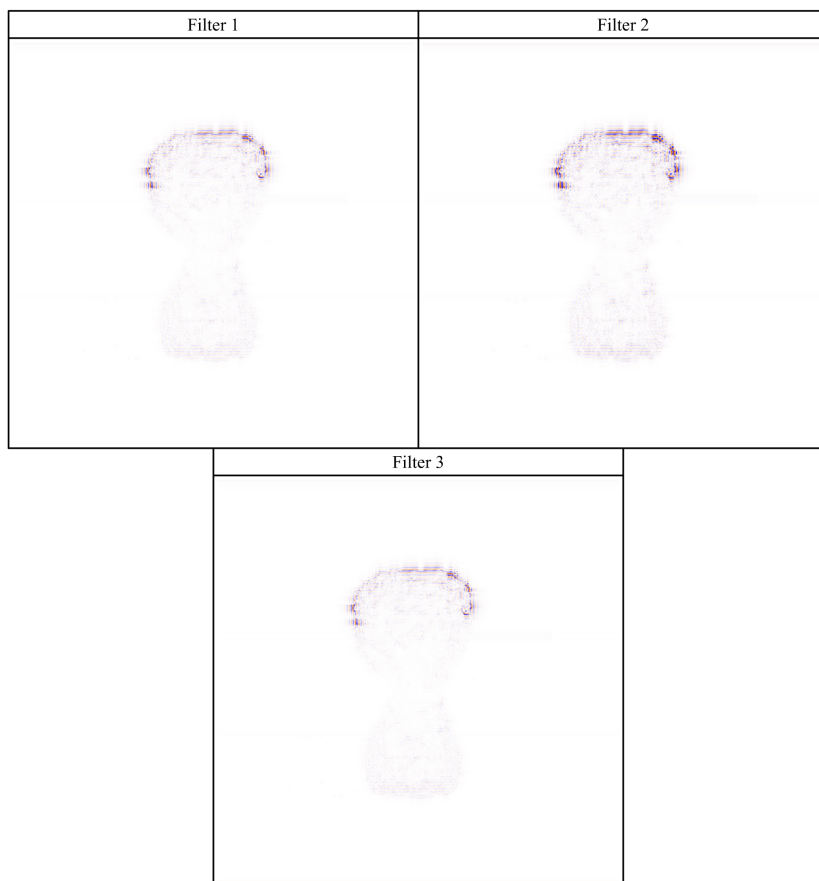


Fig. E.2. Images of normalized coefficients (normalisation at $[-100, 100]$, saturation at $[-40, 40]$), decomposition levels 1-2, filters 1-3

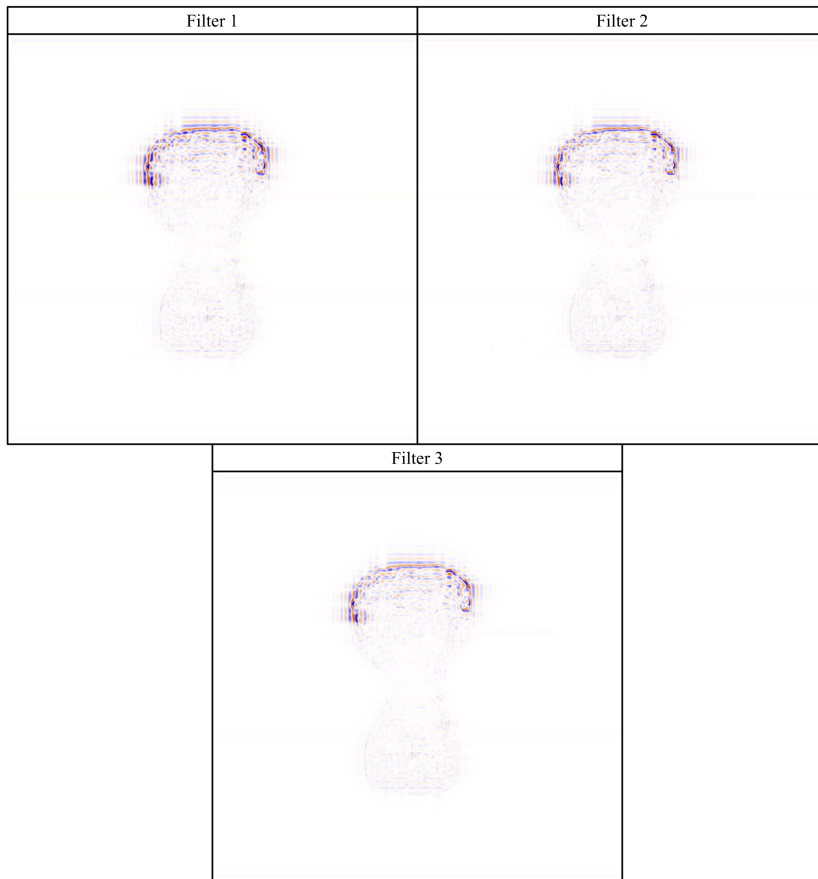


Fig. E.3. Images of normalized coefficients (normalisation at $[-100, 100]$, saturation at $[-40, 40]$), decomposition levels 1-3, filters 1-3

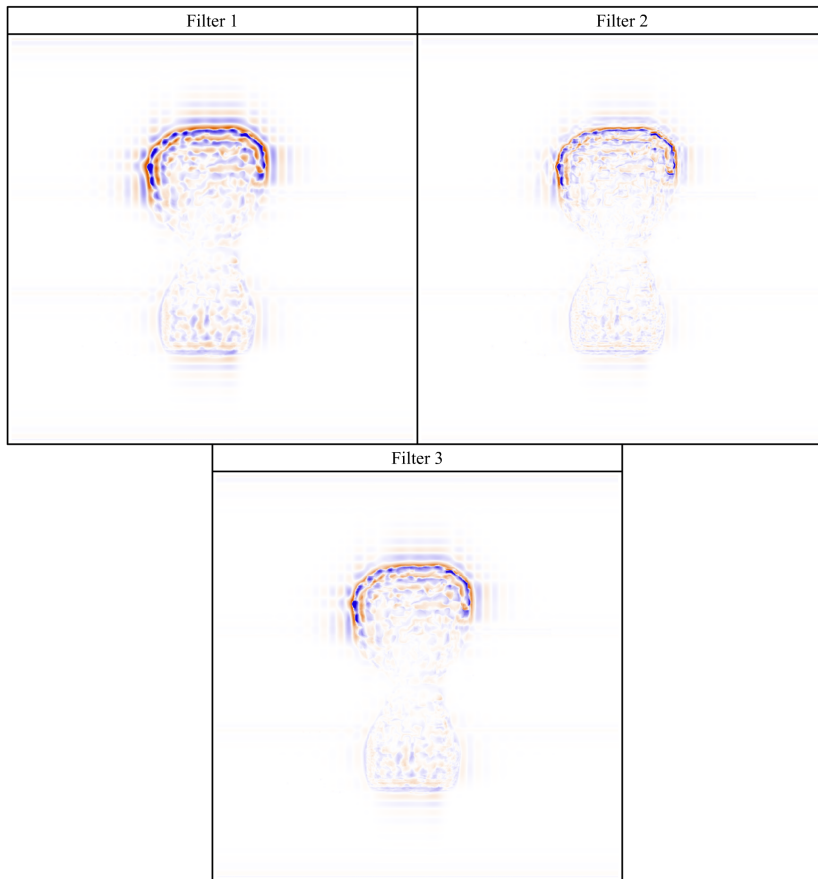


Fig. E.4. Images of normalized coefficients (normalisation at $[-100, 100]$, saturation at $[-40, 40]$), decomposition levels 1-4, filters 1-3

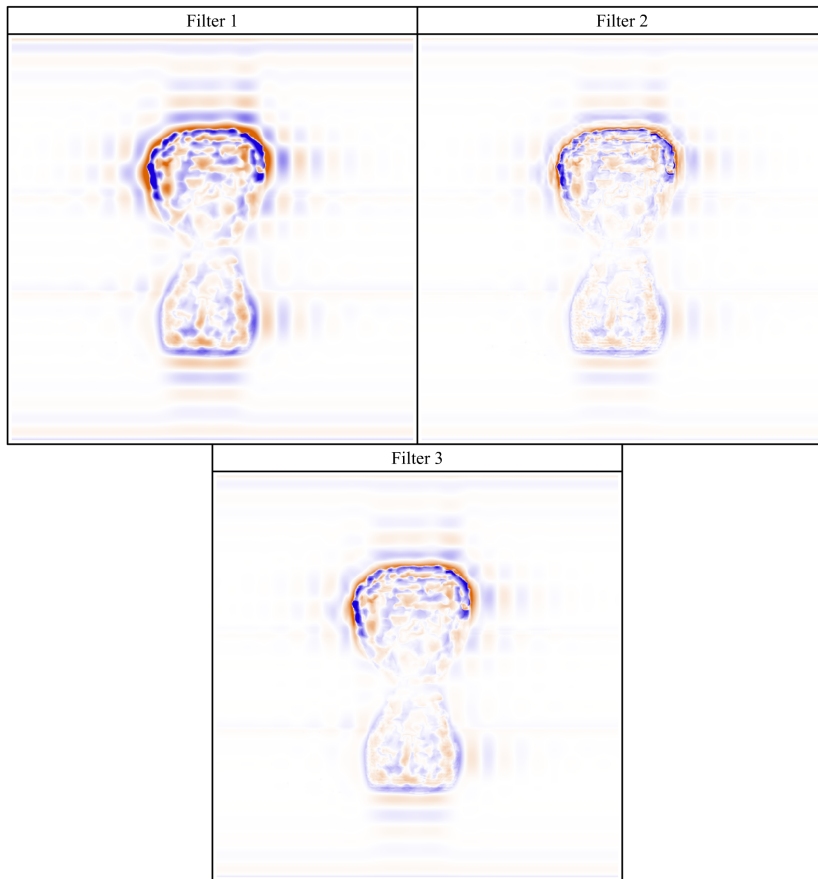


Fig. E.5. Images of normalized coefficients (normalisation at $[-100, 100]$, saturation at $[-40, 40]$), decomposition levels 1-5, filters 1-3

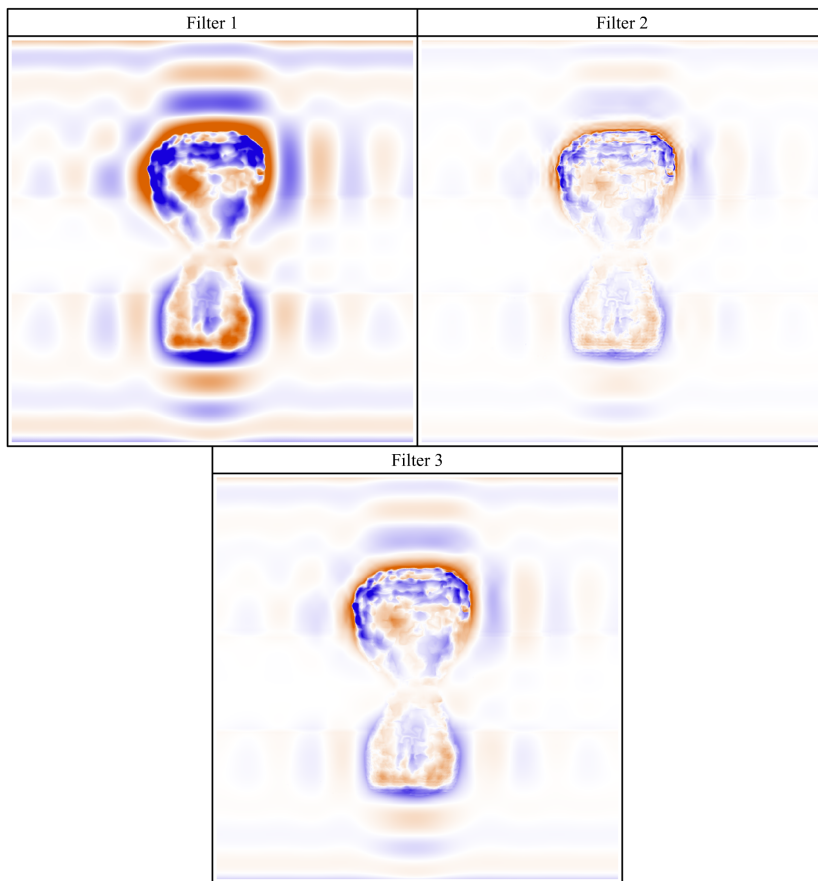


Fig. E.6. Images of normalized coefficients (normalisation at $[-100, 100]$, saturation at $[-40, 40]$), decomposition levels 1-6, filters 1-3

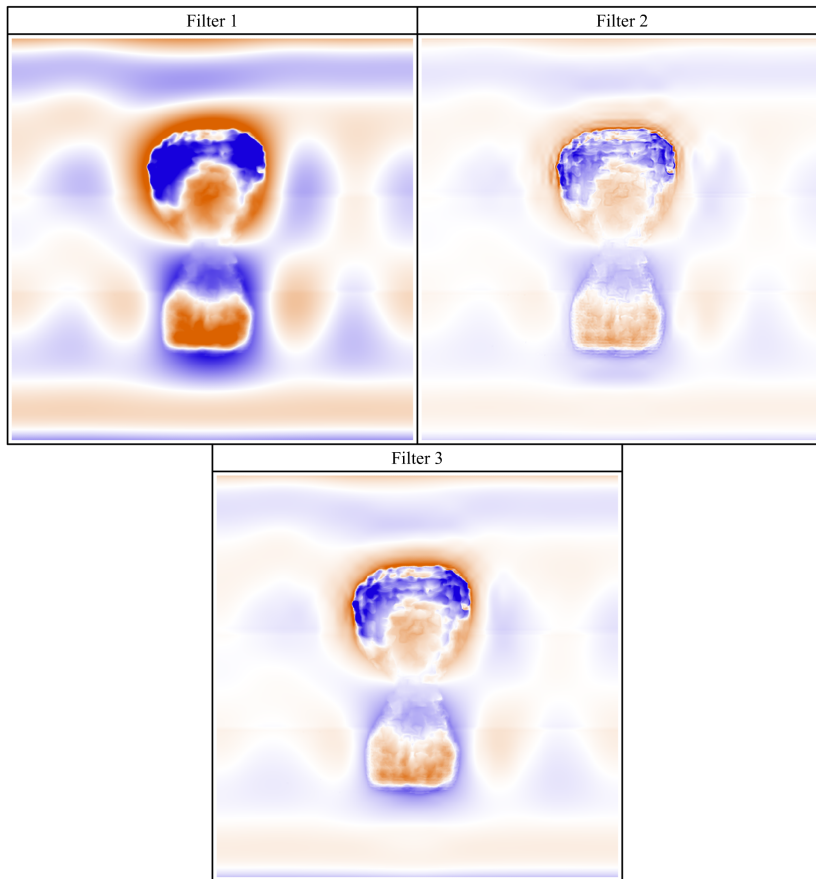


Fig. E.7. Images of normalized coefficients (normalisation at $[-100, 100]$, saturation at $[-40, 40]$), decomposition levels 1-7, filters 1-3

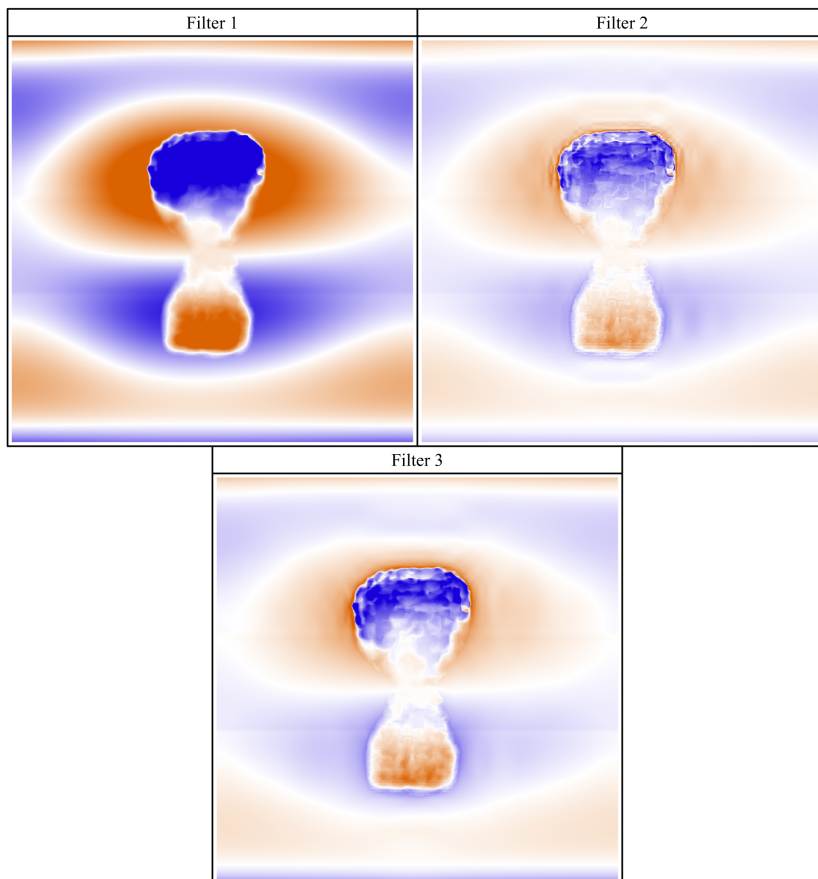


Fig. E.8. Images of normalized coefficients (normalisation at $[-100, 100]$, saturation at $[-40, 40]$), decomposition levels 1-8, filters 1-3

F. The Travers landslide description

The Travers landslide is a recent landslide which occurred on April 10th 2007. It is located¹ in Swiss Jura (figure F.1) in the village of Travers - Canton of Neuchâtel. The factors which induced the mass movement were intense rainfall (393 *mm* rain) and active thaw the month before.

F.1 Data

This section describes the different data, that is the acquired high resolution DEM and the geological map established by Gocht (1961).

F.1.1 DEM

The DEM used for the case study was acquired nine days after the landslide occurred (19th April 2007) using the scan2map² airborne LiDAR points. The raw point density ($\sim 4 \text{ pt}/\text{m}^2$) enabled the interpolation of a 1 *m* DEM using a TIN. The resulting DEM is a matrix of 1280×768 pixels with a 1 *m* resolution (figure F.2). Local authorities built a new road in order to be able to access the uphill farms and utilities, which causes the discontinuity in the landslide zone just between the transition zone and the scarp zone. Besides, the scarp zone was also remodelled by the authorities in order to facilitate the surface water drainage coming from the three resurgences in the scarp zone.

Using the acquired DEM, contour lines (interval 5 *m*) were computed to illustrate the gentle slope on which the landslide is located. The only steep zone (figure F.4) on the DEM is located in the south-east part of the DEM, which represent the uphill zone of the Jura range.

¹ In the Swiss projection (CH-1903), the centre is: 542'270.00, 198'400.00

² scan2map is a research project of the Geodetic Engineering Laboratory at the Ecole Polytechnique Fédérale de Lausanne (TOPO-EPFL, see <http://topo.epfl.ch/laserscanning/>, accessed September 16th 2009)

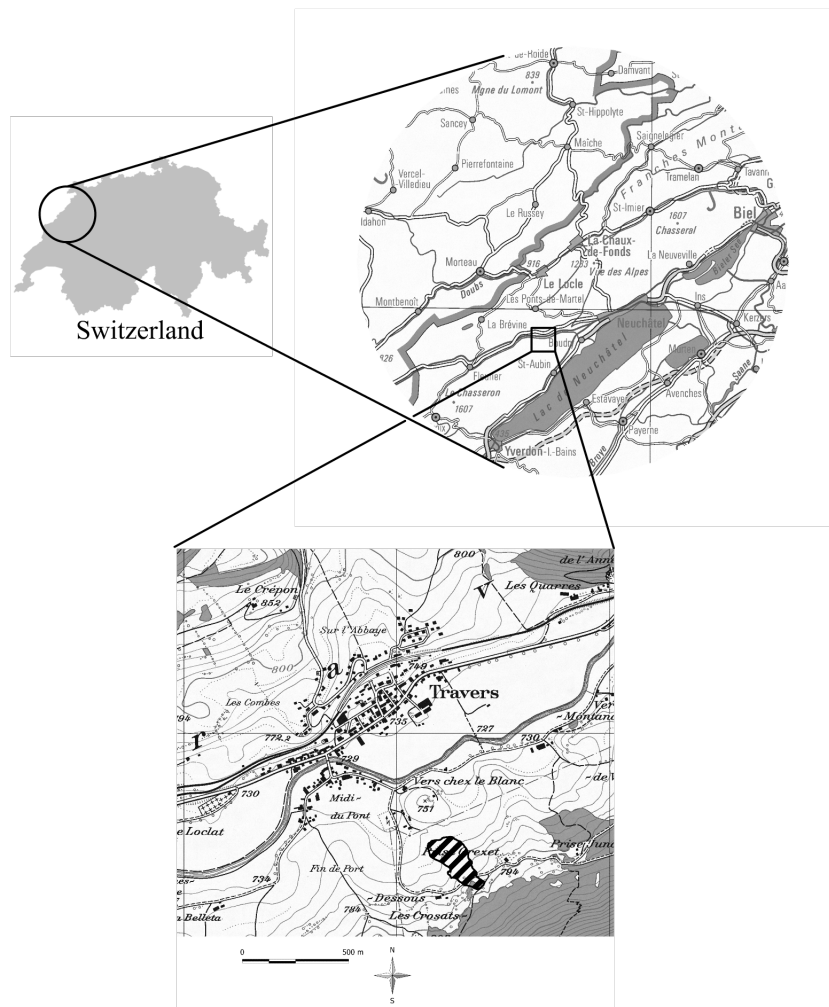


Fig. F.1. Localisation of the Travers landslide. The landslide is identified by the black and white stripped zone. CN1000,CN25©swisstopo

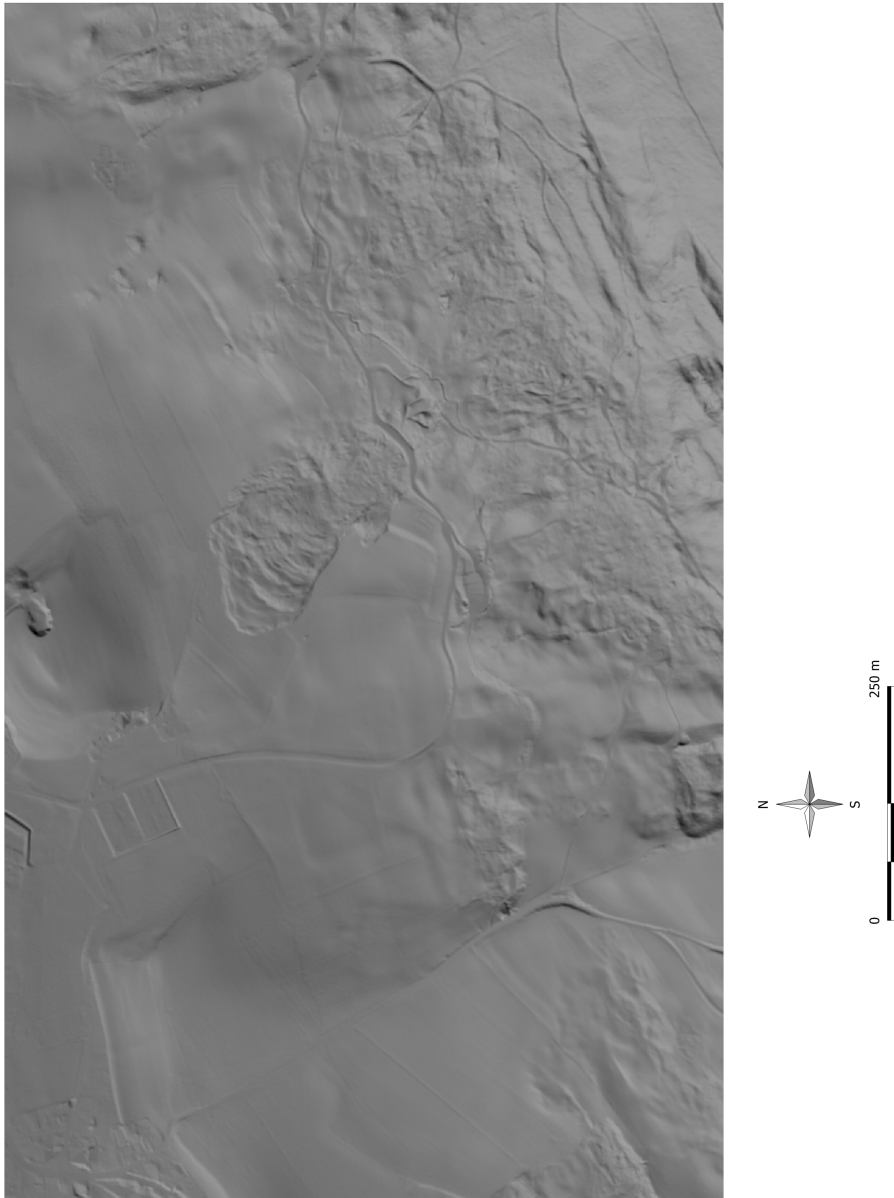


Fig. F.2. Shaded DEM of Travers - Canton of Neuchâtel, DEM©SITN

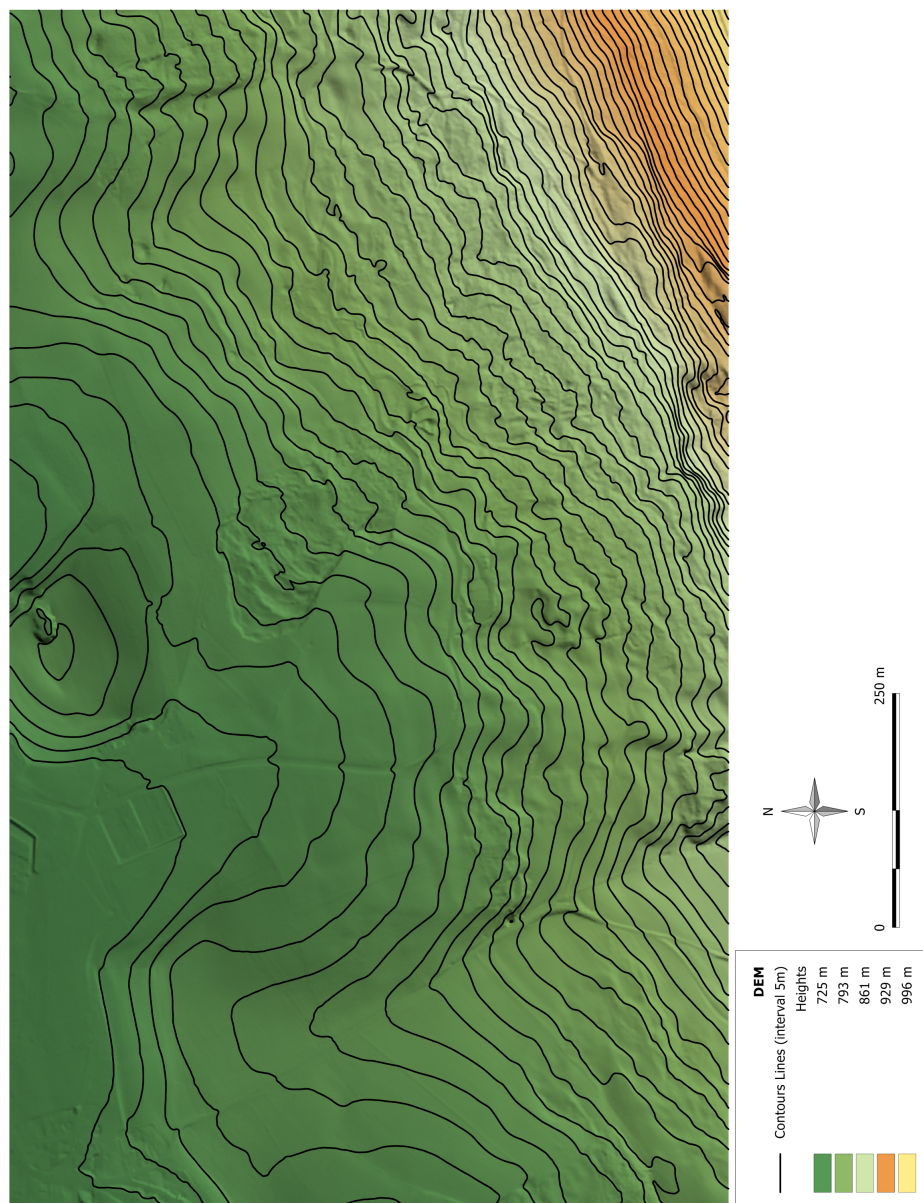


Fig. F.3. Contour lines (interval 5 m), computed using the DEM, overlaid to the shaded and height coloured DEM of Travers - Canton of Neuchâtel, DEM©SITN

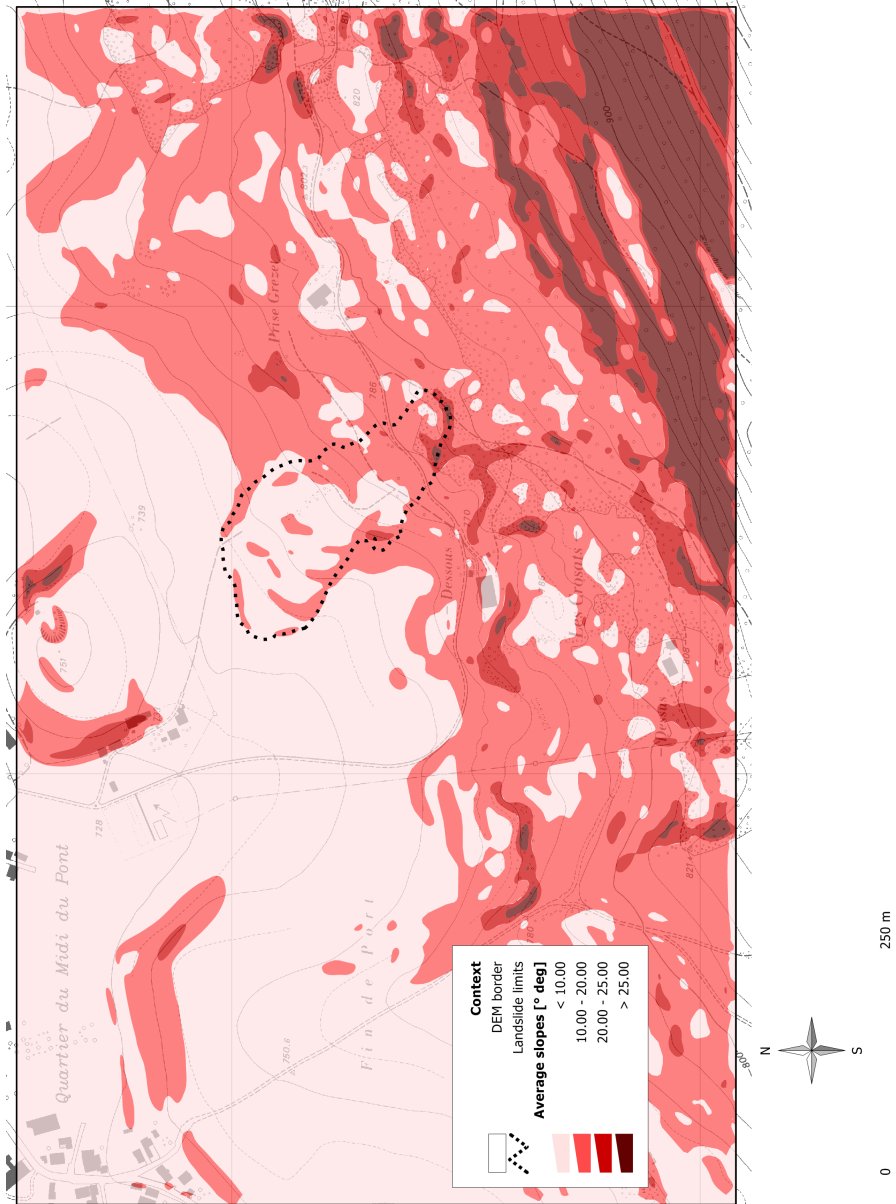


Fig. F.4. Slope map, derived and segmented from the DEM of Travers, plan d'ensemble 1 : 10 000©SITN

F.1.2 Geological Map

The surface of the DEM is composed of quaternary moraine and formations from the Cretaceous (Ablian, Hauterivian, Valangian and Purbeckian) and Jurassic (Purbeckian and Portlandian) periods. The molasse is a sedimentary clastic formation. Between the moraine and the Cretaceous-Jurassic formations, there is a fallen rock zone which is a matrix of the uphill formations. These uphill formations are organised in strata revealing some terrace-like formations.

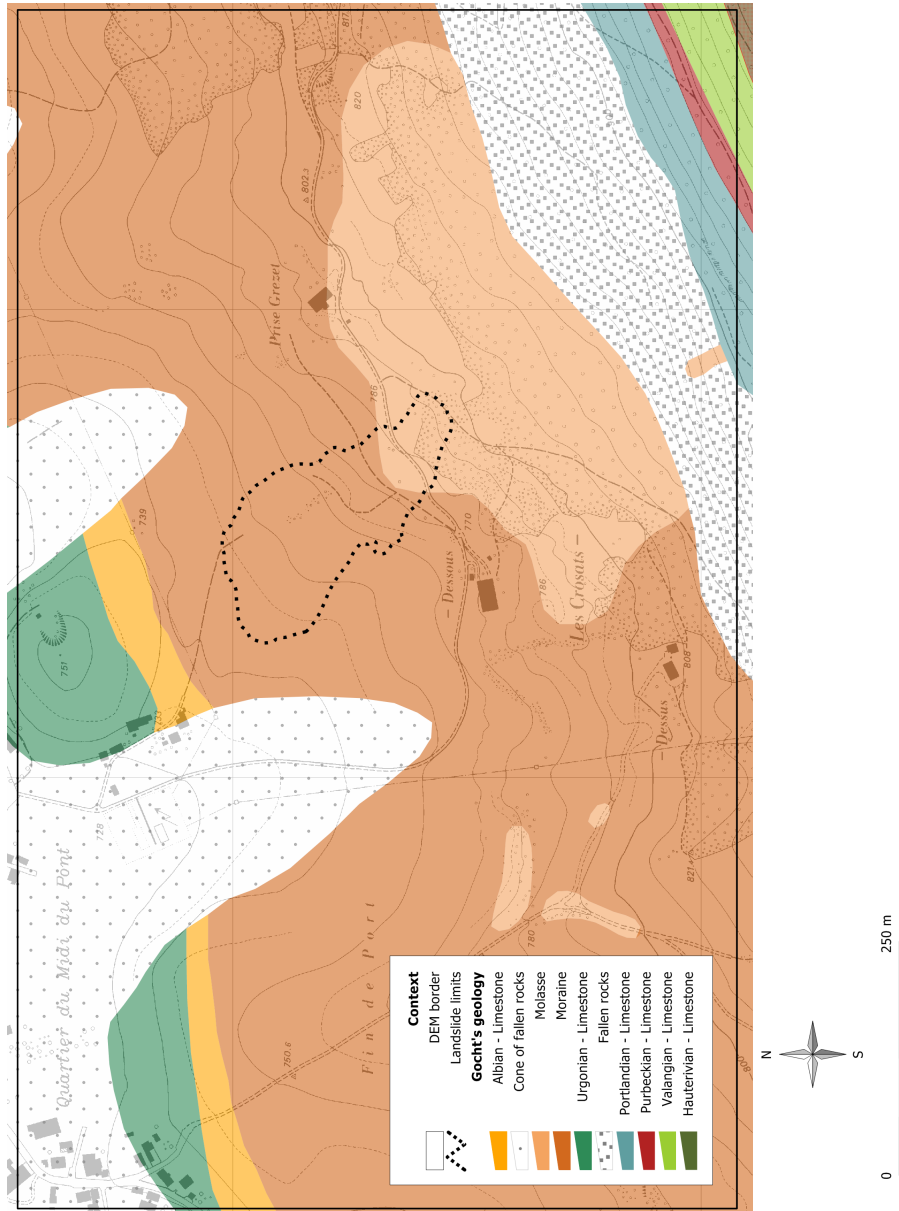


Fig. F.5. Geological map (Gocht, 1961), plan d'ensemble 1 : 10 000 ©SITN

F.2 Description of the Travers landslide

The phenomenon analysis of the landslide shows that this one is of type earth flow - landslide (Krähenbühl, 2007). In the upper part of the landslide (south-east, figure F.6), it consists of a major scarp zone made partly of morainic deposits and partly of silty sand interpreted as weathered products from the molassic bedrock. This bedrock is composed of tertiary molassic deposits made of sandstones and marl. The material slid along a surface of rupture parallel to the slope (translational landslide at the molasses' roof level) according to two different modes in the phenomenological point of view. The displaced material, rich in sandy muddy saturated material, was liquefied and produced a flow, which now occupies the upper central and oriental part of the accumulation zone. In the continuity of this first movement mode, the morainic displaced material, and its pedological coverage, slid in a more ductile way and depleted on the accumulation zone by forming folds which clearly can be distinguished on the north-west part of the accumulation zone (see figure F.6). The spatial distribution of the main landslide folds is illustrated in the phenomena map. We can see that four groundwater resurgences appeared subsequently to the landslide; three in the scarp zone and one in the middle of the accumulation zone. The displaced and bedrock material were saturated as the landslide happened. It induced the evacuation of groundwater which was under pressure. As a consequence, several wetlands, as well as ponds, appeared in the accumulation zone. The three scarp zone resurgences are drained (on surface) to a spillway. This was done in order to reconstruct a new road, which was stabilized with tree trunk stilts.

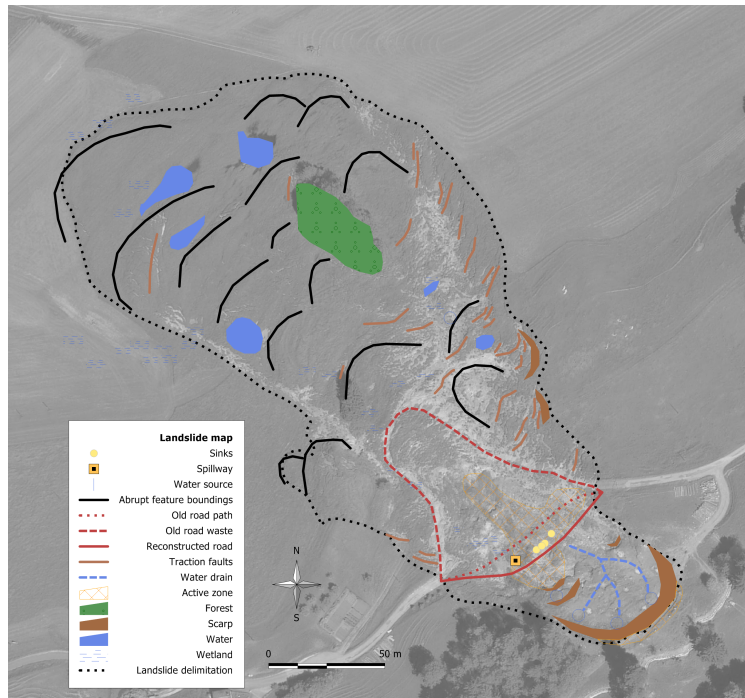


Fig. F.6. Phenomena map, July 2007, (Krähenbühl, 2007), aerial photography ©SITN

Krähenbühl (2007) undertook a study to determine what the geological issues that induced the landslide were. In situ observation and analysis were made in order to establish a phenomenological mapping (figure F.6). As conclusion it was established that the phenomenon is a combination of thaw, heavy rain (393mm in three weeks) and infiltration of water. The uphill limestone strongly influences the water infiltration due to the high porosity of the composing materials. This water spreads rapidly inside the altered masses of sandstone and high volumes of subsurface water are under pressure at the interface between sandstone and moraine. The clay composing this latter prevents the discharge of the confined groundwater, but at one point, the pressure liquefies the sandy material constituting the moraine due to the inherent increased cohesion. The moraine clay begins to slide on the sand (see figure F.7). From the scarp zone, the flow was constituted of laminated clay material. It flowed down to the north side of the landslide zone, leading to the deposit of these materials and packing down the morainic coverage of the north-west landslide area. This settlement caused the deterioration of materials (clay) and multiple water resurgences appeared in the sliding area.

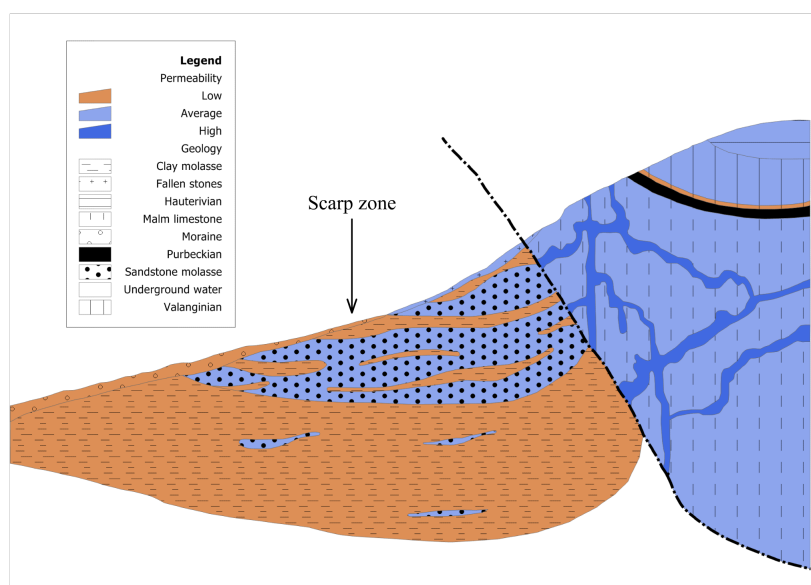


Fig. F.7. Geological cut of the Jura region (Krähenbühl, 2007)

The spread of water in the landslide area is difficult to understand due to several factors:

1. Surface water flowing from the scarp zone is drained towards the new road. The resurgent water in the transition and accumulation zones comes therefore from subsurface flows.
2. The lamination and settlement significantly altered the material in a heterogeneous mass. The material identification is complicated and uncertain.

The landslide stabilization occurs primarily through the drainage of the water that induces residual sliding of materials. However, the understanding

of the hydrological processes is difficult due to various phenomena composing the landslide.

G. Profiles on generalised DEM of Travers

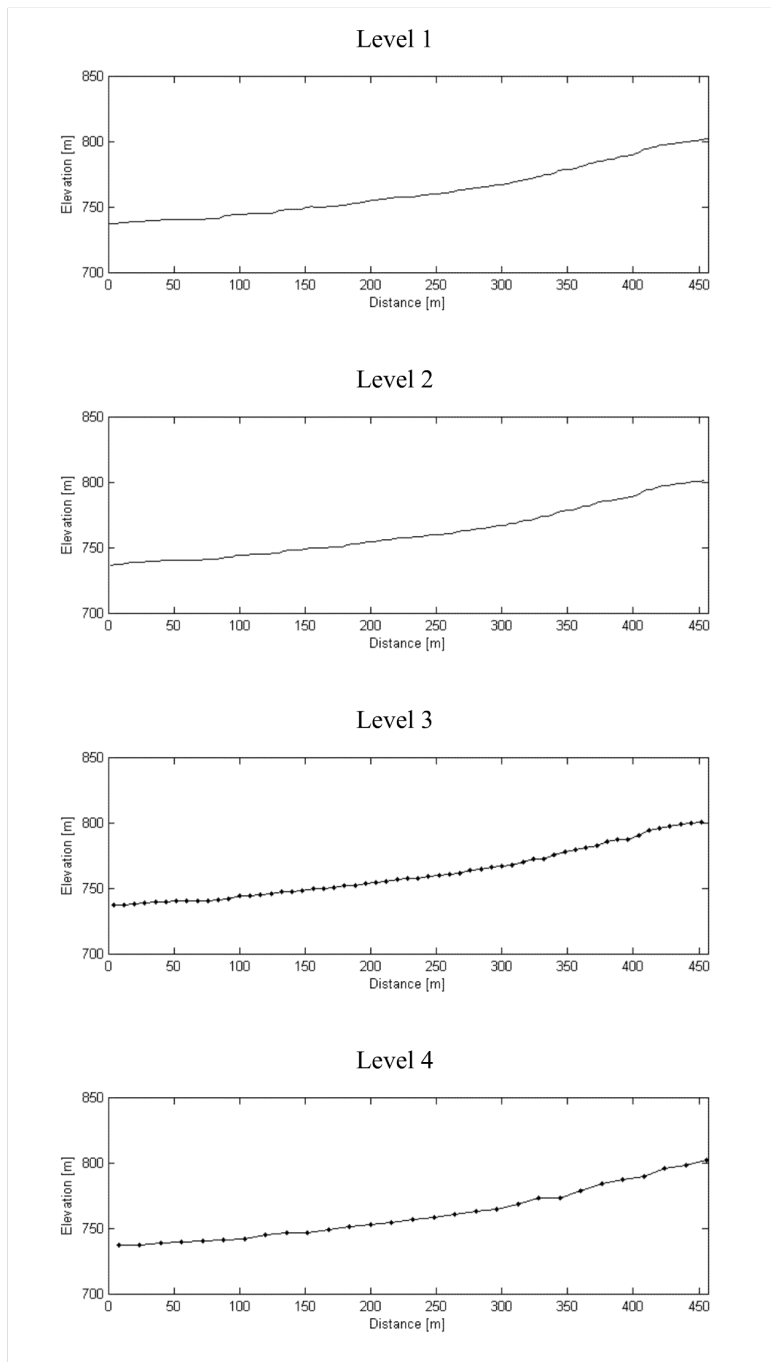


Fig. G.1. Profile 1, decomposition levels 1 to 4, (Left side is the north-western end of the profile and right side is the south-eastern end of the profile.)

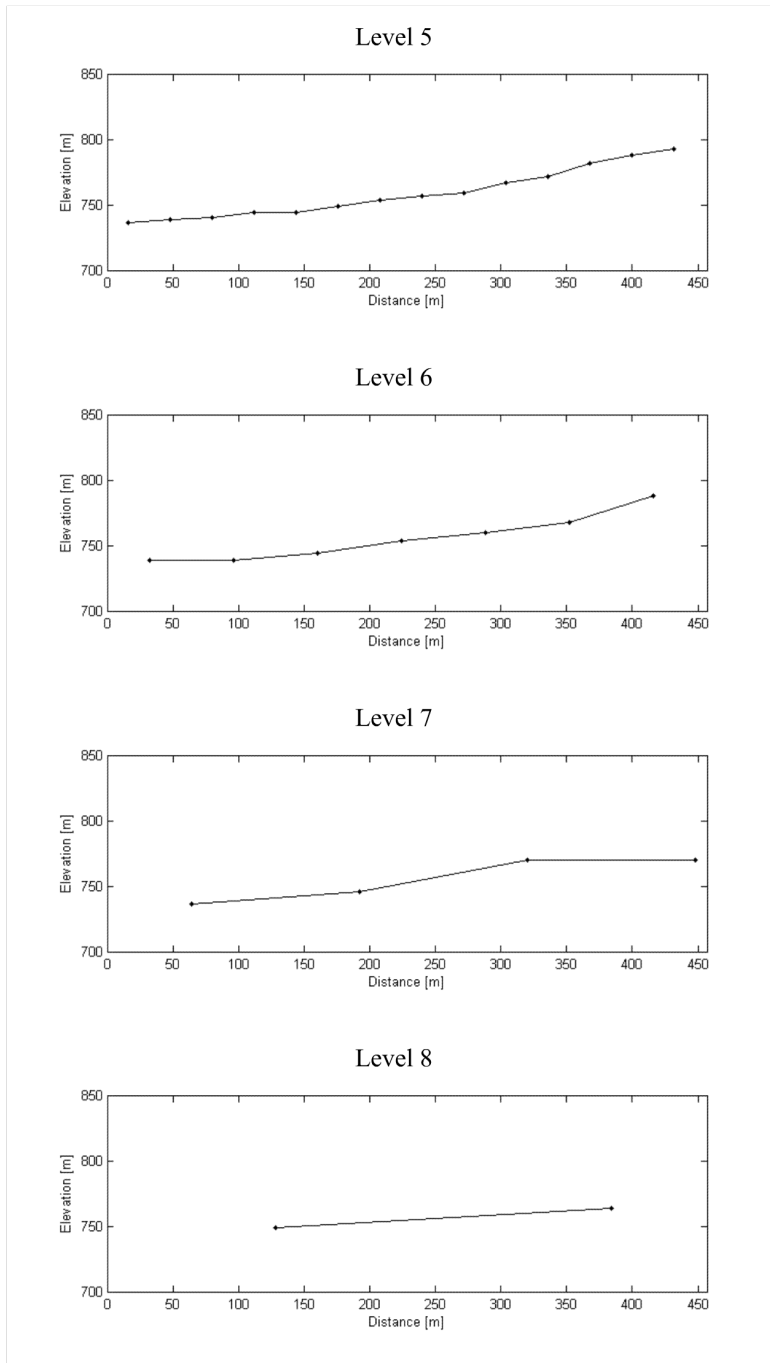


Fig. G.2. Profile 1, decomposition levels 5 to 8, (Left side is the north-western end of the profile and right side is the south-eastern end of the profile.)

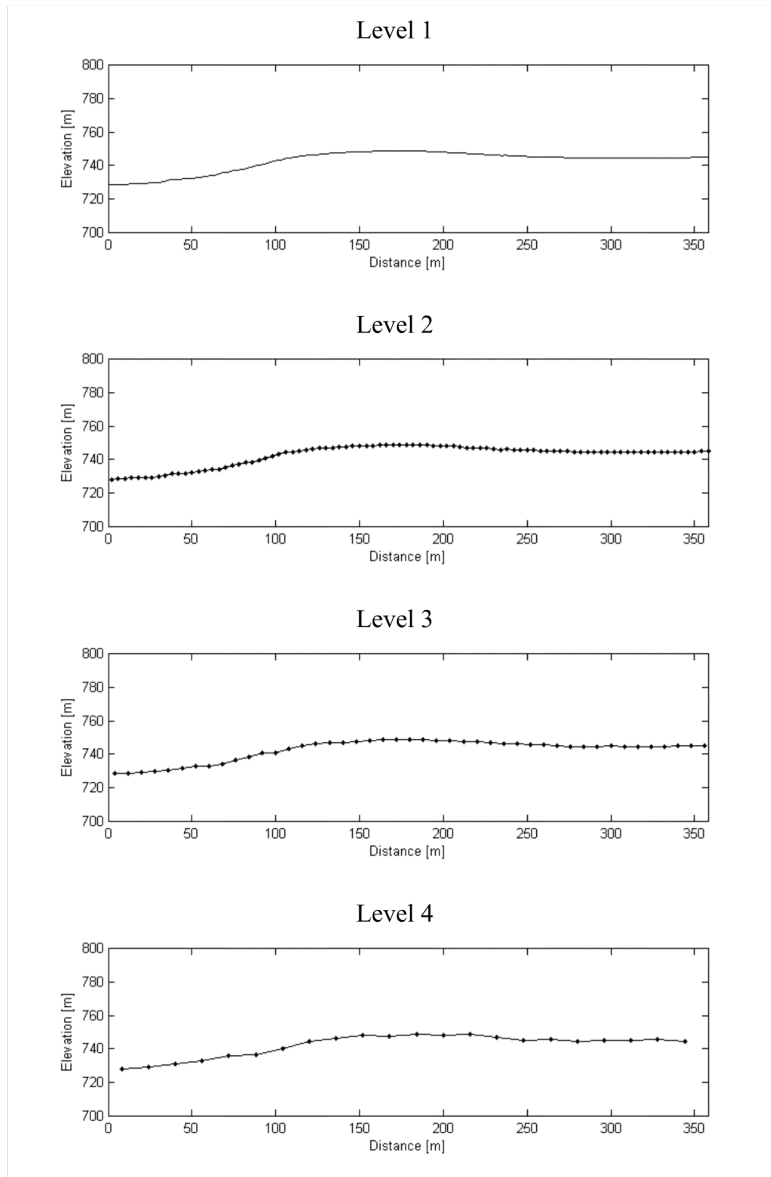


Fig. G.3. Profile 2, decomposition levels 1 to 4, (Left side is the north-western end of the profile and right side is the south-eastern end of the profile.)

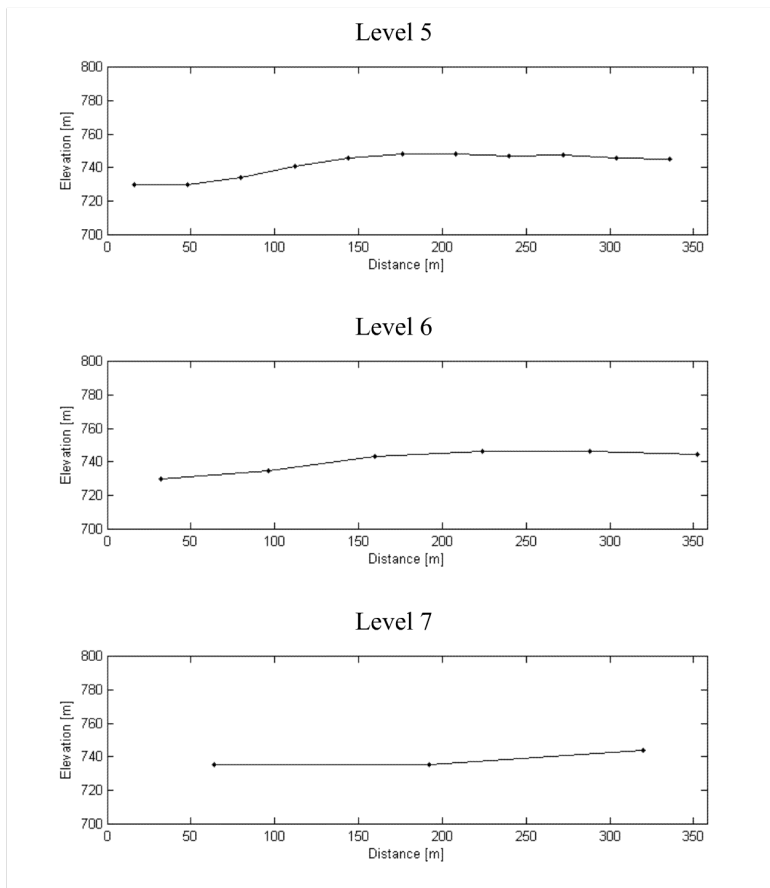


Fig. G.4. Profile 2, decomposition levels 5 to 8, (Left side is the north-western end of the profile and right side is the south-eastern end of the profile.)

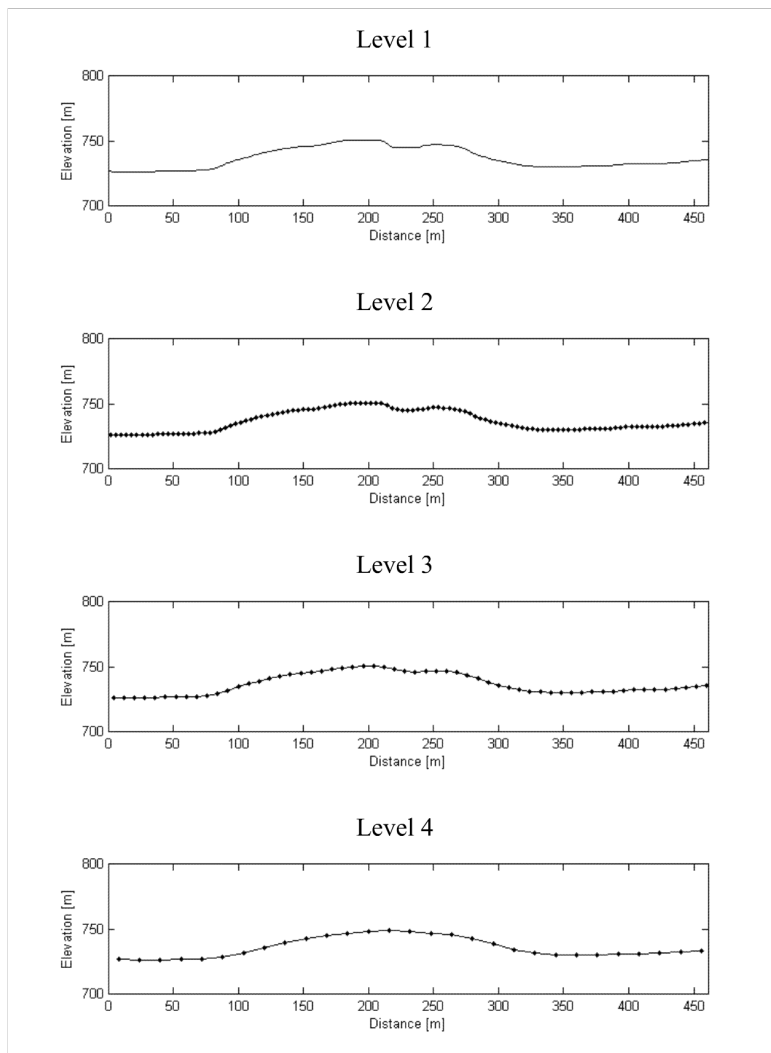


Fig. G.5. Profile 3, decomposition levels 1 to 4, (Left side is the western end of the profile and right side is the eastern end of the profile.)

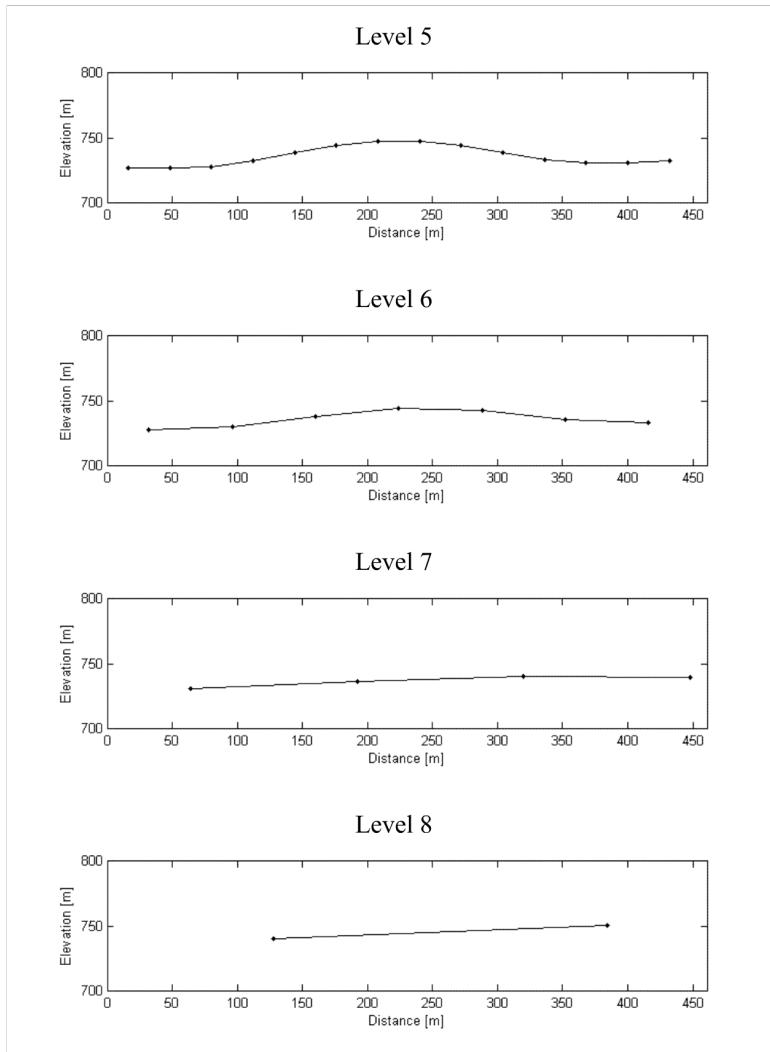


Fig. G.6. Profile 3, decomposition levels 5 to 8, (Left side is the western end of the profile and right side is the eastern end of the profile.)

H. Detail coefficients on the Travers DEM

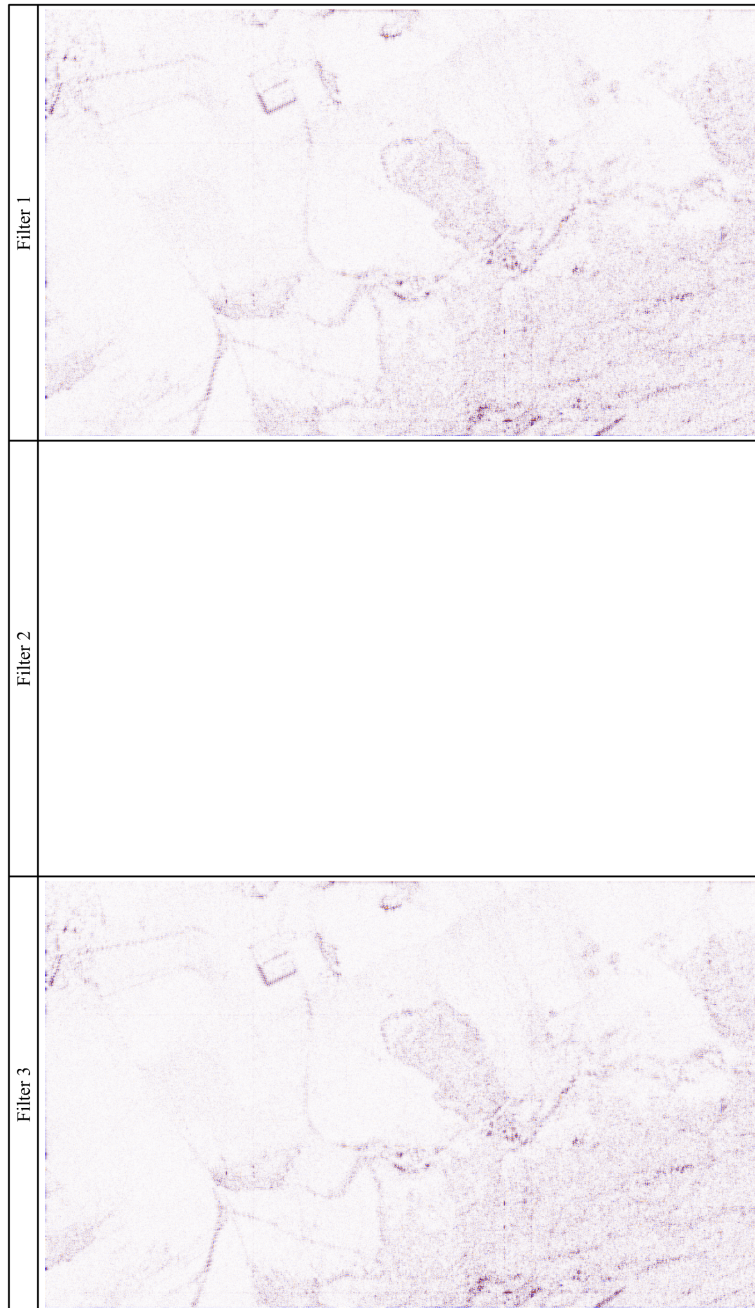


Fig. H.1. Images of normalized coefficients (normalisation at $[-100, 100]$, saturation at $[-20, 20]$), decomposition level 1, filters 1-3

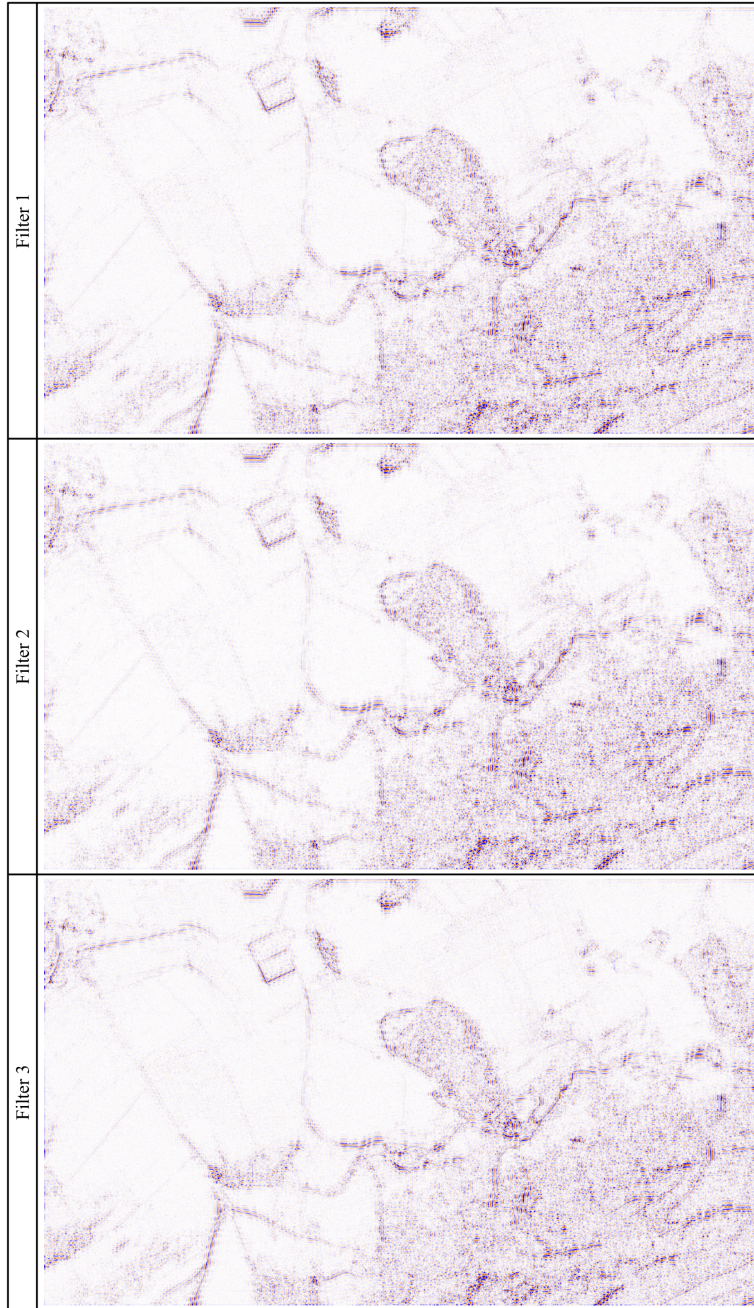


Fig. H.2. Images of normalized coefficients (normalisation at $[-100, 100]$, saturation at $[-20, 20]$), decomposition levels 1-2, filters 1-3

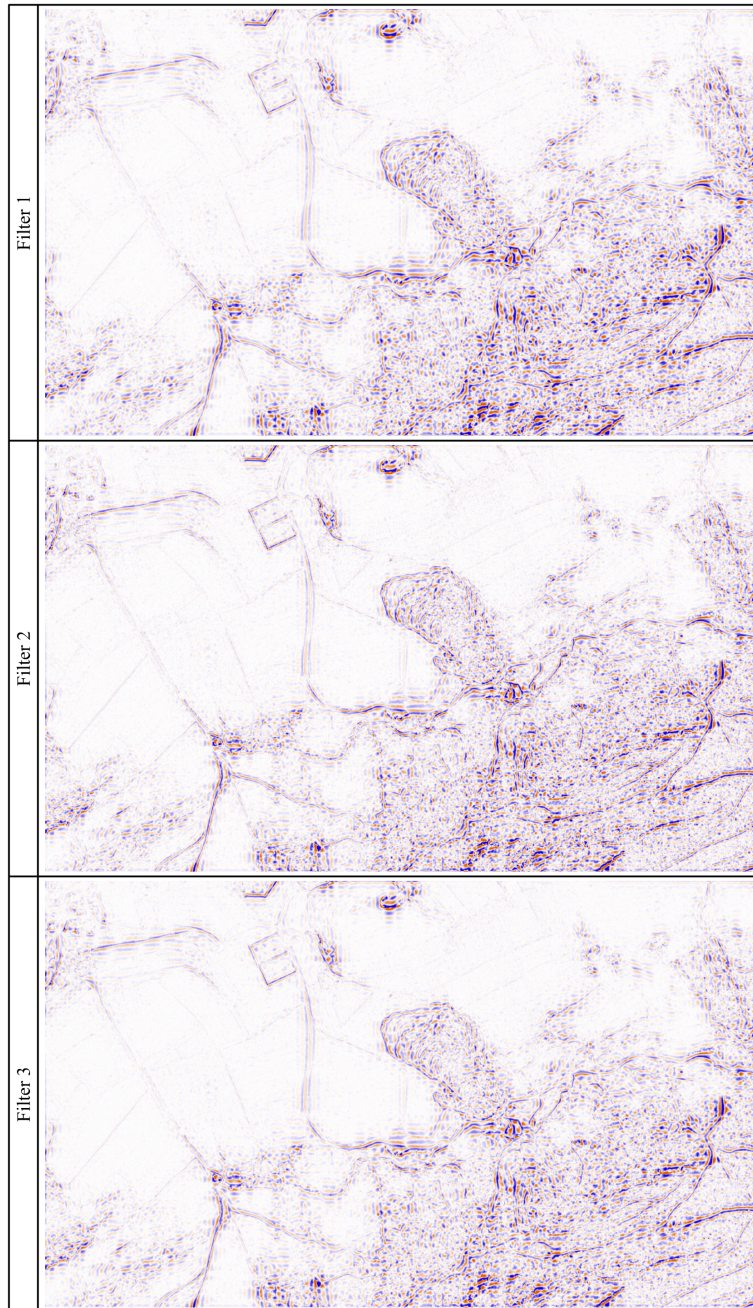


Fig. H.3. Images of normalized coefficients (normalisation at $[-100, 100]$, saturation at $[-20, 20]$), decomposition levels 1-3, filters 1-3

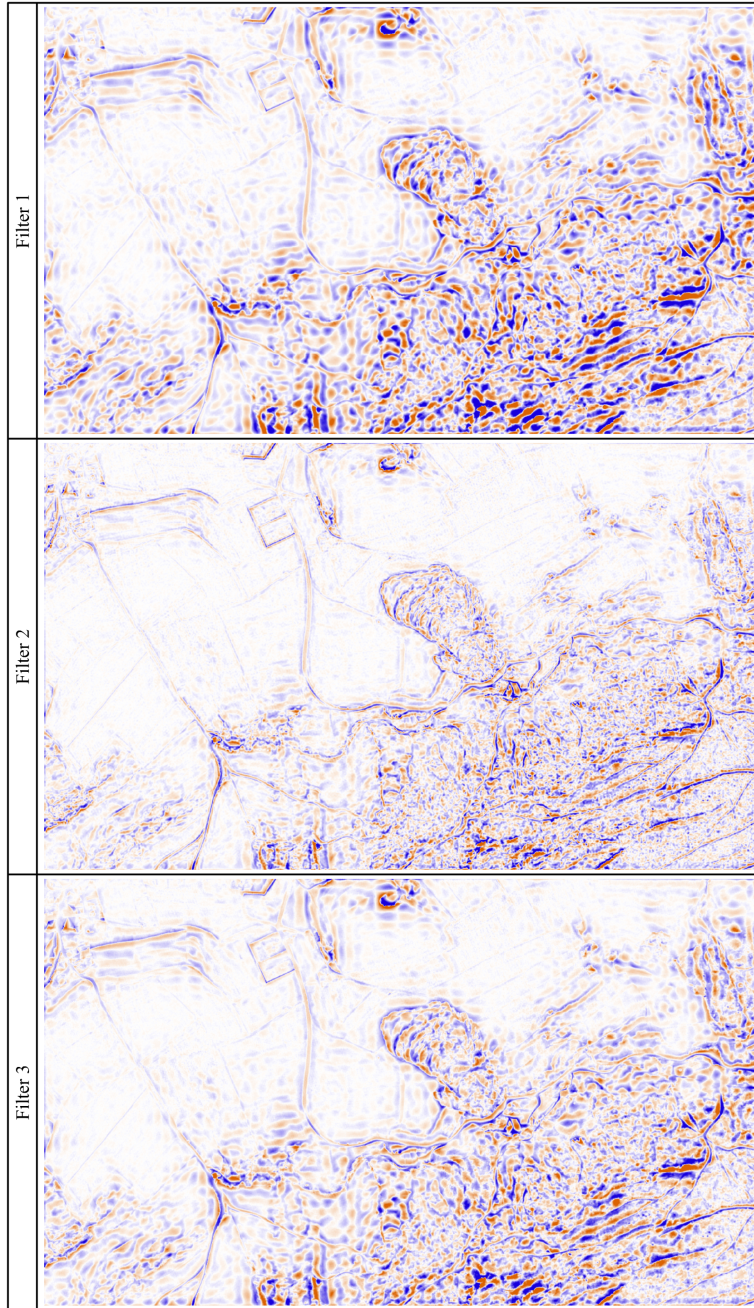


Fig. H.4. Images of normalized coefficients (normalisation at $[-100, 100]$, saturation at $[-20, 20]$), decomposition levels 1-4, filters 1-3

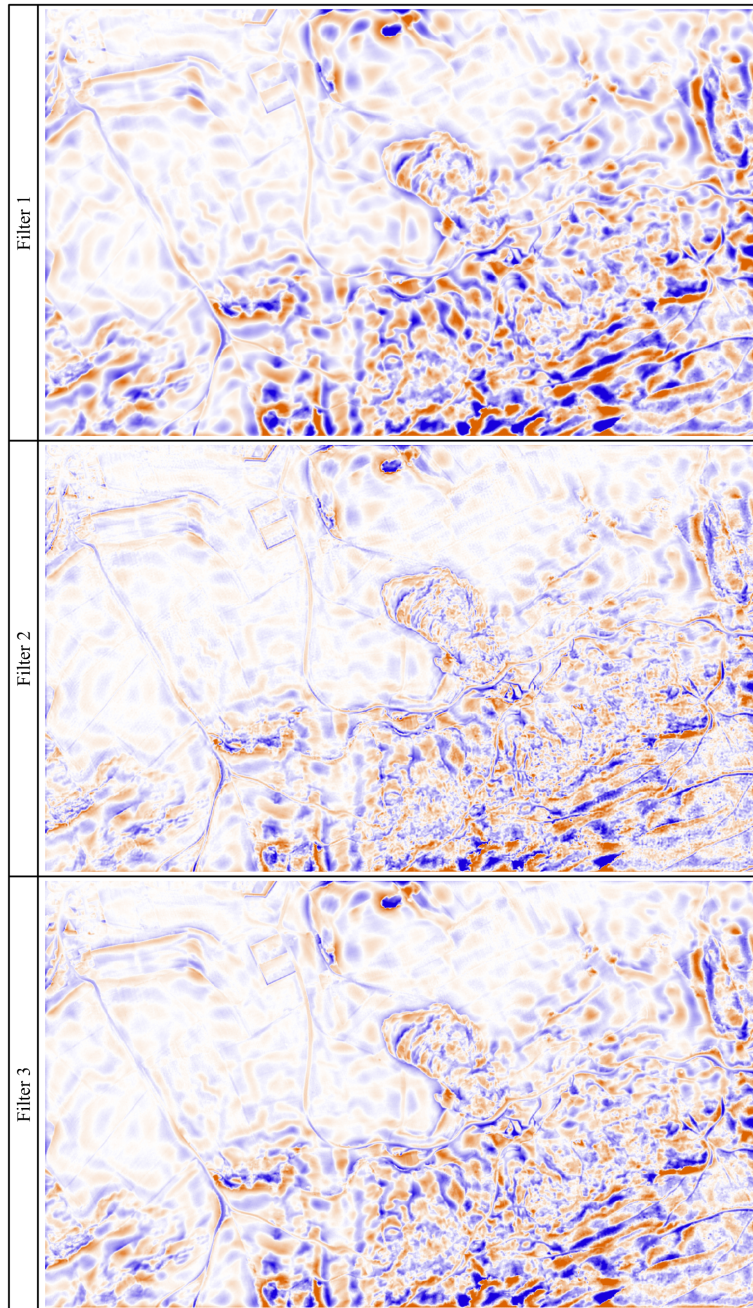


Fig. H.5. Images of normalized coefficients (normalisation at $[-100, 100]$, saturation at $[-20, 20]$), decomposition levels 1-5, filters 1-3

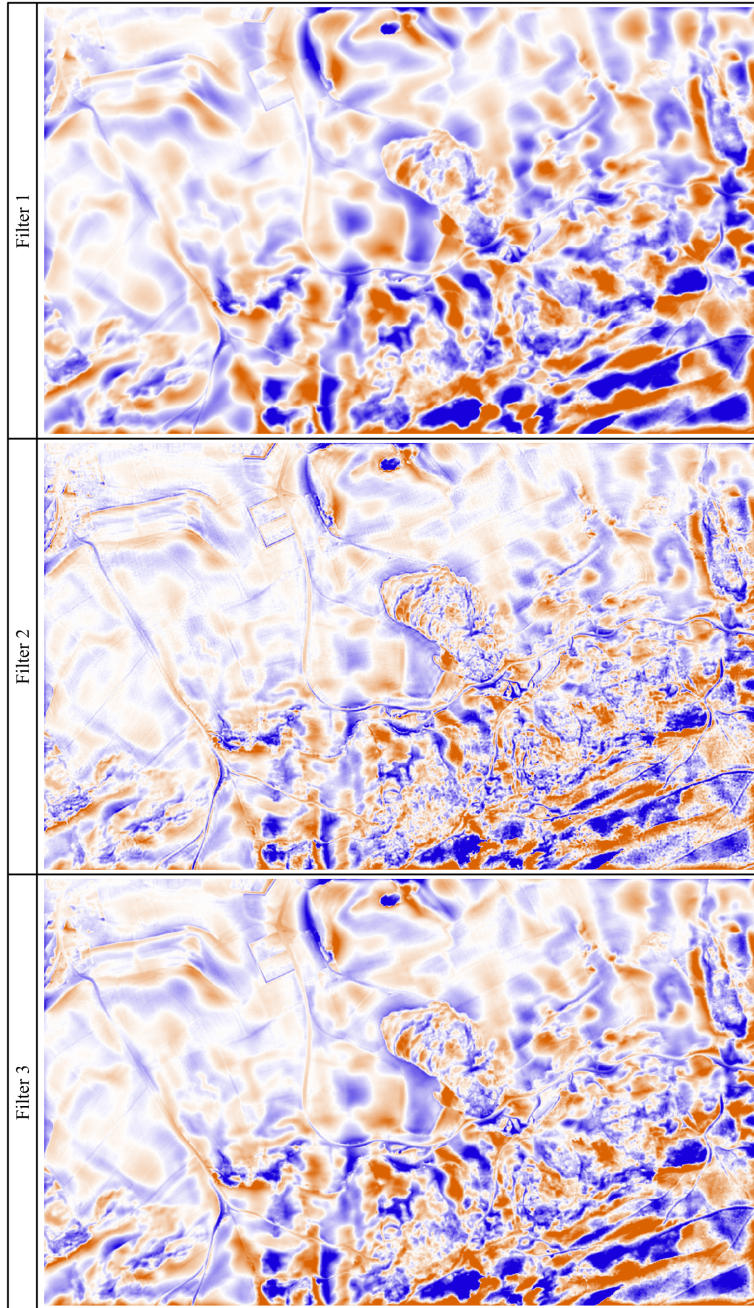


Fig. H.6. Images of normalized coefficients (normalisation at $[-100, 100]$, saturation at $[-20, 20]$), decomposition levels 1-6, filters 1-3

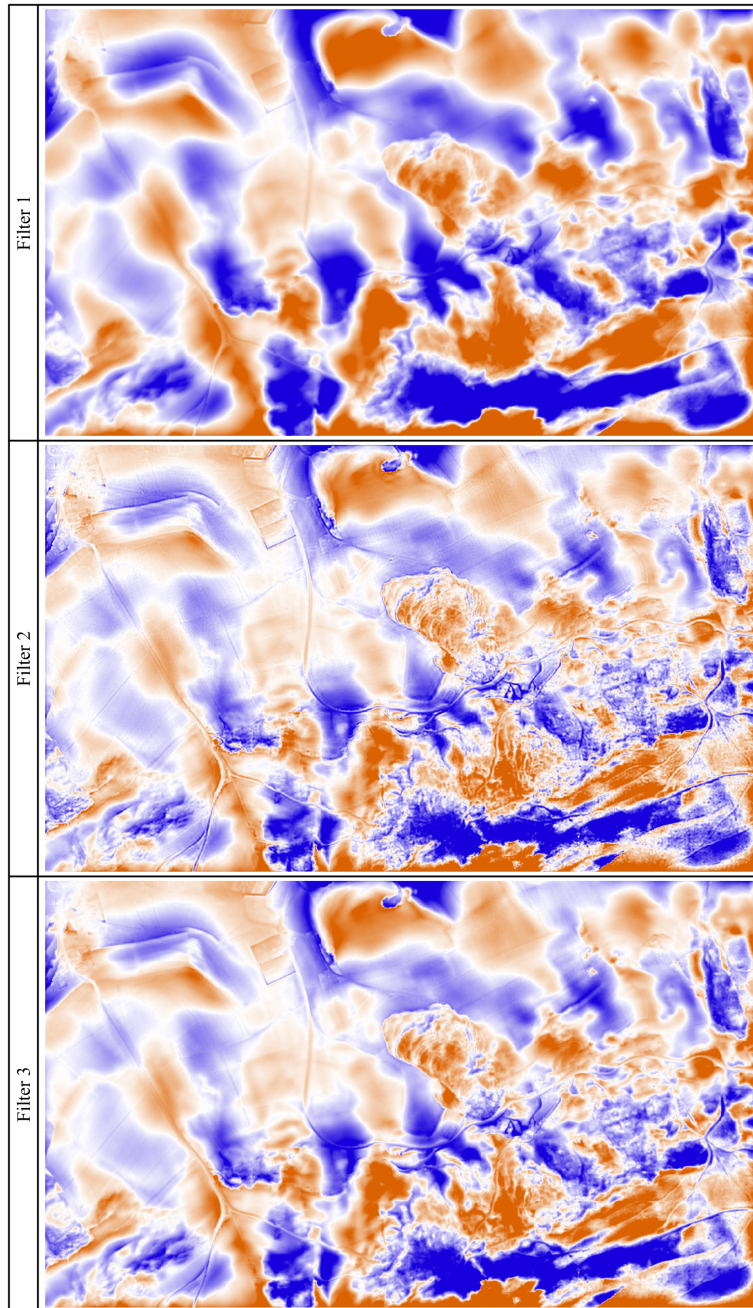


Fig. H.7. Images of normalized coefficients (normalisation at $[-100, 100]$, saturation at $[-20, 20]$), decomposition levels 1-7, filters 1-3

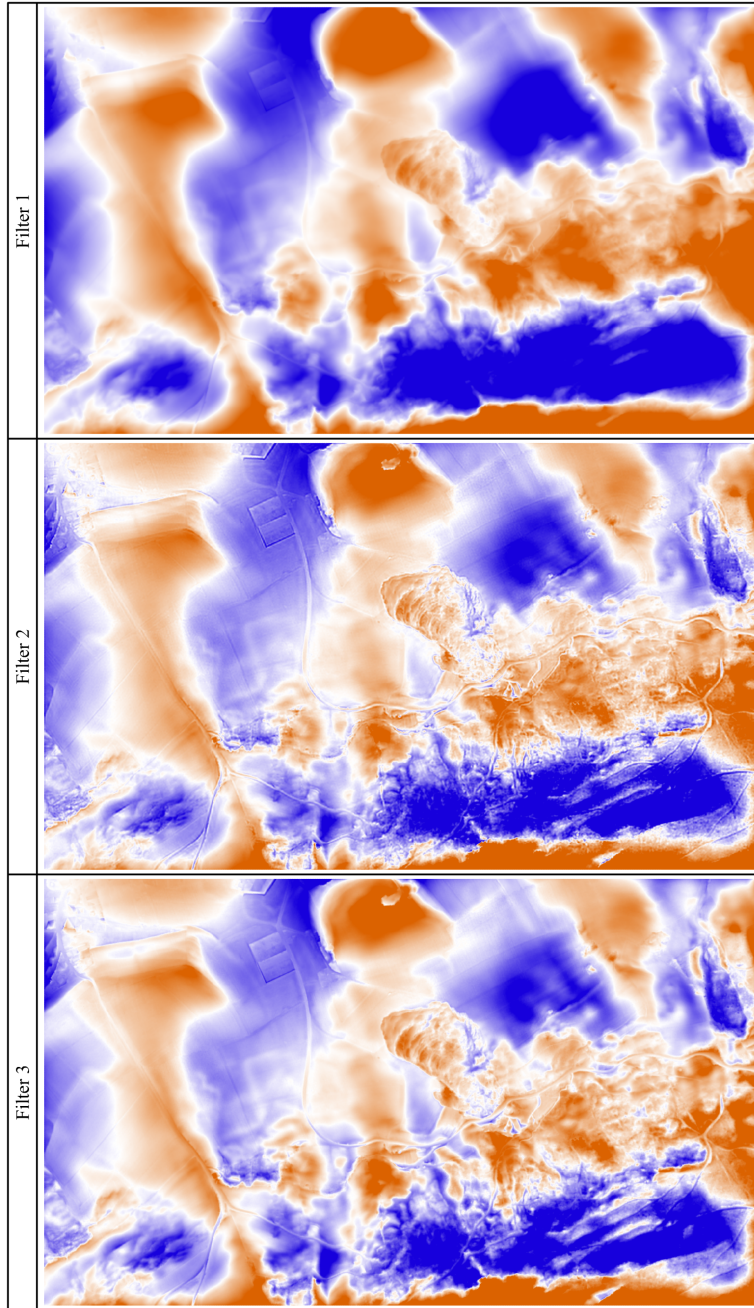


Fig. H.8. Images of normalized coefficients (normalisation at $[-100, 100]$, saturation at $[-20, 20]$), decomposition levels 1-8, filters 1-3

I. Fold profiles

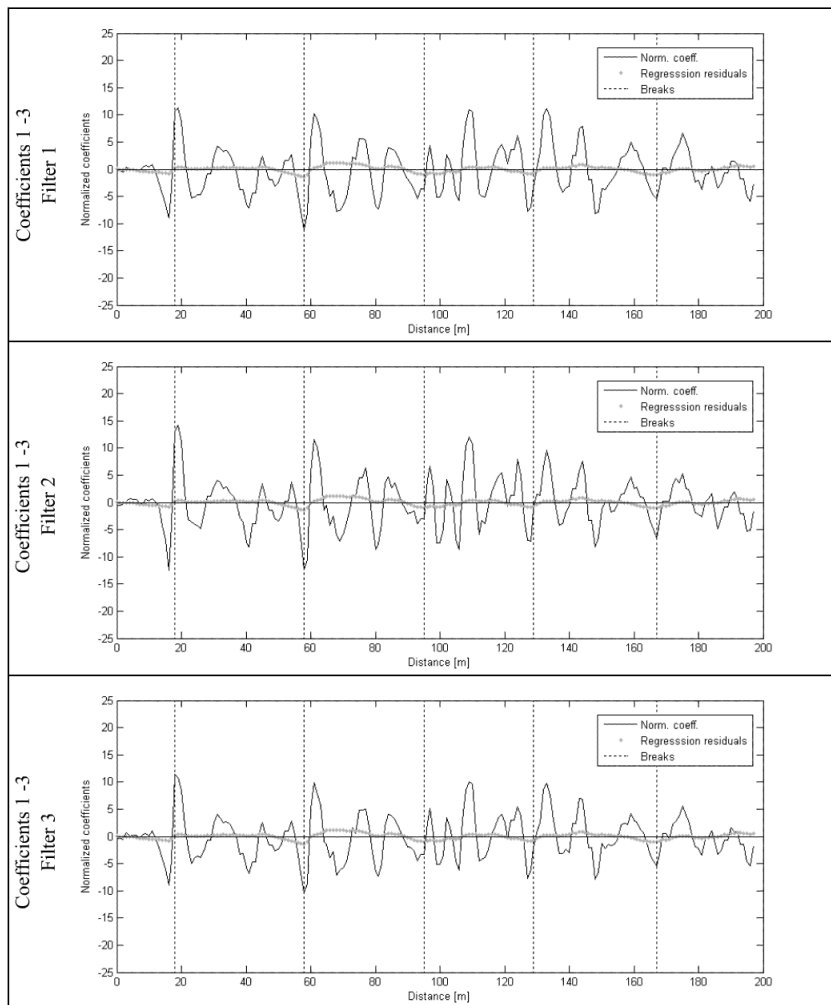


Fig. I.1. Values of normalized coefficients, decomposition levels 1-3, filters 1-3

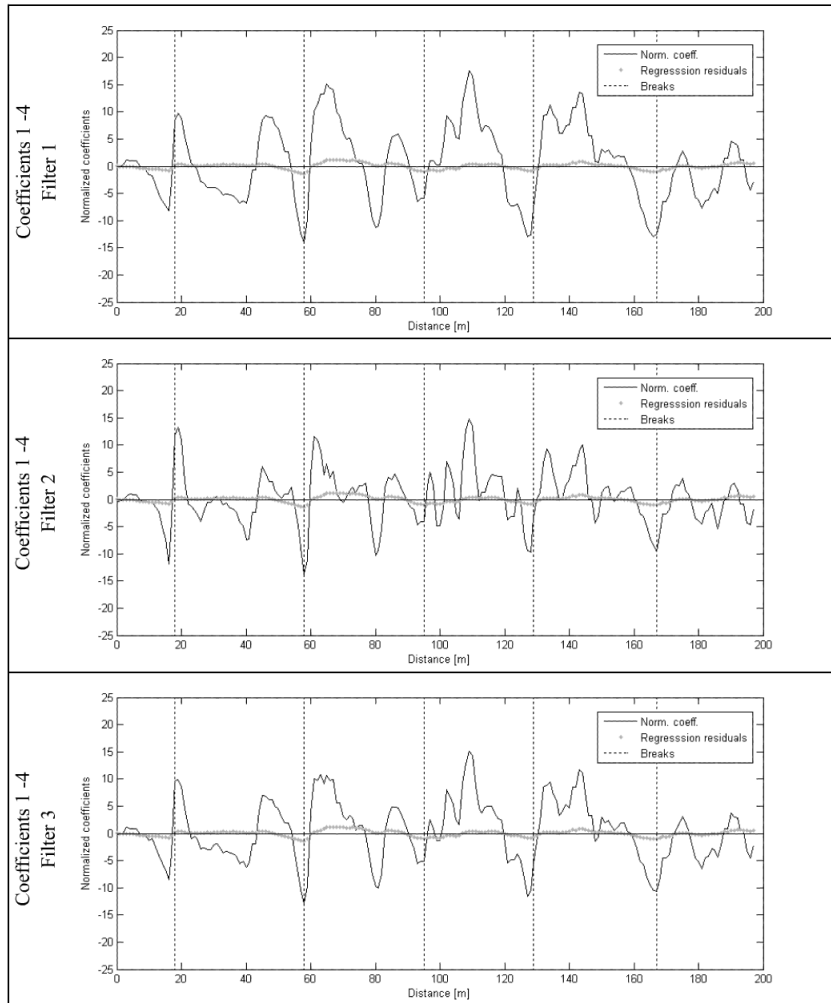


Fig. I.2. Values of normalized coefficients, decomposition levels 1-4, filters 1-3

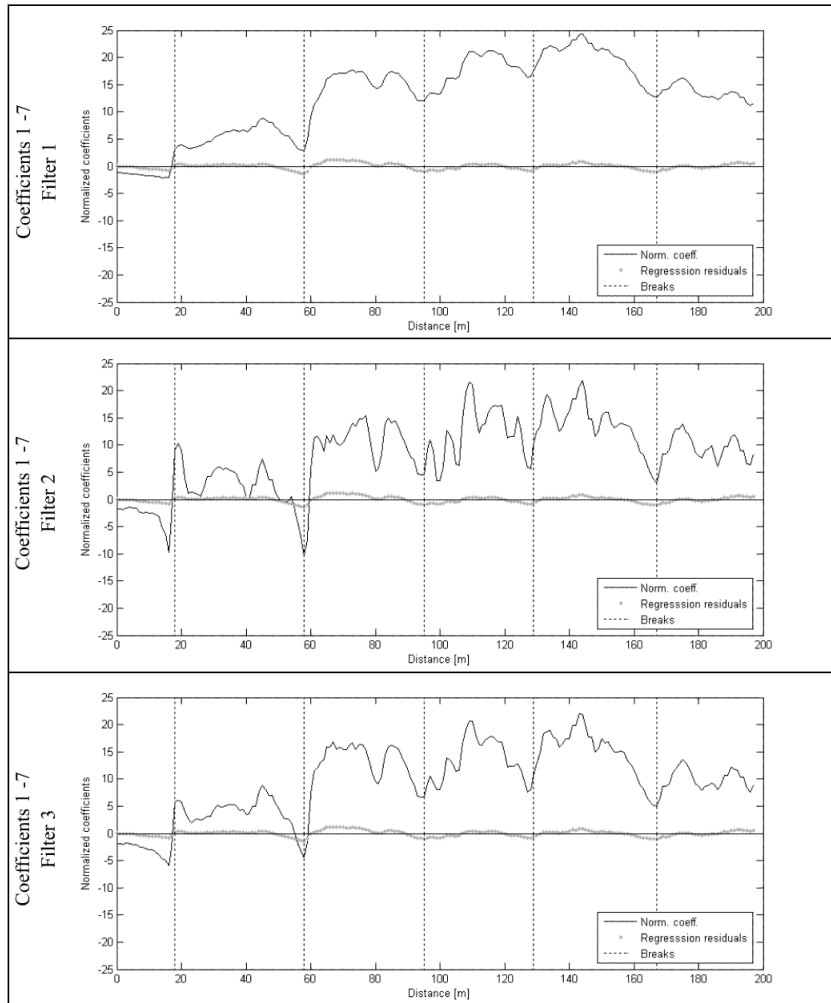


Fig. I.3. Values of normalized coefficients, decomposition levels 1-7, filters 1-3

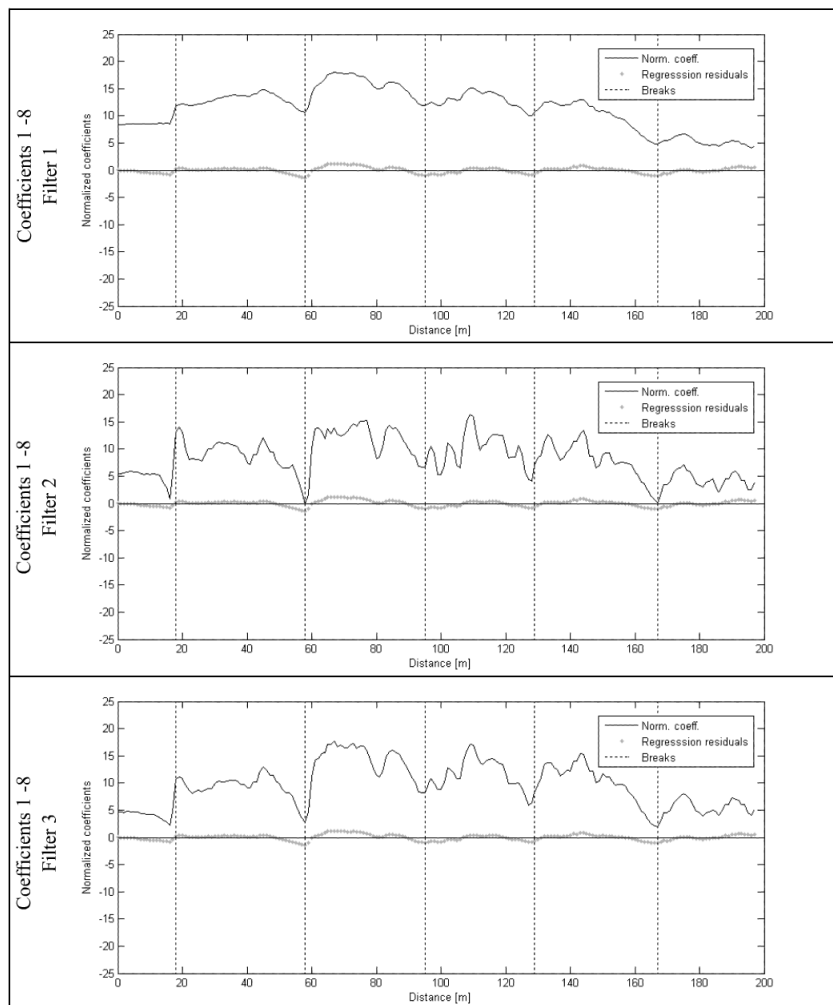


Fig. I.4. Values of normalized coefficients, decomposition levels 1-8, filters 1-3

J. Linear structural elements on the Travers DEM

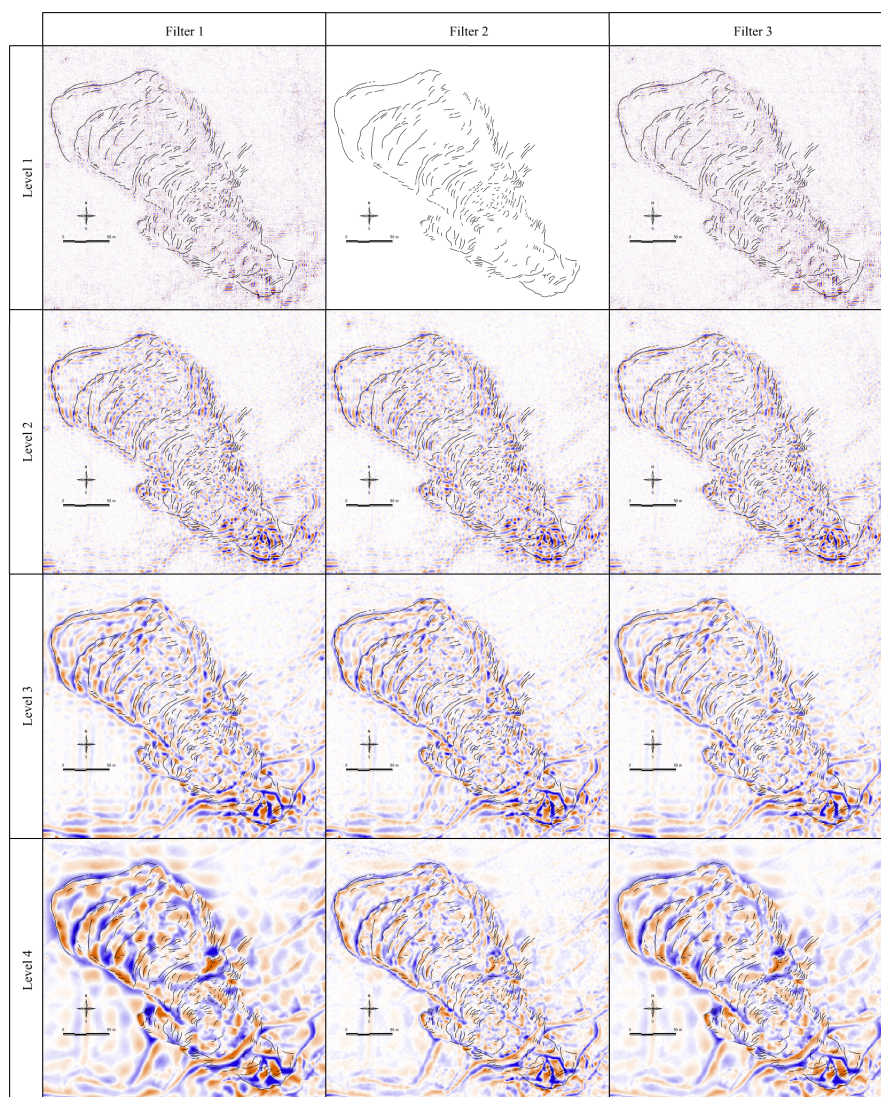


Fig. J.1. High-pass results for linear elements using the three filters, for decomposition levels 1 to 4

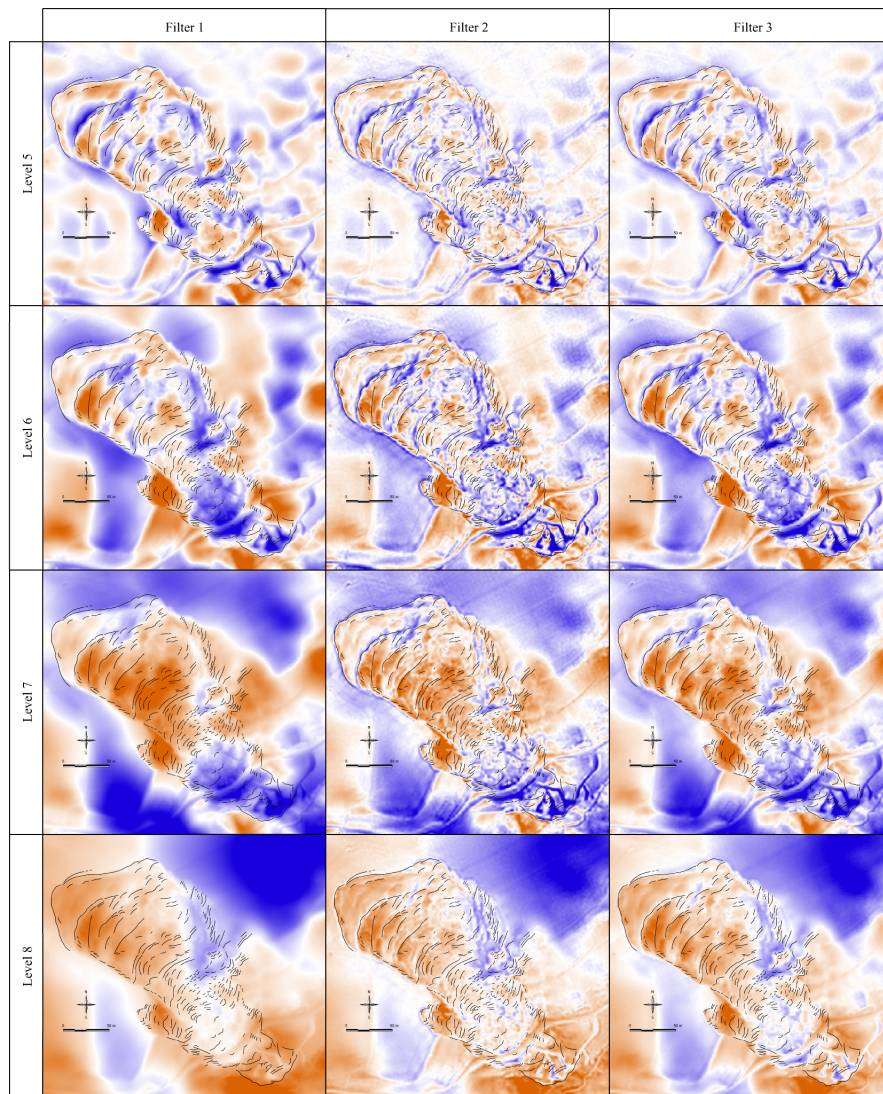


Fig. J.2. High-pass results for linear elements using the three filters, for decomposition levels 5 to 8

K. GAS - Geomorphometric Analysis System

GAS is a SVG web-mapping interface combined to an online survey. It was online from June 2009 to the end of September 2009.

The web-based questionnaires and mapping interface are composed of:

1. The SVG interface is built using PHP scripting and all terrain attribute values (elevation, slope, etc) are sent to the client (web navigator) using Javascript arrays.
2. The interaction between the user and its client is animated through Javascript which modifies the SVG content interactively.
3. All the spatial data digitized by the user is sent using HTTP requests (Javascript and PHP). At the server side, the data is stored in a postGIS¹ database.
4. The answers to the questionnaires are stored in PostgreSQL² database.

Due to the complexity of the subject and the limited potential audience, we did not have a lot of surveys. Therefore the analysis of the results will be done in a statistical manner, thus quantitative, but mostly qualitatively.

¹ postGIS: <http://postgis.refrations.net/>, accessed 17 September 2009

² <http://www.postgresql.org/>, accessed 17 September 2009

K.1 Result analysis

K.1.1 First questionnaire results

User age:	≤ 20 years	21-30 years	31-40 years	41-50 years	51-60 years	≥ 60 years
	0	4	7	2	1	1
User GIS skills:	Very bad	Bad	Intermediate	Good	Very good	
	0	0	2	7	5	
User DEM knowledge:	Yes	No				
	14	0				
User who used DEMs:	Never	Rarely	Sometimes	Often	Very often	
	2	0	5	3	4	
User ALS knowledge:	Yes	No				
	13	1				
User who used ALS DEMs:	Never	Rarely	Sometimes	Often	Very often	
	3	1	4	6	9	
User who know primary DEM derivatives:	Yes	No				
	12	2				
User who know secondary DEM derivatives:	Yes	No				
	12	2				

Table K.1. Answers to the first questionnaire of the Gemorphometric Analysis System (GAS) study. For the exact formulations of the question, refer to table K.4

K.1.2 Second questionnaire results

User satisfaction:	Satisfied	Not satisfied			
	4	10			
Estimated difficulty:	Very difficult	Difficult	Neither	Easy	Very easy
	1	2	10	1	0
Enough data?:	Yes	No			
	8	6			

Table K.2. Answers to the second questionnaire of the Gemorphometric Analysis System (GAS) study. For the exact formulations of the question, refer to table K.5

The following comments were given regarding the first question (*If not, why?*, the capital letters are an anonymous identification of users):

- A: “*Difficult to know what I see.*”
- B: “*Lack of familiarity with the technology, the data and the region.*”
- C: “*I would have liked to have seen a digital elevation model, not only its hillshade in order to have a better view on the directions of movement.*”
- D: “*I am not a geologist or geomorphologist and do not have enough knowledge about the important processes so I did not know what to map.*”
- E: “*A complete analysis takes more than 20 minutes. It is necessary to have additional documents (aerial photography). Particularly, the landslide uphill zone with the new road is hard to interpret. I limited myself to some feature relative to the landslide.*” (translated from French)
- F: “*I do not know enough.*” (translated from French)
- G: “*I am not used to the geomorphological vocabulary.*” (translated from French)
- H: “*The help bubbles of the tools are boring me! I can erase them... So I have problems to see the top of the map.*”
- I: “*Needed derivatives to be computed at multiple window sizes and grid resolutions to better assess larger features and provide context*”
- J: “*Matter of time (20min!?). I missed the elevation data itself*”

K.1.3 Third questionnaire results

User satisfaction:	Satisfied	Not satisfied			
	5	9			
Wavelet useful?:	Yes	No			
	11	3			
Wavelet understandable?:	Yes	Partially yes	Partially no	No	
	1	9	3	1	
Easy with wavelets?:	Def. yes	Yes	Neither	No	Def. no
	1	10	0	3	0

Table K.3. Answers to the third questionnaire of the Gemorphometric Analysis System (GAS) study. For the exact formulations of the question, refer to table K.6

The following comments were given regarding the first question (the capital letters represent the same user):

- B: “Same as before... (Lack of familiarity with the technology, the data and the region.)”
- C: “I find that the explanatory power of the wavelet analysis is somewhat limited. As far as I know wavelets are applied to detect frequencies in the 1D or 2D domain. I am not sure if this frequency filtering is good here except for detecting wave-like patterns in the landslide body. However, I am surprised how well larger landforms are captured by the low-pass filtered images. The high-pass images show some artefacts.”
- D: “Again, I know too little about landslides. But I definitely could distinguish more patterns with the added layers.”
- E: “The second analysis could help to affine the first one, but I see that some important elements were already detected, thus I did not digitize the whole again.” (translated from French)
- F: “Sorry, cannot do it better...” (translated from French)
- G: “Same again, not enough vocabulary” (translated from French)
- K: “Hard to detect differences in decomposed maps”
- H: “Always the same problem with the help bubbles. Perhaps a problem of web browser...”
- J: “Time again, but I am also not used to the wavelet concept”

K.1.4 General comments

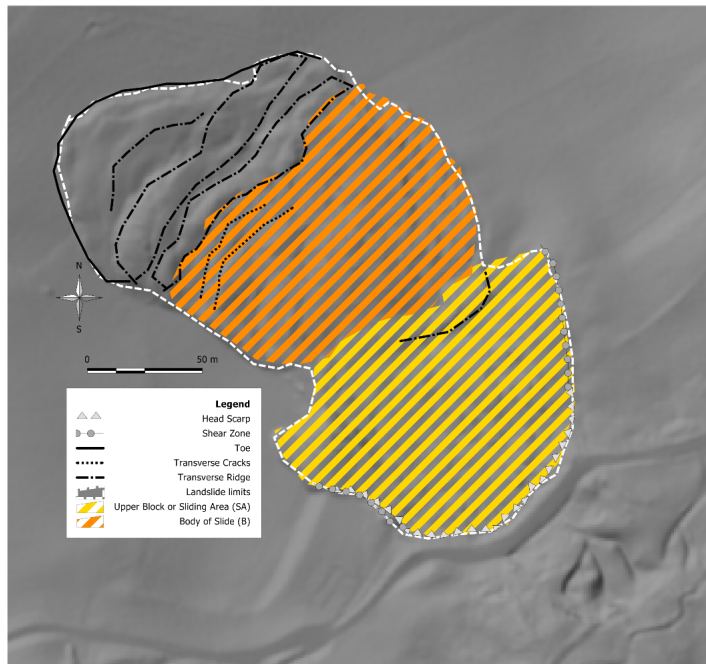
Following general remarks and comments were given at the end of the survey:

- B: “I reviewed a paper about this for a forthcoming conference in Zurich.”
- C: “Nice work.”
- D: “Maybe I should not be considered a earth science specialist...”
- E: “It is an additional element to help to do an analysis, which is always a good thing, but without being completely determining” (translated from French)

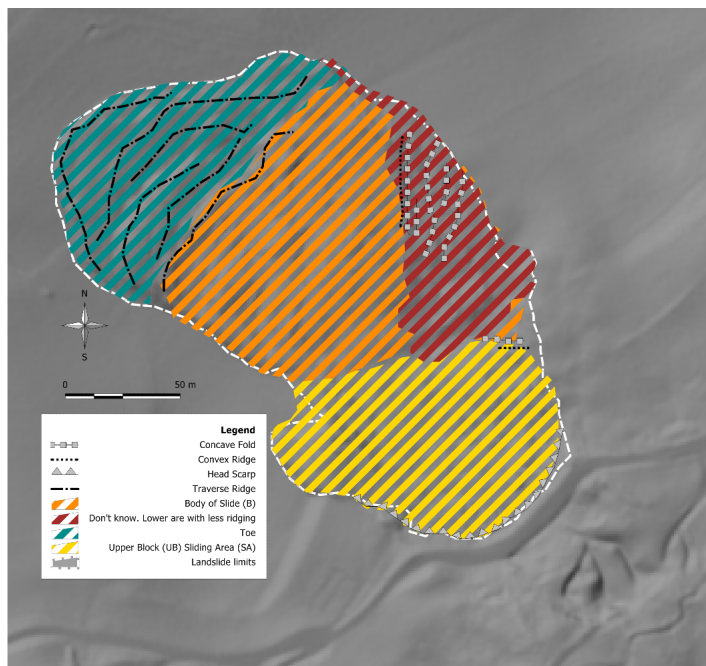
- K: *“Maps show different things for different decomposition level, it would be useful to understand what is highlighted at what decomposition level.”*
- H: *“I think that wavelet layer could be an interesting complement to the first and second derivatives of DTM. But, depending of the topographic roughness, only few wavelet layers are helpful.”*

K.2 Acknowledgement

Hereby, we would like to thank the persons who participated to the GAS experiment. Thanks (in no particular order) a lot to Matthias Pouyt, Laurent Jemelin, Massimiliano Cannata, Marianne Font, Albin Viquerat, Giuseppe Franciosi, the people from GISxpert, Andy Turner, Wolfgang Schwanghart and 5 anonymous people. We would like to thank them for the spent time and for their pertinent comments.



(a)



(b)

Fig. K.1. GAS mapping - session 7, (a) exercise 1 and (b) exercise 2

K.3 Questionnaires

Question	Possible answers
How old are you?	≤ 20 or $21 - 30$ or $31 - 40$ or $41 - 50$ or $51 - 60$ or > 60
What is your profession?	<i>GIS specialist</i> or <i>Geologist</i> or <i>Geomorphologist</i> or <i>Morphometry specialist</i> or <i>Environmental engineer</i> or <i>IT specialist</i> or <i>Image processing specialist</i> or <i>Cartographer</i> or <i>Other</i> (with description)
What is the level of your GIS skills (GIS: Geographical Information Systems)?	<i>Very bad</i> or <i>Bad</i> or <i>Intermediate</i> or <i>Good</i> or <i>Very good</i>
Do you know what a DTM (Digital Terrain Model) is?	<i>Yes</i> or <i>No</i>
Have you used DTMs to carry out geomorphological terrain analysis?	<i>Never</i> or <i>Rarely</i> or <i>Sometimes</i> or <i>Often</i> or <i>Very often</i>
Do you know what airborne laser scanning is?	<i>Yes</i> or <i>No</i>
Did you already use very high resolution DTMs generated from laser scanning?	<i>Never</i> or <i>Rarely</i> or <i>Sometimes</i> or <i>Often</i> or <i>Very often</i>
Do you know how primary topographic attributes (slope, aspect and curvature surfaces) are derived from a DTM?	<i>Yes</i> or <i>No</i>
Do you know how secondary topographic attributes (catchment area, wetness index, solar radiation and other surfaces) are derived from a DTM?	<i>Yes</i> or <i>No</i>

Table K.4. First set of questions

Question	Possible answers
Are you satisfied with the analysis you carried out?	<i>Yes or No</i>
If not, why?	User comment
Were there enough available spatial data (DTM and derivatives) for the cartography of the landslide?	<i>Yes or No</i>
How difficult was it to identify specific structures of the landslide?	<i>Very hard or Hard or Not hard, not easy or Easy or Very easy</i>

Table K.5. Second set of questions

Question	Possible answers
Are you satisfied with the second analysis you carried out?	<i>Yes or No</i>
If not, why?	User comment
Were additional wavelet layers useful for you in order to detect more features or to discover complementary information?	<i>Yes or No</i>
Did you understand what the new information was showing?	<i>Definitively yes or Yes, partially or No, not fully or Definitively no</i>
Was it easier for you to identify specific structures of the landslide using wavelet layers than using a standard DTM and associated derivative information ?	<i>Definitively yes or Yes or Did not change anything or No or Definitively no</i>
Have you any remarks/comments?	User comment
I would like to be informed about results and further developments.	E-mail address, contact address

Table K.6. Third set of questions

L. Multiscale pattern analysis results

L.1 Generalised Least-Square Errors - fuzzy k-means

If $X = \{x_1, x_2, \dots, x_n\}$ is a set of n variables. For each variable $x \in X$, we have m observations. The set of clusters $C = \{c_1, c_2, \dots, c_C\}$ is a partition of X and c_1, c_2, \dots, c_C are integers with boundaries $k \in [2, C)$. The k-means algorithm computes a membership μ for each n^{th} variable (of each m^{th} observation) to each c^{th} cluster. It is based on the minimization of the objective function J_p :

$$J_p = \sum_{k=1}^n \sum_{i=1}^C (\mu_{ik})^p \|x_k - c_i\|^2 \quad (\text{L.1})$$

The partition is an optimization of the function by iteration:

$$\mu_{ik} = \frac{1}{\sum_{k=1}^C \left(\frac{\|x_i c_j\|}{\|x_i c_k\|} \right)^{\frac{2}{p-1}}} \quad (\text{L.2})$$

and:

$$c_k = \frac{\sum_{i=1}^n \mu_{ik}^p x_i}{\sum_{i=1}^n \mu_{ik}^p} \quad (\text{L.3})$$

where:

- p is the weightening exponent, a real number $p \in [1, \infty)$.
- μ_{ik} is the degree of membership of x_i in the cluster k .
- x_i is the i^{th} of m -dimensional measured data, $X \subset \mathbb{R}^2$.
- c_k is the k^{th} centre, $k \in [2, C)$.
- C is the number of chosen centers.

The norm can be computed using the Euclidean distance or the distance of Manhattan. In this study, the Euclidean distance was used for norm computation. There are a few methods / indicators to assess the quality of the classification.

L.1.1 Confusion Index

The confusion index (CI) indicates how good the classification of each observation (separately) is. For each set of membership values (of each observation), it is possible to calculate the ratio of the second dominant value to the first dominant value:

$$CI = \frac{\max fuzz2}{\max fuzz1} \quad (\text{L.4})$$

- *maxfuzz1*: first dominant value
- *maxfuzz2*: second dominant value

It is commonly admitted that if the resulting confusion index CI is lower than 0.6, then the cluster k from which the first dominant value is taken is a hard class. Thus, the pixel has been hard classified and that there almost no chance that the pixel is part of another cluster.

Two tests are described to assess the quality of the clustering in general:

L.1.2 F, partition coefficient

The F test is calculated following:

$$F = \frac{1}{n} \sum_{i=1}^n \sum_{k=1}^C (\mu_{ik})^2, \quad 1/C < F < 1 \quad (\text{L.5})$$

The number of chosen clusters changes the boundaries of the F value. In order to be able to compare the different F values obtained through the different number of chosen clusters, we need to normalise it:

$$F_{scaled} = \frac{F - 1/C}{1 - 1/C} \quad (\text{L.6})$$

when F_{scaled} tends to 1, then the clusters are the most significant.

L.1.3 H, classification entropy

$$H = \frac{1}{n} \sum_{i=1}^n \sum_{k=1}^C -\mu_{ik} \ln(\mu_{ik}) \quad (\text{L.7})$$

Like for the F value, we need to normalise the H value:

$$H_{scaled} = \frac{H - 1 + F}{\ln(C)1 + F} \quad (\text{L.8})$$

When H_{scaled} tends to 0, then the number of clusters is the most significant.

L.2 Results for the Travers DEM

L.2.1 Correlation of geomorphometric information

<i>Level 0</i>	Elevation	Slope	Solar irrad	Profile curv.	Plan curv.	Wetness I.	Ridge dist.
Elevation	1	0.66	0.01	0.01	-0.65	0.07	-0.4
Slope	0.66	1.00	-0.89	-0.01	0.01	-0.52	0.04
Solar irrad.	0.01	-0.89	1.00	0.03	0.01	0.40	-0.02
Profile curv.	0.01	-0.01	0.03	1.00	0.43	-0.08	0.02
Plan curv.	-0.65	0.01	0.01	0.43	1.00	-0.23	0.04
Wetness I.	0.07	-0.52	0.40	-0.08	-0.23	1.00	-0.29
Ridge dist.	-0.4	0.04	-0.02	0.02	0.04	-0.29	1.00
<i>Level 1</i>	Elevation	Slope	Solar irrad	Profile curv.	Plan curv.	Wetness I.	Ridge dist.
Elevation	1	0.69	0.01	0.01	-0.68	0.29	-0.43
Slope	0.69	1.00	-0.90	-0.02	0.01	-0.56	0.22
Solar irrad.	0.01	-0.90	1.00	0.04	0.01	0.43	-0.20
Profile curv.	0.01	-0.02	0.04	1.00	0.38	-0.08	0.03
Plan curv.	-0.68	0.01	0.01	0.38	1.00	-0.27	0.08
Wetness I.	0.29	-0.56	0.43	-0.08	-0.27	1.00	-0.44
Ridge dist.	-0.43	0.22	-0.20	0.03	0.08	-0.44	1.00
<i>Level 2</i>	Elevation	Slope	Solar irrad	Profile curv.	Plan curv.	Wetness I.	Ridge dist.
Elevation	1	0.72	0.02	0	-0.71	0.52	-0.47
Slope	0.72	1.00	-0.91	-0.04	0.01	-0.60	0.35
Solar irrad.	0.02	-0.91	1.00	0.05	0.01	0.47	-0.33
Profile curv.	0	-0.04	0.05	1.00	0.38	-0.06	0.03
Plan curv.	-0.71	0.01	0.01	0.38	1.00	-0.27	0.09
Wetness I.	0.52	-0.60	0.47	-0.06	-0.27	1.00	-0.54
Ridge dist.	-0.47	0.35	-0.33	0.03	0.09	-0.54	1.00
<i>Level 3</i>	Elevation	Slope	Solar irrad	Profile curv.	Plan curv.	Wetness I.	Ridge dist.
Elevation	1	0.77	0.02	0.00	-0.76	0.44	-0.52
Slope	0.77	1.00	-0.91	-0.07	0.01	-0.63	0.27
Solar irrad.	0.02	-0.91	1.00	0.09	0.02	0.49	-0.25
Profile curv.	0.00	-0.07	0.09	1.00	0.37	-0.05	0.03
Plan curv.	-0.76	0.01	0.02	0.37	1.00	-0.28	0.07
Wetness I.	0.44	-0.63	0.49	-0.05	-0.28	1.00	-0.44
Ridge dist.	-0.52	0.27	-0.25	0.03	0.07	-0.44	1.00
<i>Level 4</i>	Elevation	Slope	Solar irrad	Profile curv.	Plan curv.	Wetness I.	Ridge dist.
Elevation	1	0.82	0.03	-0.02	-0.81	0.65	-0.57
Slope	0.82	1.00	-0.93	-0.11	0.00	-0.65	0.43
Solar irrad.	0.03	-0.93	1.00	0.13	0.04	0.52	-0.40
Profile curv.	-0.02	-0.11	0.13	1.00	0.39	-0.04	0.03
Plan curv.	-0.81	0.00	0.04	0.39	1.00	-0.31	0.09
Wetness I.	0.65	-0.65	0.52	-0.04	-0.31	1.00	-0.55
Ridge dist.	-0.57	0.43	-0.40	0.03	0.09	-0.55	1.00

Table L.1. Correlation between the variables for the k-means clustering for each decomposition level

L.2.2 Confusion index

The confusion index results show that the highest number of well-classified pixels is by using only two classes. The threshold was set to 0.6.

Regarding the dyadic subsampling, a \log_2 was applied to the values. Each level line (see table L.2) should be spaced by a factor 2 (relation between the dyadic subsampling and the number of pixels).

		Proportion of well-classified pixels for each class			
Level	Number of pixels	2	3	4	5
0	668160	92%	87%	85%	84%
1	167040	90%	83%	85%	83%
2	41760	86%	84%	85%	81%
3	10440	92%	89%	81%	79%
4	2610	93%	86%	83%	77%

		Proportion of well-classified pixels for each class			
Level	Number of pixels	6	7	8	9
0	668160	83%	82%	80%	79%
1	167040	80%	80%	80%	78%
2	41760	81%	79%	79%	78%
3	10440	82%	83%	83%	78%
4	2610	80%	79%	79%	80%

Table L.2. Confusion index for the different levels and the different number of clusters

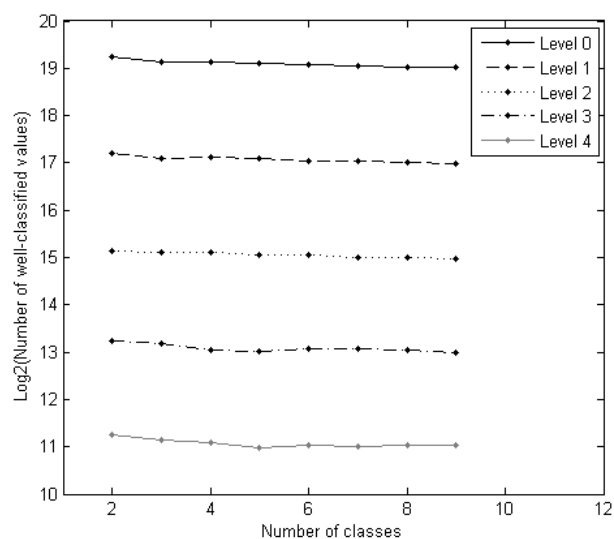


Fig. L.1. Confusion index analysis

L.2.3 Result of the fuzzy k-means classification

It is not the characteristics of the clusters that we want to explain and explore in our case, but rather the interactions of the latter through the decomposition levels, i.e. the multiscale classification. For all decomposition levels, a similarity was visually made in order to give to the same clusters the same colour. Visually this increases the comparative capabilities between the levels. But, this does not mean that clusters having the same colour or the same topographical typology represent the same topographical effect.

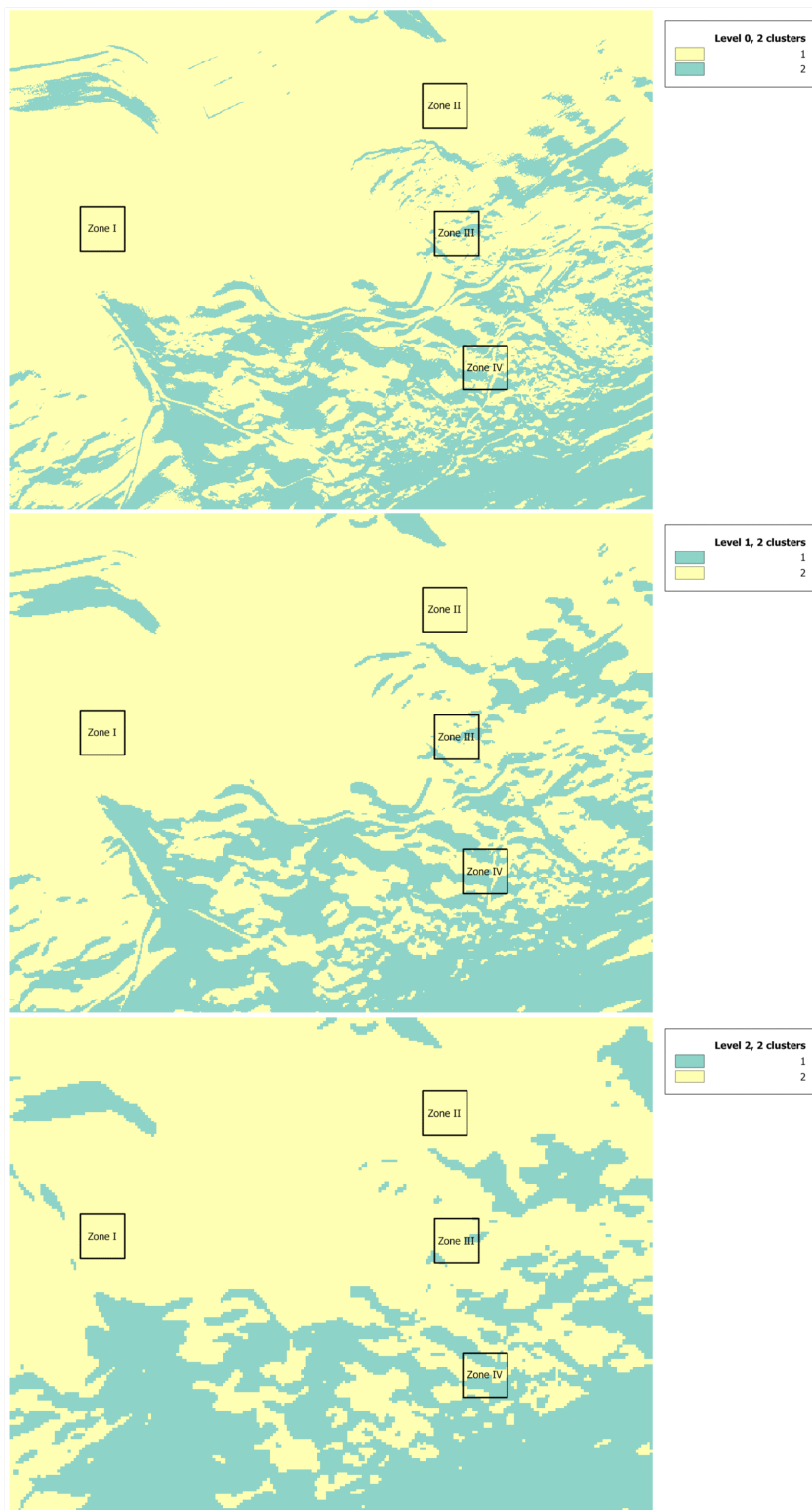


Fig. L.2. Decomposition levels 0 to 2, 2 clusters



Fig. L.3. Decomposition levels 3 to 4, 2 clusters

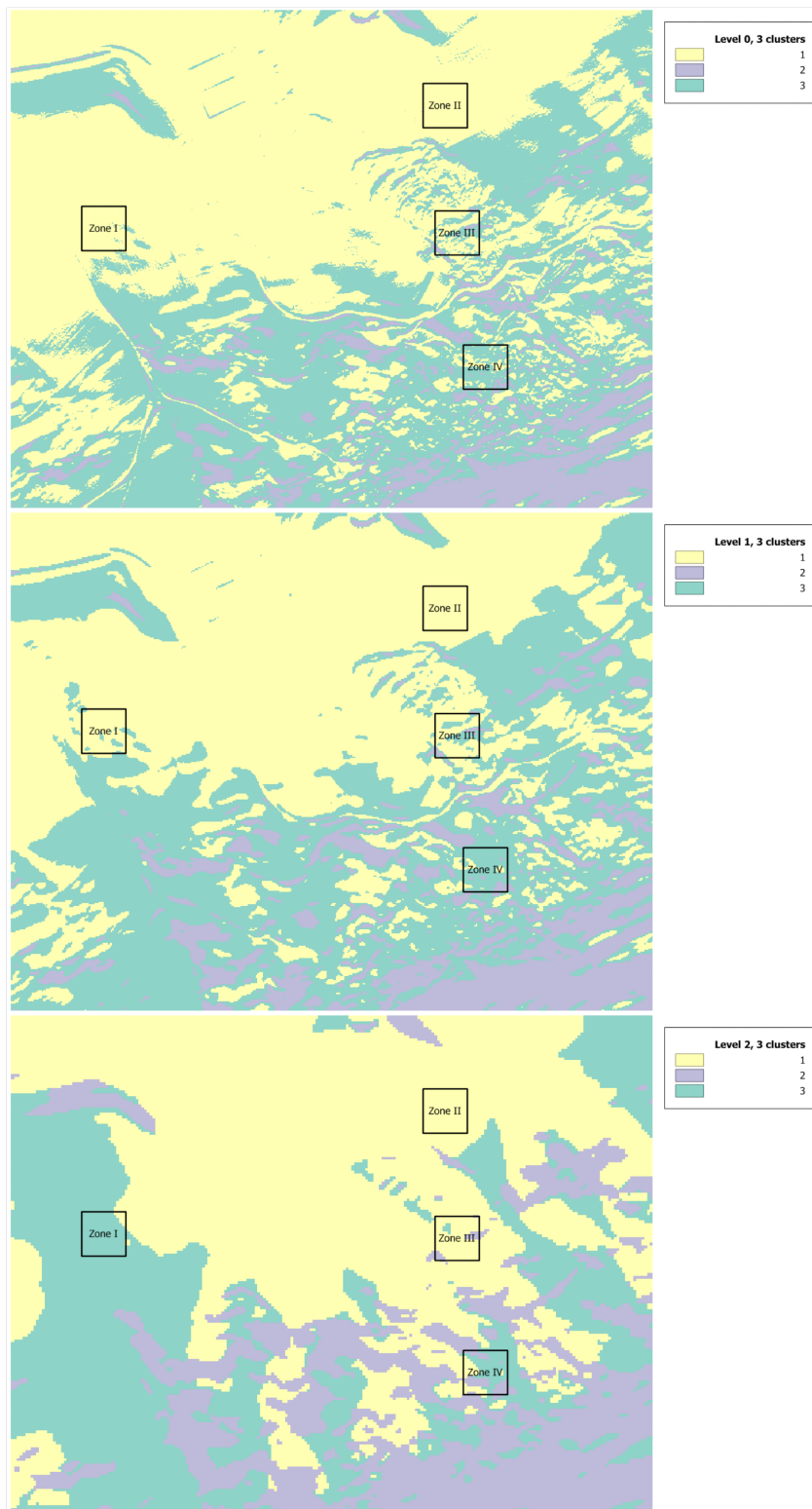


Fig. L.4. Decomposition levels 3 to 4, 3 clusters



Fig. L.5. Decomposition levels 3 to 4, 3 clusters

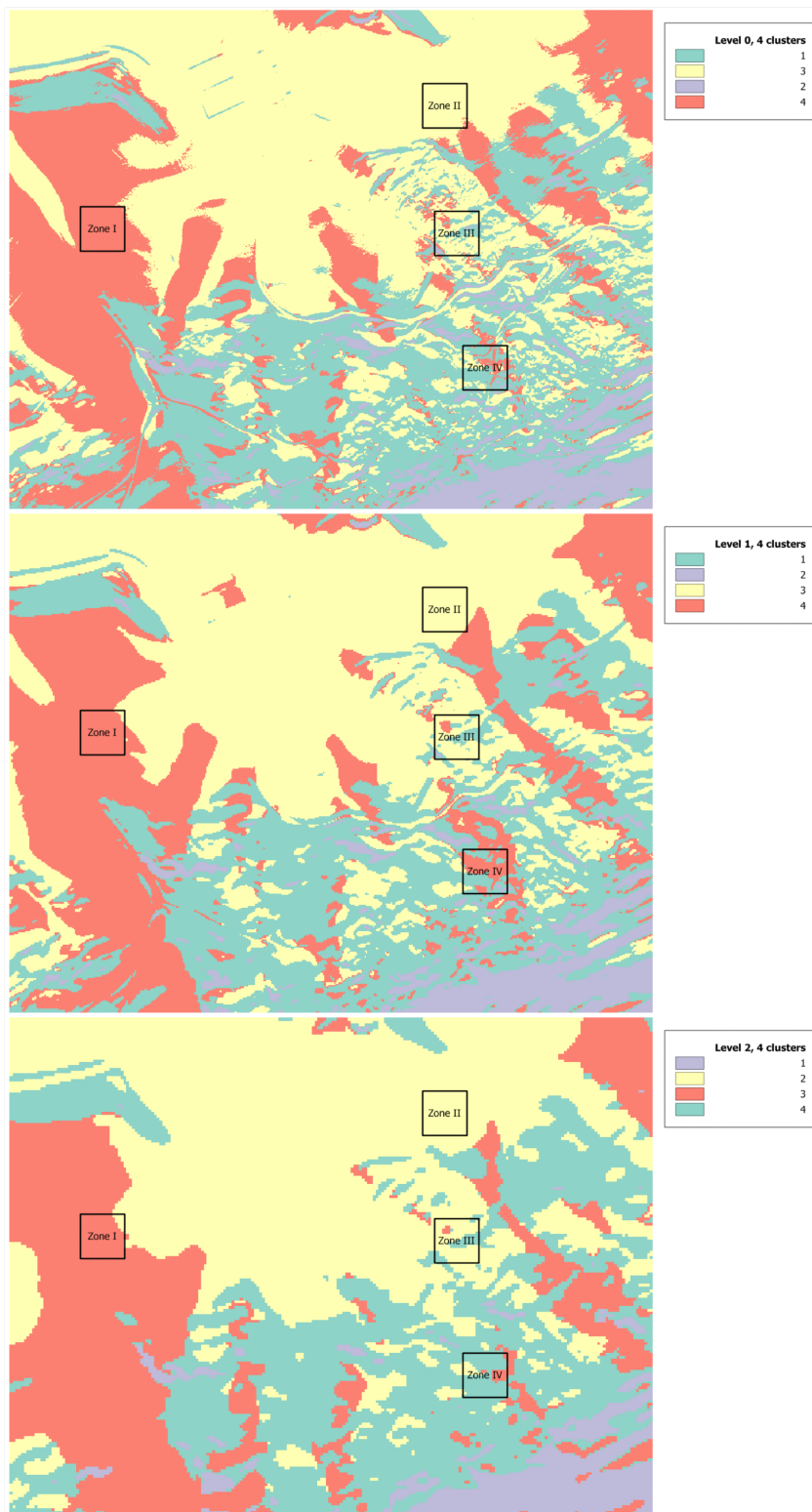


Fig. L.6. Decomposition levels 3 to 4, 4 clusters

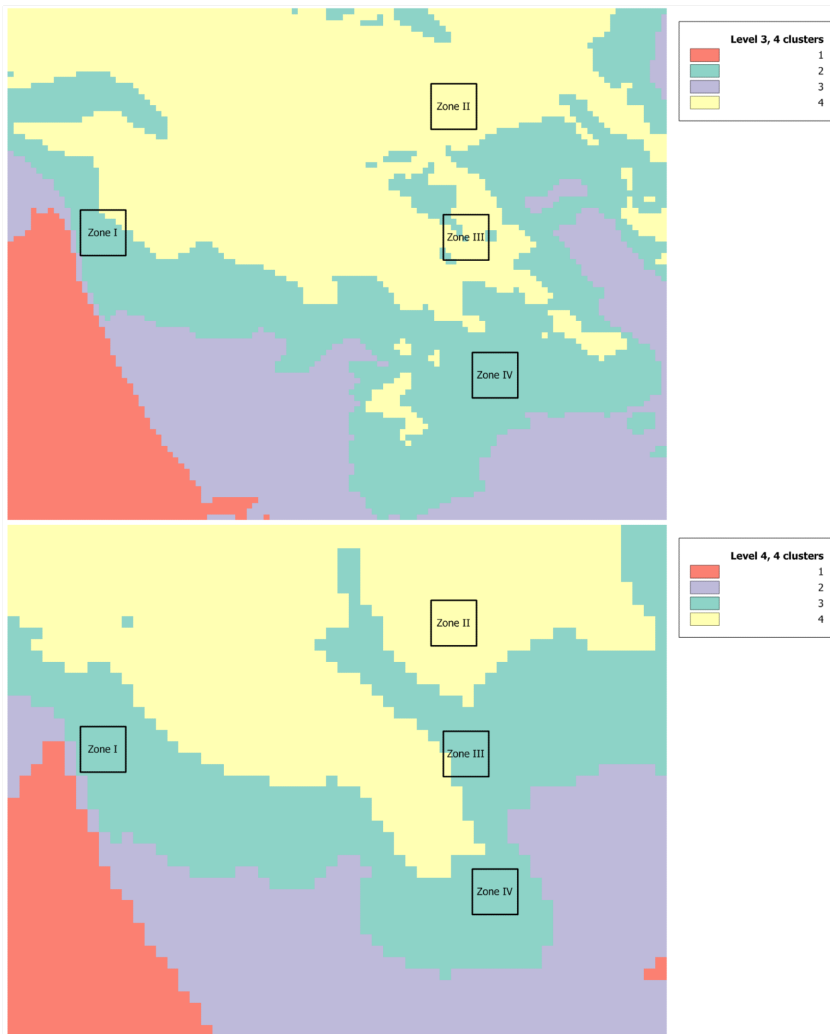


Fig. L.7. Decomposition levels 3 to 4, 4 clusters

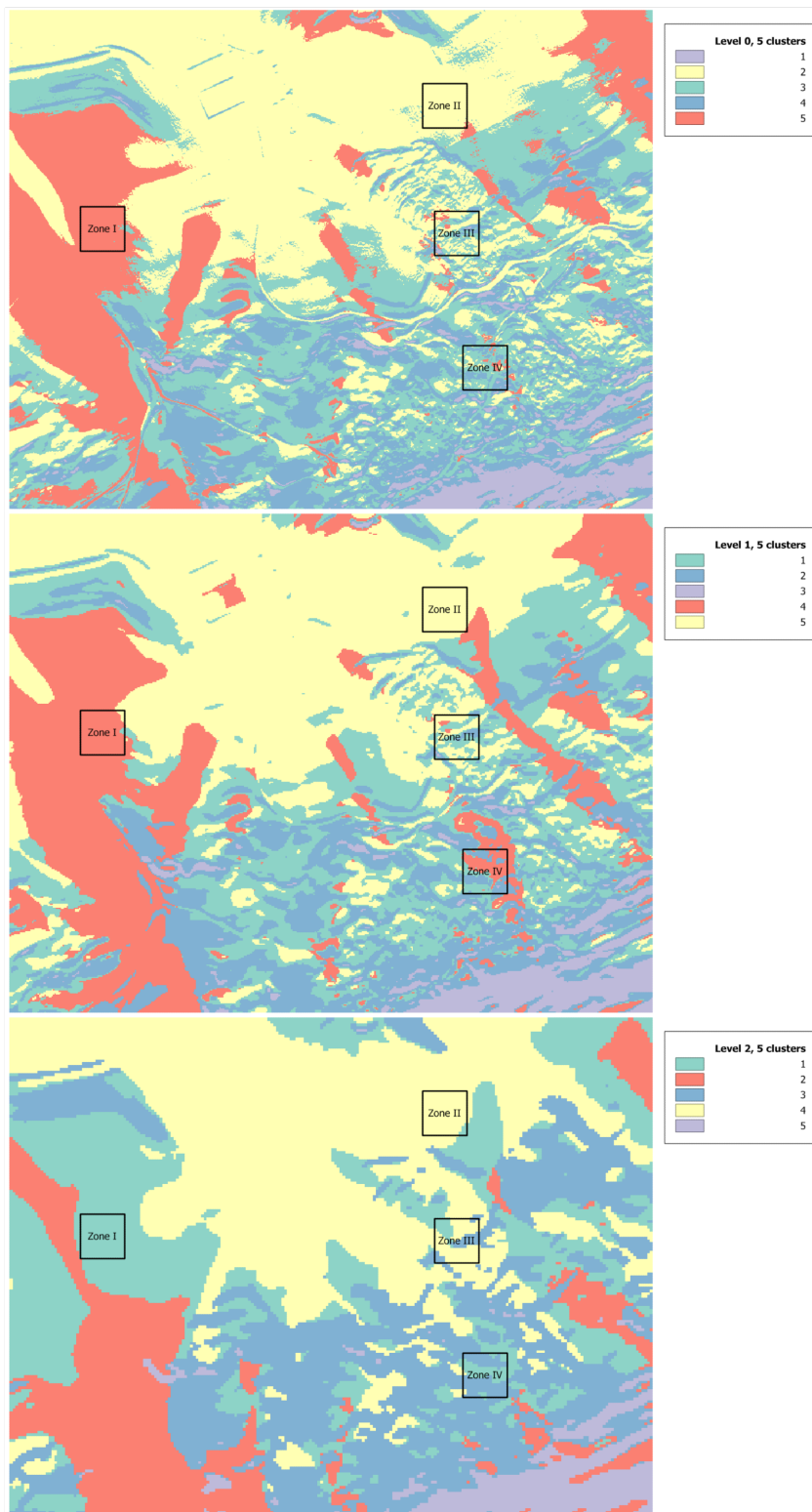


Fig. L.8. Decomposition levels 3 to 4, 5 clusters

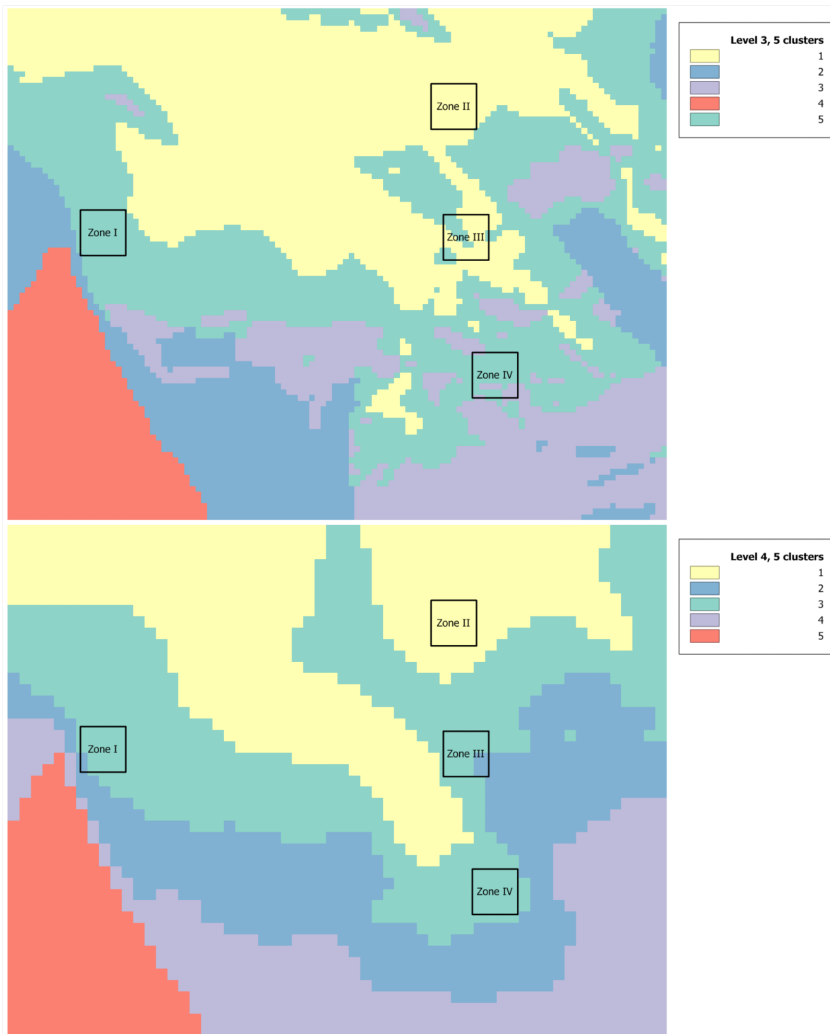


Fig. L.9. Decomposition levels 3 to 4, 5 clusters

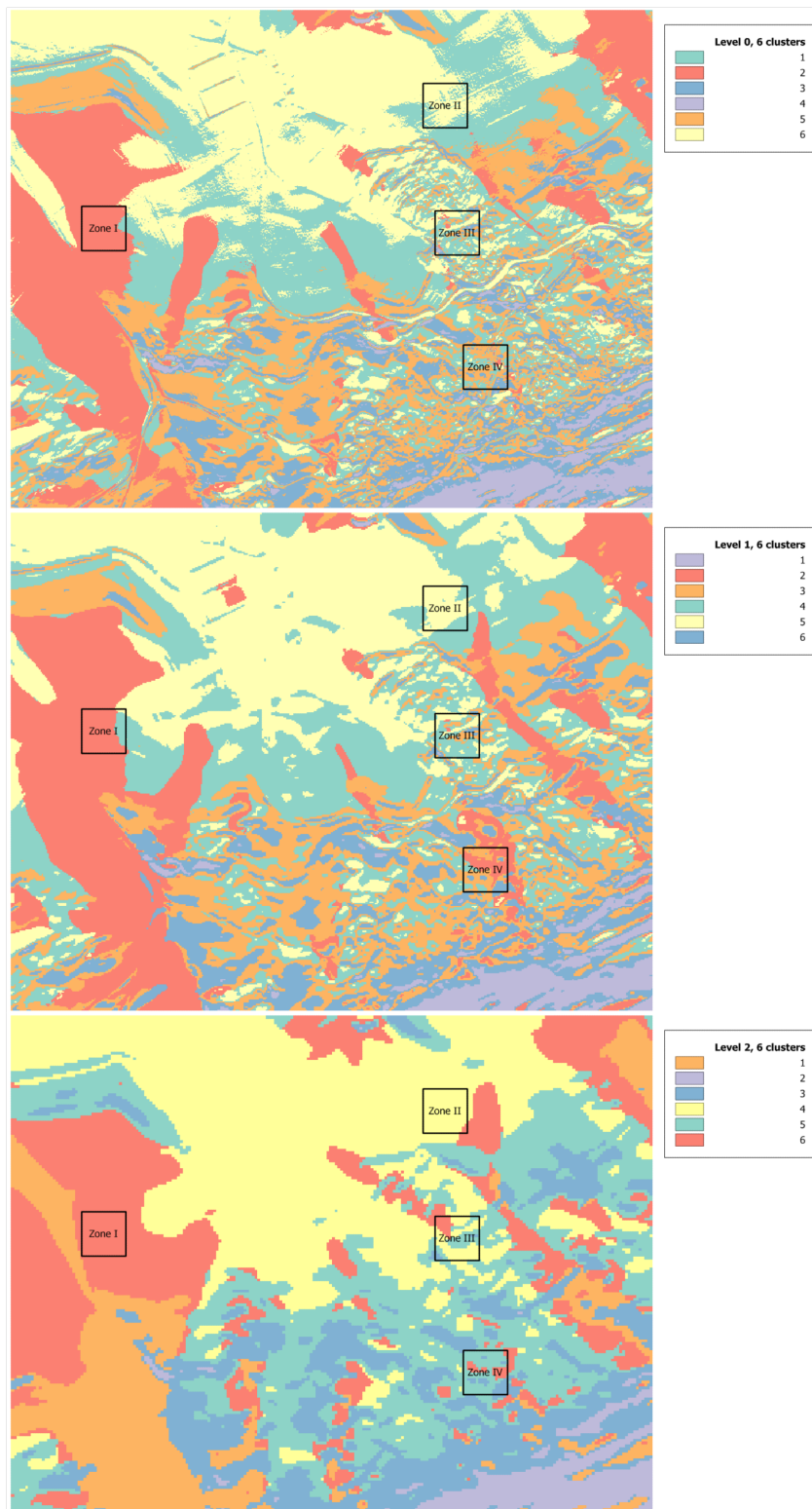


Fig. L.10. Decomposition levels 3 to 4, 6 clusters

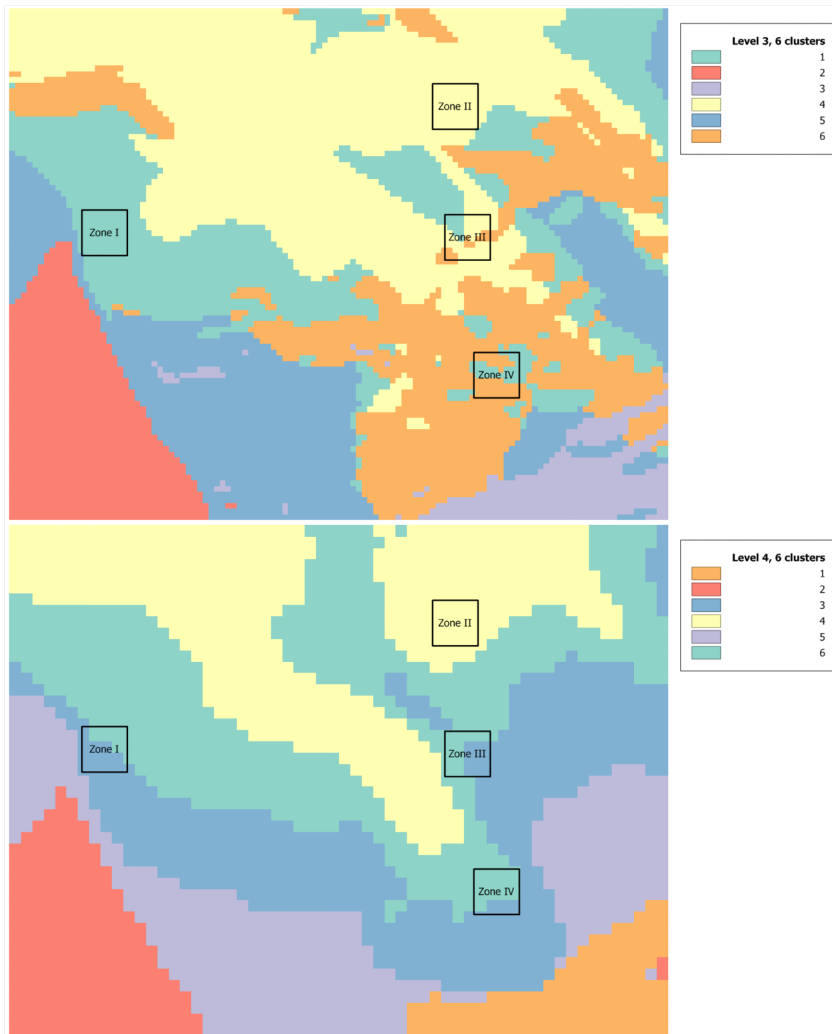


Fig. L.11. Decomposition levels 3 to 4, 6 clusters

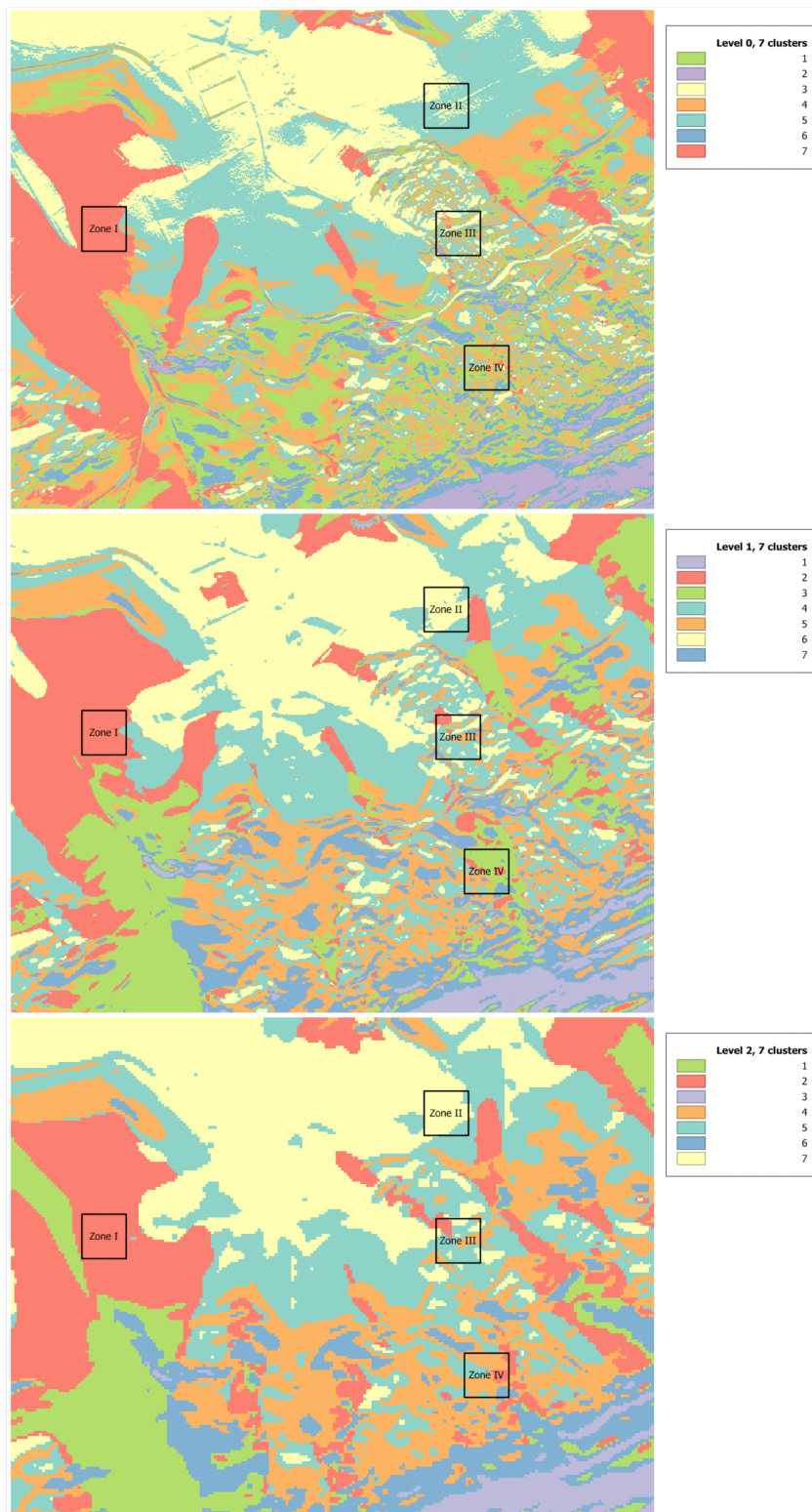


Fig. L.12. Decomposition levels 3 to 4, 7 clusters

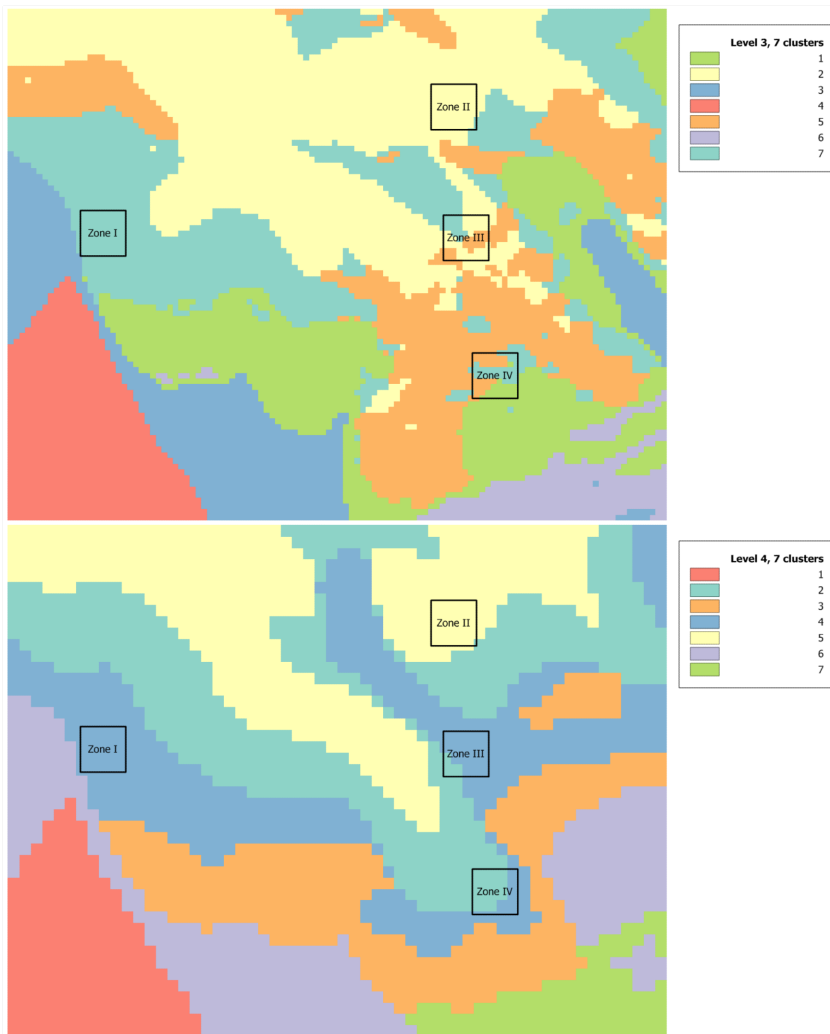


Fig. L.13. Decomposition levels 3 to 4, 7 clusters

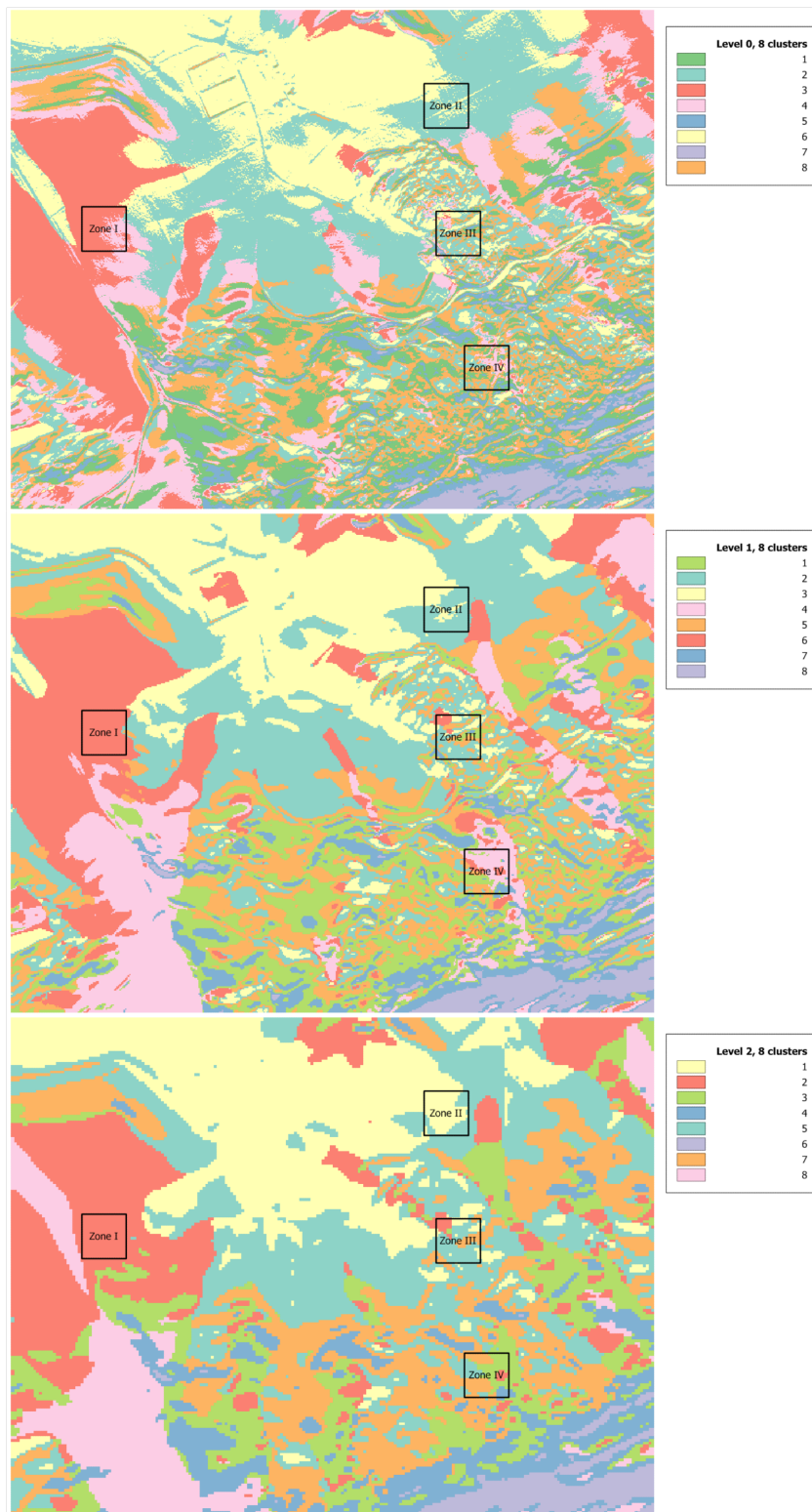


Fig. L.14. Decomposition levels 3 to 4, 8 clusters

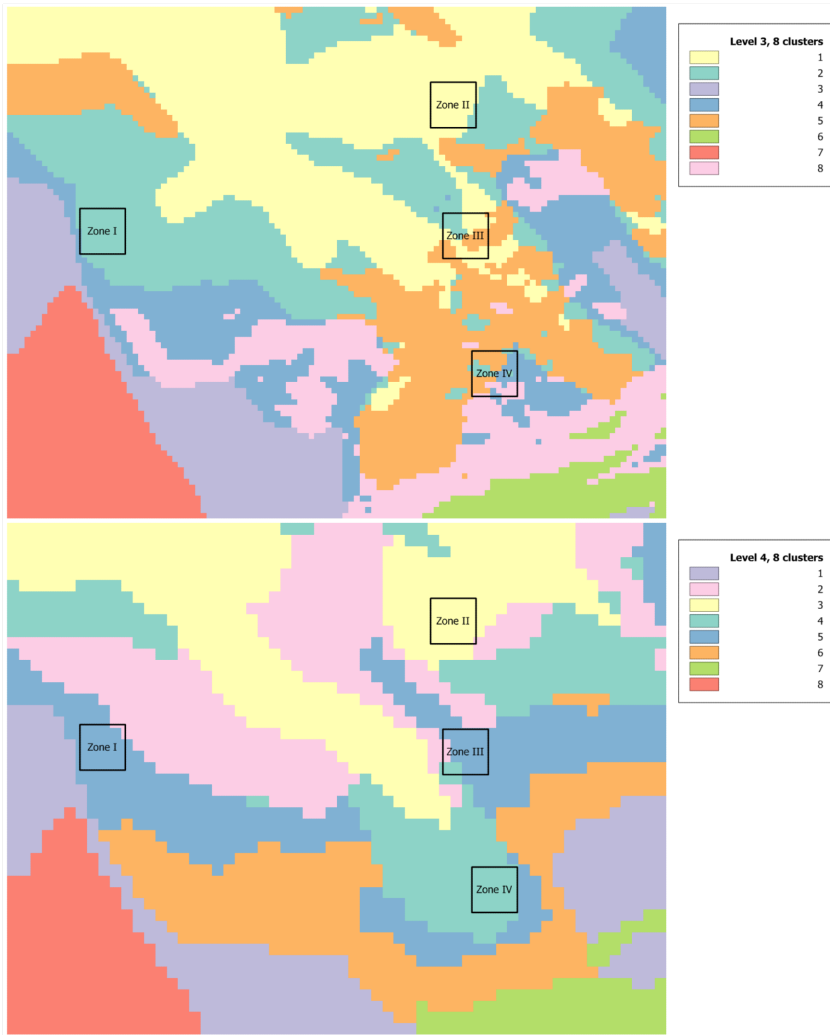


Fig. L.15. Decomposition levels 3 to 4, 8 clusters

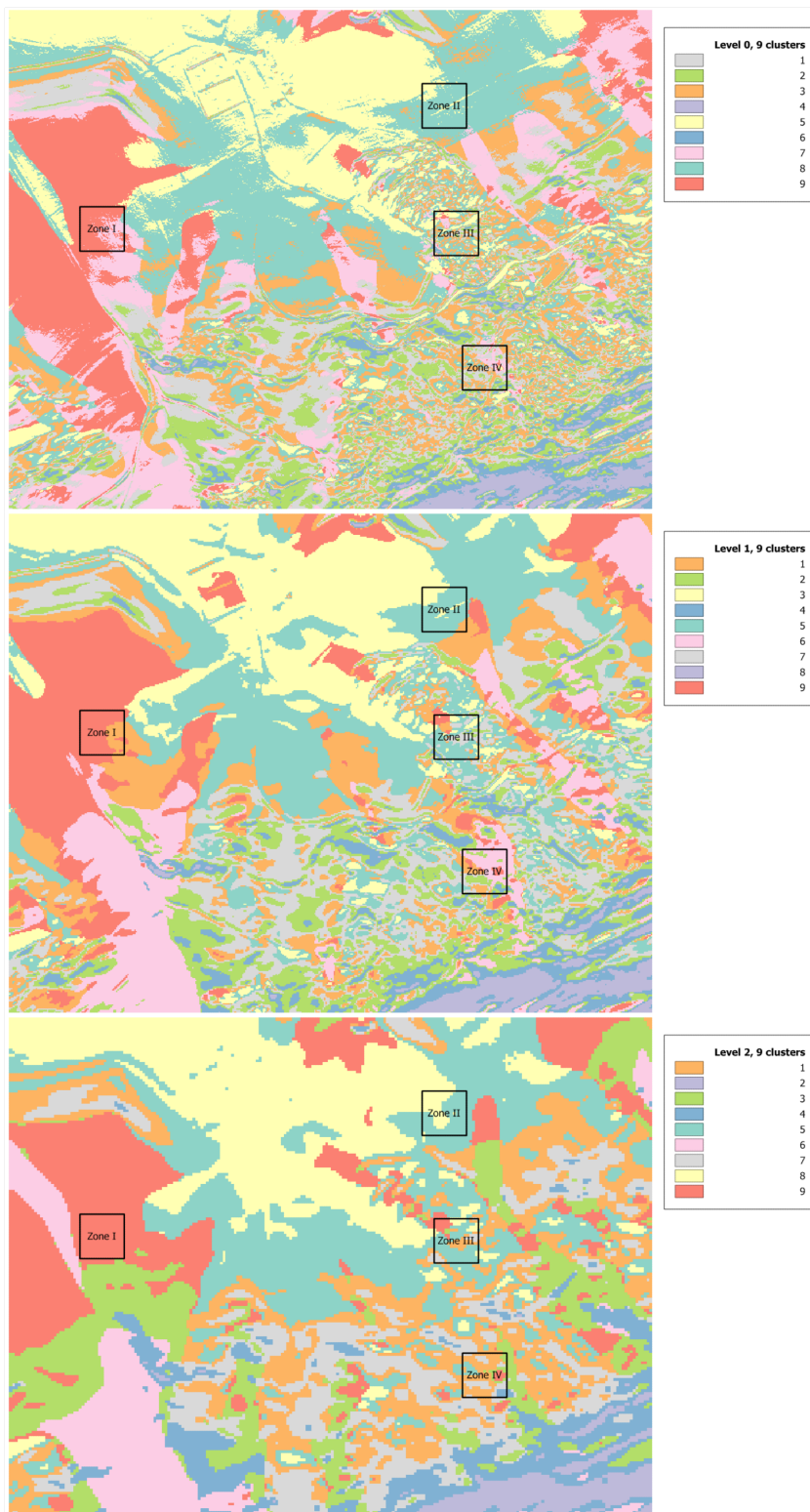


Fig. L.16. Decomposition levels 3 to 4, 9 clusters

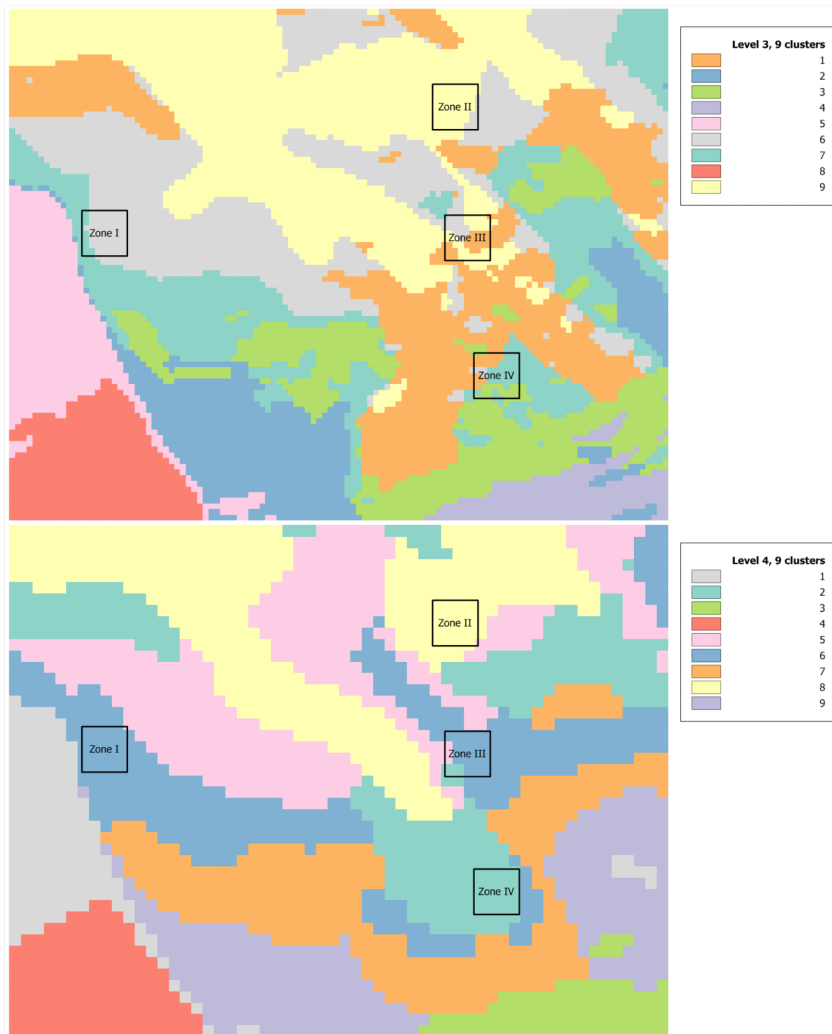


Fig. L.17. Decomposition levels 3 to 4, 9 clusters

M. Laplace-gradient wavelet pyramid and structure tensor

All the developments and theory presented in this appendix are taken from following publications: Jähne (2005); Unser *et al.* (2009); Unser and Van De Ville (2008); Van De Ville *et al.* (2005, 2008); Van De Ville and Unser (2008); Madych and Nelson (1990); Bigun *et al.* (2004)

M.1 Laplace-gradient wavelet pyramid

A Laplacian operator is defined as the second derivative of a signal. In its real notation and in the spatial domain (\mathbb{R}^2), it is usually described as:

$$\Delta f = \nabla^2 f = \nabla \cdot \nabla f = \frac{\partial^2 f}{\partial x^2} + \frac{\partial^2 f}{\partial y^2} \quad (\text{M.1})$$

and in the Fourier domain:

$$\Delta f \xleftrightarrow{F} -\|\boldsymbol{\omega}\|^2 \hat{f}(\boldsymbol{\omega}), \quad \boldsymbol{\omega} = (\omega_1, \omega_2) \quad (\text{M.2})$$

As starting point to the wavelet pyramid and combining the 2D definition of the laplacian operator in the complex domain, we can identify the Laplace-complex gradient, which characterizes the complete family of shift-invariant, scale-invariant, and rotation-covariant convolution operators (Van De Ville and Unser, 2008):

$$L_{\gamma, N} = (-\Delta)^{\frac{\gamma-N}{2}} \left(-j \frac{\partial}{\partial x} - \frac{\partial}{\partial y} \right)^N \quad (\text{M.3})$$

with:

- $\gamma \in \mathbb{R}^+$ ($\gamma > 1/2$): the order of the isotropic Laplacian
- $N \in \mathbb{N}$: the order of the complex gradient

In association with this, we have a complex polyharmonic B-spline $\beta_{\gamma, N}$ (Van De Ville and Unser, 2008; Van De Ville *et al.*, 2005) which is a distribution annihilated by discrete iterations of the complex Laplacian (Madych and Nelson, 1990). Its scaling relation for dyadic subsampling (factor of 2 in each dimension) can be expressed conveniently in the Fourier domain (Van De Ville and Unser, 2008):

$$\hat{\beta}_{\gamma, N}(\boldsymbol{\omega}) = \frac{V_{\gamma, N}(e^{j\boldsymbol{\omega}})}{\|\boldsymbol{\omega}\|^{\gamma-N} (\omega_1 - j\omega_2)^N} = \frac{V_{\gamma, N}(e^{j\boldsymbol{\omega}})}{\hat{L}_{\gamma, N}(\boldsymbol{\omega})} \quad (\text{M.4})$$

where:

- $L_{\gamma, N}(\boldsymbol{x}) \xleftrightarrow{F} \hat{L}_{\gamma, N}(\boldsymbol{\omega})$

- $V_{\gamma,N}$ is a polar representation of the interpolation localisation. It can be decomposed into: $V_{\gamma,N}(e^{j\omega}) = V_{\gamma}(e^{j\omega}) \cdot e^{j\theta_N(\omega)}$
- $V_{\gamma}(e^{j\omega}) = (8/3(\sin^2(\frac{\omega_1}{2}) + \sin^2(\frac{\omega_2}{2})) + 2/3(\sin^2(\frac{\omega_1 + \omega_2}{2}) + \sin^2(\frac{\omega_1 - \omega_2}{2})))^{\gamma/2}$
- $\theta_N = \angle(j[\omega_1] - j[\omega_2])^N$ is the phase¹

The complex polyharmonic B-spline satisfies all properties for a dyadic multiscale analysis of $L_2(\mathbb{R})$ (Riesz basis, unity and scaling relation), thus in the Fourier domain (Van De Ville *et al.*, 2008):

$$\hat{\beta}_{\gamma,N}(2\omega) = \frac{1}{2} \underbrace{H(e^{j\omega})}_{\text{Scaling filter}} \hat{\beta}_{\gamma,N}(\omega) \tag{M.5}$$

$$H(e^{j\omega}) = 2 \frac{\hat{\beta}_{\gamma,N}(2\omega)}{\hat{\beta}_{\gamma,N}(\omega)} \tag{M.6}$$

By using the semi-orthogonality properties $W_{i-1}^+ = V_i \ominus_{\perp} W_i$, we can define the wavelet basis. The wavelet function is embedded in the finer approximation scale; i.e., the high-pass filter W expresses the relationship in equation M.7. This associated wavelet function is a multiscale version of the complex Laplacian operator; i.e., the wavelet is defined as $\psi_{\gamma,N} = L_{\gamma,N}(\phi)$, where ϕ is an appropriate smoothing kernel (Van De Ville *et al.*, 2008):

$$\hat{\psi}_{\gamma,N}(2\omega) = \frac{1}{4} \underbrace{W(e^{j\omega})}_{\text{Wavelet filter}} \hat{\beta}_{\gamma,N}(\omega) \tag{M.7}$$

$$W(e^{j\omega}) = 4 \frac{\hat{\psi}_{\gamma,N}(2\omega)}{\hat{\beta}_{\gamma,N}(\omega)} \tag{M.8}$$

Here, we use $\gamma = 3$ (number of vanishing moments) and $N = 1$ (order of the complex gradient). Consequently, the wavelet transform corresponds to a multiscale version of the operator $L_{3,1}$:

$$L_{3,1} = -\Delta \left(-j \frac{\partial}{\partial x} - \frac{\partial}{\partial y} \right) = \Delta \left(j \frac{\partial}{\partial x} + \frac{\partial}{\partial y} \right) \tag{M.9}$$

Thus:

$$\psi(\mathbf{x}) = \Delta \left(j \frac{\partial}{\partial x} + \frac{\partial}{\partial y} \right) \{\beta_2(2\cdot)\}(\mathbf{x}) \tag{M.10}$$

This shows that the Marr-like wavelet spans the augmented wavelet space. Finally, we can define the coefficients:

$$\begin{aligned} d_i[\mathbf{k}] &= \langle f(\cdot), 2^i \psi_{3,1}(2^i \cdot - \mathbf{k}/2) \rangle \\ c_i[\mathbf{k}] &= \langle f(\cdot), 2^i \beta_{3,1}(2^i \cdot - \mathbf{k}) \rangle \end{aligned} \tag{M.11}$$

To obtain the pyramid decomposition of the signal, we apply the efficient filterbank algorithm depicted in figure M.1. The decomposition is applied iteratively to the low-pass coefficients $c_{i+1}[\mathbf{k}]$. The wavelet coefficients are not subsampled, which leads to a pyramid structure with mild redundancy. In this paper, we chose up to eight decomposition levels ($i = 0, \dots, 7$).

¹ where $[\omega]$ stands for the unique $\omega \in [-\pi, \pi[$ such that $\omega - [\omega] = 2n\pi$ for some integer n (Van De Ville *et al.*, 2008).

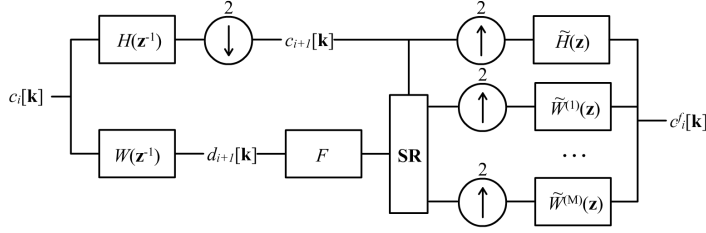


Fig. M.1. Laplace-gradient wavelet pyramid filterbank using the z -transform representation (adapted from Van De Ville and Unser (2008))

Before applying the synthesis procedure, we can process the wavelet coefficients ($d_{i+1}[\mathbf{k}]$), as embodied in the box F of figure M.1. The synthesis procedure uses a so-called subband regression method to obtain the most consistent reconstruction with respect to the (redundant) decomposition (box SR in figure M.1, see Unser and Van De Ville (2008) for more details).

The synthesis (reconstruction) is done using a subband regression because of the information redundancy between the $c_{i+1}[\mathbf{k}]$ and the $d_{i+1}[\mathbf{k}]$. We want get rid of the less informative part in order to accomplish an perfect reconstruction. Thus we have to minimise the redundancy using least squares between the coefficients.

M.2 Structure Tensor

As we use a pure Laplacian operator ($\gamma = 3, N = 1$), we might use structure tensor theory directly without needing to compute the second order derivative, the Laplacian being already one (Van De Ville *et al.*, 2008):

$$d_i[\mathbf{k}] = \begin{bmatrix} \Im(d_i[\mathbf{k}]) \\ \Re(d_i[\mathbf{k}]) \end{bmatrix} = 2^i \underbrace{\begin{bmatrix} \partial/\partial x \\ \partial/\partial y \end{bmatrix}}_{\nabla} \underbrace{\Delta\{f(\cdot) * \beta_6(2^i \cdot)\}}_{g_i[\mathbf{k}]} (2^{-i-1}\mathbf{k}) \quad (\text{M.12})$$

The structure tensor is defined by the maximisation of the cosine between the gradient of the directions and an orientation vector \bar{n} (Jähne, 2005):

$$(\nabla g^T \bar{n})^2 = |\nabla g|^2 \cos^2(\angle(\nabla g, \bar{n})) \rightarrow \max \quad (\text{M.13})$$

If we want to maximise that in a local neighbourhood w of size \mathbf{k}' (where w is a fixed-size smoothing window with positive weights), in the continuous space, it follows that the maximisation is undertaken in:

$$J_i(\mathbf{k}) = \int_{\Omega} w(\mathbf{k} + \mathbf{k}') (\nabla g(\mathbf{k} + \mathbf{k}') \nabla g^T(\mathbf{k} + \mathbf{k}')) d\mathbf{k}' \quad (\text{M.14})$$

In the discrete space, this gives (Ω is the window):

$$J_i(\mathbf{k}) = \sum_{\mathbf{k}' \in \Omega} w[\mathbf{k}'] (\nabla g(\mathbf{k} + \mathbf{k}') \nabla g^T(\mathbf{k} + \mathbf{k}')) \quad (\text{M.15})$$

The norm of g_i along the orientation of any direction is given using a vector $\mathbf{u} = [\cos(\theta), \sin(\theta)]^T$:

$$\|D_u g_i\|_w^2 = \langle \mathbf{u}^T \nabla g_i, \nabla g_i^T \mathbf{u} \rangle_w = \mathbf{u}^T J \mathbf{u} \quad (\text{M.16})$$

If we maximise that (with $\|\mathbf{u}\| = 1$ as constrain), we have an eigenvector equation system. We can link the complex coefficient directly to the complex moments of the system (Bigun *et al.*, 2004; Van De Ville *et al.*, 2008):

$$M_i^{(1)}(\mathbf{k}) = 2^{-2i} \langle d_i[\mathbf{k}], d_i[\mathbf{k}] \rangle_w = (\lambda_{max} - \lambda_{min}) e^{j2\theta} \quad (\text{M.17})$$

$$M_i^{(2)}(\mathbf{k}) = 2^{-2i} \langle |d_i[\mathbf{k}]|, |d_i[\mathbf{k}]| \rangle_w = \lambda_{max} + \lambda_{min} \quad (\text{M.18})$$

Thus, we do not need to construct J and the following structure tensors can then be built:

- *Energy* = $\lambda_{max} + \lambda_{min} = M_i^{(2)}(\mathbf{k})$.
- *Orientation* = $\theta = \frac{\arg(M_i^{(1)}(\mathbf{k}))}{2} \in [-\pi/2, \pi/2]$ which is the direction of minimal inertia.
- *Coherency* = $\frac{\lambda_{max} - \lambda_{min}}{\lambda_{max} + \lambda_{min}} = \frac{|M_i^{(1)}(\mathbf{k})|}{M_i^{(2)}(\mathbf{k})} \in [0, 1]$.

Michael Kalbermatten

ing. env. dipl. EPF

Rue Aimé Steinlen 5
1004 Lausanne

+41 79 798 76 12

✉ michael.kalbermatten@epfl.ch

Date of birth: 27.04.1980

Education

- 2004 **Master's degree in Geographical Information & Environmental Sciences**, *Ecole Polytechnique Fédérale de Lausanne - EPFL*, Switzerland.
- 1999–2003 **Rural and Environmental Engineering Studies**, *Ecole Polytechnique Fédérale de Lausanne - EPFL*, Switzerland.
- 1999 **Maturité, type C**, *Gymnase cantonal de Morges*, Switzerland.

Experience

- 2009 **Lecturer in UUE06 - Urban Jam**, *EPFL*.
- 2006–2007 **Teaching assistant in Territorial image analysis II**, *EPFL*.
- 2006–2009 **Teaching assistant in Spatial analysis**, *EPFL*.
- 2004–2006 **Teaching assistant in GIS**, *EPFL*.
- Since 2004 **PhD student at the GIS laboratory**, *EPFL*.
- 2003–2004 **Teaching assistant in databases**, *EPFL*.
- 2002–2005 **Teaching assistant in topography**, *EPFL*.

Languages

- French **Native**
- Swiss German **Native**
- German **Good knowledge**
- English **Good knowledge**

1 year in the USA

Computer skills

- | | | | |
|----------------|--------------------------------------|---------------|---------------------------|
| GIS software | Manifold, ArcGIS, MapInfo, FME, SAGA | Database | PostgreSQL, MySQL |
| Mathematical | Matlab, R | Web languages | PHP, XML, Javascript, SVG |
| Image analysis | Erdas, Idrisi, Definiens, ImageJ | | |

Publications

- S. Joost, M. Kalbermatten, and A. Bonin. Spatial Analysis Method (SAM): a software tool combining molecular and environmental data to clarify candidate loci for selection. *Molecular Ecology Resources*, 8:957–960, 2008.
- M. Kalbermatten. Etude et méthodologie de production de courbes de niveau à partir de données altimétriques laser. Technical report, LaSIG-EPFL, 2005.
- M. Kalbermatten. Landscape characterization using wavelet detail coefficients - the landslide case study. In *European Geoscience Union meeting*, 2008.
- M. Kalbermatten, R. Caloz, A. Pointet, and F. Golay. Generalization of very high resolution DEM using wavelets. In *3rd Swiss Geoscience Meeting*, 2005.
- M. Kalbermatten, F. Golay, and J. Ingensand. Manuel de modélisation standardisée des géodonnées. Technical report, ASIT-VD, 2005.
- M. Kalbermatten and P. Turberg. Analysing landslide features through scale using the wavelet transform - theory and application to the earth flow type landslide of Travers (Switzerland). In *6th Swiss Geoscience Meeting*, 2008.
- M. Kalbermatten, D. Van De Ville, S. Joost, M. Unser, and F. Golay. Laplace-gradient wavelet pyramid and multiscale tensor structures applied on high resolution DEMs. In *Proceedings of Geomorphometry 2009*, 2009.
- G. Massard, M. Kalbermatten, and S. Erkman. Geographic information system applied to industrial symbiosis: A case study in Geneva, Switzerland. In *Environmental Informatics and Industrial Ecology*, 2008.